Queen Mary
University of London

The effects of particulate filters on the strain energy function and crack growth in rubbers.

De, Dilip Kumar

The copyright of this thesis rests with the author and no quotation from it or information derived from it may be published without the prior written consent of the author

For additional information about this publication click this link.
http://qmro.qmul.ac.uk/jspui/handle/123456789/1675

Information about this research object was correct at the time of download; we occasionally make corrections to records, please therefore check the published record when citing. For more information contact scholarlycommunications@qmul.ac.uk

The effect of particulate fillers on the strain energy function and crack growth in rubbers

A Thesis Presented to
Department of Materials
Queen Mary and Westfield College
(University of London)
for the Degree of
Doctor of Philosophy

By

DILIP KUMAR DE

MARCH 1994

BIBL
LONDON
UNIV

ABSTRACT

The thesis presents a wide range of studies on carbon black and silica particulate reinforced rubbers. These include stress-strain, strain energy function, static and cyclic stress relaxation (stress softening), trouser test piece tearing and cyclic crack growth studies.

The novel features of the work include the development of a simple strain energy function which is shown to represent the stress-strain behaviour of carbon black and silica filled rubbers up to strains of 100%. The numerical values of the constants in this function are shown to vary in a meaningful and systematic manner with the fraction of reinforcing filler and with the crosslink density.

The cyclic stress relaxation studies are the first of their kind and demonstrate a significantly increased relaxation rate resulting from cycling in filled rubbers.

The trouser tearing studies give some insight as to the materials and experimental variables that determine the type of tear growth and regime of tearing. The process of stress whitening around the tear tip during steady tearing in silica filled compounds provide the first opportunity to quantitatively relate the tearing energy to the hysteresis energy loss in a known volume of rubber at the tear tip.

The cyclic crack growth studies show for the first time a systematic decrease in crack growth per cycle (dc/dn) at a given tearing energy as the carbon black filler content is systematically increased and as the crosslink density is decreased. A novel feature of the work is the demonstration of the effect of pre-strain in one direction on the cyclic growth rate of a crack in this direction when cyclically strained in a direction at right angles. The very large increase in dc/dn with increasing pre-strain is discussed in terms of pre-orientation of the rubber/carbon black structure.

Acknowledgements

I would like to thank my supervisors, Dr C.K.L.Davies and Prof. A.G.Thomas, for their tremendous help and guidance throughout the course of this research programme.

I am indebted to Peradin Limited for the manufacture and provision of the majority of the materials used in this project together with financial support.

I am also indebted to Department for Science and Education, UK for a Overseas Research Award.

Acknowledgement is made to the Department of Materials and all the members of the lecturing staff and technicians at Queen Mary and Westfield College for the provision of facilities and technical assistance throughout this project.

Thanks are also due to Mr P. Goodwin and his colleagues at MRPRA for the use of their rubber mixing and moulding facilities. The author would also like to thank Dr R.N. Stevens for writing the computer programme used in this work.

Last but not least, I would like to thank to my wife and all my family for their continuous support and encouragement.

CONTENTS

Page No.

List of Tables

Chapter 3.

Chapter 4.

Chapter 5.

Chapter 7.

Chapter 8.

List of Figures

Chapter Two.

Chapter Three.

Chapter Four.

Chapter Five.

Chapter Six.

Page No.

Chapter Seven.

Chapter Eight.

CHAPTER ONE

I.0 INTRODUCTION

The work in this thesis was initiated as a result of the need to design rubber/metal components as antivibration devices largely for use in the automobile industry. These components are subjected to static loads on which are superimposed cyclic loading. The rubber in the components is subjected to complex non uniform stresses. In most cases the rubbers are reinforced with a carbon black reinforcing filler.

The important initial design criteria is that the components should deflect a given maximum amount when the initial static load is applied. It is hence necessary during design to model the behaviour of a component stressed in a complex manner using a Finite Element Analysis Programme. To carry this out successfully there is a need to develop a strain energy function to represent the stress-strain behaviour of a filled rubber, preferably in any stressing mode, at least up to strains of 100% encountered in practice. In association with this is clearly the need to be able to simply obtain the numerical constants in such a function for a given material.

Chapter two of this thesis investigate the various forms of strain energy function previously used, with varying degrees of success, to predict the stress-strain behaviour of rubbers. The chapter ends with a simple proposed strain energy function which may represent the stress-strain behaviour of a filled rubber up to strains of 100% in any stressing mode. **Chapter three** describes the procedures to be used in an attempt to validate the proposed function which involve carrying out stress-strain experiments in tension, compression, pure shear and simple shear on a range of filled rubbers. In **chapter four and five**, the results of these experiments on carbon black and silica filled rubbers are presented and discussed. The validity of the proposed strain energy function is examined in light of both experimental results in this thesis and in light of published data. The variation in the magnitudes of the parameters in the strain energy function with filler content, crosslink density etc, are discussed.

Following initial loading rubber/metal components are subject to cyclic stresses of varying magnitude. These may lead to failure of components as a result of creep/stress relaxation or due to crack growth.

In **chapter six** the subject of cyclic and static stress relaxation in filled rubbers is discussed. Cyclic stress relaxation experiments are

described which utilize the same carbon black filled rubbers characterized in chapter four. The results are discussed in terms of the effect of carbon black content on the strain crystallization behaviour during loading and unloading.

In **chapter seven and eight** the subject of crack growth during tearing and during cyclic loading are discussed in terms of the tearing energy. In **chapter seven** the tearing energy results obtained in the present work for a variety of rubbers filled with carbon black and silica are presented and discussed in terms of the effect of materials and experimental variables on the rate and regime of tearing. In **chapter eight** the cyclic crack growth results are presented for the carbon black filled rubbers as a function of filler content, crosslink density and pre-extension ratio. The results are discussed in terms of the factors that control the increment of crack growth per cycle.

Chapter nine summarizes the significant results obtained in this thesis, their implications and gives suggestions for future work.

CHAPTER TWO

2.0 STRESS-STRAIN BEHAVIOUR OF FILLED RUBBERS

2.1 GENERAL INTRODUCTION

Rubbers filled with carbon black or silica are used extensively as the major elements in antivibration devices and other engineering rubber/metal components particularly in transportation vehicles e.g., cars, lorries, trains, aircraft etc. The most numerous components are rubber bushes and engine mounts as illustrated in figures 2.1. Rubber bushes are essentially two metal cylinders (A, A') separated by a rubber tube (B). The main purpose of the rubber tube is to isolate the vibration of one of the rigid cylinders from the other and at the same time to fix the cylinders in place through the metal/rubber bond. The rubber is deformed in a complex manner of combined shear, tension, compression and the deformation is in no sense uniaxial. These components are also required to operate under a given load which may be static or dynamic and are required to retain their structural integrity for a given time or a given number of loading cycles. Hence, these components must be designed to experience complex stressing modes under both static and dynamic conditions usually at relatively modest strains of up to 100%. The primary design criterion is the maximum allowed deflection on application of a specific force. This is determined by geometrical aspects and the mechanical behaviour of the rubber, which determine the shape and size of the rubber components. The other essential design criterion is that of component life in service. This will depend on the strain energy and stress, distributions in the component under load (both geometric and rubber property dependent) and the fracture mechanics/crack growth behaviour of the rubber. The subject of crack growth in rubbers will be addressed in subsequent chapters.

The geometry of components can be designed using an appropriate finite element package to predict the load/deflection behaviour if a simple strain energy function applicable for all stressing modes is available for rubbers. It is of course also necessary to have a simple means of determining the parameters in such a function for a given rubber and preferable to develop an understanding of how these parameters depend on materials variables such as filler content and crosslink density.

The numerical values of parameters in strain energy functions are obtained by curve fitting stress-strain behaviour determined in a given stressing mode. In filled rubbers this in not a simple matter because the stress-strain curves are highly non-linear, particularly at the low extensions of interest to the current applications. Furthermore, a strain energy function obtained by a regression analysis fit to the experimentally determined stress-strain curve in one stressing mode may not be applicable to predict the load/deflection behaviour in other stressing modes. Many researchers have included experimental data from more than one type of stressing mode in their regression analysis in order that their postulated form of strain energy function may be shown to be as general as possible. These approaches not only complicate the testing requirements to obtain a strain energy function for each rubber used but also as Treloar[1] points out, the process of modifying or correction of a strain energy function to suit a given set of data is nothing more than the "three-dimensional analogue of simple curve fitting, which has no physical basis". What is required is a simple strain energy function which can be shown to have some physical basis hence giving confidence in its use. The function must be applicable to all stressing modes, at least over the range of strain of interest. Furthermore, it must be possible to determine the magnitude of the parameters in such a function simply and reliably.

This chapter deals largely with a review of methods of measurement and types of strain energy function which other workers have used to represent the stress-strain behaviour of filled rubbers. It ends with a proposal for a new function. This function is examined experimentally utilizing commercial carbon black filled rubbers in chapter four and silica filled rubbers in chapter five. The experimental approach and procedures used are presented in chapter three. It will be shown in chapters four and five that such a function can be measured easily, is applicable to all stressing modes and that the parameters in the function vary in a meaningful manner with the physical structure of different rubber compounds.

2.2 STRESS-STRAIN BEHAVIOUR/STRAIN ENERGY FUNCTIONS

2.2.1 Introduction

There are two main approaches which attempt to describe the elastic behaviour of rubber in terms of a strain energy function for the most general types of strains. They are the molecular and the phenomenological approaches. The molecular approach, also commonly known as the simple statistical theory or gaussian theory, is based on the random fluctuations of rubber chain molecules in three dimensional networks and the response of this network to the application of a force. The phenomenological approach is based on the classical continuum mechanics, and is not molecular or structural specific. The magnitudes of the parameters in such a strain energy function can only be obtained by curve fitting appropriate experimentally obtained stress-strain data. The molecular approach is discussed first, even through its application is likely to be limited to simple unfilled rubbers, as it is important to develop some physical understanding of any phenomenological approach. This is followed by a discussion of various strain energy functions developed by other workers on a phenomenological basis.

2.2.2 Simple statistical theory/Gaussian theory

The theory[1] assumes that the entropy change per unit volume (Δs) of a network of molecular chains is only a function of the change in the chain length on application of a pure homogeneous strain; (i.e., a strain not involving rotation of the principal axes, as shown in figure 2.2)

$$\Delta s = -(1/2)\ \rho R M_c^{-1} [\ (\lambda_1)^2 + (\lambda_2)^2 + (\lambda_3)^2 - 3\ ] \qquad (2.1)$$

where ρ is the density of rubber, R is the universal gas constant, M_c is the mean molecular weight of segments of molecules between successive crosslinks, $\lambda_1, \lambda_2, \lambda_3$ are the three principal extension ratios and the corresponding principal stresses are t_1, t_2, t_3. The theory assumes constant volume ($\lambda_1\lambda_2\lambda_3 = 1$) and that the deformation is affine (i.e., Each network point moves in the same way as the bulk deformation of the specimen).

The work done (W) is equal to the change in the Helmholtz free energy and is given by $-T\Delta s$ if it is assumed that the internal energy is unchanged i.e.,

$$W = (1/2)\ \rho RT M_c^{-1} [\ (\lambda_1)^2 + (\lambda_2)^2 + (\lambda_3)^2 - 3\ ] \qquad (2.2)$$

If no energy is lost, the work done is equal to the elastically stored energy per unit volume of rubber or the stored energy density or strain energy function.

The derivatives of the strain energy function can be used to determine the principal stress differences i.e.,

$$t_1 - t_2 = \rho RT M_c^{-1} [(\lambda_1)^2 - (\lambda_2)^2], \text{ etc.} \quad (2.3)$$

From these can be determined the stress-strain relationships for a given stress system i.e., for simple extension $\lambda_1 = \lambda$, $\lambda_2 = \lambda^{-1/2}$ and $t_2 = 0$

$$\text{Thus the tensile stress } t = \rho RT M_c^{-1} [(\lambda)^2 - (\lambda)^{-1}] \quad (2.4)$$

t is the tensile stress referred to the deformed dimensions also known as the true stress. The corresponding engineering stress or nominal stress σ referred to the undeformed dimensions is given by $\sigma = t / \lambda$ and equation (2.4) becomes;

$$\sigma = \rho RT M_c^{-1} [\lambda - (\lambda)^{-2}] \quad (2.5)$$

Or

$$\frac{\sigma}{[\lambda - (\lambda)^{-2}]} = \rho RT M_c^{-1} \quad (2.6)$$

For simple shear the corresponding relationship between shear stress τ and shear strain γ is

$$\tau = \rho RT M_c^{-1} \gamma \quad (2.7)$$

The theory predicts simple relationships between stress and strain. In simple shear, the shear stress is linearly related to the shear strain by the shear modulus G ($= \rho RT M_c^{-1}$). The form of the relationships are similar for all rubbers being only scaled by the magnitude of the distance between crosslinks. A linear shear stress-strain relationship is found experimentally for unfilled rubbers at small strains. The measured values of the elastic constants agree well with the theory up to strains of 50%. However, the statistical theory does not of course purport to attempt to explain the high strain behaviour even of unfilled rubbers. Furthermore, it will not explain either the marked non-linearity in the low strain range, nor the high strain

behaviour of filled rubbers. The phenomenological theories, to be discussed next, concentrate largely on trying to represent the high strain behaviour of unfilled rubbers, with little attempt to expand these ideas to filled rubbers.

2.2.3 Mooney Equation

Mooney[2] developed the first phenomenological theory in 1940 prior to the statistical theory, to account for the large elastic deformation of rubber. His theory assumed that rubber is incompressible, isotropic in the unstrained state and obeys Hooke's law in simple shear or in simple shear superposed in a plane transverse to a prior uniaxial extension or compression. Mooney derived a strain energy function of the form;

$$W = C_1 [(\lambda_1)^2 + (\lambda_2)^2 + (\lambda_3)^2 - 3] + C_2 [(\lambda_1)^{-2} + (\lambda_2)^{-2} + (\lambda_3)^{-2} - 3] \quad (2.8)$$

which contains two elastic constant C_1 and C_2. If equation (2.8) is compared to equation (2.2), it can be seen that the Mooney function contains an additional term, C_2, compared to the statistical theory. At small strains, for unfilled rubbers, when $C_2 \rightarrow 0$, the function approximates to the statistical theory with $C_1 = (1/2)\ \rho\ RT\ M_c^{-1}$. Equation (2.8) yields the stress-strain behaviour in simple extension as;

$$\frac{\sigma}{[\ \lambda - (\lambda)^{-2}\ ]} = 2 [\ C_1 + C_2 (\lambda)^{-1}\ ] \quad (2.9)$$

A plot of the term on the left hand side of equation (2.9) versus λ^{-1} should give a straight line of slope $2C_2$ and intercept $2C_1$. A typical plot for an unfilled rubber is as shown in figure 2.3. The usual procedure to obtain the constants is to fit a straight line through the data at the lower strains and to ignore the upturn which has been associated with the finite extensibility of the macromolecular network. Furthermore, the lowest strain data points are often unreliable due to uncertainty of the precise unstrained length. The slope and intercept are taken as the Mooney constants. For an unfilled rubber, the upturn occurs at a relatively large extension ($\lambda = 2.5$ i.e., $\lambda^{-1} = 0.4$ in figure 2.3), and a substantial part of the curve approximates to a straight line. Thus the Mooney equation can be used to approximately represent the behaviour of an unfilled rubber in simple extension. Yeoh[3] examined the applicability of the Mooney equation in the course of his study to characterize carbon black filled rubbers. One of his plots is shown in

figure 2.4, for a natural rubber containing 70 pphr carbon black and indicates only a small straight portion (dotted line) at the initial part of the curve. To obtained Mooney constants using only the initial part of the curve one has to reject most of the available data at high strains. The resulting strain energy function hence, at best, only represents the behaviour over a very small strain range. Also the fitted curve ignores the data at the very small strains. In filled rubbers this region can not be excluded as the observed marked non-linearity is significant and not just experimental error. The line fitted to the tensile data in figure 2.4 was used to determine the Mooney constants C_1 and C_2. These are used here to attempt to predict the behaviour in compression. This is shown in figure 2.5 together with the actual experimental compression stress-strain curve. It can be seen that the predicted behaviour is quite different from the experimental one. Thus, in this case, the Mooney constants derived from a simple extension test are unsuitable for predicting behaviour in compression. It has also been pointed out by others[4,5] that Mooney constants determined from tensile data have only a limited value in predicting the behaviour in other stressing modes, even in unfilled rubbers.

2.2.4 General theory of Rivlin

The strain energy function proposed by Rivlin[6] is the result of the most extensive and systematic study of the continuum mechanics approach to large scale elastic deformation and most subsequent theoretical and experimental studies are based on his framework. He proposed that W must be a symmetrical function of the three principal extension ratios λ_1, λ_2, and λ_3, in case of rubber which is isotropic in the unstrained state. The strain energy function due to Rivlin is;

$$W = \sum_{i,j,k=0}^{\infty} C_{ijk} (I_1 - 3)^i (I_2 - 3)^j (I_3 - 3)^k \qquad (2.10)$$

Where I_1, I_2, and I_3 are the three strain invariants of the Green deformation tensor and are given by;

$$I_1 = (\lambda_1)^2 + (\lambda_2)^2 + (\lambda_3)^2 \qquad (2.11)$$

$$I_2 = (\lambda_1)^2(\lambda_2)^2 + (\lambda_2)^2(\lambda_3)^2 + (\lambda_3)^2(\lambda_1)^2 \qquad (2.12)$$

$$I_3 = (\lambda_1)^2 (\lambda_2)^2 (\lambda_3)^2 \quad (2.13)$$

The above three expressions are independent of the particular choice of co-ordinate axes.

For rubber, an incompressible material, $I_3 = 1$ and equation (2.10) reduces to;

$$W = \sum_{i,j=0}^{\infty} C_{ij} (I_1 - 3)^i (I_2 - 3)^j \quad (2.14)$$

and C_{00} is set equal to zero to reflect zero strain energy in the unstrained state. Thus the strain energy function W is a function of I_1 and I_2 only.

Equation (2.14) is a power series, the first term of the equation is of the same form as statistical theory with $C_{10} = (1/2) \rho RT M_c^{-1}$, [see equation (2.2)] i.e.,

$$W = C_{10} (I_1 - 3) \quad (2.15)$$

Considering only the first two terms of equation (2.14) yields Mooney's equation [see equation (2.8)] i.e.,

$$W = C_{10} (I_1 - 3) + C_{01} (I_2 - 3) \quad (2.16)$$

The power series allows the possibility of fitting a strain energy function involving higher order terms to experimental stress/strain curves, to describe the behaviour of rubbers and many forms are proposed[7,8,9,10]. A popular form is the so-called third-order deformation approximation proposed by James et al for both unfilled and filled rubbers[8,11] i.e.,

$$W = C_{10} (I_1 - 3) + C_{01} (I_2 - 3) + C_{20} (I_1 - 3)^2 + C_{11} (I_1 - 3) (I_2 - 3) + C_{30} (I_1 - 3)^3 \quad (2.17)$$

Clearly this type of formulation can be carried to any desired degree of refinement if it is intended to represent the stress-strain data for a particular type of rubber in a purely empirical manner. An example of this kind of elaboration is provided by the work of Tschoegl[12], who showed that the complete force-extension curve for a carbon-black filled natural rubber vulcanizate in simple extension could be represented by the relationship;

$$W = C_{10}(I_1 - 3) + C_{01}(I_2 - 3) + C_{11}(I_1 - 3)(I_2 - 3) \qquad (2.18)$$

while for an unfilled styrene-butadiene rubber the best fit was obtained with the relationship;

$$W = C_{10}(I_1 - 3) + C_{01}(I_2 - 3) + C_{22}(I_1 - 3)^2 (I_2 - 3)^2 \qquad (2.19)$$

While it is possible to fit strain energy functions involving higher order terms to experimental data to a good precision at high strains, the marked non-linearities at small strains, which are shown by filled rubbers, in practice, make these power series difficult to use, as an inconveniently large number of terms of varying sign may have to be used to give an adequate representation of the small strain region. Furthermore the apparent dependence of W on both I_1 and I_2 make it difficult to believe that values of the constants determined from one stressing mode could be used to predict behaviour in another stressing mode. It should also be noticed that no molecular interpretation is given or intended for any of the constants in these formulations.

2.2.5 Alternative forms of representation

Other empirical relationships for W have been reported[13,14,15]. These diverge from the Rivlin type of relationship in discarding the principle that the strain invariants I_1 and I_2 are even-powered functions of the extension ratios and are written in terms of strains or extension ratios rather than in terms of strain invariants.

For an incompressible rubber Ogden[14] expresses W in the form of a series;

$$W = \sum_n \frac{\mu_n}{\alpha_n} \left[(\lambda_1)^{\alpha_n} + (\lambda_2)^{\alpha_n} + (\lambda_2)^{\alpha_n} - 3 \right] \qquad (2.20)$$

in which the μ_n are constants and the α_n are not necessarily integers, and may be either positive or negative. This representation includes the statistical theory ($\alpha_1 = 2$) and the Mooney equation ($\alpha_1 = 2, \alpha_2 = -2$), as special cases. It is shown that a three-term expression is required to represent simple extension, pure shear and equi-biaxial extension for an unfilled rubber, containing six adjustable parameters.

The degree of agreement with experiment is quite satisfactory for unfilled rubbers. Ogden's formulation has the merit of mathematical simplicity, although the magnitudes of a large number of independent constants have to be determined, because all the terms in the equation are of identical form. However, the relationship, while fitting the whole stress-strain curve relatively well is poor at representing the marked non-linear behaviour at small strains in the case of filled rubbers.

Valanis and Landel[15] express the strain energy function W as the sum of separate functions of the three principal extension ratios, i.e.,

$$W = w(\lambda_1) + w(\lambda_2) + w(\lambda_3) \qquad (2.21)$$

in which, by symmetry, the three functions $w(\lambda_i)$ are identical. It has been shown that the Valanis-Landel relationship is in reasonable agreement with the experimental data over a wide range of strain for unfilled rubbers[1], and that it is capable of providing a convenient representation of general strain data in the form of an explicit algebraic function of the single variable λ. However the usefulness of this function in the case of filled rubbers is unknown.

2.2.6 Biaxial Extension

Rivlin[6] has shown that for a pure homogeneous general strain, a set of relationships exist between the principal stresses t_1, t_2, and t_3, the principal extension ratios λ_1, λ_2, and λ_3 and the partial derivatives of W with respect to the invariants I_1 and I_2;

$$\frac{t_1 - t_2}{(\lambda_1)^2-(\lambda_2)^2} = 2\left[\ \partial W/\partial I_1 + (\lambda_3)^2\ \partial W/\partial I_2\ \right] \qquad (2.22)$$

$$\frac{t_1 - t_3}{(\lambda_1)^2-(\lambda_3)^2} = 2\left[\ \partial W/\partial I_1 + (\lambda_2)^2\ \partial W/\partial I_2\ \right] \qquad (2.23)$$

$$\frac{t_2 - t_3}{(\lambda_2)^2-(\lambda_3)^2} = 2\left[\ \partial W/\partial I_1 + (\lambda_1)^2\ \partial W/\partial I_2\ \right] \qquad (2.24)$$

From these, the stress-strain relations for simple stressing modes can be derived as;

Tension and compression

$$\frac{\sigma}{[\lambda-(\lambda)^{-2}]} = 2\left[\ \partial W/\partial I_1 + (1/\lambda)\ \partial W/\partial I_2\ \right] \qquad (2.25)$$

$\lambda > 1$ for tension, $\lambda < 1$ for compression

Pure shear

$$\frac{\sigma}{[\lambda-(\lambda)^{-3}]} = 2\left[\ \partial W/\partial I_1 + \partial W/\partial I_2\ \right] \qquad (2.26)$$

Simple shear:

$$\tau / \gamma = 2\left[\ \partial W / \partial I_1 + \partial W / \partial I_2\ \right] \qquad (2.27)$$

where $\sigma_i = t_i / \lambda_i$

These relationships, of course, require a knowledge of the form of the strain energy function W and/or the derivatives $\partial W / \partial I_1$ and $\partial W / \partial I_2$ to enable stress strain curves to be calculated for rubbers. Equations (2.25), (2.26), and (2.27) provide a basis for the experimental examination of the form of W which would represent the mechanical behaviour resulting from a pure homogeneous strain of the most general type. This has been carried out by Rivlin and Saunders[4] by straining a sheet of an unfilled rubber unequally in two directions (biaxial testing) and measuring the resulting stresses. They then calculated $\partial W / \partial I_1$ and $\partial W / \partial I_2$ in terms of I_1 and I_2. They found, assuming incompressibility, that $\partial W / \partial I_1$ was substantially constant (a function of neither I_1 nor I_2) and that $\partial W / \partial I_2$ was independent of I_1 but varied with I_2. From their observations, they concluded that the strain-energy function could be represented by;

$$W = C_1 (I_1 - 3) + \phi (I_2 - 3) \qquad (2.28)$$

This form of the strain energy function was utilized by Hart-Smith[16] and by Alexander[17] who determined the numerical parameters of two complex functions of (I_1 - 3) and (I_2 - 3) using simple extension and equi-biaxial data. The resulting functions were shown to represent the stress-strain data of an unfilled natural rubber and an unfilled polychloroprene rubber up to strains of 200% and 500% respectively.

While the broad conclusions of the Rivlin and Saunders experiments stand, there remains considerable doubt about the relative magnitudes of $\partial W / \partial I_1$, $\partial W / \partial I_2$ and their dependences on I_1 and I_2 particularly in the region of small strains in unfilled rubbers, where the experimental errors

are greatest. Obata, Kawabata, and Kawai[18] using an automatic biaxial stretching machine suggest that both $\partial W / \partial I_1$ and $\partial W / \partial I_2$ were functions of I_1 and I_2. Furthermore, they suggest that dW / dI_2 increases monotonically with increasing I_2, which is quite contrary to the findings of Jones & Treloar[19] who suggest that dW / dI_2 decreases monotonically with increasing I_2. These differences may arise from the fact that, as reported by Obata et al[18], that dW / dI_2 contributes only a small fraction (< 10%) to the total stress in extension for unfilled rubbers and may be numerically close to zero for filled rubbers[20,21,22].

Biaxial testing has been adopted by various workers[10,11,19,21] in an effort to determine W for filled rubbers. The problems referred to above are now exaggerated as the non-linear small strain region assumes a greater significance. As the method requires the calculation of small differences between relatively large strains and stresses, the inaccuracy at small strains is large. The functional dependences of $\partial W / \partial I_1$, $\partial W / \partial I_2$ on I_1 and I_2 hence become even less clear. Furthermore, the method requires complex testing equipment and very careful experimentation. It would therefore not appear advisable to adopt a biaxial testing approach as a means of characterizing the material behaviour of filled rubbers in the strain range 1-100%, unless no other method is available.

2.3 PROPOSED FORM OF STRAIN ENERGY FUNCTION FOR FILLED RUBBERS

It can be seen from the previous discussion that most of the attempts to determine the form of the strain energy function for rubbers have largely concentrated on representing the whole of the stress-strain curves and particularly the behaviour at large strains. This makes the functions unreasonably complicated and unreliable in the small strain regions, the region of interest in the present work.

Furthermore, direct measurement of $\partial W / \partial I_1$ and $\partial W / \partial I_2$ to determine experimentally a suitable strain energy function using a biaxial test leads to the small strain difficulty mentioned earlier and is also experimentally elaborate. The problem is that the relationships in equations (2.25), (2.26), and (2.27) require a knowledge of the dependence of W on both I_1 and I_2. If the strain energy function W could be shown to be a function of I_1 only, for filled rubbers (at least to within experimental limits), and not a significant function of the second invariant I_2, then simple relationships could be obtained between the reduced stress terms on the left hand sides of equations (2.25), (2.26), and (2.27) and the single strain invariant I_1.

Such a simple relationship would exist if,
(a) $\partial W/\partial I_1$ was much larger than $\partial W/\partial I_2$ and
(b) $\partial W/\partial I_1$ was independent of I_2.

The justification for these assumptions is helped by the fact that if the deformation is not large then the predicted stress-strain relation is not very sensitive to the exact way in which W depends on both I_1 and I_2. In practice, $\partial W / \partial I_2$ for filled rubbers is not only smaller than $\partial W / \partial I_1$, but is also numerically close to zero[20,21,22]. Recently, Yeoh[3,23] proposed a strain energy function for a carbon black filled rubber which is a cubic equation in the invariant (I_1 -3) only. He derived his equation from the modified Rivlin function given in equation (2.17) by considering $\partial W / \partial I_2 = 0$. His proposed function represented the experimental data obtained in different stressing conditions well for a carbon black filled rubber, except at small strains. This is again due to the problem of using a Rivlin type of power series in the small strain range as mentioned earlier. Furthermore, during the course of a survey of the effect of carbon-black fillers on the

stress-strain properties of natural rubber vulcanizates Gregory[24] noted that a simple relationship existed between stress-strain data obtained in tension, compression, and simple shear. He showed that a plot of the reduced stress terms on the left-hand sides of equations (2.25) and (2.27) [i.e., $G = \tau/\gamma$, $H = \sigma / \{ \lambda - (\lambda)^{-2} \}$] against the invariant $(I_1 - 3)$ gave only a single curve for data for all these stressing modes, at least for strains of up to 100% in shear as shown in figure 2.6.

Taken together, the above suggests that assumptions (a), (b) may well prove valid enough in practice, at least at low strains, to allow the use of a strain energy function which depends only on I_1. If this is the case equation (2.27) for simple shear would reduce to;

$$\frac{t}{\gamma} = 2\,\partial W/\partial I_1$$

$$\text{or } G = 2\,\partial W / \partial I_1 \qquad (2.29)$$

where G is the chord modulus = τ/γ, and $(I_1 - 3) = \gamma^2$

From close examination of published results in the MRPRA engineering data sheets[25] (EDS), it can be seen that the chord modulus strain dependence can, to a fair approximation, be represented, over the published strain range (1- 100%), by a power law as shown in figure 2.7. This was also observed by Stacer et al[26] from results on highly filled materials over a more restricted strain range.

$$\text{Thus,} \qquad G = A\,\gamma^{-n} \qquad (2.30)$$

where A and n are constants for a given rubber formulation.
Combining equations (2.29) and (2.30) gives;

$$W = \frac{A}{2\,(1 - n/2)}\,(I_1 - 3)^{(1 - n/2)} \qquad (2.31)$$

This is a simple two constant strain energy function which while derived here for simple shear should be generally applicable. It could be used to characterize the stress-strain behaviour of filled rubbers in the strain range

of 1-100%, the range of interest for many engineering applications, if values of n and A could be simply determined.

2.3.1 Determination of n and A

Combining, equations (2.29), and (2.30) gives;

$$G / 2 = \partial W / \partial I_1 = (A/2)\, \gamma^{-n} = (A/2)\, (I_1 - 3)^{-n/2} \qquad (2.32)$$

Hence, taking logs gives for **simple shear ;**

$$\log G / 2 = \log (A/2) - (n/2) \log (I_1 - 3) \qquad (2.33)$$

Similarly for,

Tension and compression; Putting $\partial W / \partial I_2 = 0$ in equation (2.25), gives;

$$\sigma / 2 [\, \lambda - (\lambda)^{-2} \,] = \partial W / \partial I_1 \qquad (2.34)$$

If the strain energy function in equation (2.31) represents the behaviour in tension and compression, then

Equation (2.32) and (2.34) give;

$$\sigma / 2 [\, \lambda - (\lambda)^{-2}] = (A/2) (I_1 - 3)^{-n/2} \qquad (2.35)$$

Taking logs gives;

$$\log \sigma / 2 [\, \lambda - (\lambda)^{-2}] = \log (A/2) - (n/2) \log (I_1 - 3) \qquad (2.36)$$

Pure shear; The equivalent equation is

$$\log \sigma / 2 [\, \lambda - (\lambda)^{-3}] = \log (A/2) - (n/2) \log (I_1 - 3) \qquad (2.37)$$

Double log plots of the reduced stress terms on the left hand sides of equations (2.33), (2.36), and (2.37) against the invariant (I_1 - 3) should give a straight line of slope n/2 and an intercept of log A/2 in all the four stressing modes if the strain energy function in equation (2.31) represents the behaviour in all stressing modes.

If this is the case then values of n and A determined from any single stressing mode for a given rubber could then be used in equation (2.31) to calculate the strain energy function which could be used to predict the behaviour of the filled rubber in any other simple or complex stressing mode.

Figure 2.1: Rubber bushes

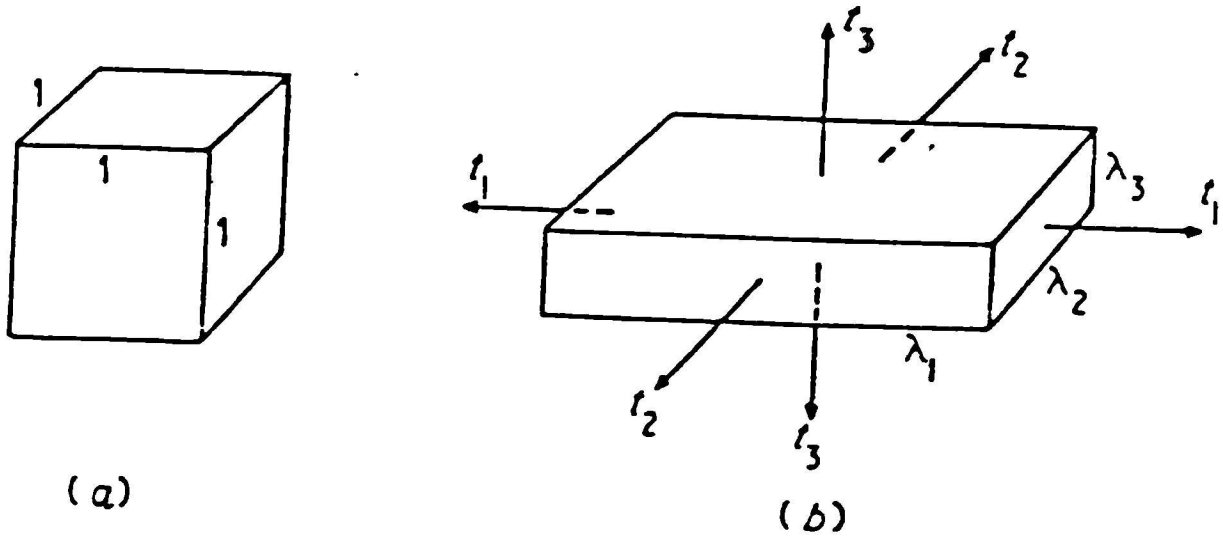

Figure 2.2: Pure homogeneous strain:
(a) unstrained state; (b) strained state

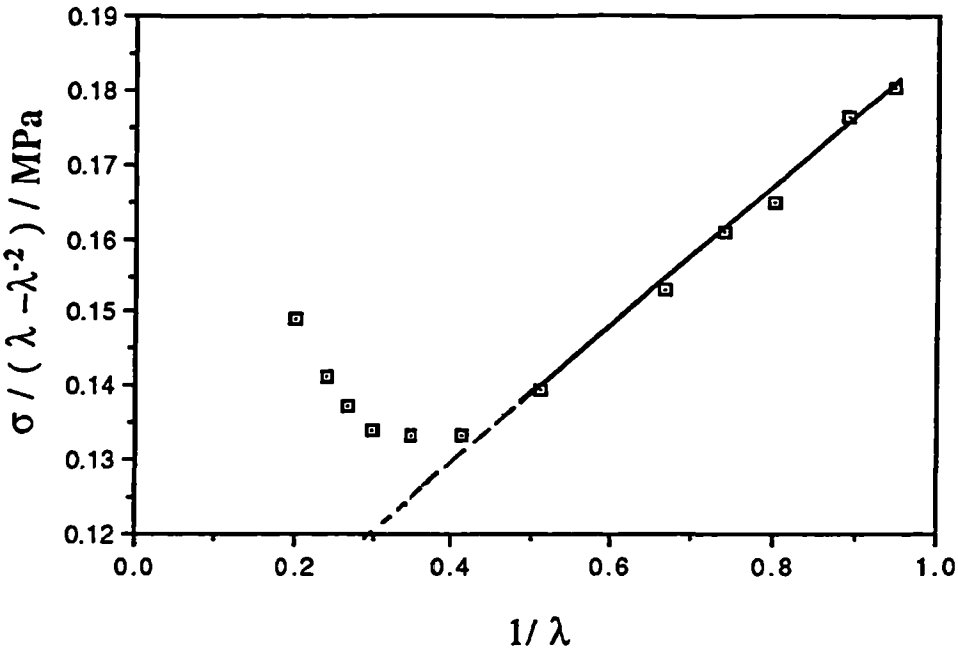

Figure 2.3 :Mooney plot for an unfilled natural rubber cured with peroxide, crosslink density 5.02 x 10^{-2} g. mol / g RH [fig 6.13 curve (b), ref 1]

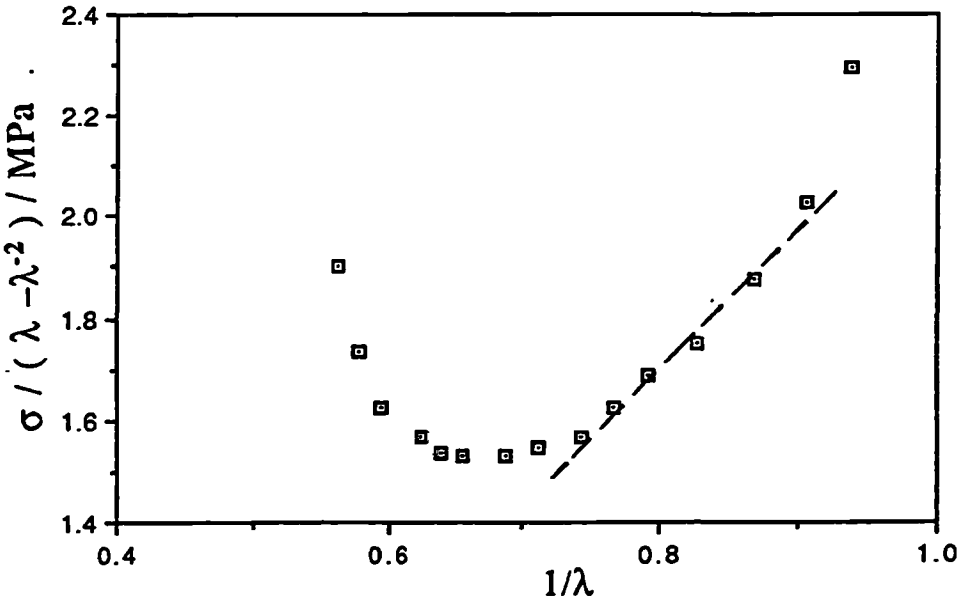

Figure 2.4 : Mooney plot for a natural rubber vulcanizate containing 70pphr of carbon black in tension. The broken line is the Mooney equation fitted to the tensile data over the approximately linear region [figure 1, ref 3].

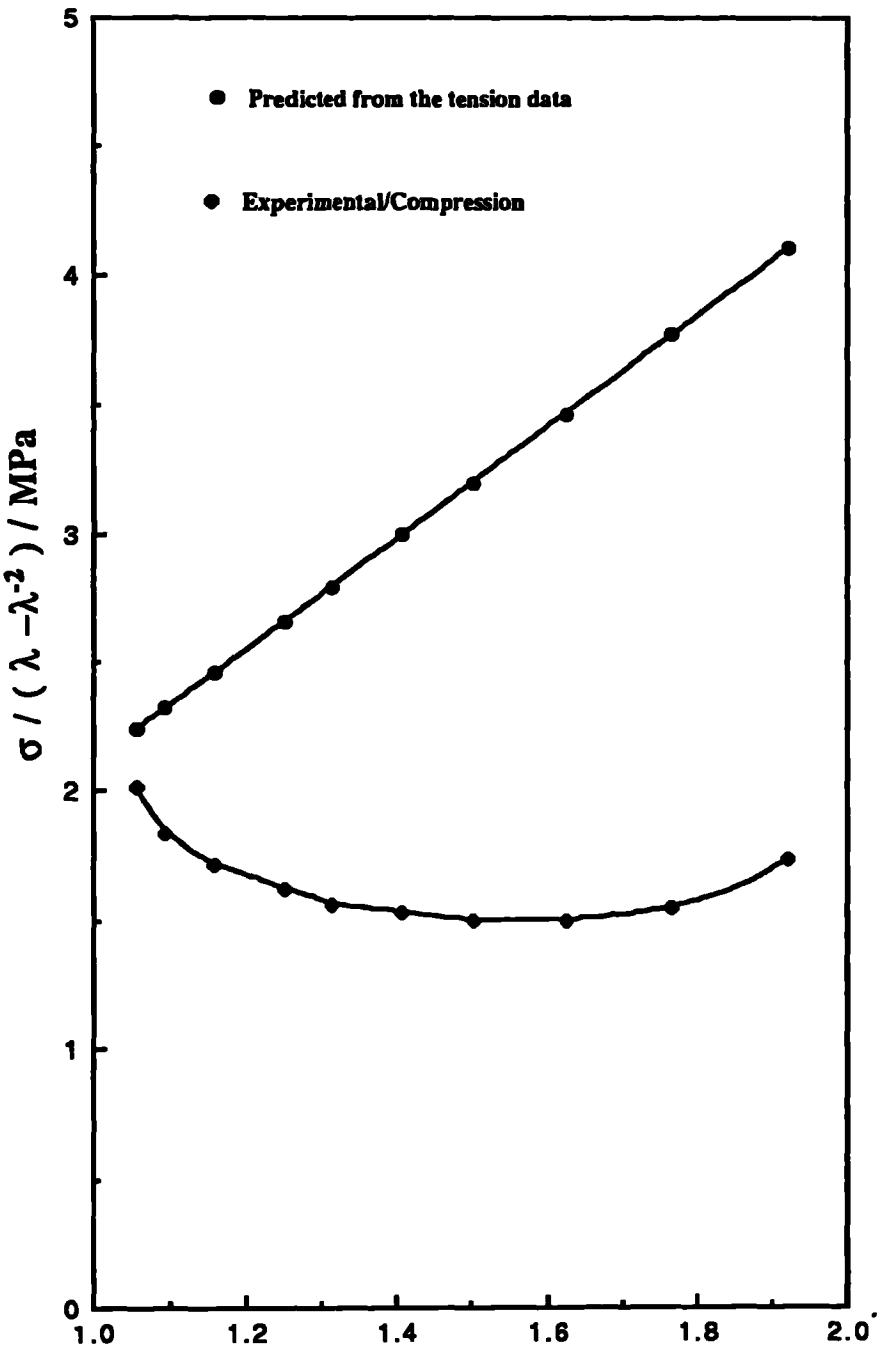

Figure 2.5 : Mooney plot for a natural rubber vulcanizate, containing 70pphr of carbon black, in compression together with the predicted curve using the Mooney constants obtained from the tension data of the same vulcanizate.

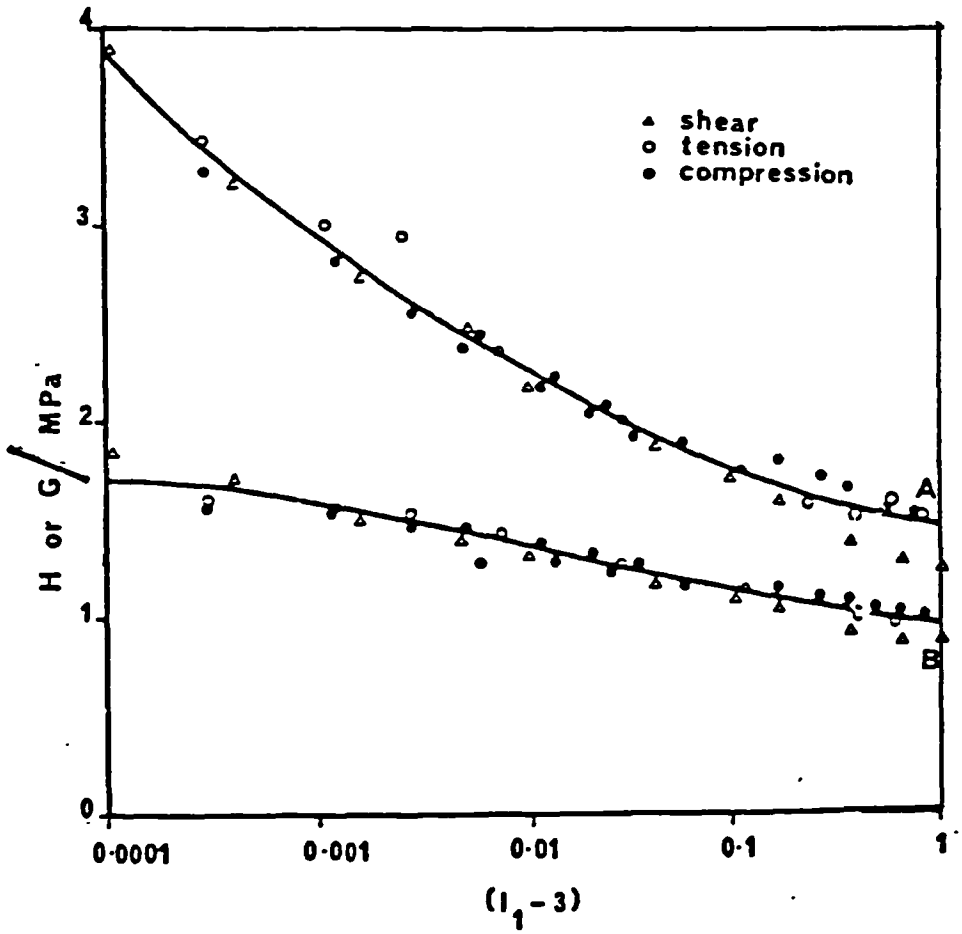

Figure 2.6: Variation of H and G with the strain invariant I_1 for HAF carbon black filled natural rubber vulcanizates, A-60 pphr, B-40 pphr, (fig-2, ref 24)

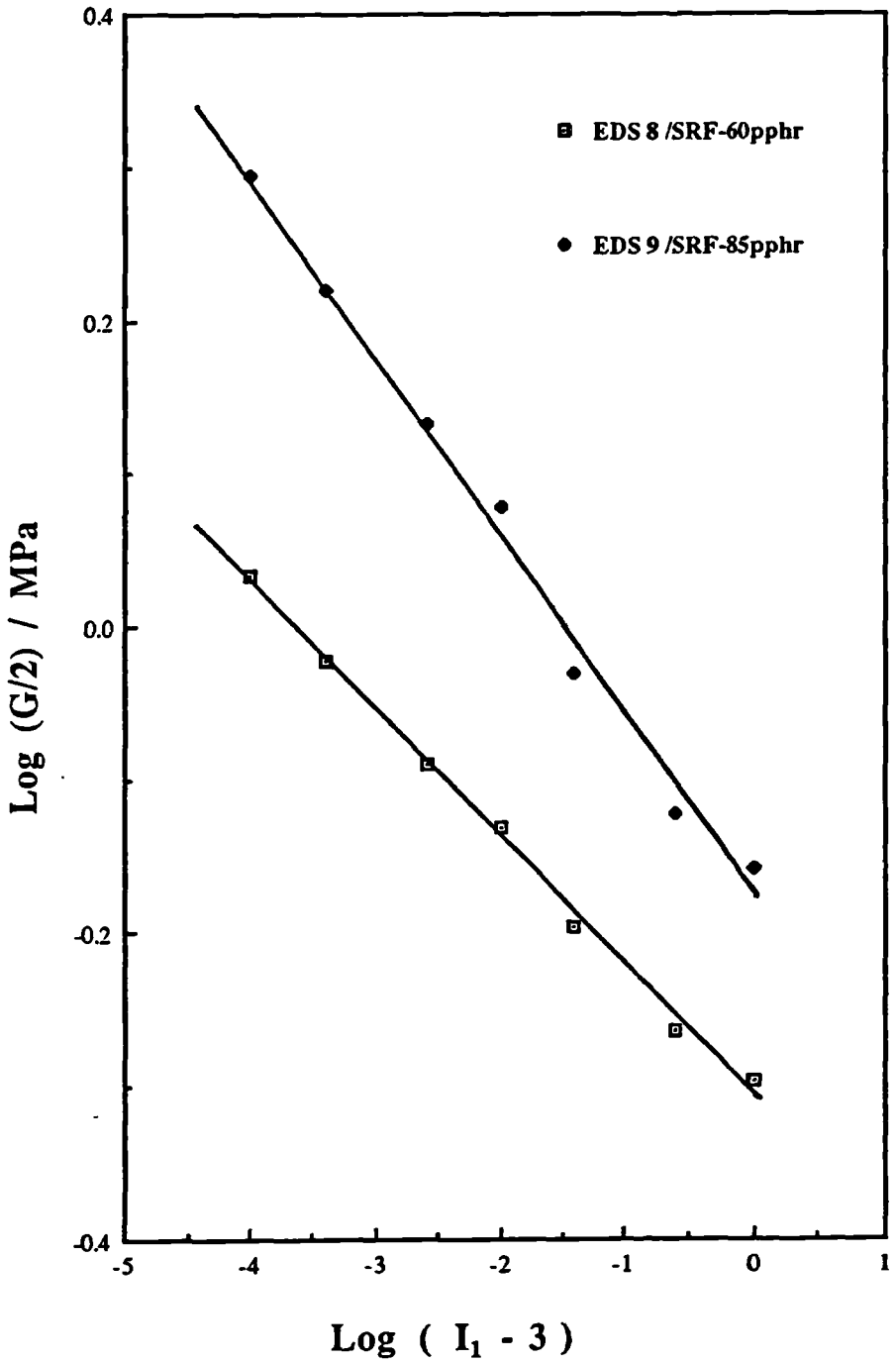

Figure 2.7: Cord modulus versus (I_1-3) for carbon black filled vulcanizates, data obtained from Engineering data sheets (ref 25)

CHAPTER THREE

3.0 EXPERIMENTAL APPROACH AND PROCEDURES

3.1 INTRODUCTION

In the previous chapter, a simple two constant strain energy function was proposed to characterize the stress-strain behaviour of filled rubbers in the strain range of 1-100%. It was postulated that this simple strain energy function could represent all the stress-strain data whether the rubbers were tested in simple tension, compression or shear. The present work intends to test this hypothesis, on a series of filled rubbers containing a range of carbon black contents, currently used by Peradin Ltd in anti-vibration devices, by moulding the appropriate geometry test pieces with which to carry out tension, compression, pure shear and simple shear, stress-strain tests. To do this successfully great care must be taken to ensure that all the types of test pieces have the same resultant crosslink density for each particular vulcanizate. Furthermore, great care must be taken with the measurements of extension and force in the tests, using the appropriate types of specimen grips, if the simple strain energy function is to be validated or otherwise for all the various test geometries. Tests are to be carried out on rubbers of various crosslink densities with a fixed carbon black content in order to explore the physical significance of the parameters n and A in the strain energy function. It is then intended to extend this process to the testing of silica filled rubbers to explore the general applicability of this strain energy function.

3.2 MATERIALS AND FORMULATIONS

The main materials used in this study were either natural (NR) or synthetic cis-polyisoprene (IR) with limited testing using a styrene butadiene rubber (SBR). The rubbers were filled with carbon black or fine silica and crosslinked with sulphur or a peroxide system. Tables 3.1-3.4 detail the constituents in each rubber.

The carbon black filled systems were commercial rubbers developed by Peradin Ltd for use in antivibration devices. Four carbon black-filled NR vulcanizates were used containing 23, 32, 49, and 69 pphr of high abrasion furnace black (HAF N330) and an SBR rubber filled with 50 pphr HAF carbon black. They were all sulphur cured. Table 3.2 also shows a set of formulations for a 49 pphr HAF carbon black system with different ratios of sulphur and accelerator in order to obtain networks with a range of crosslink densities for a fixed filler content. The values of crosslink density shown in table 3.2 were determined by the equilibrium swelling method which will be discussed latter.

The silica filled rubbers used were crosslinked with peroxide and all contained 40 pphr of silica. The silica filled vulcanizates opened up the possibility of studying a reinforcing system other than the more widely studied carbon black system. Furthermore, vulcanizates cured with peroxide were translucent and offered the possibility of optical observation of the behaviour of the filler/rubber interface as a function of strain; without and with the presence of a silane coupling agent.

The rubbers were mixed in a internal mixer with a batch mass of approximately 20 kg. The total mixing time was six minutes and the average mixing temperature at the time of dumping was 150°C. The rubber sheets were allowed to cool overnight. Curatives were added separately on a two roll mill before use. The vulcanization time for each compound was determined by using a Monsanto oscillating disc cure meter (type R100). The vulcanization temperatures and the time taken to achieve a maximum state of cure are given in tables 3.1-3.4.

3.3 MOULDING OF TEST PIECES

It was necessary to produce flat sheets for tensile and pure shear tests, compression buttons for compression tests and double shear test pieces for simple shear tests. This required three separate moulding operations using the same batch of a given rubber. It was also necessary to ensure that all the rubber test pieces attained the same crosslink density. This was achieved by curing all types of samples at the same nominal temperature (155^{o}C for the carbon black filled compounds) but with appropriate nominal cure times for each type of sample. Moulding was carried out at pressure of 21 MPa on an electrically heated press at Peradin Ltd or at QMW.

3.3.1 Flat sheet

Vulcanization was carried out using two compression moulds to produce flat vulcanized sheets of sizes 185x185x2 mm (Peradin) and 224x224x1-2 mm (QMW). The times taken to vulcanize (cure time) are given in tables 3.1-3.4.

3.3.2 Compression buttons

Vulcanization was carried out using a special compression mould with 10 mould cavities to produce compression samples (figure 3.1) at Peradin Ltd. The compression buttons were cured for an additional three minutes, compared to the flat sheets, at the same temperature, to allow for the longer heating up period of the thicker samples.

3.3.3 Double shear test piece

The test-piece, as shown in figure 3.2, comprised two rubber disks (A), bonded between three cylindrical mild steel pieces (B1, B2, B3). The surface of the mild steel was first sandblasted and then degreased in a suitable solvent for two days to remove any rust and oil contamination to ensure satisfactory rubber/metal bonding. The cleaned surfaces were painted with commercial bonding agents, Chemlok 203 (primer coat) and Chemlok 220 (top coat). Vulcanization was then carried out using a transfer moulding technique at Peradin Ltd. The temperatures and times were the same as for the flat sheets.

3.4 MATERIAL CHARACTERIZATION

3.4.1 Determination of the crosslink density

Equilibrium swelling in n-decane was used to determine the crosslink densities to check the consistency of the material in a given batch or to check the variability between the different types of samples. The details of the method are contained in appendix-(3.1).

Graphs were plotted of the mass uptake of solvent (n-decane), against the square root of time as shown in figure 3.3. The equilibrium mass uptake (M_∞) was used to calculate the physically manifested crosslink density or apparent crosslink density $[X]_{phys}$ using the equations (3A-3C) in appendix-(3.1). The filler volume was excluded from the calculation. Table 3.5 shows the average values of $[X]_{phys}$, so calculated for the NR vulcanizates in the form of flat sheets containing different amounts of carbon black. The formulations of these materials are given in the table 3.1.

3.4.2 Variation of the crosslink density between the different geometry test pieces

The variation of $[X]_{phys}$, in this study, from sheet to sheet cured from the same batch of a compound was ± 0.8 % of the average value. The variation of the average values of $[X]_{phys}$ between the flat sheets, the compression buttons and the shear specimens was ± 1.2%.

The effect of this variation of $[X]_{phys}$ on the value of the tensile stress for a given strain can be estimated, approximately, using the statistical theory of rubber like elasticity[1]. The tensile stress, σ, is related to extension ratio λ by;

$$\sigma = 2\,[X]_{phys}\,\rho\,RT\,[\lambda - (\lambda)^{-2}] \qquad (3.1)$$

Where ρ is the mass per unit volume of the network, and R is the gas constant.

Thus the observed variation of $[X]_{phys}$ between different flat sheets will vary the tensile stress at a given extension ratio by only ± 0.8%. The observed variation of the crosslink density between different types of specimen will vary the stress by only ±1.2%. These resulting stress differences lie within the experimental errors of the stress-strain measurements. Thus it can be considered that, in effect, the same crosslink density was achieved within experimental error, in this study, for the different geometry test pieces.

3.4.3 Effect of carbon black loading on crosslink density

It can be seen from the table 3.5 that the apparent crosslink density $[X]_{phys}$ obtained from the swelling measurements increases with increasing carbon black content. The observed variation between NR23 and NR69 is 26%. This has been attributed to the restricted mobility (reduced swelling) of the rubber through interaction at the filler surface which increases with increasing filler content[27]. Porter[27] developed an empirical relationship which allows the actual physical crosslink density in any natural rubber containing a known volume of HAF carbon black to be determined i.e.,

$$[X]_{act} = \frac{[X]_{phys}}{1 + k\Phi} \qquad (3.2)$$

where $[X]_{act}$ is the actual physical crosslink density in the vulcanizate network, k is a constant characteristic of the filler and has a value of 2.6 for HAF carbon black, and Φ is the volume fraction of carbon black in the vulcanizate.

The above relationship was used to calculate the actual crosslink densities of the carbon black filled vulcanizates and the results are given in table 3.5. The observed variation between NR23 and NR69 is now only 4% and the maximum variation of crosslink density between the four carbon black filled vulcanizates is only 6%. Thus it can be considered that, in effect, the same crosslink density (actual) was achieved within experimental error, in this study, for the different carbon black filled vulcanizates, when the effect of filler content on swelling is taken into account.

3.4.4 Effect of filler and coupling agent on crosslink densities determined by Swelling in the case of silica filled vulcanizates

The effect of the addition of a silica filler and a coupling agent on the apparent crosslink density of an unfilled IR (cariflex 305, 92% cis polyisoprene) cured with dicumyl peroxide (formulation IR/00), observed in this study, is as shown in table 3.3. The effect of the filler will be discussed first. It can be seen from the table that the addition of 40 pphr silica to the unfilled IR (resulting formulation IR40/01) increased the apparent crosslink density by a factor of 1.68. This effect results from the restriction of swelling due to the addition of filler, as mentioned earlier. The addition of 1pphr coupling agent, alone, to the unfilled IR showed an increase of 5% in apparent crosslink density, suggesting only a small participation of the

coupling agent (A174) in the crosslinking process. The same amount of coupling agent when added to the silica filled IR (resulting formulation IR40/02), resulted in an increase of the apparent crosslink density by a factor of 1.5. This is in addition to the factor of 1.68 due to filler addition alone. According to Wagner[28] the increases are due to the formation of coupling bonds between filler and rubber which are indistinguishable from network bonds under swelling conditions, resulting in small swelling strains. He also observed that the silane effect was specific to silica, being virtually absent with carbon black. These effects will be discussed again in chapter five in connection with the stress-strain behaviour of silica filled vulcanizates.

3.5 DESIGN OF SPECIMEN GRIPS

3.5.1 Tension

Parallel-sided test pieces (150x10x2 mm) were used for the tensile measurements. The advantage of this type of test piece is that the grip separation can be used as a fair measure of the elongation, if the initial length between the grips can be determined accurately and no slippage from the grips occurs during testing. To prevent slipping positive gripping is required. This can create a problem as if an excessive compressive force exists on the rubber at the edges of the grips it is difficult to measure the initial unstrained length of the sample between the grips. Special spring loaded grips (figure 3.4) were used to avoid excessive compression of the rubber while maintaining positive gripping and preventing slippage.

3.5.2 Compression

The compression test buttons and compression platens used are shown in figures 3.1 & 3.5 respectively. The important parameters in testing are that the compression platens must be flat, and parallel, as should the specimens, and the platen/specimen interface must be friction free. These conditions ensure a uniform distribution of forces over the compression test piece surfaces. The friction free condition was achieved, during tests, by using a medium viscosity silicone oil at the platen/specimen interface.

3.5.3 Pure shear

Pure shear deformation is achieved by straining a rectangular sheet in its height direction as illustrated in figure 3.6, so as to produce an extension ratio λ_1, while maintaining the perpendicular or transverse dimension unchanged (λ_2=1). Pure shear deformation requires the application of a tensile force F_1 in one direction and F_2 in a transverse direction. However, if the width of the sheet is very much greater (minimum 6 times[1]) than its height, the direct application of a transverse force is not required, the force being automatically generated as a result of the restraints introduced by the grips. It has been demonstrated previously[1,29] that except in the immediate vicinity of the free edge, the state of strain in such a test piece is substantially uniform pure shear. This has also been demonstrated in the present work by measuring the change in the length along parallel lines in the transverse direction before and after stretching up to 100% strain.

The dimensions of the test pieces in this study were 185 mm width (w) x16-18 mm height (L_o). The width was approximately 10 times the height. The grips are essentially similar to tensile grips but are larger and hence capable of gripping samples of up to 240 mm width (figure 3.11).

3.5.4 Simple shear

Simple shear is a type of strain obtained by sliding a plane which is parallel to a given plane, through a distance which is proportional to the distance from the given plane[1], as shown in figure 3.7. The lateral faces of a cube are transformed by simple shear into parallelograms. There is no strain in the plane normal to the XOY plane, and the extension ratio in that direction is therefore unity. A simple shear type of deformation was achieved in this study by using double shear test pieces and a set of special shear grips, as shown in figure 3.8. The grips had two halves (M&N). The half M had two semicircular bottoms (R&P) and two semicircular tops (r & p) of diameter 28 mm. They were screwed together to house the mild steel pieces (B1&B2) of the sample (figure 3.12). The half N with a semicircular bottom (Q) and a semicircular top (q) of diameter 28 mm was used to house the central mild steel piece (B3) of the sample. The two rubber disks (A) experience a simple shear deformation when the central piece was moved parallel to its diameter by the application of a force.

3.6 MECHANICAL TESTING TECHNIQUE

Tests were carried out on screw driven Instron universal testing machines, 1122 or 1195 (capacity 5 KN and 100 KN respectively) or on a servo-hydraulic machine which was constructed as a part of a Teaching company scheme. The strain rate was 10% per minute in the case of tension, compression and pure shear tests. This was achieved by adjusting the crosshead speed according to the straining length of the different types of samples. Simple shear tests were carried out at a strain rate of 30% per minute (i.e., 2 mm/minute cross head speed) The applied force could be measured using the Instron load cell which was calibrated using dead weights before each set of experiments. The applied force could be measured to ± 0.5% of the indicated load. Dynamic simple shear tests were carried out at 1 Hz. The methods of measuring strain are described below for each geometry of testing. All measurements were carried out at 23°C and on previously unstrained samples. Results of five test pieces of a given geometry were averaged to give representative stress-strain data for the material in that given geometry.

3.6.1 Tension

The experimental set up is shown in figure 3.9. The thickness and width of each sample was measured, using a micrometer by taking an average of ten measurements along the length. Two gauge marks parallel to one another were drawn approximately 100 mm apart using a silver ink pen. The sample (C) was clamped along one of those lines by the upper grip (A) which was attached to the load cell. The weight of the sample was balanced off by rotating the zero adjusting knob at the control panel of the machine. Then, the lower grip (B) was used to clamp the sample alone the other line. Two screws (S) along with two springs on each grip were used for clamping the sample. The screws of the grips were tightened carefully ensuring minimum change in the zero force, but sufficiently tightly to avoid any specimen slippage during straining. The small change in the zero force measured by the load cell was due to a compressive force on the rubber generated by the grips. This compression force was balanced off by moving the crosshead down slowly to attain zero force. The initial length between the grips was measured accurately using a Cathetometer (X ± 0.01 mm). Tests were carried out at a specified strain rate (10%/minute) by moving the crosshead downwards. The force-time curves were recorded on a chart

recorder attached to the machine. The available chart speeds ranged from 1 to 1000 mm/minute. The nominal stress, σ i.e., force per unit cross-sectional area referred to the unstrained state and the percentage strain referred to the grip separation were calculated.

3.6.2 Compression

The experimental set up is shown in figure 3.10. The upper platen (A) was connected to the load cell and the lower platen (B) was connected to the crosshead. The lower platen was fitted with an Aluminium block (M) which had two holes of 12.5 mm diameter to house two transducer bodies (T), one in each hole. A similar block (M) attached to upper platen had two holes of 5mm diameter which housed two adjusting screws (U) connected to the movable cores (J) of the transducers. The transducers were D.C. linear variable differential transformers (LVDT). They required ± 15 VDC power supply to operate and produced a ± 10 VDC output for ± 12.5 mm full scale extension. The scale factor was 0.8 volts/mm. The power supply and outputs from the transducers were monitored using an Analogue summing unit (average outputs) constructed by the Electronics Department at QMW which was connected to an X-Y chart recorder.

The thickness and diameter of each sample were measured using a micrometer by taking an average of ten measurements. The flat surfaces of the sample were lubricated with a medium viscosity silicone oil to avoid friction at the platen-sample interface. The lubricated sample was placed at the centre of the two platens. The crosshead was so adjusted so that both platens touched the surfaces of the sample. The sample was given a rotating movement, by hand, to ensure zero force and proper contact of the sample surfaces by both the platens. Tests were carried out by moving the crosshead continuously towards the load cell for strains of up to 50% [$(I_1-3)=1.25$], which is equivalent to 80% in tension and 110% in simple shear. This limit was set as at greater strains slippage of the samples from the centre of the platens occurred.

Force-displacement curves were recorded on an X-Y plotter using the outputs from the Instron load cell (Y-axis) and the average voltage outputs from the transducers (X-axis). The nominal compression stress i.e., force per unit cross-sectional area referred to the unstrained state and the percentage strain referred to the unstrained thickness of the sample were calculated and plotted.

B L
LO N
U

3.6.3 Pure shear

The experimental set up is as shown in figure 3.11. The upper grip (A) and the lower grip (B) were attached to the load cell and crosshead respectively. The lower grip was fitted with two Aluminium blocks (M) to house the two transducer bodies (T). Two Aluminium plates (P) with holes were attached to the upper grip which housed two adjusting screws (U) connected to the cores (J) of the transducers. Transducer outputs were connected to an X-Y plotter in the same manner as for the compression test. The thickness of each sample was measured using a micrometer by taking an average of ten measurements. A pair of lines were drawn parallel to one another on the surface of the sample. The sample (C) was clamped along one of those lines by the upper grip. The weight of the sample was balanced by rotating the zero knob on the control panel of the machine. The lower grip was used to clamp the sample along the other line. The screws (S) at the grips were tightened carefully to ensure minimum change in the zero force but sufficiently tightly to avoid any slippage from the grips during tests. While tightening up the screws, the sample buckled a little due to the compression of the rubber at the edges of the grips. This compressive force was balanced off by moving the crosshead down slowly. The initial distance between the grips was measured using a Cathetometer. Tests were carried out at a strain rate of 10%/minute by adjusting the crosshead speed in relation to the measured height between the grips. The force-displacement curves were recorded using the same procedure as for the compression tests from which were determined the nominal stress versus percentage strain curves.

3.6.4 Static simple shear

The experimental set up is as shown in figure 3.12. The upper grip (A) and the lower grip (B) were attached to the load cell and the crosshead of the machine respectively. The lower grip was fitted with an Aluminium block (M) to house the transducer body (T). The aluminium plate (P) attached to the upper grip houses an adjusting screw (U) connected to the core (J) of the transducer. The double shear sample (figure 3.2) was clamped firmly to the three mild steel holders (figure 3.8) as described in section 3.5.4. The tests were carried out at a crosshead speed of 2 mm/minute.

The force-displacement curves were recorded up to strains of 100% using the same procedure as for the compression tests and from these were determined the nominal stresses and percentage strains.

3.6.5 Dynamic simple shear

The tests were carried out on a servo-hydraulic testing machine. A sinusoidal waveform was used for all the work reported. The force and extension measuring devices were connected to a TANDON PCA 40+ computer via an analogue input. The Tandon computer provided a precise means to capture the force-displacement data from the outputs of a flat load cell (2.5 KN) and a LVDT transducer, and to subsequently analyze it using the software programmes available from the manufacturer (CAVSMO2). The grips and the samples used were the same as for the static simple shear tests. The tests were carried out with different strain amplitudes (half strain range) up to 100% strain at 1 Hz. The printouts obtained from the computer were used to determine the dynamic shear modulus and strain, based on the unstrained dimensions of the samples.

TABLE 3.1 : Formulations of NR and SBR vulcanizates-carbon black filled

(All ingredients are parts by weight per hundred rubber; pphr)

INGREDIENTS	NR23	NR32	NR49	NR69	SBR50
[1]NR	100.0	100.0	100.0	100.0	-
[2]SBR	-	-	-	-	100.0
Zno	5.0	5.0	5.0	5.0	5.0
Stearic acid	2.0	2.0	2.0	2.0	2.0
[3]Antioxident 2246	2.0	2.0	2.0	2.0	2.0
[4]Carbon black N330	23.0	32.0	49.0	69.0	50.0
Sulphur	1.0	1.0	1.0	2.0	1.5
[5]CBS	1.6	1.4	1.5	1.5	1.5
[6]TMTD	1.0	1.0	1.0	2.0	-
Cure time, minutes 155 ± 1°C	12	12	12	17	60
Vr	0.3300	0.3460	0.3596	0.3712	0.4771
$[X]_{phys} \times 10^{-5}$ g mol /g RH	9.9	11.2	12.0	13.4	9.0
Mc/g	5036	4461	4037	3772	5555
Stress at $\lambda = 2$ MPa	1.21	1.53	2.33	3.46	2.71

[1] SMR CV60- Constant viscosity standard Malaysian rubber with producer's viscosity limit at 55-65
[2] Intal 1500- Cold emulsion grade SBR
[3] 2,2'-Methylene-bis-(4-methyl-6-tert. butyl-phenol)
[4] HAF- High abrasion furnace black, particle diameter 28-36 nm
[5] N-Cyclohexyl-2-benzothiazyl sulphenamide
[6] Tetramethyl thiuram disulphide

TABLE 3.2 : Formulations of NR vulcanizates- a fixed carbon black content but different crosslink densities

(All ingredients are parts by weight per hundred rubber; pphr)

INGREDIENTS	NR49/A	NR49/B	NR49[1]	NR49/C
[2]NR	100.0	100.0	100.0	100.0
Zno	5.0	5.0	5.0	5.0
Stearic acid	2.0	2.0	2.0	2.0
Antioxident 2246	2.0	2.0	2.0	2.0
Carbon black N330	49.0	49.0	49.0	49.0
Sulphur	1.0	1.0	1.0	1.0
CBS	0.3	0.7	1.5	1.5
TMTD	0.3	0.7	1.0	2.0
Cure time, minutes 155 ± 1°C	15	17	12	15
Vr	0.2849	0.3385	0.3596	0.3881
$[X]_{phys}$ x 10^{-5} g mol /g RH	6.9	9.8	12.4	15.2
Mc/g	7246	5102	4037	3290
Stress at λ = 2 . MPa	1.21	1.70	2.33	2.93

NR49[1]-same vulcanizate as in table 3.1
[2]SMR CV60

TABLE 3.3: Formulations of IR vulcanizates-silica filled

(All ingredients are parts by weight per hundred rubber, pphr)

INGREDIENTS	IR00	IR40/01	IR40/02	IR40/03
[1]Cariflex 305	100	100	100	100
Antioxident2246	1	1	1	1
[2]Ultrasil VN3	-	40	40	40
Dicumyl peroxide	1	1	1	1
[3]Silane A174	-	-	1	2
Cure time, minutes 160 ± 1°C	45	45	45	45
Vr	0.2263	0.2748	0.3326	0.3602
$[X]_{phys}$ x 10^{-5} gr mol /gr RH	4.00	6.73	10.13	12.44
Mc/g	12500	7429	4761	4019
Stress at $\lambda = 2$ MPa	0.43	1.05	1.65	1.82

[1]Cariflex 305- Synthetic cis (92%) polyisoprene (IR)
[2]Ultrasil VN3- Silica filler
[3]Silane A174- coupling agent-gamma-methacryloxypropyltri methoxysilane

TABLE 3.4 : Formulations of NR and SBR vulcanizates- silica filled

(All ingredients are parts by weight per hundred rubber, pphr)

INGREDIENTS	NR40/01	NR40/02	SBR40/01	SBR40/02	SBR40/03
[1]NR	100.0	100.0 -		-	-
[2]SBR	-		100.0	100.0	100.0
Antioxident2246	1.0	1.0	1.0	1.0	1.0
Ultrasil VN3	40.0	40.0	40.0	40.0	40.0
Dicumyl peroxide	1.0	1.0	1.0	1.0	1.0
Silane A174	-	1	-	1.0	1.5
Cure time, minutes 160 ± 1°C	45	45	45	45	45
V_r	0.2725	0.3023	0.4729	-	-
$[X]_{phys} \times 10^{-5}$ g: mol /g. RH	6.7	8.0	8.6	-	-
Mc/g	7462	6273	5841	-	-
Stress at $\lambda = 2$	1.209	1.360	2.220	-	-

[1]SMR CV60
[2]Intal 1500

TABLE 3.5: The apparent and actual crosslink densities of carbon black filled vulcanizates

Compound.	Carbon black, pphr	$[X]_{phys}$ /10^{-5} g mol /g RH	Φ	$[X]_{act}$ /10^{-5} g mol /g RH
NR23	23	9.9	0.0943	8.0
NR32	32	11.2	0.1260	8.4
NR49	49	12.4	0.1753	8.5
NR69	69	13.4	0.2378	8.3

$$[X]_{act} = \frac{[X]_{phys}}{1 + k\,\Phi}$$

$[X]_{act.}$ = actual crosslink concentration , g mol /g RH

$[X]_{phys}$= physically manifested crosslink concentration, g mol /g RH

k = 2.6 for HAF carbon black -constant characteristic of the filler

Φ = Volume fraction of carbon black in the vulcanizate

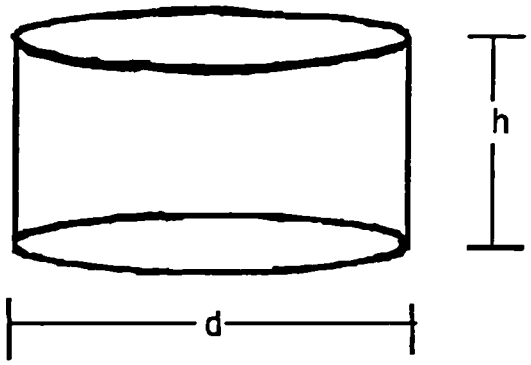

Figure 3.1: Schematic diagram showing a compression button, height, h = 12.5 mm, diameter, d = 29 mm

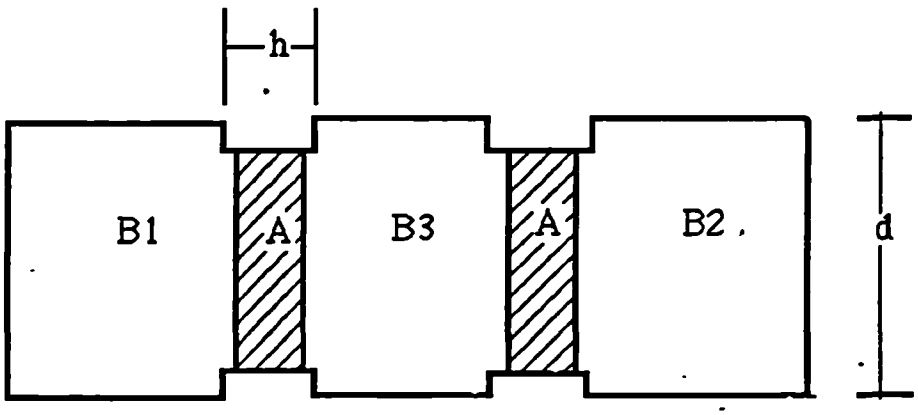

Figure 3.2: Schematic diagram showing a double shear test piece A, A - rubber disks, B1, B2, B3 -mild steet pieces, thickness, h = 6.0 mm, diameter, d = 25.4 mm

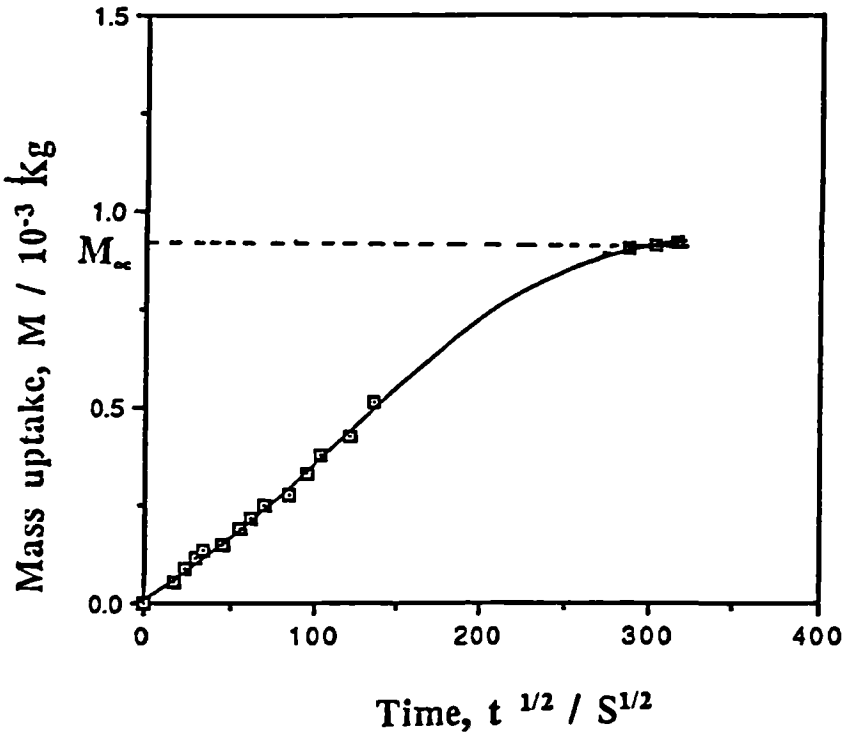

Figure 3.3: The mass of liquid, M, absorbed by a NR vulcanizated sheet immersed in n-decane as a function of time, temperature-23^{0}C

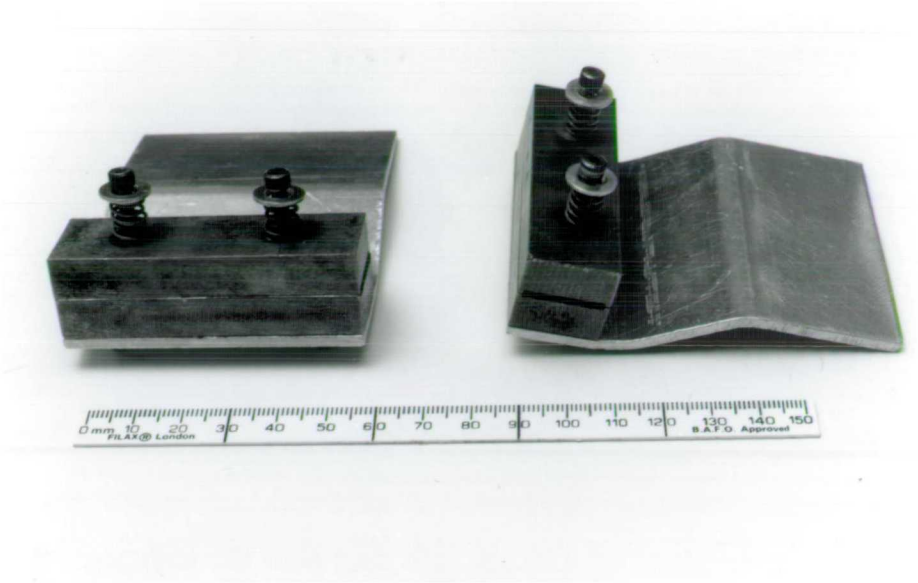

Figure 3.4: Tensile grips

Figure 3.5: Compression grips, diameter of the platens = 75 mm

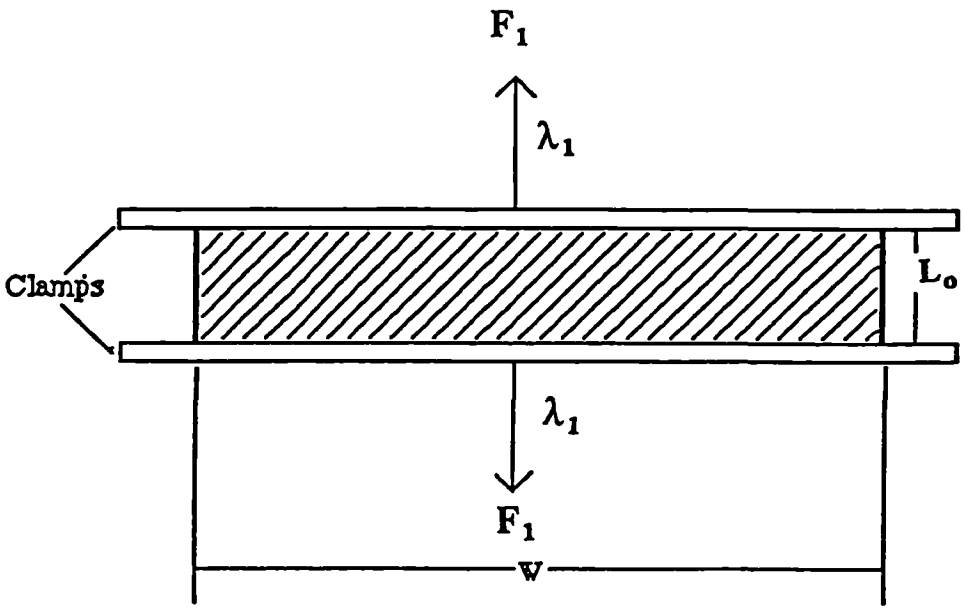

Figure 3.6: Pure shear specimen, height L_o =16-18 mm, width, w = 185 mm.

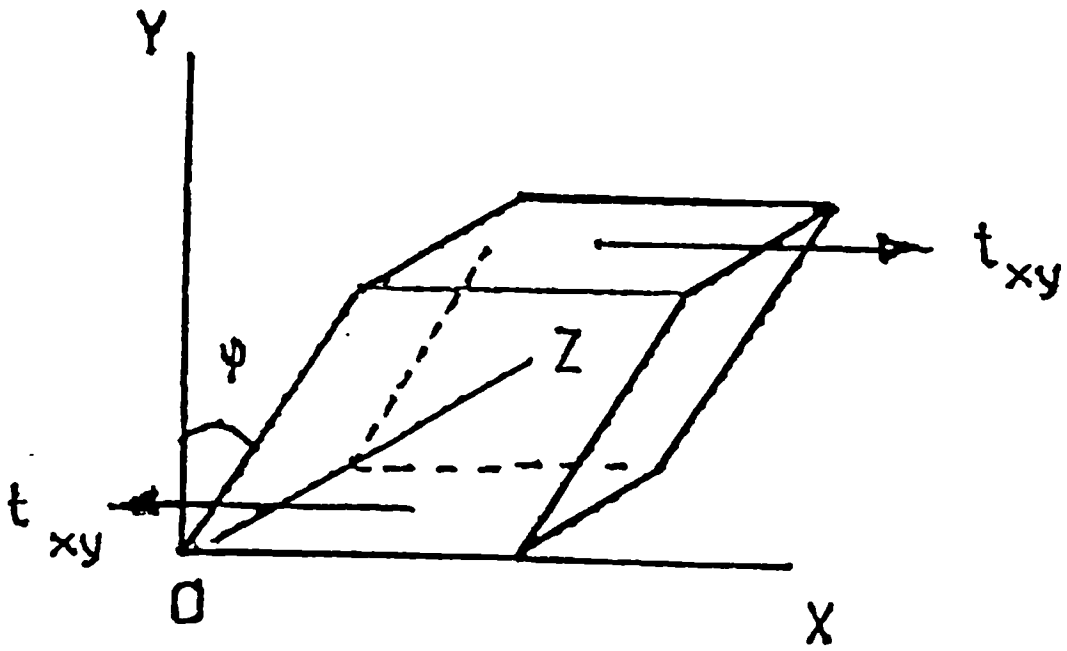

Figure 3.7: Simple shear in a cubic sample

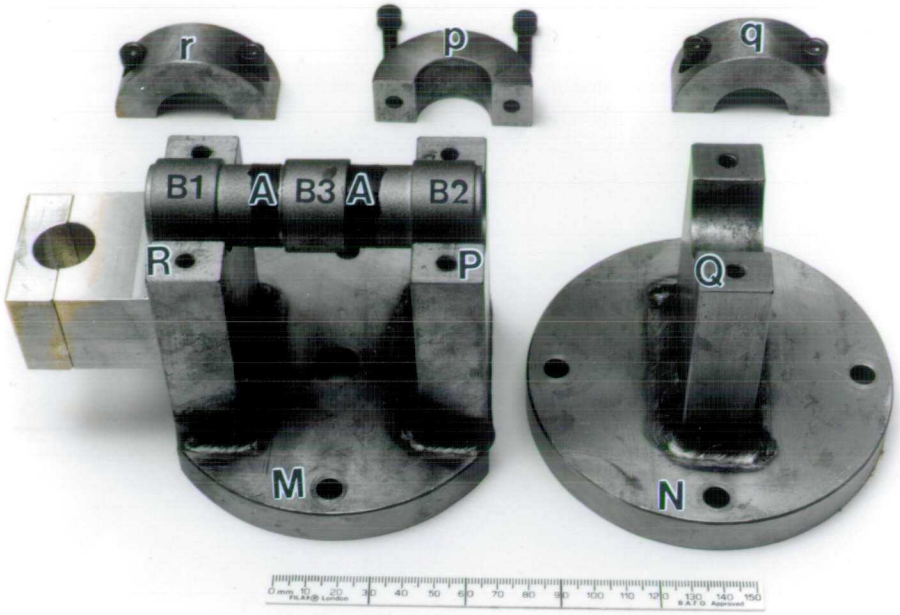

Figure 3.8: Simple shear grips

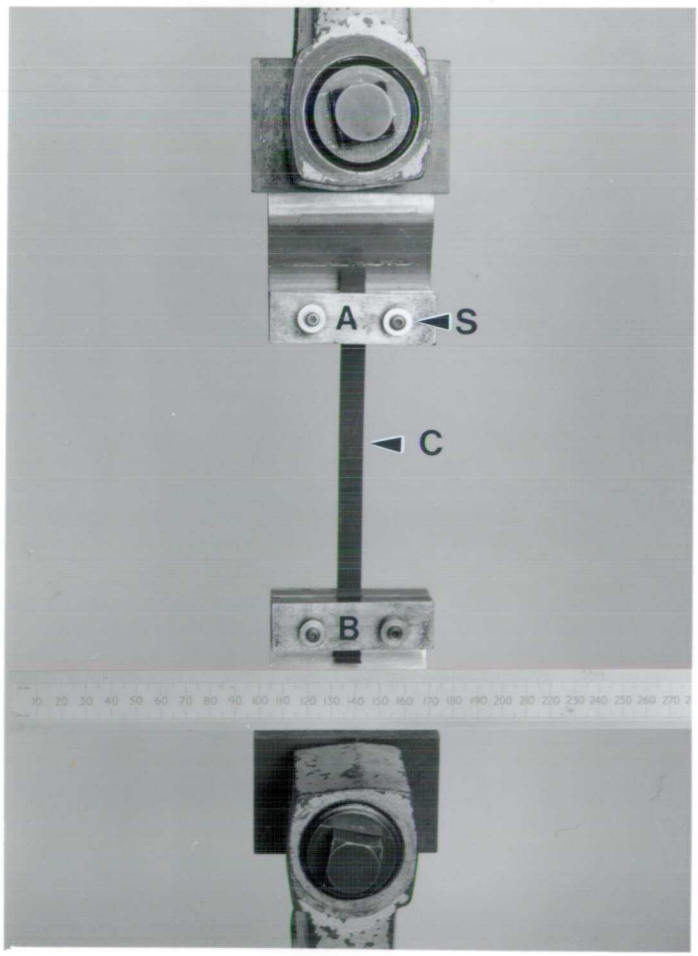

Figure 3.9: Tensile testing set-up

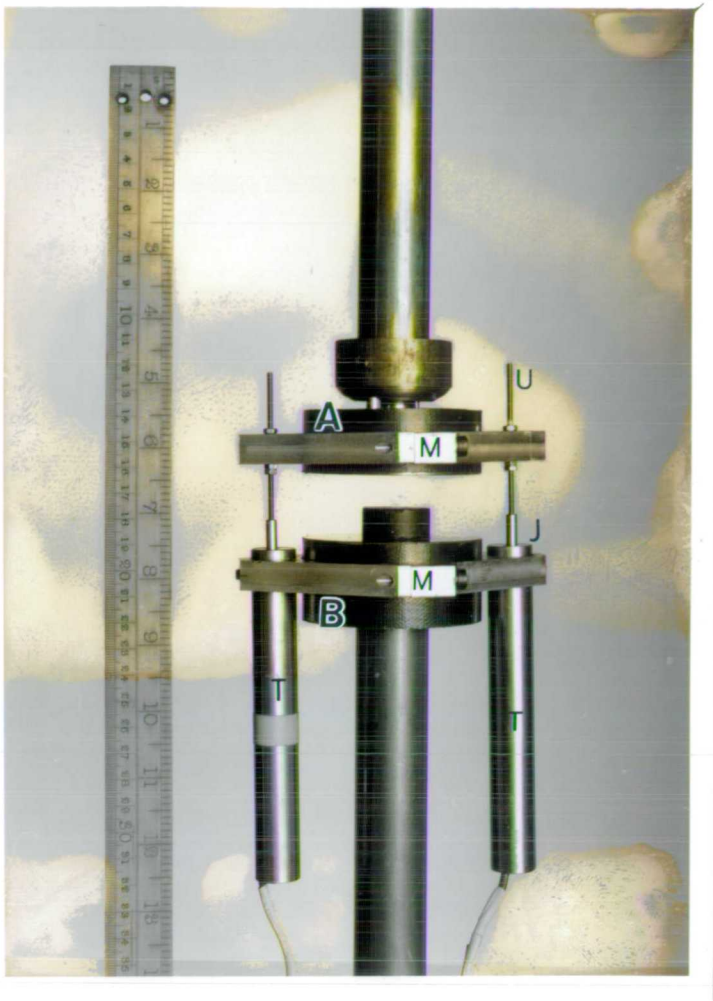

Figure 3.10: Compression testing set-up

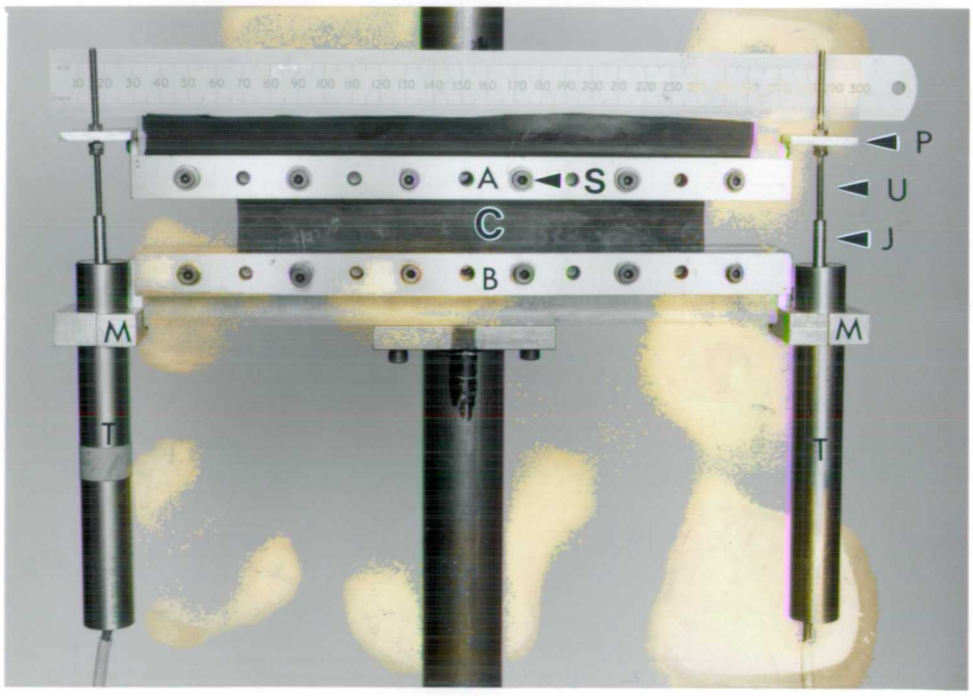

Figure 3.11: Pure shear testing set-up

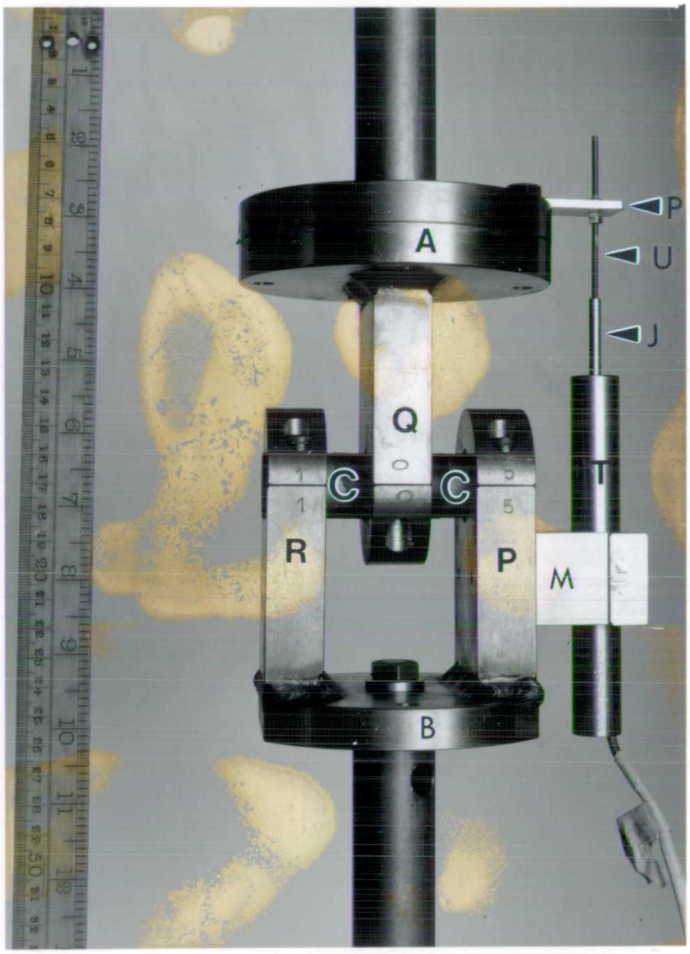

Figure 3.12: Simple shear testing set-up

CHAPTER FOUR

4.0 RESULTS AND DISCUSSION-CARBON BLACK FILLED RUBBERS

In this chapter, the results of the stress-strain tests which have been carried out in four different stressing modes on a series of carbon black filled NR-vulcanizates (Peradin compounds) as described in chapter three are presented and discussed. The validity of the strain energy function proposed in chapter two is examined and its applicability to all stressing modes is demonstrated. The materials constants in the function are determined using a non-linear least squares fitting routine. The magnitudes of the constants and their physical significance are examined utilizing experimental data obtained in this study and data obtained from the published literature. The effects of testing under static (1st cycle) and dynamic (10th cycle) conditions are examined.

The general applicability of strain energy function to other particulate filled rubbers will be examined utilizing silica-filled rubber data in chapter five.

4.1 STRESS-STRAIN DATA AND STRAIN ENERGY FUNCTION FOR CARBON BLACK-FILLED VULCANIZATES

4.1.1 Stress-strain curves

The nominal stress (i.e., force per unit cross-sectional area referred to the unstrained state) and the percentage strain were calculated as described in section 3.6 for tension, pure shear, and static simple shear up to 100% strain and 50% in compression on previously unstrained samples. The tests were carried out on four carbon black-filled NR vulcanizates containing 23, 32, 49, and 69 pphr of high abrasion furnace black. The formulations are shown in table 3.1. The carbon black filled systems were commercial rubbers developed by Peradin Ltd for use in antivibration devices. The stress-strain curves for all stressing modes are shown in figures 4.1-4.4 and the stresses to produce given strains are as shown in table 4.1. It can be seen that the stress at a particular strain increases with increasing carbon black content. It is also observed that all the filled rubbers show considerable non-linearity at low strains i.e., the stress versus strain curves (figures 4.1 & 4.4) are concave downwards. The curvature increases with increasing carbon black content. This may be due to the effect of carbon black

structure within the material which does not breakdown at small strains but breaks down as the strain increases. The carbon black structure becomes more well developed as the carbon black content increases. Hence one would anticipate a greater degree of breakdown and more curvature with increasing carbon black content. It can also be seen that an upturn in the stress-strain curve appears at high strains in the case of the highly filled rubbers in the range of strain applied in this study (figure 4.1). The strain at which the upturn appears decreases with increasing concentration of carbon black. This upturn has been associated with finite extensibility of the macromolecular network chains[30]. The magnitudes and forms of the curves are consistent with those previously reported for carbon black filled rubbers[31,32].

4.1.2 Use of the simple strain energy function to rationalize stress-strain data derived from different stressing modes

The strain energy function proposed in chapter two i.e

$$W = \frac{A}{2\,(\,1 - n/2\,)}\,(\,I_1 - 3\,)^{(\,1 - n/2\,)} \qquad (4.1)$$

was derived by assuming that the rubber behaviour was largely dependent only on the strain invariant I_1 and that the second invariant I_2 had a minimal effect at strains of 1-100% for filled rubbers. One test of this hypothesis is that use of the function should rationalize the data from any stressing mode and enable prediction from one stressing mode to another to be made. The first step was to re-analyze the stress-strain data referred to in section 4.1.1 by plotting the reduced stress terms against (I_1 - 3) according to equations 2.33, 2.36 and 2.37 previously derived in chapter two. They are reproduced in this chapter with new equation numbers i.e., 4.2, 4.3 and 4.4 respectively, for the convenience of the discussion.

SIMPLE SHEAR;

$$\log G/2 = \log (A/2) - (n/2) \log (I_1 - 3) \qquad (4.2)$$

TENSION AND COMPRESSION;

$$\log \sigma / 2\,[\,\lambda - (\lambda)^{-2}\,] = \log (A/2) - (n/2) \log (I_1 - 3) \qquad (4.3)$$

PURE SHEAR:

$$\log \sigma / 2 [\lambda - (\lambda)^{-3}] = \log (A/2) - (n/2) \log (I_1 - 3) \qquad (4.4)$$

Such double log plots of the reduced stress-terms (left hand sides of equations 4.2-4.4) versus the invariant (I_1 -3) are shown in figures 4.5 &4.6 for the four NR vulcanizates with the four different carbon black contents. It is seen that the data points in all stressing modes are very close and all describe similar curves. It should be noted that these plots are a very severe test of the comparability of the stress-strain behaviour of the rubbers tested in different stressing modes. The agreement, to within 2-4 percent, is hence very satisfactory. The small differences between the plots for different stressing modes are not in the order or the sense expected if they resulted from the assumption that $dW/dI_2 = 0$ was incorrect. It seems likely then that general experimental uncertainty accounts for the small differences, especially bearing in mind the problems arising from the imperfect elasticity of filled rubbers. Thus it can be concluded, within the small experimental uncertainty, that data from all the stressing modes lie on a similar curve. This observation is consistent with the earlier findings of Gregory[24]. However, Gregory's work did not include the pure shear mode of deformation which has been included in this study and his study was limited to two NR carbon black filled vulcanizates although he referred to other published data. These results hence support the assumption that W is simply a function of I_1 only and that the second invariant I_2 has a minimal effect.

All the plots exhibit a long straight portion, with deviations from this line at both low and high strains. The low strain deviations, occurring at strains of < 4%, are due to a combination of experimental difficulty (determination of the initial zero force specimen length) and genuine differences in the behaviour of the rubbers. The strain at which the upturns appears at the high strain end decreases with increasing carbon black content. The upturn occurs at log (I_1 - 3) = 0 which is equal to a strain of 70% in tension/shear, 45% in compression and 100% in simple shear for NR23 (see figure 4.5). The corresponding values for NR69 are log (I_1 - 3) = - 0.23 and 50%, 35% and 70% respectively. This is associated with the finite extensibility of the macromolecule network chains as mentioned in section 4.1.1.

For each compound, the mean slope of the straight line portions of the plots yields a value of n/2 and the mean intercept yields a value of log A/2.

These measured single average values of n and A for each rubber for all stressing modes are shown in table 4.2. These average values of n and A for each rubber have been used to predict the stress-strain behaviour in the different stressing modes using equations (4.2), (4.3) & (4.4). Examples of the predicted stress-strain curves are shown, compared to the measured curves in figures 4.7 (a),(b) and 4.8 (a),(b). The agreement is seen to be excellent upto 100% and 70% shear strain for NR23 and NR69 respectively. It is also interesting to note that the deviation at small strains seen in figures 4.5 & 4.6 is not reflected in the above plots and indicates that the plots of log (reduced stress) versus log (I_1 -3) are a very severe test of the comparability of the stress-strain behaviour of the rubbers tested in different stressing modes. Now the question arises as to whether from values of A and n obtained from any stressing mode, say in tension, it is possible to predict the behaviour in other stressing modes. The values of A and n as determined from the NR23 tension data were used in the strain energy function to predict the stress-strain behaviour in simple shear as shown in figure 4.9. It can be seen again that the agreement is excellent. Thus, it would be possible to use the tension data to predict the behaviour in shear or in any other stressing mode. These results suggest that the use of equation 4.1 as a two constant strain energy function containing I_1 only, is quite satisfactory in predicting stress-strain curves up to these moderate strains at least for the different carbon black filled vulcanizates used in this study.

It can be seen in figures 4.8 (a) &(b) that considerable deviation occurs between the measured and predicted stress-strain curves for the 69 pphr carbon black rubber (NR69) at the highest strains studied. This deviation is due to the inability of the strain energy function in equation 4.1 to represent the upsweep at the higher strains attributable to the finite extensibility effects (figure 4.6).

In order to attempt to produce a strain energy function to represent the data for all carbon black contents over the whole of the strain range studied (upto 100%) and to retain the assumption that W is a function of I_1 only, an additive term $K(I_1-3)^2$ was included in equation (4.1). A somewhat similar approach to modelling this region has been proposed by Yeoh[3]. He used square and cubic terms of (I_1 - 3) to model strains of upto 250%. For the present purposes an attempt is not being made to model the stress-strain behaviour at these very high strains because the strains encountered in most engineering applications are relatively modest. Furthermore, attempts to fit

these high strain regions invariably lead to loss of accuracy at low strains. Thus it is proposed that equation (4.1) be modified to;

$$W = \frac{A}{2\,(\,1 - n/2\,)}\,(\,I_1 - 3\,)^{(\,1 - n/2\,)} + K\,(I_1 - 3)^2 \qquad (4.5)$$

where K is another material constant.

Differentiating equation (4.5) with respect to I_1 gives;

$$dW/dI_1 = \quad (A/2)\ (I_1 - 3)^{-n/2} + \quad 2K\,(I_1 - 3) \qquad (4.6)$$

Taking equation (4.6) and using the expression for dW/dI_1 in equation (2.34) gives;

$$\sigma\,/2\ [\lambda - (\lambda)^{-2}] = \quad (A/2)\,(I_1 - 3)^{-n/2} + \ 2K\,(I_1 - 3) \qquad (4.7)$$

(for tension and compression)

and similarly for;

Simple shear

$$G/2 = \quad (A/2)\,(I_1 - 3)^{-n/2} + \quad 2K\,(I_1 - 3) \qquad (4.8)$$

and for

Pure shear

$$\sigma/2\ [\lambda - (\lambda)^{-3}\,] \ = \ (A/2\,)\,(I_1 - 3)^{-n/2} \ + 2K\,(I_1 - 3) \qquad (4.9)$$

Equations (4.7), (4.8), & (4.9) replace equations (4.2), (4.3), & (4.4) if the three term (n, A, and K) strain energy function of equation (4.5) is used instead of the two term function (n, A) in equation (4.1)

To determine the numerical values of K, n and A in the modified function, a computer programme was used as detailed in appendix 4.1. This programme accepted data from rubbers deformed in a number of stressing modes and fitted the data to an equation, using a non-linear least squares technique. The equation fitted was;

$$\psi \ = \ (A/2)\,\zeta^{-n/2} \ + \ 2K\zeta \qquad (4.10)$$

where ψ is the reduced stress term of equations 4.7-4.9 and ζ is $(I_1 - 3)$.

The basic process, in brief, was to input data in the form of $(I_1 - 3)$ and

the reduced stress terms for each of the four stressing modes into a common input file. The output file was the values of (I_1 -3) and the reduced stress term for the best fitted curve as shown in figures 4.5 &4.6. It can be seen that it provides a very good fit over the range covered by the present experiments, except at the lowest strains for the lowest carbon black content materials. The programme also tabulated the values of n, A and K. These values were used in the modified three term strain energy function, equation 4.5, to predict the behaviour in each stressing mode. An example using the predicted stress-strain curve in tension compared to the measured curve is given in figure 4.10. The three constant function is seen to fit the experimental data over a much larger strain range than the two constant function (compare figure 4.8b and figure 4.10). The numerical values of K for all the NR vulcanizates are shown in table 4.2. They are seen to increase with increasing carbon black content.

4.1.3 Small strain portion of the stress-strain curve

The proposed form for W gives a good fit to the experimental data over the strain range of about 1 to 100% which is the main region of engineering interest. However, the form chosen would give an infinite value of the modulus at zero strain. For a finite element programme, it is important that a stress-strain relation is used which yields a finite modulus at small strains (<1%). From this point of view alone choosing a realistic value of the modulus would suffice as its effect on predicting the stress-strain relationship at higher strains would be negligible. However in some practical cases the very small strain behaviour is important e.g., the flexing of a running automobile tyre (0.2-1%) or the even smaller strains involved in vibration damping. The present work was not undertaken to study this area specifically and hence the currently measured very low strain data is limited in both quantity and quality. It is hence proposed to use literature data in an attempt to modify the function and then to compare the predictions of this new function with the current experimental data. For this purpose the dynamic data of Payne & Whittaker[33] was used as shown in figure 4.11 for a butyl rubber containing different amounts of HAF carbon black. The curves are seen to asymptote to a finite dynamic inphase shear modulus (G'_o) at very low strains [log (I_1 -3) = -8 equals to 0.01% shear strain]. To accommodate this small strain behaviour of filled rubbers, one extra term was incorporated into equation (4.5) to yield;

$$W = \frac{A}{2\,(\,1 - n/2\,)}\,(\,I_1 - 3 + C^2)^{(\,1 - n/2\,)} + K\,(I_1 - 3)^2 \qquad (4.11)$$

giving;

$$dW/dI_1 = A/2\,[\,(\,I_1 - 3 + C^2\,)\,]^{-n/2} + 2K\,(I_1 - 3) \qquad (4.12)$$

This gives a shear modulus of;

$$G/2 = (A/2)[\,(\,I_1 - 3 + C^2\,)\,]^{-n/2} + 2K\,(I_1 - 3)$$

or

$$G/2 = (A/2)[\,(\,\gamma^2 + C^2\,)\,]^{-n/2} + 2K\,\gamma^2 \qquad (4.13)$$

The significance of the new parameter C is that it is the shear strain at which the modulus begins to tend to its finite small-strain value. This value is given by;

$$G'_o = A\,C^{-n} \qquad (4.14)$$

The applicability of equation (4.11) was checked by comparison of Payne's results in figure 4.11, for example for the vulcanizate containing 20.2 % by volume of carbon black, with a curve obtained from equation 4.13. Three fitting constants are needed, n, A and C. The K value is zero since data was not available at high strains. The constants n and A were obtained from straight portion of the curve at strains of 1% and greater, the values of C having little effect in this region. The values were A= 0.68 MPa and n = 0.31 respectively for the 20.2% by volume of HAF carbon black filled butyl rubber vulcanizate (45 pphr HAF carbon black). The value of G'_o was taken as the modulus where the near horizontal portion of the curve intercepted the X axis (4.47 MPa, i.e., log G/2 = 0.35 MPa in figure 4.11). The constant C was determined from equation (4.14) by inserting these values of n, A and G'_o. The value of C was 2.9×10^{-3}. These n, A, and C values were used to plot equation 4.13 on figure 4.11 and the fit is seen to be very good.

The current study has shown that stress-strain results in tension, compression, pure shear and simple shear were all consistent with W being a function of I_1 only at strains of 1-100%, and if this is also true down to strains of less than 1%, then the strain energy function given in equation (4.11), should be valid in tension, compression and pure shear. For very small strains of course the form of W is not important, as the classical

theory requires that E = 3G (E is tensile modulus), so that the assumption that W is a function of I_1 only is much less critical. In fact, several small strain studies[34] have found that both dynamic shear and extensional experiments gave consistent results as the ratio of E/G approached 3. The expectation is therefore that deductions from (4.11) are likely to be satisfactory for all stressing modes.

To test this hypothesis, the computer programme was modified to fit the current data using the strain energy function in equation 4.11 and hence to calculate n, A, K, and C.

An example of this four parameter fit is shown for NR23 in figure 4.12 and shows that the new function fits all the data over the whole strain range. The values of C for all the Peradin carbon black filled compounds are shown in table 4.2 and are seen to decrease with increasing carbon black content.

It should be re-emphasized that for many purposes a two parameter strain energy function, (n, A) is adequate. The inclusion of K is only necessary if high strain data is needed and the inclusion of the exact value of C is only necessary if the application involves very low strain amplitudes.

4.1.4 Dynamic shear

Table 4.3 shows the values of shear moduli at different shear strains obtained from experiments carried out using double shear test pieces under static (i.e., previously unstrained and first cycle) and dynamic conditions (data was taken at 10th cycle). The dynamic moduli are in general lower than the static moduli and this effect is more prominent in the case of highly filled rubbers. For example at 100% shear strain, the dynamic modulus is 2.5% lower than the static modulus in the case of NR23 compared to 33% lower at the same strain in the case of NR69. This may be due to the stress-softening, termed the Mullin's effect. This softening has been attributed to breakdown or slippage of linkages between filler and rubber, breakdown of filler-filler aggregates, and breaking of molecular network chains[35].

It is important to know if the strain energy function proposed here can be similarly used to predict dynamic data as much of the literature data was obtained dynamically. Hence the function was fitted to the dynamic data and the results are shown in figures 4.13 (a) & (b) as solid lines. The values of A and n obtained are shown in table 4.3(a). The function can clearly be used to fit the data. This is also important as in section 4.2 in some cases dynamic data will be used to illustrate the effect of materials variables on n, A, K,

and C. The corresponding simple shear static data is also reproduced in figure 4.13 (a) & (b) for the purpose of comparison. The main difference between the 1st cycle (static) and 10th cycle (dynamic) is seen to be in the A values, which are lowered for the softened dynamically tested specimens. It should be noted that K values were not obtained as this dynamic data does not extend to high enough strains to obtain this parameter.

4.2 EFFECT OF MATERIALS VARIABLES ON n, A, K AND C

The proposed form for the strain energy function, with up to four constants, gives a good fit to the stress-strain data from the smallest of strains used in the published data, around 0.01 %, up to about 100%. The question now arises as to whether the materials constants in the function vary in a sensible way, with the materials variables. The initial results presented in table 4.2 indicate the general dependence of n, A, K and C on carbon black content. This section discusses the effect of carbon black content along with other variables such as filler type, crosslink density etc. on n, A, K and C using experimental data obtained in this study and data obtained from the engineering data sheets[25]. The latter provides a considerable body of data on the shear modulus as a function of strain for a wide range of natural rubber vulcanizates strained from 1 to 100% under dynamic conditions.

4.2.1 Effect of carbon black content on values of n

The values of n as a function of carbon black content (pphr), for the rubbers NR23, NR32, NR49 and NR69 of similar given crosslink density, are shown in figure 4.14. It can be seen that n can be represented as increasing approximately linearly with carbon black content. The extrapolated value for zero carbon black content is near to zero. The numerical value of n is derived from the slope of the reduced stress versus (I_1 - 3) plot. The slope of such a plot increases as the curvature of the stress-strain curve increases. The curvature of the stress-strain curves (in the strain range 1-100%) increases with increasing carbon black content and hence n increases. The curvature results from the breakdown in the carbon black structures. The carbon black structure becomes more well developed as the carbon black content increases. Hence one would anticipate a greater degree of breakdown and more curvature with increasing carbon black content. The increasing value of n with increasing carbon black content represents this effect. If n is identified with the breakdown of the carbon black structure

with strain, it is expected that these numerical values of n will not depend on crosslink density for a similar carbon black content. It should be noted that the numerical values of n obtained here are for HAF carbon black filled rubbers and are unlikely to be the same for different carbon blacks.

4.2.2 Effect of carbon black content on values of A

The values of A as a function of carbon black content (pphr), for the rubbers NR23, NR32, NR49 and NR69 of similar given crosslink density, are shown in figure 4.15. It can be seen that A increases approximately linearly with carbon black content. If the line is extrapolated to zero parts carbon black (in effect an unfilled rubber) a value of A = 0.39 MPa is obtained. A is in effect the shear modulus at 100% strain in simple shear (see equation 2.30). The numerical value of the shear modulus at 100% strain for a similarly crosslinked unfilled natural rubber is 0.44 MPa[25] which is very close to the extrapolated value of A, for zero filler content. Given the definition of A above, any parameter which stiffens the rubber will increase the numerical value of A. The values of A given here are hence for a given crosslink density and can not be generalized to other vulcanizates. However there is no reason to suppose that A should not increase in a similar manner with carbon black content for any system.

4.2.3 Effect of carbon black content on values of K

The values of K as a function of carbon black content (pphr), for the rubbers NR23, NR32, NR49 and NR69 of similar given crosslink density, are shown in figure 4.16. It can be seen that K increases approximately linearly with carbon black content. K is associated with the point at which the upturn occurs in the plot of log (reduced stress term) versus log (I_1-3) as shown in figures 4.5&4.6. The upturn occurs at lower (I_1-3) values as the carbon black content increases. In terms of stress-strain curves, this is associated with the approach of the strain at which the modulus stops decreasing and starts to increase. It is hence associated with the finite extensibility effect; the strain amplification effect of the carbon black causing it to occur at apparently smaller strains. As for A, the form of the variation of K with carbon black content is expected to be similar for any crosslink density, but the numerical values of K must depend on crosslink density.

4.2.4 Effect of carbon black content on values of C

It has been mentioned already that C is the shear strain at which the modulus begins to tend to its finite small strain value. In order to check the effect of carbon black content on the numerical values of C, values of C were determined from the published dynamic shear strain data of Payne as shown in figure 4.11 by fitting the 4 parameter programme to the curves and the results are tabulated in table 4.4. The K value is zero since data was not available at high strains. The values of A and n are also tabulated in and are seen to increase with increasing carbon black content as expected. It can be seen that the C values decrease with increasing carbon black content. The carbon black structure becomes more well developed as the carbon black content increases. Hence it is expected that the carbon black structures would start to breakdown at smaller strains which is reflected by the decrease in the C values with increasing carbon black content. The values of C calculated from data obtained in this study show a similar tend (see table 4.2) and the numerical values are very close. For example, the value of C for NR 69 (23.8% by volume of HAF carbon black) is 2.2 $x10^{-3}$ which is very close to the C value (2.8 $x10^{-3}$) for a butyl rubber vulcanizate containing 23.3% by volume of HAF carbon black.

4.2.5 Effect of crosslink density on values of n, A, and K

In order to study the effect of crosslink density alone, a series of vulcanizates was prepared based on the compound NR49 but with a range of accelerator/sulphur levels (table 3.2). The measured tensile stress-strain relations for these vulcanizates are shown in figure 4.17 as a double log plot of the reduced stress term versus (I_1-3) All the curves exhibit a long straight portion with departure from this line at high strains. The values of n, A and K were determined using the three parameter fitting programme and are shown in table 4.5. The parallelism seen in the straight portion of these curves in the figure is confirmed by the constancy of n in the table, indicating that n is governed primarily by the filler content. n is hence clearly dependent on the rate of breakdown of carbon black structure with strain and as such is dependent on carbon black content but is independent of crosslink density.

The variation of the numerical values of A and K as a function of crosslink density are as shown in figures 4.18(a) &(b) respectively. It can be seen that both A and K increase approximately linearly with crosslink density. Given the definition of A earlier as the shear modulus at 100%

strain, any factor which stiffens the rubber will increase the numerical values of A. Hence one would anticipated a greater stiffening effect for vulcanizates with increasing crosslink density. The increasing value of A with increasing crosslink density represents this effect.

The value of K is associated with the point at which the upturn occurs in the plot of log (reduced stress terms) versus log (I_1-3) as shown in figure 4.17. The upturn occurs at lower (I_1-3) values as the crosslink density increases. It is associated with the finite extensibility of the rubber chain network. For a fixed carbon black loading, with increasing crosslink density, the rubber network becomes more rigid, causing the upturn to occur at apparently small strains. The increasing value of K with increasing crosslink density represents this effect.

4.2.6 Effect of type of carbon black on values of A and n

The influence of type of carbon black i.e., HAF, FEF, and SRF on the derived values of A and n is illustrated graphically in figures 4.19 &4.20 using data for NR vulcanizates from the EDS[25] for a CV system. In all cases A and n increase with increasing carbon black content in a similar manner. The more reinforcing carbon blacks result in higher A values, as A is in effect the shear modulus at 100% strain. The values of n depend on the rate of breakdown of carbon black structure. It is hence not surprising that both the numerical values of n and the rate of change of n with carbon black content are both highest for the carbon black system (HAF) known to have the most well developed structure[36].

The figures also include the A and n values obtained in this study. It can be seen that the A values obtained in the current study (HAF carbon black filled NR vulcanizates) are close to the A values calculated from the published data for the HAF carbon black filled NR vulcanizates. The observed differences may be attributed to the differences in the crosslink density. However, the n values for both the sets of vulcanizates are very close as the values of n are largely independent of crosslink density.

4.2.7 Effect of dispersion of carbon black on values of n and A

Payne[37] studied the effect of mixing time, varying from 1-16 minutes, on the dispersion of the carbon black for an SBR vulcanizate containing 70 pphr ISAF carbon black. He showed that the small strain in-phase modulus of the materials decreased with increased mixing time. The shape of these stress-strain curves were similar to the shape of the curves in figure 4.11. The

values of n and A for these curves have been determined here for mixing times of 1.5, 2.5 and 4-8 minutes and are shown in table 4.6. It can be seen from the table that there is a considerable drop in the n value from 0.39 to 0.29 when the mixing time was increased from 1.5 to 2.5 minutes. Any additional mixing time had little effect on n; the value of n being 0.28 when the mixing time was 4-8 minutes. The initial decrease was attributed to the breakage of some of the loose carbon black aggregate structures[33]. Once this breakdown occurred, the shear forces generated during mixing had little further effect on the filler structures and the dispersion was said to be homogeneous[33,38]. The mixing time used in the current study was six minutes, the usual time used by Peradin Ltd for their commercial production. The n value for NR69 is 0.3 which is very close to the n value for the 70 pphr ISAF carbon black mix obtained at 4-8 minutes. This illustrates that 4-8 minutes are suitable mixing times for commercial production of carbon black filled mixes and that the n values could give an indication of the homogeneity of dispersion. The A values are less affected, as they are a measure of the shear modulus at 100% strain, by which time the carbon black structure tends to have homogenized.

4.3 SUMMARY

It has been shown that the stress-strain behaviour of carbon black filled rubbers can be derived from a strain energy function of the form;

$$W = \frac{A}{2\,(\,1 - n/2\,)}\,(\,I_1 - 3 + C^2)^{(\,1 - n/2\,)} + K\,(I_1 - 3)^2 \qquad (4.11)$$

where the constants, n, A, K, and C are characteristic of a given rubber/filler mixture.

The function is seen to be applicable over the strain range 0-100%, a range of very significant engineering interest.

It has been demonstrated that the constants can be derived from stress-strain data obtained in any single simple stressing mode. The function can then be used to predict the stress-strain behaviour in any other stressing modes simple or complex.

It is demonstrated that it is only necessary to obtain numerical values for the two constants n and A for most purposes. A precise value for C is only necessary when very accurate values of the stress-strain relationship are needed in the strain range of 0-4%. For all except the rubber with the

highest carbon black content, it is not necessary to obtain a value of K for shear strains of less than 80%. In fact a simple two constant strain energy function, containing only n and A will accurately predict the stress-strain data for most engineering purposes.

It is demonstrated that the numerical values of the constants vary in a systematic, reasonable manner with the materials variables. The numerical value of n increases linearly with carbon black content and is independent of the crosslink density. n is clearly related to the extent and rate of breakdown of the carbon black structure. The constant A is in effect the modulus at 100% shear strain and as such increases with both crosslink density and carbon black content. The constant K describes the upturn in the stress-strain behaviour at higher strains and is associated with the finite extensibility of the rubber network. As such it increases with carbon black content, due to the strain amplification effect of the filler and with increasing crosslink density. The constant C is the shear strain at which the modulus begins to tend to its finite small strain value and as such decreases with increasing carbon black content.

It has been demonstrated that the proposed strain energy function is simple to determine and is an accurate predictor of the stress-strain behaviour of carbon black filled rubbers both on the basis of data obtained in this work and for previously published data in the literature. Furthermore for all data examined to date the numerical constants are consistent in value and vary in a systematic manner with the usual materials variables.

TABLE 4.1: Stress to produce a given strain obtained from figures 4.1-4.4

COMP-OUND	CARBON BLACK PPHR	STRESS / MPa											
		TENSION STRAIN / %			COMPRESSION STRAIN / %		PURE SHEAR STRAIN / %			SIMPLE SHEAR STRAIN / %		
		20	50	100	20	50	20	50	100	20	50	100
NR23	23	0.40	0.75	1.21	0.60	2.45	0.49	0.85	1.33	0.17	0.38	0.70
NR32	32	0.47	0.87	1.53	0.70	2.99	0.57	1.00	1.68	0.20	0.43	0.83
NR49	49	0.65	1.20	2.33	0.95	4.32	0.79	1.39	2.48	0.29	0.60	1.19
NR69	69	0.95	1.70	3.46	1.47	6.48	1.26	2.09	4.07	0.45	0.88	1.72

TABLE -4.2: Values of the materials constants n, A, K, and C for the fitted curves in figures 4.5 and 4.6 for carbon black filled NR vulcanizates.

COMP-OUND	CARBON BLACK /PPHR	n	A / MPa	K / MPa	C
NR23	23	0.120	0.70	0.009	$3.1 X10^{-2}$
NR32	32	0.137	0.80	0.024	$1.2X10^{-2}$
NR49	49	0.220	1.00	0.050	$7.5X10^{-3}$
NR69	69	0.300	1.40	0.090	$2.2X10^{-3}$

TABLE 4.3: Static simple shear (1st cycle) and dynamic simple shear (10th cycle) elastic chord moduli at different strains

		SHEAR MODULUS, G / MPa					
COMPOUND	CARBON BLACK/ PPHR	STATIC SIMPLE SHEAR (1 ST CYCLE) STRAIN / %			DYNAMIC SHEAR (10TH CYCLE) STRAIN / %		
		20	50	100	20	50	100
NR23	23	0.86	0.76	0.70	0.87	0.76	0..69
NR32	32	1.00	0.87	0.83	0.96	0.85	0.78
NR49	49	1.45	1.21	1.19	1.32	1.11	0.97
NR69	69	2.32	1.76	1.72	1.87	1.39	1.14

TABLE 4.3(a): Values of the materials constants n and A for the fitted line in figures 4.13 (a) & (b) for carbon black filled NR vulcanizates.

COMPOUND	CARBON BLACK / PPHR	n	A / MPa
NR23	23	0.120	0.695
NR32	32	0.132	0.780
NR49	49	0.206	0.960
NR69	69	0.310	1.130

TABLE 4.4: Values of the materials constants n, A, and C for a butyl rubber containing various % by volume of HAF carbon black obtained from curves in figure 4.11

% BY VOLUME OF CARBON BLACK	n	A / MPa	C
13.2	0.17	0.50	8.6×10^{-3}
16.8	0.24	0.55	4.6×10^{-3}
20.2	0.31	0.68	2.9×10^{-3}
23.2	0.44	0.71	2.8×10^{-3}

TABLE 4.5: Values of the materials constants n, A and K for the fitted curves in figure 4.17 for NR49 vulcanizates of different crosslink densities.

Crosslink density $[X]_{phys}/10^{-5}$ (g mol / g RH)	n	A / MPa	K / MPa
6.9	0.232	0.55	0.020
9.8	0.228	0.73	0.035
12.4	0.225	1.00	0.049
15.2	0.231	1.20	0.067

TABLE 4.6: Values of the materials constants n and A for a SBR rubber containing 70 pphr ISAF carbon black, as a function of mixing time (ref 37)

MIXING TIME (MINUTES)	n	A / MPa
1.5	0.39	0.77
2.5	0.29	0.76
4-8	0.28	0.69

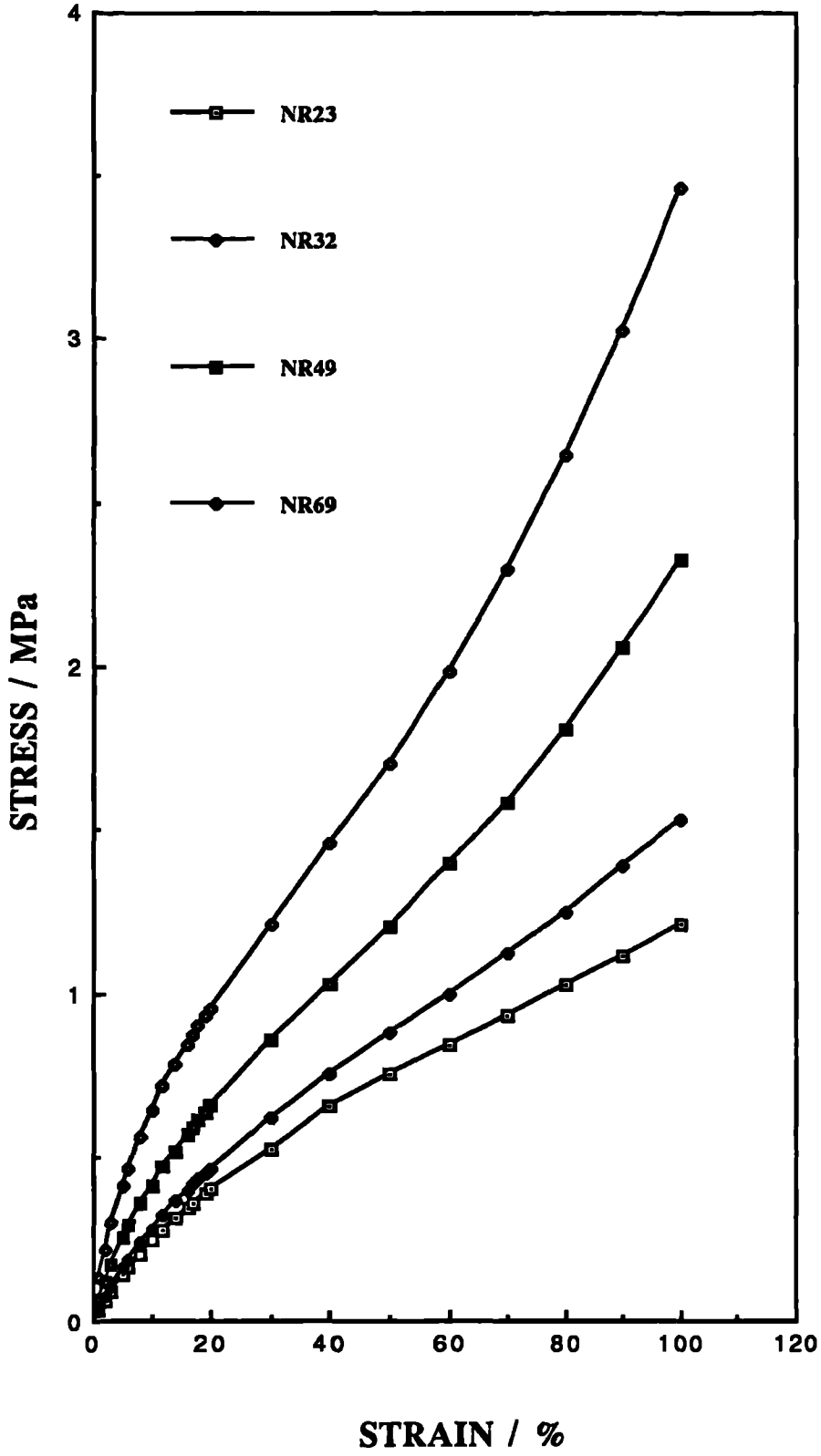

Figure 4.1 : Tensile stress-strain curves for carbon black filled NR vulcanizates

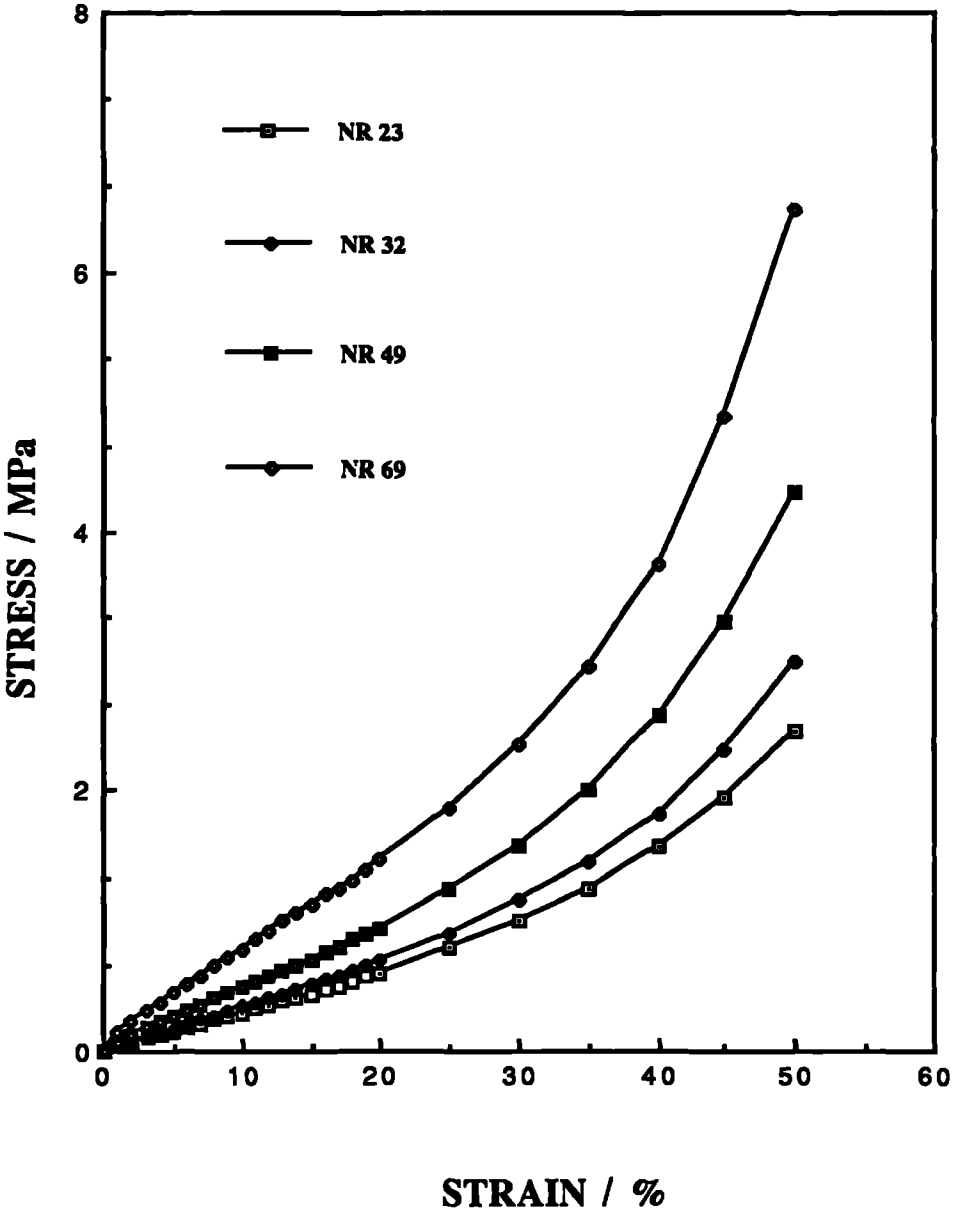

Figure 4.2 : Compression stress-strain curves for carbon black-filled NR vulcanizates

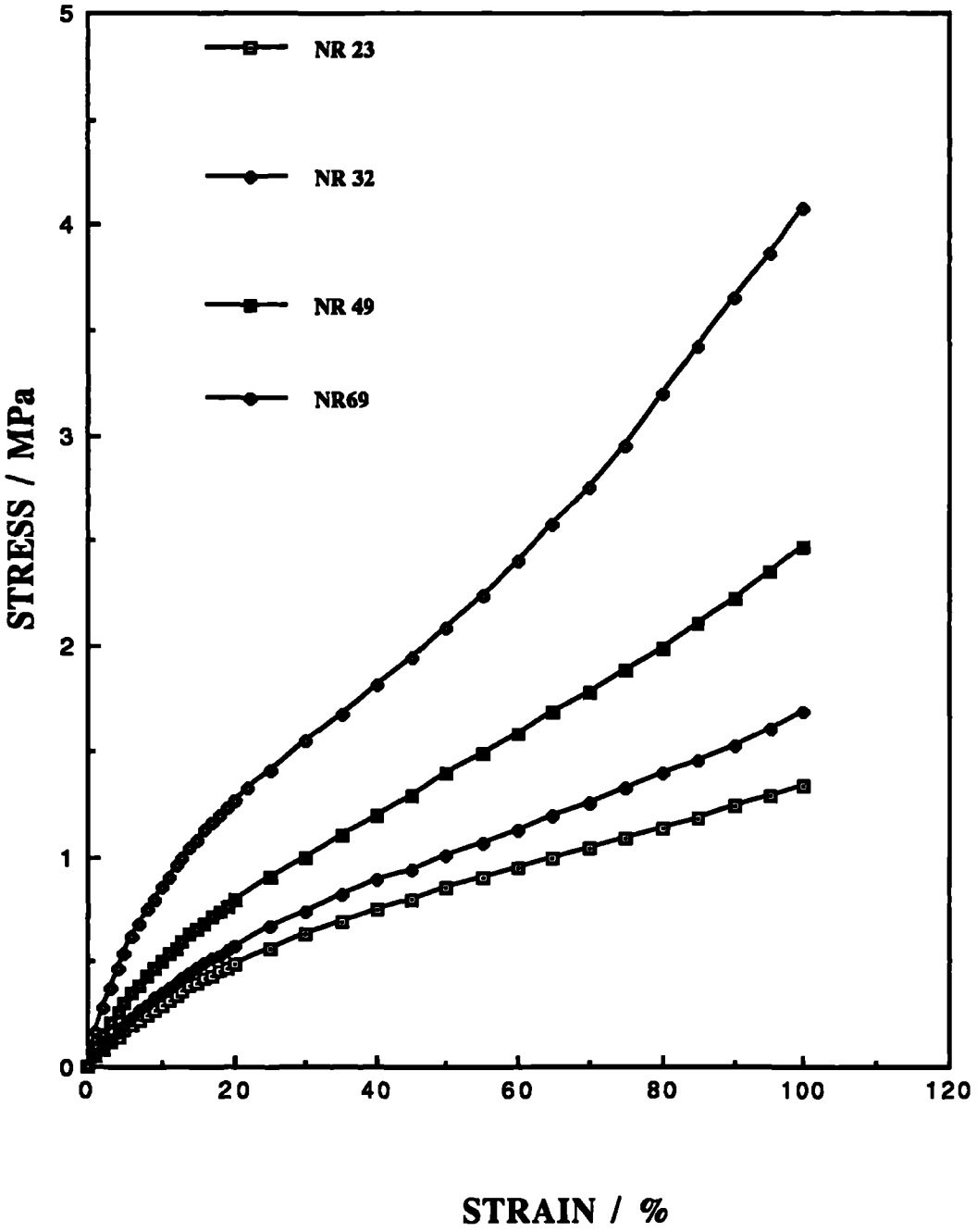

Figure 4.3 : Pure shear stress-strain curves for carbon black-filled NR vulcanizates

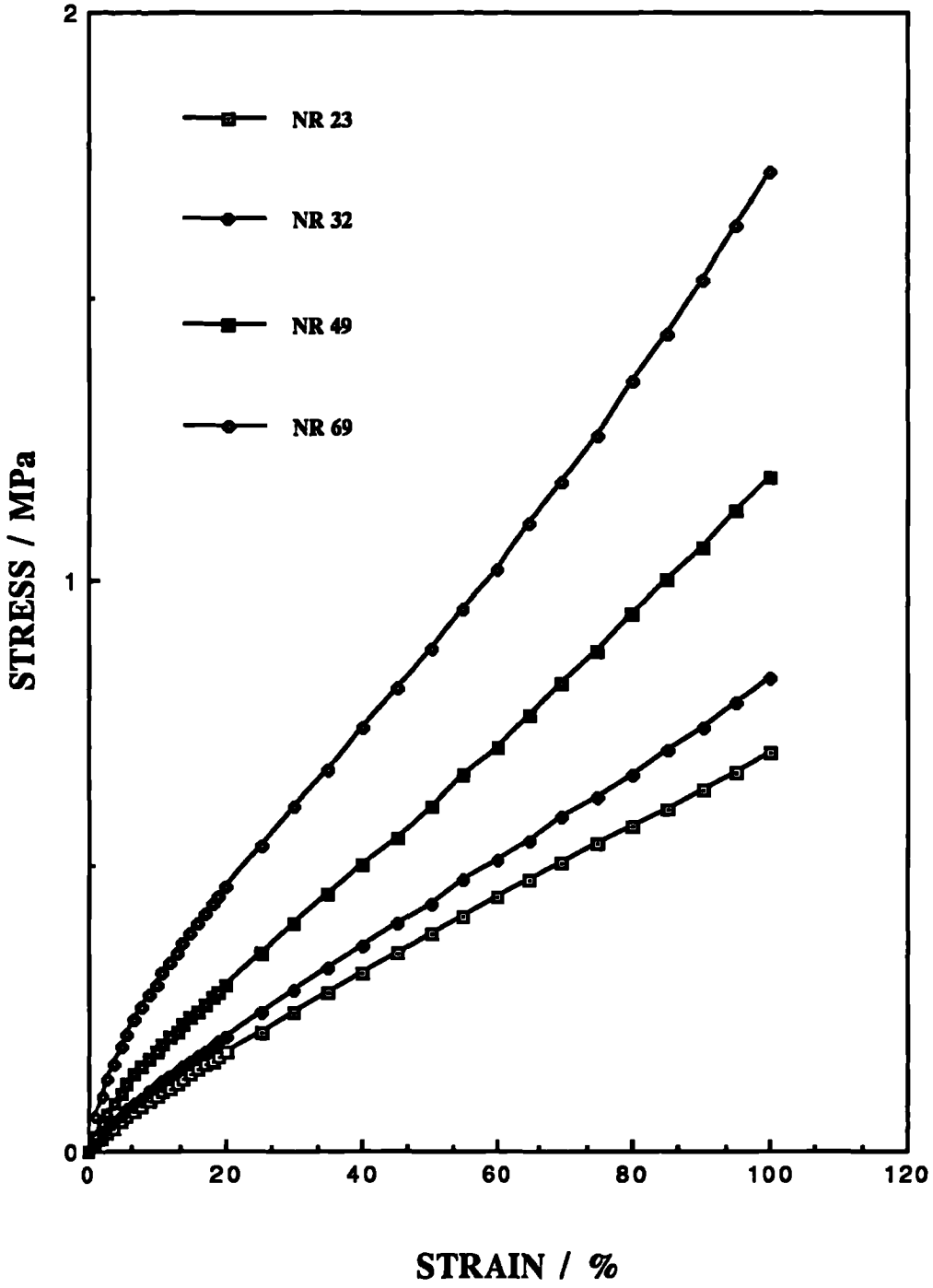

Figure 4.4 : Static simple shear stress-strain curves for carbon black-filled NR vulcanizates

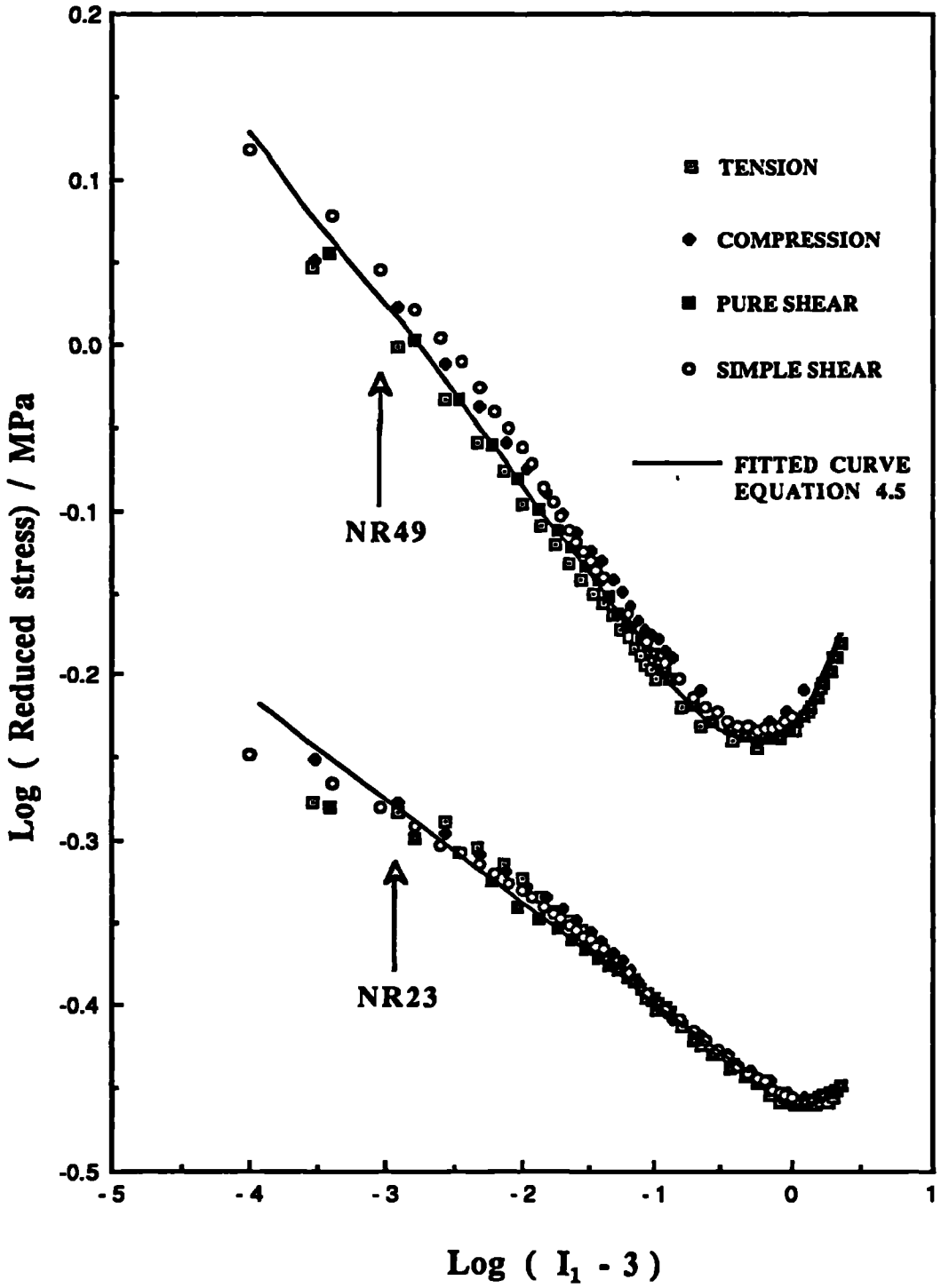

Figure 4.5 : Reduced stress as a function of (I_1 - 3) for NR23 and NR49

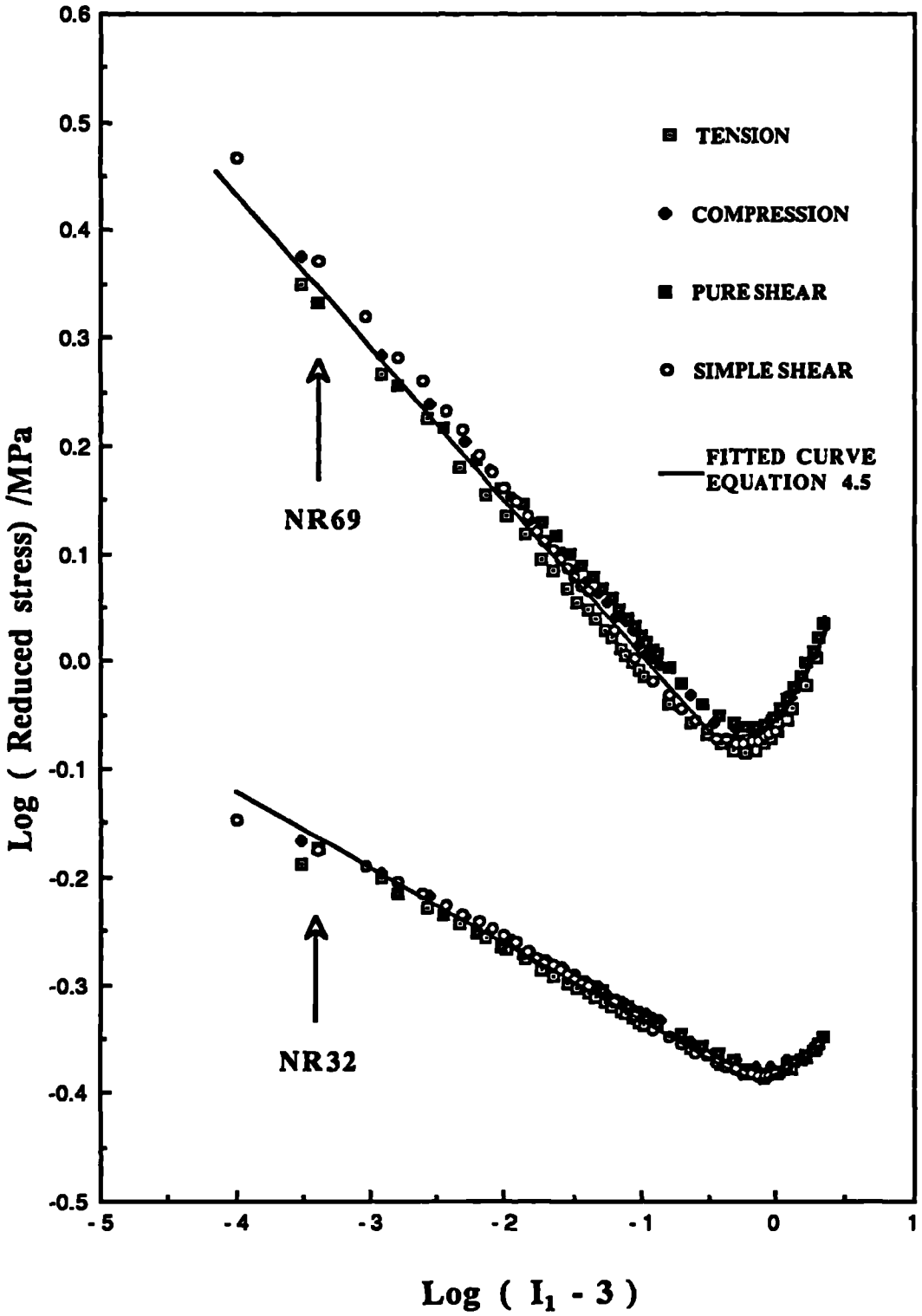

Figure 4.6 : Reduced stress as a function of (I_1 - 3) for NR32 and NR69

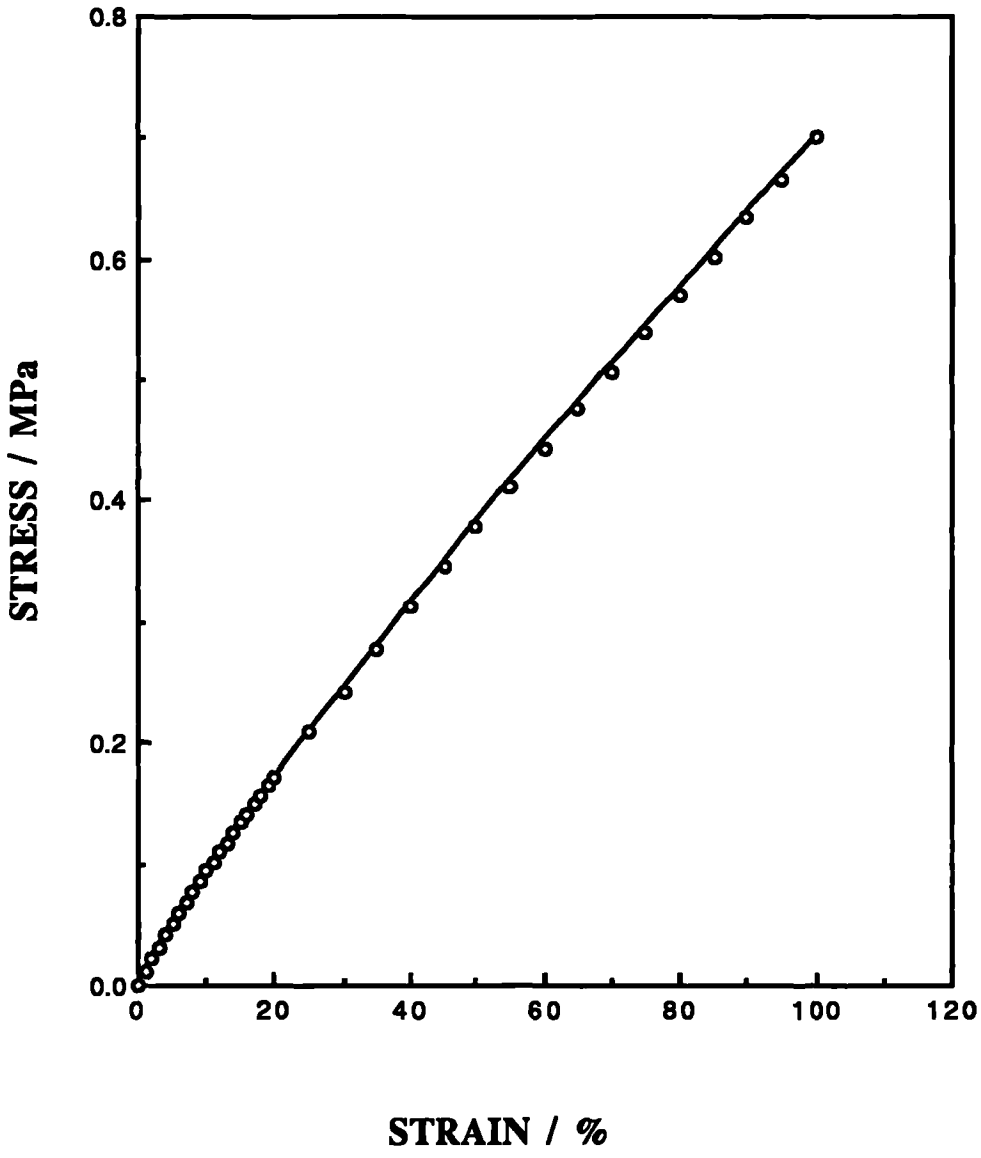

Figure 4.7 (a) : Simple shear stress-strain data points for NR23 with the curve predicted for equation (4.1) using the average values of n and A

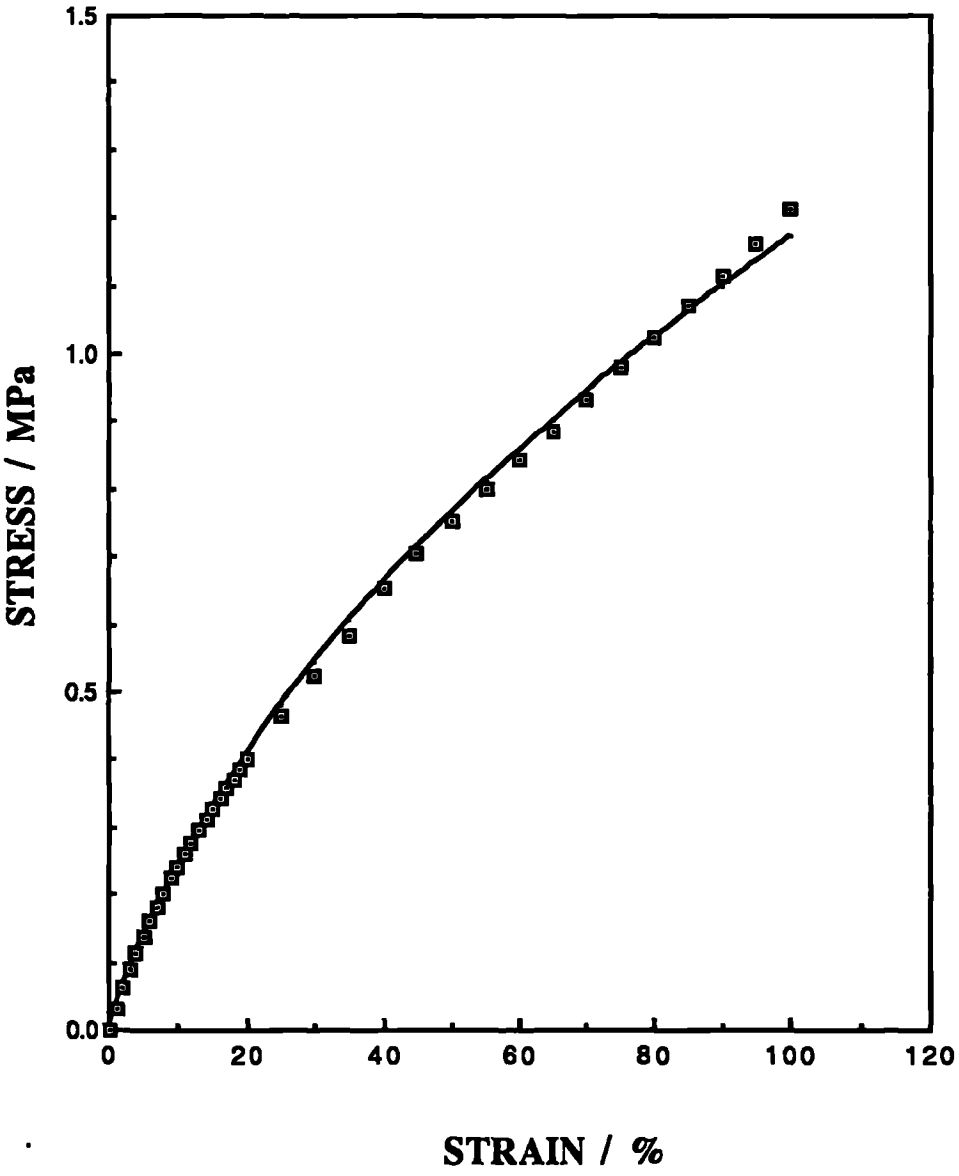

Figure 4.7 (b) : Tensile stress-strain data points for NR23 with the curve predicted from equation (4.1) using the average values of n and A

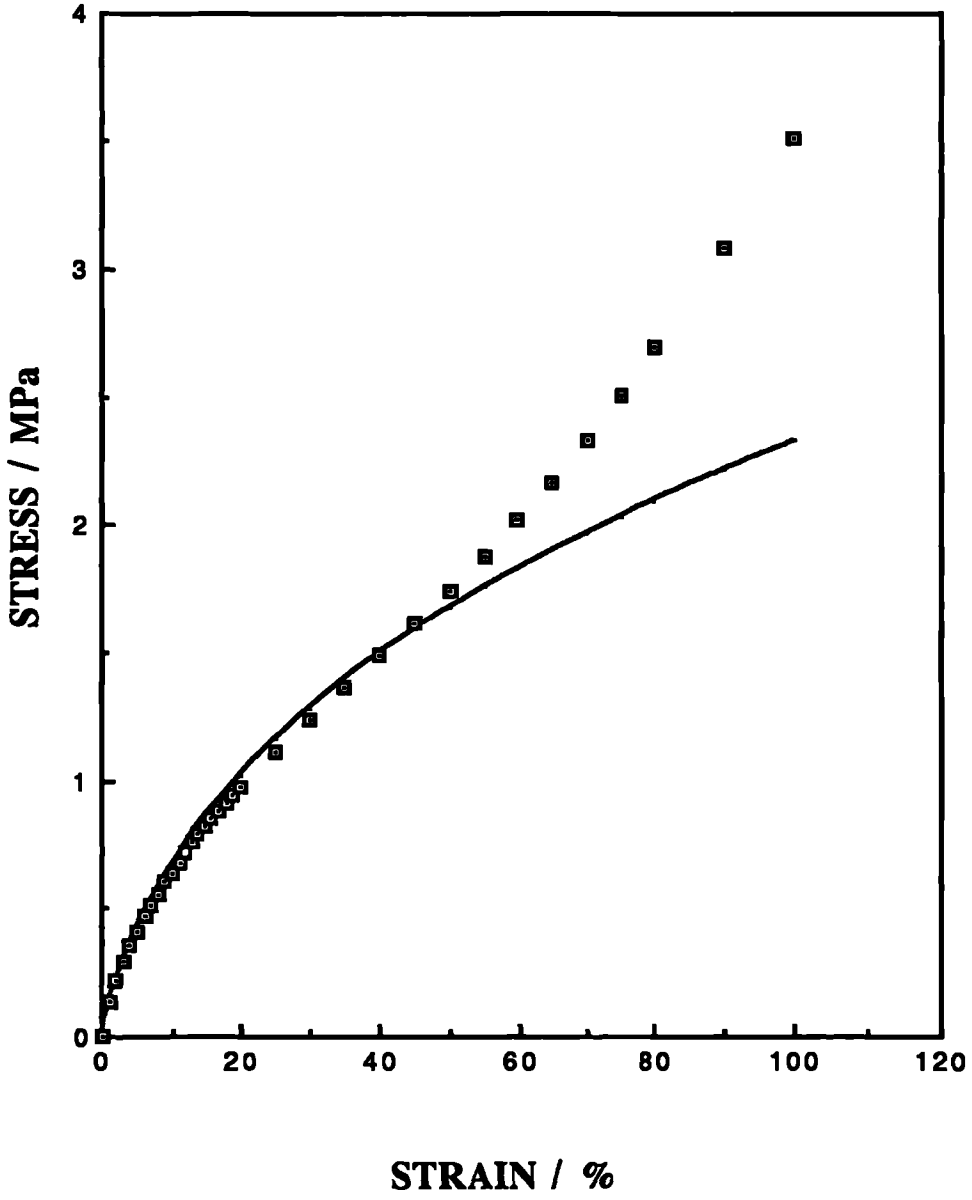

Figure 4.8 (a) :Tensile stress-strain data points for NR69 with the curve predicted from equation (4.1) using the average values of n and A

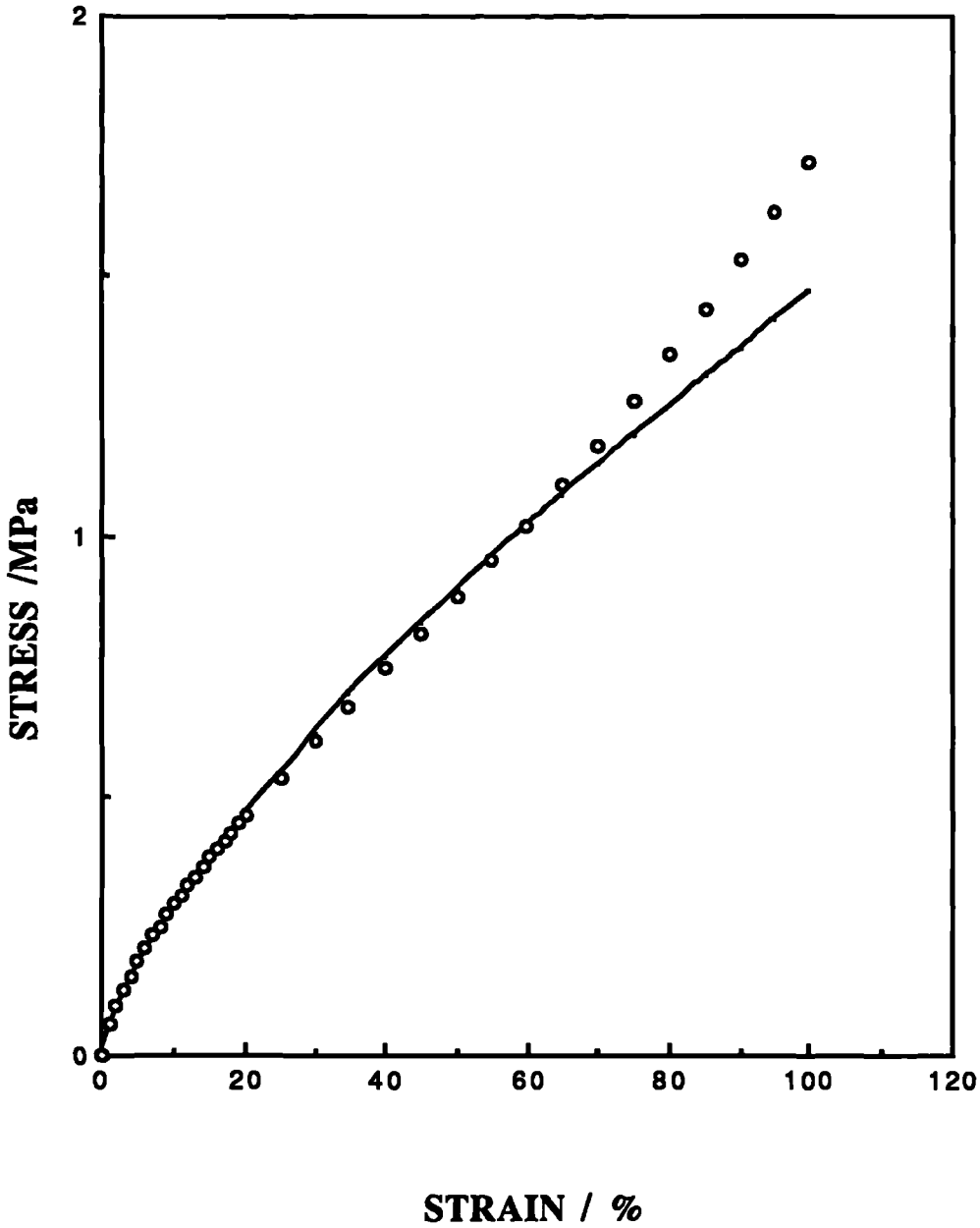

Figure 4.8 (b) : Simple shear stress-strain data points for NR69 with the curve predicted from equation (4.1) using the average values of n and A

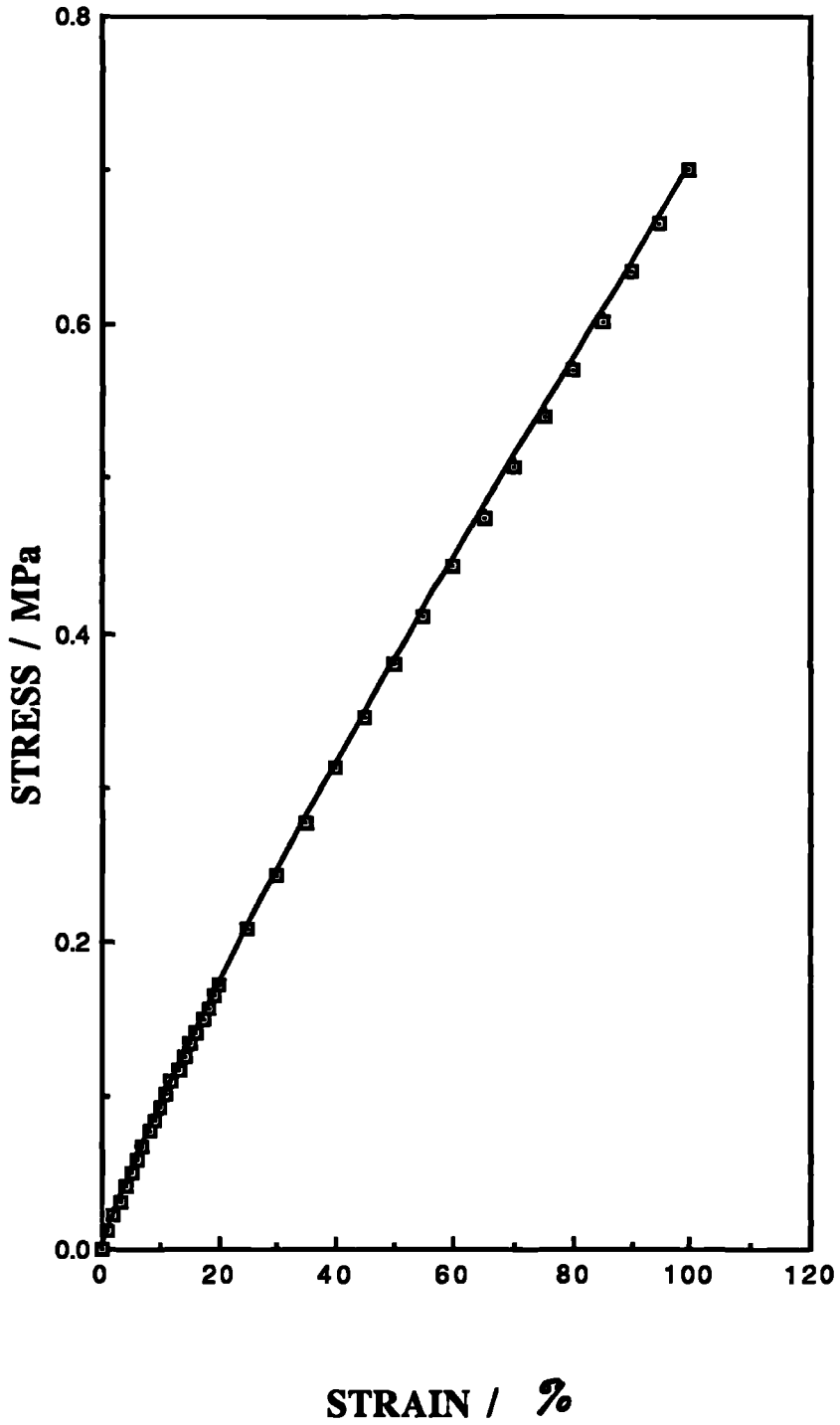

Figure 4.9 : Simple shear stress-strain data points for NR23 with the curve predicted from equation (4.1) using the values of n & A obtained from tension data

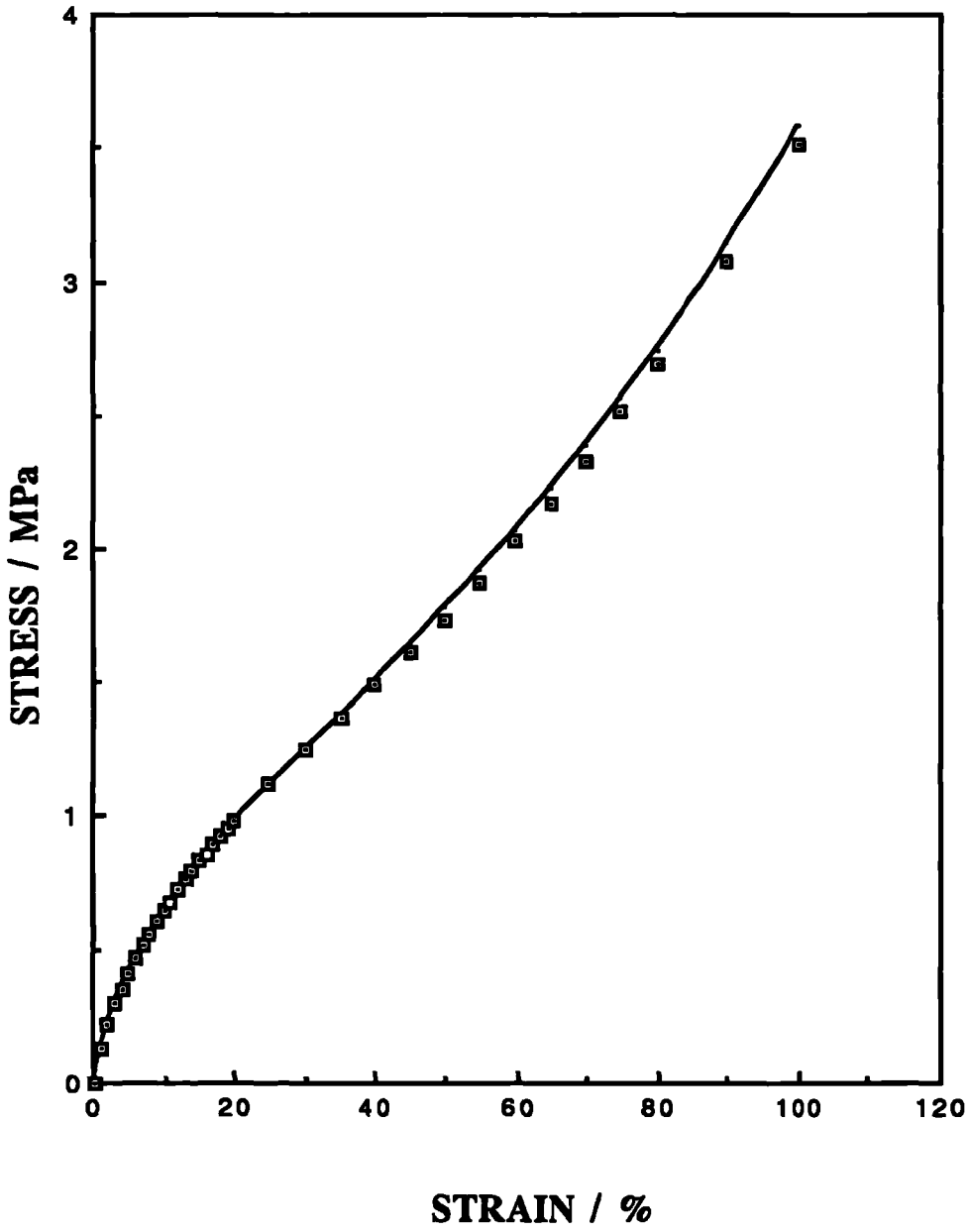

Figure 4.10 : Tensile stress-strain data points for NR69 with the curve predicted from equation (4.5) using the average values of n, A and K.

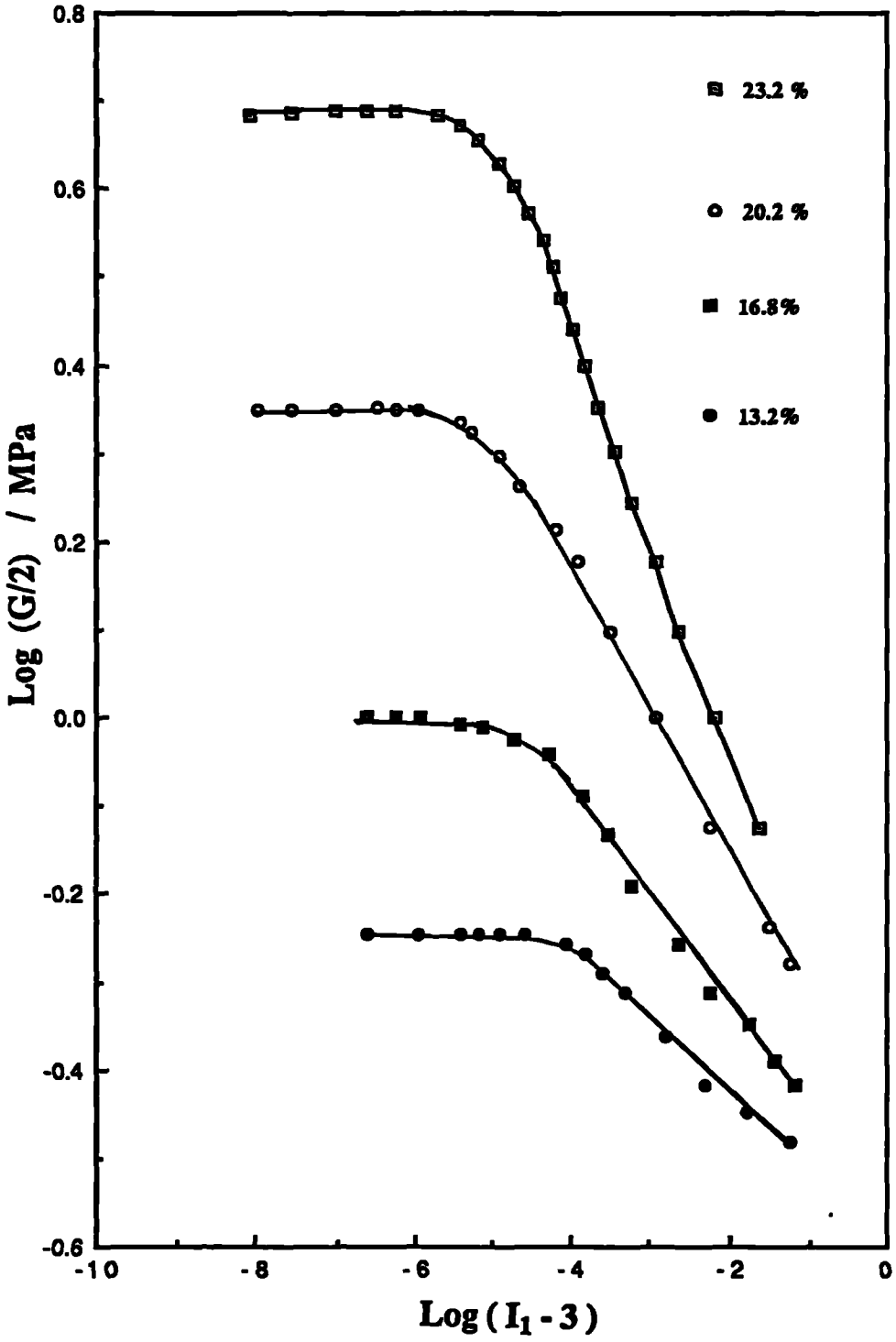

Figure 4.11 : Dynamic shear modulus as a function of (I_1 - 3) for a butyl rubber containing various % by volume of HAF carbon black data reproduced from figure 3, ref 33, fitted curves from equation 4.13.

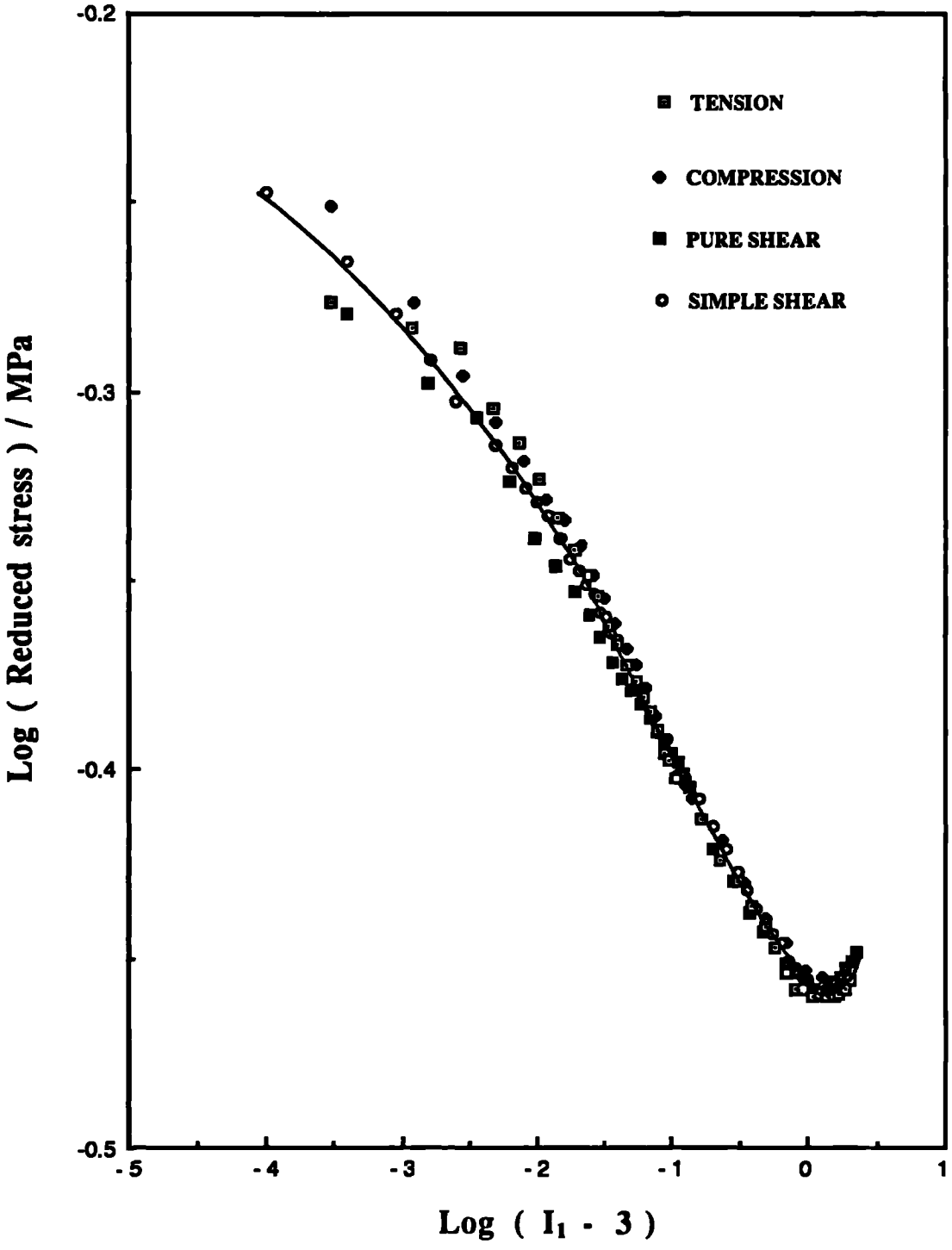

Figure 4.12 : Four parameter fit for NR23

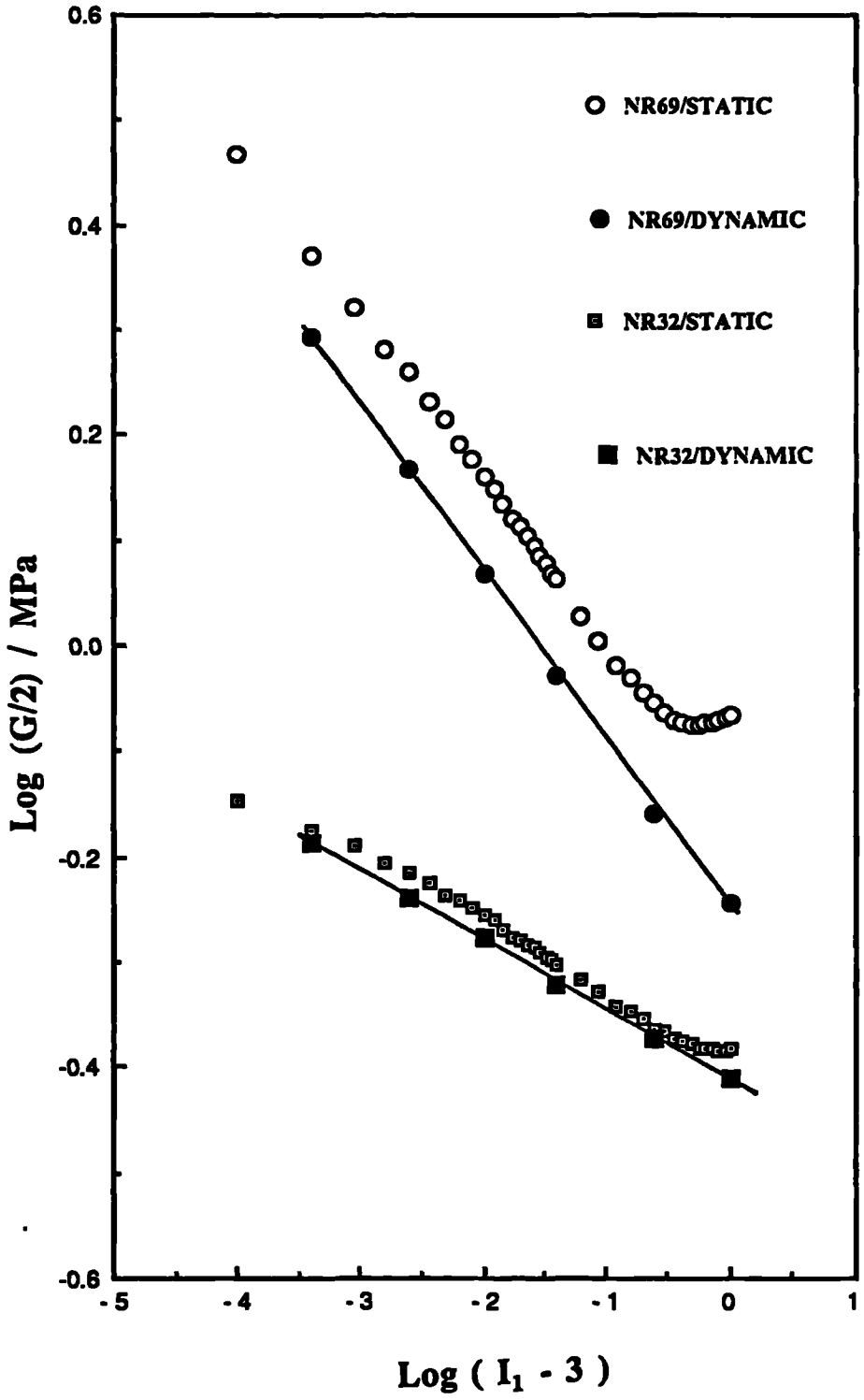

Figure 4.13(a): Shear modulus as a function of (I_1 - 3) for NR32 & NR69 under static (1st cycle) and dynamic (10th cycle) conditions, fitted curves from equation (4.11)

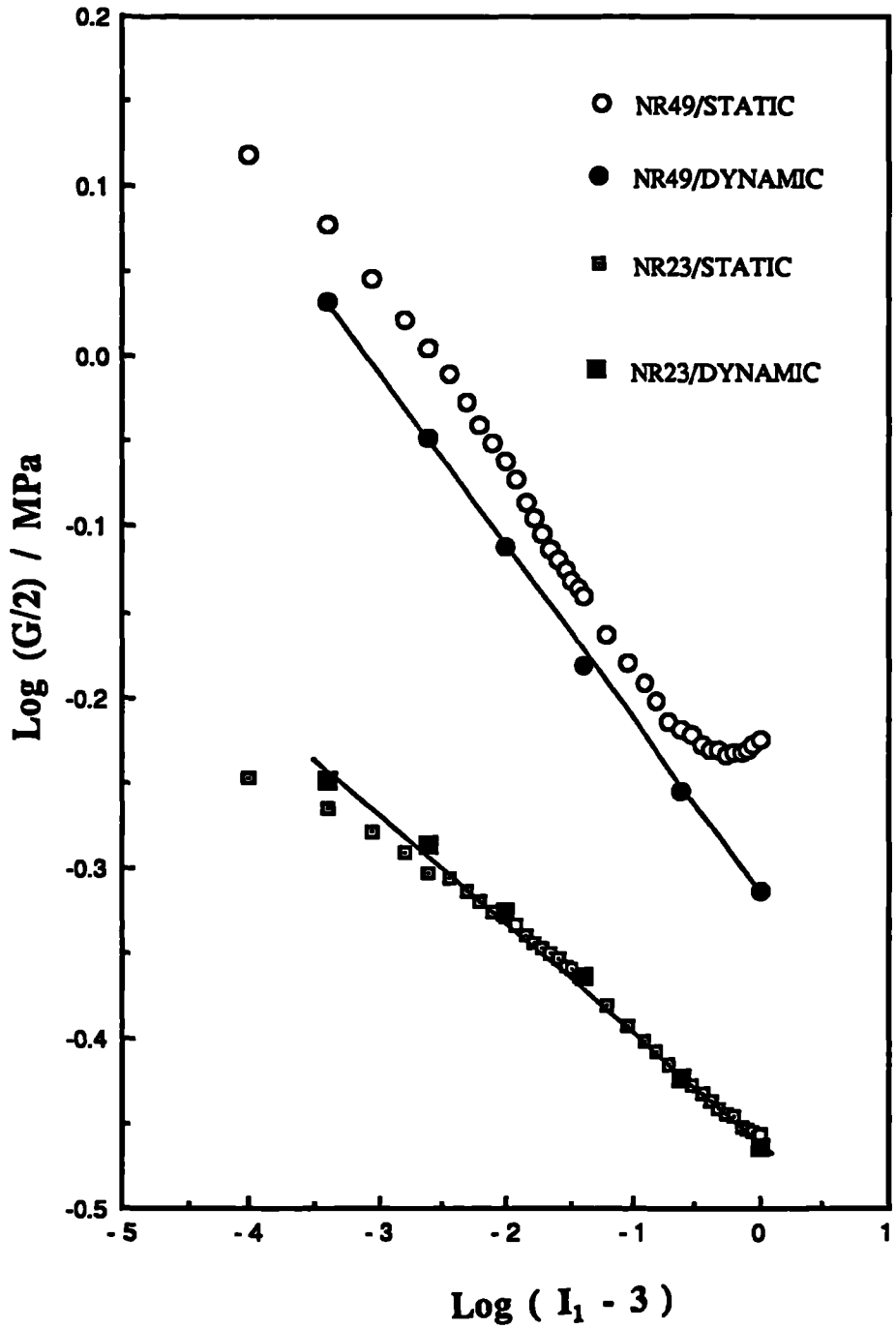

Figure 4.13 (b): Shear modulus as a function of (I_1 - 3) for NR23 & NR49 under static (1st cycle) and dynamic (10th cycle) conditions fitted curves from equation (4.11)

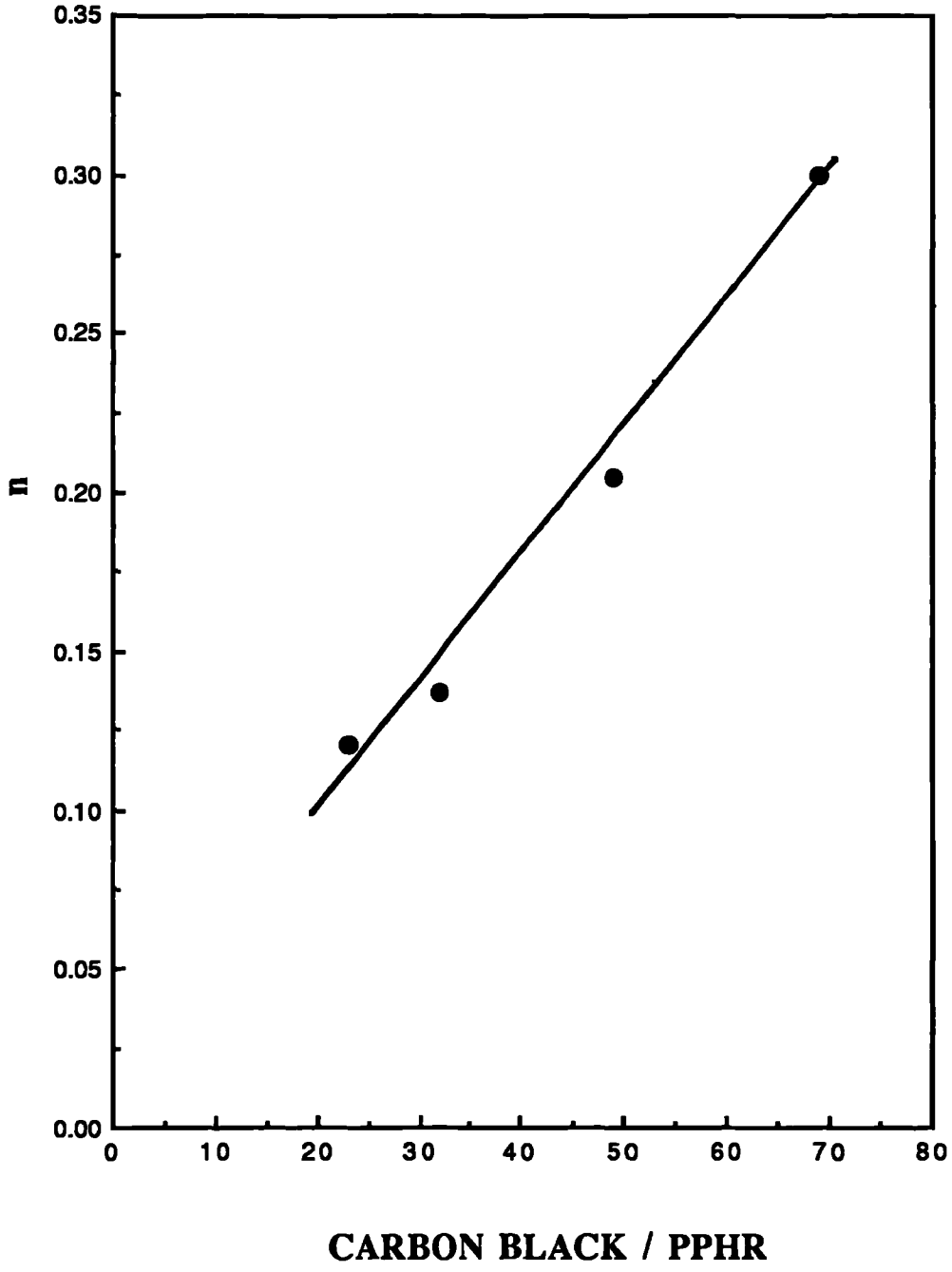

Figure 4.14 : Effect of carbon black content on values of n for NR vulcanizates (Peradin compounds)

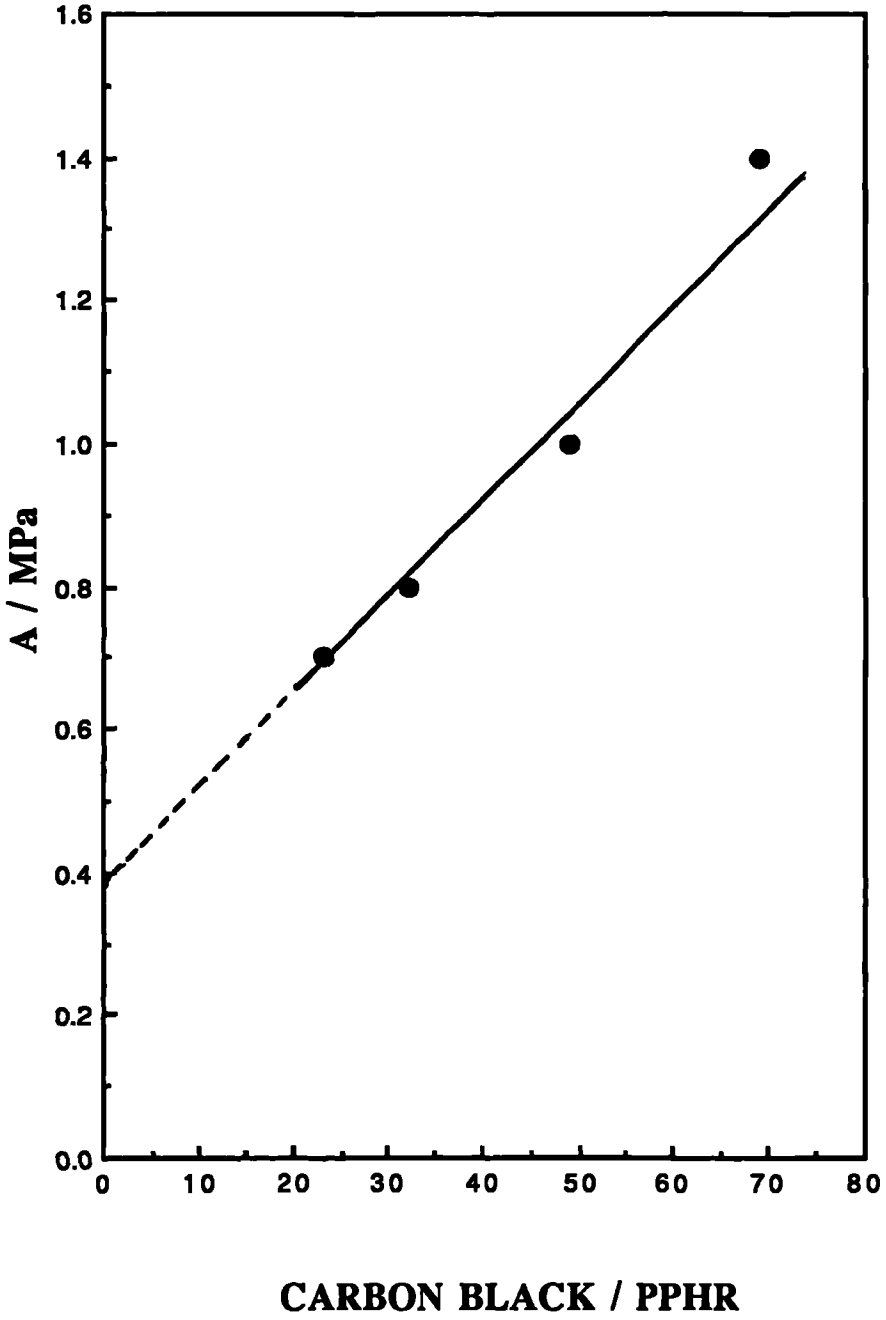

Figure 4.15 : Effect of carbon black content on values of A for NR vulcanizates (Peradin compounds)

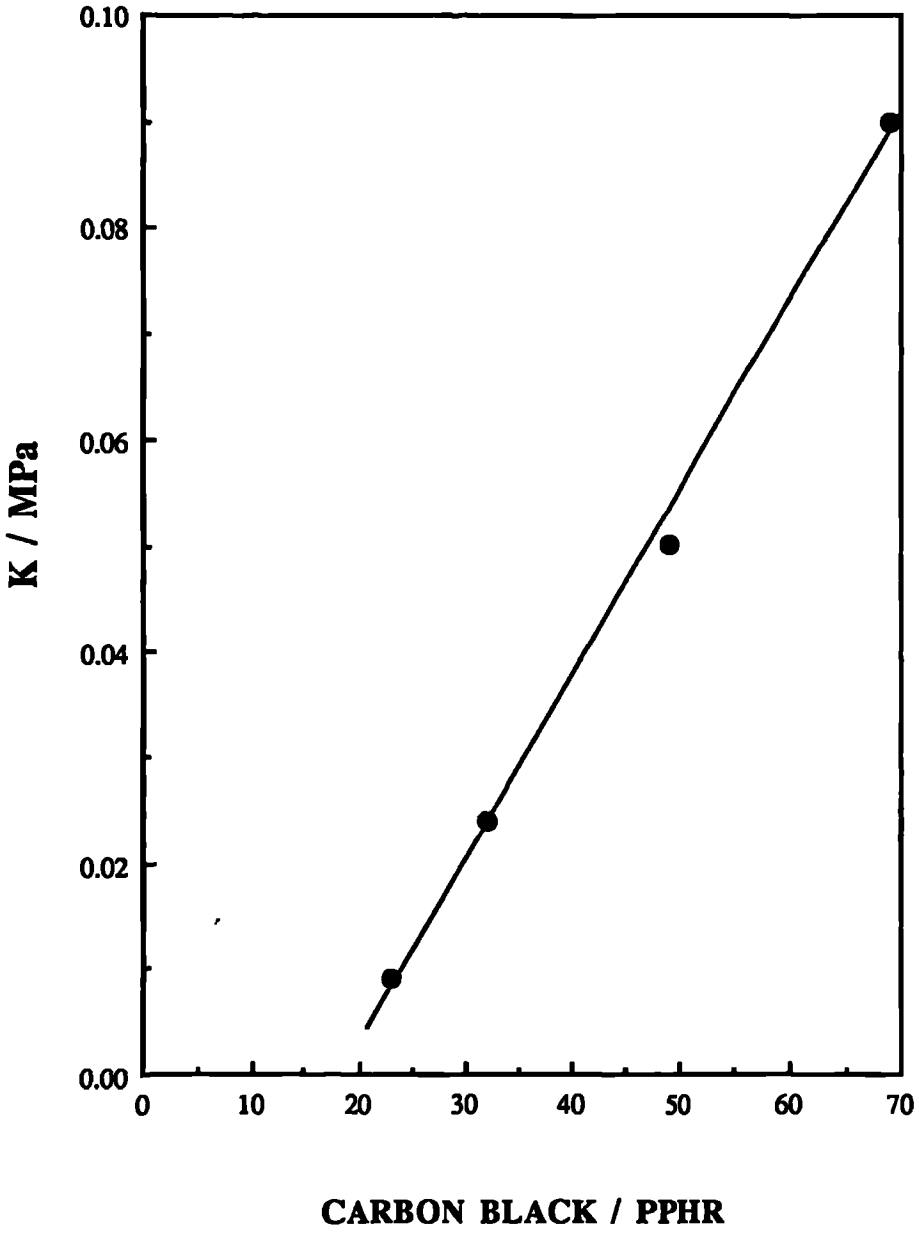

Figure 4.16: Effect of carbon black content on values of K for NR vulcanizates [Peradin compounds]

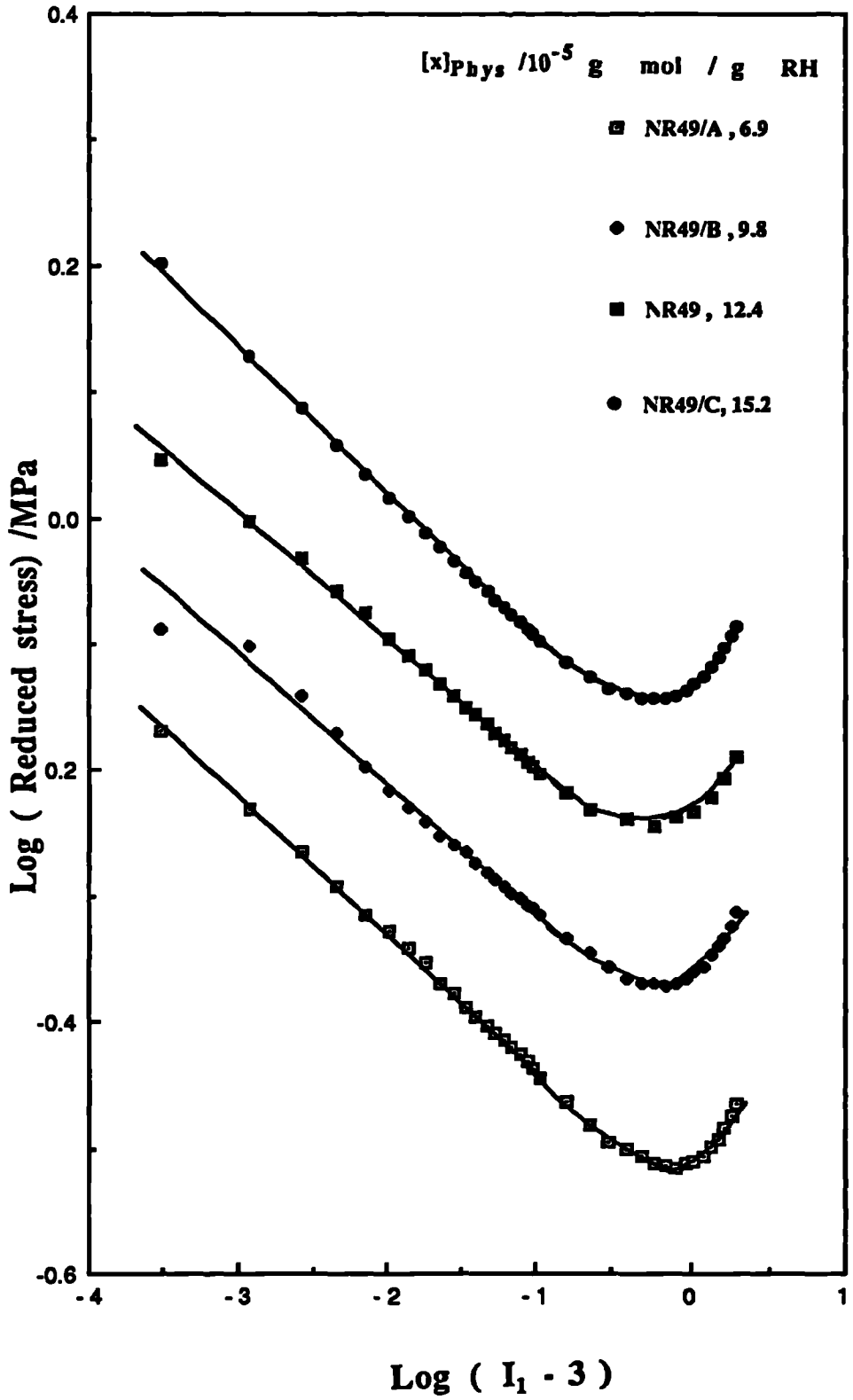

Figure 4.17: Effect of crosslink density on values of n, A and K. Compound NR49 of different crosslink densities

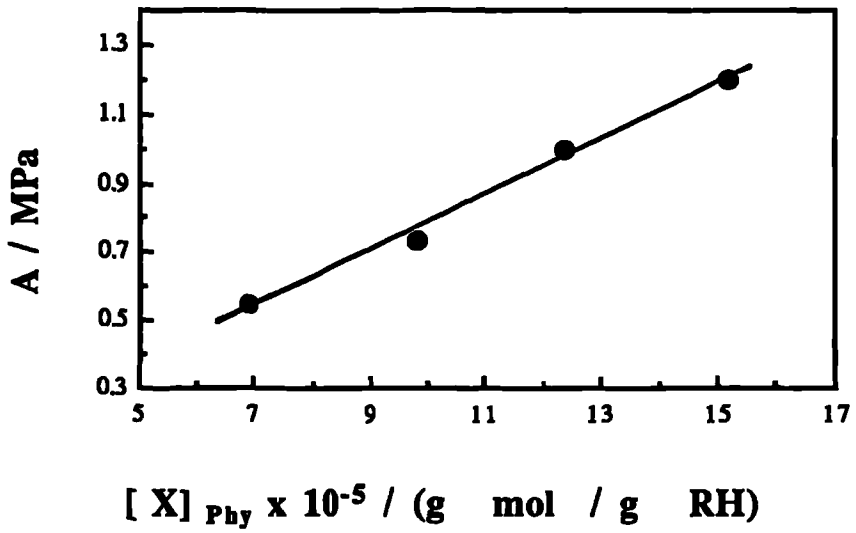

Figure 4.18(a) Crosslink density versus A for NR vulcanizates containing 49 pphr HAF carbon black

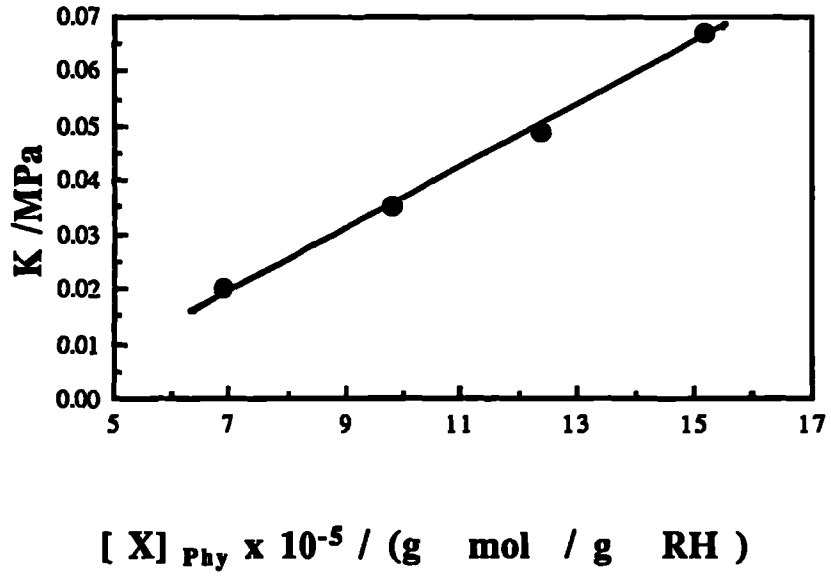

Figure 4.18(b) Crosslink density versus K for NR vulcanizates containing 49 pphr HAF carbon black

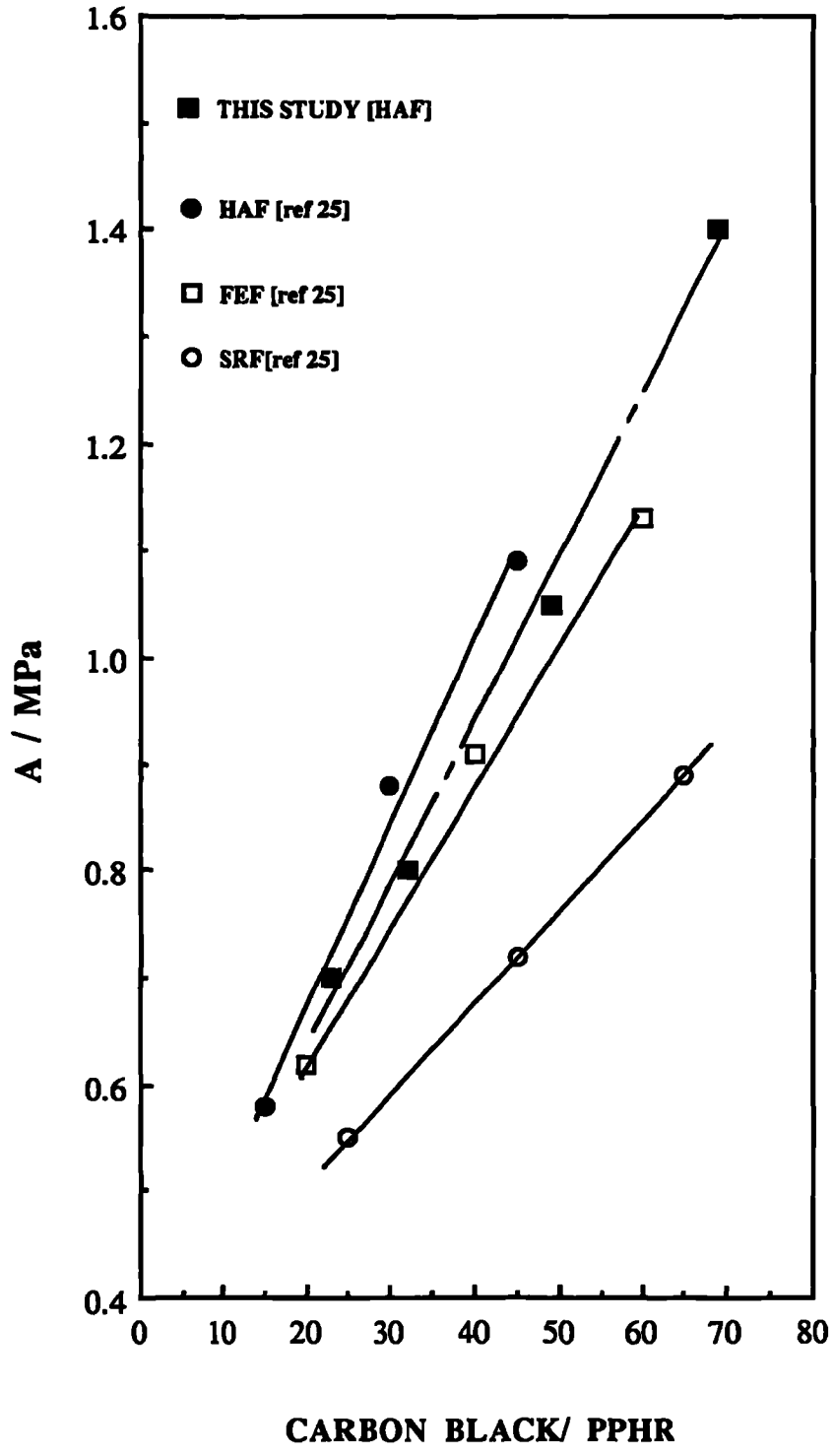

Figure 4.19 : Effect of type of carbon black on values of A

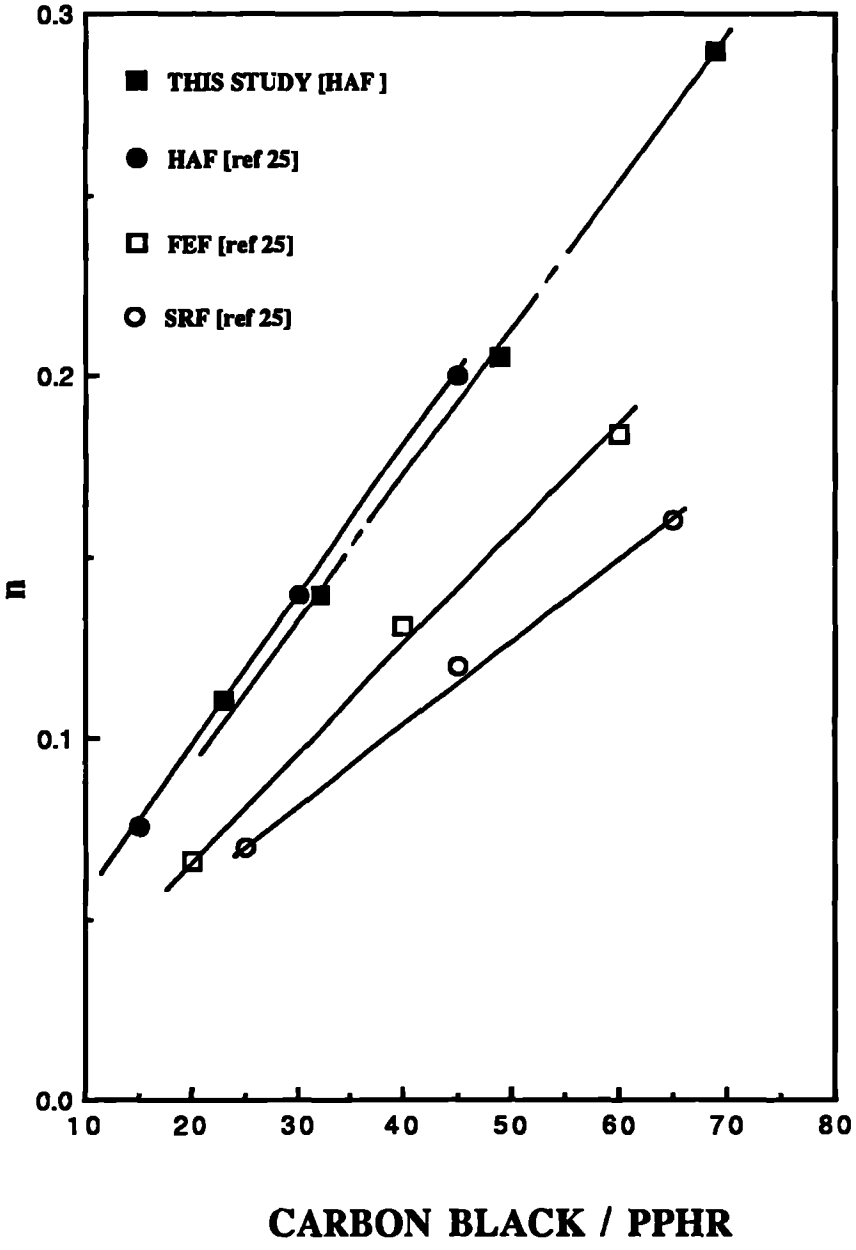

Figure 4.20 : Effect of type of carbon black on values of n

CHAPTER FIVE

5.0 SILICA FILLED RUBBERS

5.1 INTRODUCTION

Carbon black is the most common particulate filler used in rubbers and is believed to yield the highest degree of reinforcement. This is reflected in the fact that by far the most research carried out so far concerns carbon black-filled vulcanizates. A consequence of this has been a lack of understanding of the behaviour of rubber vulcanizates reinforced with other types of fillers, such as silica. Silica seems to be the most highly reinforcing filler after carbon black[39]. Thus silica filled vulcanizates seemed the most relevant to study after the more widely studied carbon black system. It has been reported[39,40] that one of the major differences between carbon black and silica was the degree of filler agglomeration in the rubber; silica fillers being agglomerated to a greater extent than carbon black. This is because the aggregates of fused silica particles (called primary structures) interact through hydrogen bonding to produce extensive agglomerates called secondary structures due to the presence of silanol groups on the filler surfaces. Furthermore silica filler surfaces have little affinity for hydrocarbon rubbers such as NR due to the polar nature of their surfaces and wetting of the surface by rubber is difficult to achieve. In most rubber applications, coupling agents are added to improve interaction between filler and rubber.

In this chapter, the results of the limited stress-strain studies of silica-filled vulcanizates will be presented and discussed. The compositions and formulations for the silica filled NR, IR and SBR rubbers are given in table 3.3 & 3.4. The strain-energy function established in the previous chapter will be used to obtain materials constants for these silica filled vulcanizates and these will be compared with those for the carbon black system. The effect of the addition of a coupling agent on the mechanical behaviour of a silica filled vulcanizate will be examined.

5.2 STRESS-STRAIN DATA OF SILICA FILLED VULCANIZATES

Typical tensile stress-strain curves for a 40 pphr silica filled NR vulcanizate cured with a peroxide, without (uncoupled) and with (coupled) a coupling

agent, are shown in figures 5.1&5.2. Similar curves for IR vulcanizates are shown in figures 5.3&5.4.

It can be seen that the rubber vulcanizate without a coupling agent appears abnormally stiff at small strains (figures 5.1&5.3). At a given stress (0.7-0.8 MPa) the material actually behaves some what as though it had reached a yield point. This sharp yield point is much smoothed by the addition of 1.0 pphr silane as a coupling agent.

The differences in behaviour result from the role of the coupling agent. The coupling agent will both improve the homogeneity of the dispersion, reducing the maximum size of aggregates and improve rubber/filler particle adhesion. At these low stresses the effects observed are most likely to be due to the breakdown of the aggregates, with the effects being much less in the case of the better dispersed coupled materials.

In figure 5.1 this low strain behaviour is compared with that of NR32, one of the Peradin carbon black compounds. There is no direct equivalent carbon black filled compound used in this study but NR32 is the closest, having a rather lower filler content but a rather higher crosslink density, resulting in a very similar tensile stress at 100% strain to that of the coupled silica filled material. It can be seen that the curvature at low strains is even less than that exhibited by the coupled silica filled compound. NR32 contains a very homogeneous dispersion of carbon black and this adds weight to the argument that the sharp yield point in the uncoupled silica filled material is primarily due to the breakdown of the coarse silica aggregates.

At higher stresses (figure 5.2) the coupled materials always exhibit a significantly higher stress for a given strain. This effect is now probably more dependent on the improved adhesion of rubber/silica as a result of addition of coupling agent, evidenced by the fact that stress whitening occurs in the uncoupled material at high stresses. In fact the mechanical behaviour of the coupled NR silica material is now very similar to that of the carbon black filled NR32 (figure 5.5). This suggests that silica filled rubbers with appropriate coupling can be equally stiff to carbon black filled rubbers[39]. It should be noted that in this higher stress region the curves for the IR rubbers always lie below those for the NR rubbers. It must be reiterated here that the IR (cariflex 305) is a synthetic natural rubber with 92% cis-polyisoprene compared to the NR which contains more than 99% cis. These differences may well result in a much reduced strain crystallization effect in the IR rubber vulcanizate, hence resulting in lower stresses for a given

strain. It should also be noted that in the IR rubber a further increase in the amount of coupling agent (1.0-2.0 pphr) caused a further increase in stiffness at high strains (figure 5.4). Care must therefore be taken when comparing the reinforcing role of fillers in rubbers which strain crystallize to different extents.

5.3 SMALL STRAIN PORTION OF THE STRESS-STRAIN CURVES

It has been observed that the stress-strain curves of the silica filled rubbers are highly non-linear, particularly at low extensions from 1 to 100%, which is the region of major concern in most engineering applications. Furthermore the uncoupled rubbers exhibit a relatively sharp 'yield point'. It has been postulated here that the mechanical behaviour in this region is more likely to be due to the breakdown of silica/silica aggregates than to the breakdown of silica/rubber adhesion. A series of experiments was hence carried out in an attempt to separate these effects although it was recognised that they must always be interrelated.

5.3.1 Effect of a solvent

It was recognised that solvents like benzene and carbon tetrachloride could produce linear swelling strains of as much as 50-60%. Such strains could take the rubbers well past the yield point effect (figure 5.1). It must be recognised however that the actual stresses/strains generated are hydrostatic and that their effects may be different in kind to those produced by the application of an uniaxial tensile stress. It was hence decided to investigate whether the stresses developed during solvent swelling were sufficient to breakdown the filled aggregates structures in any way and whether any such changes remained after the solvent had been removed.

Strips of the rubbers were swollen in carbon tetrachloride for 3 days to a linear swelling strain of 65%. The samples were then dried at room temperature in the dark. The strips were then tested in tension producing the stress-strain curves shown in figures 5.6 & 5.7.

Comparison of the stress-strain curves produced before and after the swelling show that significant effects has occurred particularly at low strains in the uncoupled material. In this case the swelling treatment had made the yield point much less sharp, causing a reduction in the stress to a given strain of about 30%. It is most likely that this effect resulted from the swelling stresses breaking up some of the loose silica particle

aggregates reducing the effective stiffness at low strains. The effect on the coupled material is much less, presumably due to the fact that the silica dispersion in this material is more homogeneous with the largest aggregates being both smaller in size and number. The stress-strain curves for the uncoupled and coupled materials in this low strain region are now more similar as a result of the filler dispersion being more similar.

At higher stresses the effect to the swelling treatment is proportionally much less. Any effect of the silica particle aggregate breakdown due to swelling stresses has been totally masked by the aggregate breakdown resulting from the applied tensile stress. In fact there is a slight increase in the stress to a given strain for both the materials. This stiffening effect may be due to solvent extraction during swelling which would effectively cause a slight increase in the effective volume fraction of the filler.

5.3.2 Effect of prestressing on the initial modulus

It has been postulated that the higher initial modulus in the uncoupled material is a result of the poor dispersion of silica, resulting in coarse particle aggregates. It has been further suggested that the sharp yield point observed is a result of the breakdown of these aggregates. Prestressing of the material should hence breakdown the aggregates resulting in a lower initial modulus when retested. The extent of this effect would depend on the magnitude of the initially applied stress. It should be noted that the application of a tensile stress may breakdown the aggregates in a different way to that produced by the hydrostatic stresses generated during swelling. Furthermore the use of the initial tensile modulus to determine the magnitude of the effect measures only the effect in one direction; the direction in which aggregate breakdown is likely to have occurred to the greatest extent.

The results of such an experiment are shown in figure 5.8 for both uncoupled and coupled materials. The uncoupled material initially shows no change in the initial modulus suggesting that no permanent aggregate breakdown occurs at prestressing of up to 0.5 MPa (5 % strain). Over the prestressing region, 0.5-1.0 MPa, a very large drop in the initial modulus is observed. This region includes the sharp yield point which suggests that significant breakdown of coarse silica particle aggregates is occurring in this region at these stresses. The coupled material shows a similar effect but the magnitude is much reduced. This is presumably due to the fact that the

better dispersion of silica in this material yields smaller aggregate clusters less susceptible to breakdown.

At stresses larger than 1.0 MPa the effect of prestressing on the initial modulus is much reduced. In fact, in the coupled material, it would be difficult to ascert that there was an effect. In the uncoupled material the initial modulus continues to fall but at a much slower rate. This is probably due to some continuous aggregate breakdown but some contribution may be present due to rubber/filler particle debonding.

5.3.3 Effect of stressing and swelling on silica-filled vulcanizates

The extent of swelling of rubber vulcanizates is determined largely by the crosslink density. The volume change of the rubber is calculated on the basis that the inert silica filler does not swell. The filler may however restrict the swelling behaviour as a result of rubber/silica adhesion and/or as a result of silica/silica particle agglomeration. If a vulcanizate is swollen after stressing the extent of swelling may be increased due to crosslink breakage or due to rubber/silica debonding or due to breakdown of agglomerates.

In the present case tensile strips were strained to different nominal stresses using an Instron testing machine and were then swollen in n-decane for 3 days. Following swelling the volume fraction of rubber in the swollen samples (V_r) was determined. The extent of prestressing on the swelling behaviour was represented by the quantity ΔV_r % defined as;

$$\Delta V_r \% = \frac{V_r - V_{rc}}{V_{rc}} \times 100 \qquad (5.1)$$

Where V_r is the volume fraction of rubber in the swollen vulcanizate after pre-stressing, and V_{rc} is the volume fraction of rubber in the swollen vulcanizate before pre-stressing (unstressed control samples). The changes in volume fraction of rubber in swollen samples, $\Delta V_r\%$, is shown as a function of the nominal stress, σ , in figure 5.9, for both uncoupled and coupled materials. Data for the unfilled NR is also shown for comparison purposes.

It should be noted that in all cases both stressed and unstressed samples were taken from the same vulcanized sheet and that the unstressed samples were swollen under the same conditions simultaneously with the stressed samples. This was carried out to ensure that any solvent extraction effect was similar for all samples.

At low stresses no significant variation of ΔV_r % is observed in the case of unfilled NR indicating that no significant breakage of crosslinks had occurred. At low stresses in the silica filled materials ΔV_r % decreases with increasing prestress; the effect being much greater for the uncoupled material. At large stresses the effects become much less.

Understanding this effect is by no means simple. Section 5.3.1 demonstrated that swelling itself permanently alters the scale of the silica dispersion; this effect being larger in the uncoupled material. In the present case swelling is being used as a measure of the effect of prestressing on the filled rubbers. The tool used for measuring the effect in this case clearly itself causes changes in the filled rubbers. In section 5.3.2 the initial modulus was used as a tool to measure the effect of tensile prestressing . In this case the largest degree of aggregate breakdown probably occurred in the tensile direction and utilizing the initial modulus as a measurement tool maximized the observed effect. Utillizing swelling to measure the effect of prestressing then measures the effect of aggregate breakdown in all directions, not just the tensile direction. Furthermore swelling itself causes some breakdown; an effect which is removed by the representation used in figure 5.9, but is nevertheless present differentialy in the two materials.

Tensile prestressing to 1 MPa causes a drop in the initial tensile modulus by more than 200% (figure 5.8) in the uncoupled material. However ΔV_r % drops by only 3% at this tensile prestress (figure 5.9). This would be equivalent to a drop in modulus (average in all directions) of only about 10%. Even allowing for the fact that the swelling process itself will decrease the tensile modulus by 25% (figure 5.6) there is a large difference between the two results. It must be that there is a large degree of breakdown in the large weak aggregates in the tensile direction but little or no effect in all other directions. As a result there is a large drop in the initial tensile modulus but only a small average change in the effect of the silica particles in restricting swelling in all other directions, resulting in only a small change in ΔV_r %. Nevertheless this effect is less for the coupled materials in line with the fact that the better dispersion breaks down less readily.

The decrease in the measured initial tensile modulus is much less as the prestress is increased to more than 1 MPa (figure 5.8), where as ΔV_r % continue to decrease at a not dissimilar rate (figure 5.9). Presumably aggregates initially breakdown in the tensile direction but with increasing strain, breakdown in directions normal to this becomes significant resulting

in a continuous decrease in average stiffness and a continuous increase in swelling (decrease in ΔV_r %). As the stress increases it becomes difficult to separate effects due to aggregate breakdown and rubber/silica debonding. Both effects presumably causing ΔV_r % to be greater for the uncoupled materials. It is interesting to note however that the rate of change of ΔV_r % with stress becomes less for the uncoupled material compared to the coupled material at the highest stresses. The region of stress at which this occurs coincides with stress whitening occurring in the uncoupled material. Presumably once significant rubber/silica decoupling occurs further decreases in apparent stiffness become much less and the resultant change in ΔV_r % becomes much smaller. In the coupled material where stress whitening does not occur ΔV_r % continues to decrease although at a slower rate presumably because decoupling does not occur until significantly higher local stresses.

5.4 DETERMINATION OF MATERIALS CONSTANTS USING THE STRAIN ENERGY FUNCTION PREVIOUSLY DERIVED

Double log plots of the reduced stress term versus the invariant (I_1 -3) are shown in figure 5.10 for NR, and figure 5.11 for IR filled vulcanizates, containing 40 pphr silica without and with the coupling agent. It is interesting to note that all plots exhibit a long straight portion with deviation from these lines at both low and high strains as observed in the case of carbon black filled vulcanizates. The numerical values of the materials constants i.e., n, A, K and C were determined using the 4 parameter fitting routine as described in appendix 4.1. They are shown in tables 5.1 and 5.2. In general, the values of n and C are seen to decrease as a result of the addition of the coupling agent, where as the numerical values of the A and K are seen to increase. These values were used in the 4 term strain energy function, equation (4.11), to predict the behaviour in tension for the uncoupled and the coupled silica filled NR and IR vulcanizates as shown in figure 5.5 and figure 5.3 as solid lines together with the actual experimental points. The agreement is seen to be excellent. It is clear then that, at least for the present data, the four constant strain energy function, can represent the silica filled rubbers stress-strain behaviour in a similar manner to that for the carbon black filled rubbers.

5.5 MATERIALS CONSTANTS OF SILICA FILLED RUBBERS-EFFECT OF COUPLING AGENT

This section discusses the numerical values n, A, K and C for the silica filled rubbers, compares these values with those for the carbon black filled rubbers and in particular discusses the effect of the addition of the coupling agent.

5.5.1 Effect of coupling agent on values of n

The numerical values of n, which are the slopes of the linear section of the log (reduced stress) versus log(I_1 - 3) plots in figures 5.10 and 5.11 decrease upon the addition of the coupling agent for both the NR and IR rubbers.

The n values for the uncoupled materials (0.8-0.9) are very large even when compared to the most highly filled carbon black material (0.3). In the case of the carbon black filled materials it was suggested (see section 4.2.1) that the value of n represented the rate of breakdown of the carbon black structure with strain. n was found to increase with carbon black content and this was attributed to a more well developed structure with some increase in the size of particle aggregates. Furthermore, poorly dispersed carbon black systems (short mixing times) yield values of n as large as 0.39 as a result of the presence of relatively large particle aggregates. TEM studies of uncoupled silica filled rubbers[41] showed the presence of large aggregates of silica which were largely discontinuous. The aggregates tended to be larger and more tightly clustered than those for carbon black systems because the interaction of rubber hydrocarbon with silica is weaker than that for carbon black. The large values of n obtained for uncoupled materials probably results from the rate of breakdown of these coarse structures. These large values of n are reflected in the large curvature of the stress-strain curves over the range 0-30% (figure 5.1).

The addition of the coupling agent has a very significant effect on these materials causing a reduction in the values of n by a factor of 2. TEM evidence[41] suggests that a major effect of the coupling agent is to produce a better dispersion of the filler with a large number of smaller particle aggregates resulting from the enhanced wetting and increased interaction

with the rubber. However the n values obtained, 0.4, are still significantly larger than those for a similar carbon black filled rubber (NR32) of 0.14. This suggests that even with the addition of a coupling agent the silica dispersion is still poorer than the equivalent carbon black dispersion with the addition of further coupling agent (1-2 pphr) having a minimal effect (0.44-0.45). This is evidenced by the fact that even though the addition of coupling agent causes a marked decrease in curvature of the stress-strain curves, this curvature is still larger than that for the equivalent carbon black filled compound (figure 5.1).

5.5.2 Effect of coupling agent on values of A & K

Discussing the effect of materials variables on the numerical values of A and K is more difficult as both depend on crosslink density as well as on filler content. Furthermore higher strain data is limited causing the K values to be less reliable particularly for the IR rubbers.

The values of A correspond to the shear stress at 100% strain. By this strain considerable breakdown of the silica particle aggregates has taken place as evidenced by both the swelling and prestressing experiments; the effects being greater for the uncoupled materials. Furthermore the coupled materials have an apparently higher crosslink density but this may merely reflect both the better dispersion of the silica and better rubber/silica adhesion, both restricting the extent of swelling.

The addition of the coupling agent increases the value of A from 0.6 to 0.8 which may result from both the better dispersion and/or the apparent increased crosslink density. It is interesting to note that the A value of 0.8 is very close to that for the equivalent carbon black filled rubber NR32, suggesting that by 100% shear strain the scale of the dispersion and the effect on mechanical properties is similar for the two fillers. This is evidenced by the similarity of the two tensile stress-strain curves at strains greater than 100% (figure 5.5). The effect of increasing the amount of coupling agent (1 to 2 pphr) is marginal on n but does seem to increase A (table 5.2). This suggests that while the scale of dispersion is not significantly different the better rubber/silica adhesion is beginning to play a role by 100% strain.

The values of K are associated with the points at which the upturn occurs in the plot of log (reduced stress) versus log (I_1 - 3). It is associated with strain at which finite extensibility effect occurred. K was found to increase considerably with both carbon black content and crosslink density

for the carbon filled rubbers as finite extensibility effects occurred at progressively low strains. The values for the silica filled materials are very close to that for the equivalent carbon black filled material NR32, of about 0.02. This even though the filler content of NR32 is slightly lower but the crosslink density slightly higher. Furthermore K does not change greatly with the addition of coupling agent when compared to changes of 0.02 to 0.06 with crosslink density and 0.01 to 0.09 with carbon black content. This suggests that at a sufficiently large strain, when larger particle aggregates have broken down, that K depends mostly on the magnitude of the filler content whether silica or carbon black, both having a similar effect on finite extensibility.

5.5.3 Effect of coupling agent on values of C

The value of C is determined by the strain at which the modulus begins to tend to its finite small strain value. Alternatively it is the strain at which aggregates of particles begin to breakdown. In the case of the carbon black filled materials C decreased with increasing carbon black content suggesting that the larger particle aggregates broken down more easily.

In the case of the silica filled materials the aggregates are likely to be stronger particularly in the uncoupled material as the silica particles have more affinity towards themselves than to the rubber. The resultant C values are hence significantly larger than for the carbon black filled materials.(12-13 x 10^{-2} compared to 1.2 x 10^{-2} for NR32). The effect of adding a coupling agent is to very much reduce the C values as the strength of the aggregates are much reduced (tables 5.1 and 5.2). The values are however, still larger than for the carbon black materials suggesting that the aggregates remain stronger.

5.6 SUMMARY

It has been demonstrated that the proposed strain energy function can represent the stress-strain behaviour of these particular silica filled rubbers very good. The magnitudes of the parameters n, A, K, and C are shown to be consistent with those obtained for carbon black filled rubbers. Furthermore changes in the magnitudes of the parameters with the addition of coupling agents can be adequately interpreted in terms largely of changes in the extent and strength of silica particle aggregation.

TABLE 5.1: Values of materials constants n, A, K, and C for the fitted curves in figure 5.10 for silica filled NR vulcanizates and compared to a carbon black filled NR vulcanizate (NR32).

Compound	silica/car-bon black, /pphr	crosslink density/ 10^{-5} g mol /g RH	Volume fraction (Φ)	n	A / MPa	K / MPa	C
NR40/01 without CA	40	6.7	15.5	0.91	0.64	0.020	$13.4X10^{-2}$
NR40/02 with CA (1.0 pphr)	40	9.4	15.5	0.41	0.82	0.028	$5.4X10^{-2}$
NR32	32	11.2	12.6	0.137	0.80	0.024	$1.2X10^{-2}$

TABLE 5.2 : Values of materials constants n, A, K and C for the fitted curves in figure 5.11 for silica filled IR vulcanizates.

Compound	silica/ pphr	crosslink density /10^{-5} g . mol /g. RH	n	A / MPa	K / MPa	C
IR40/01 with out CA	40	6.8	0.81	0.61	0.016	$12.0X10^{-2}$
IR40/02 with CA (1.0 pphr)	40	10.1	0.44	0.92	0.02	$8.0X10^{-2}$
IR40/03 with CA (2 pphr)	40	12.4	0.45	0.97	0.026	$8.0X10^{-2}$

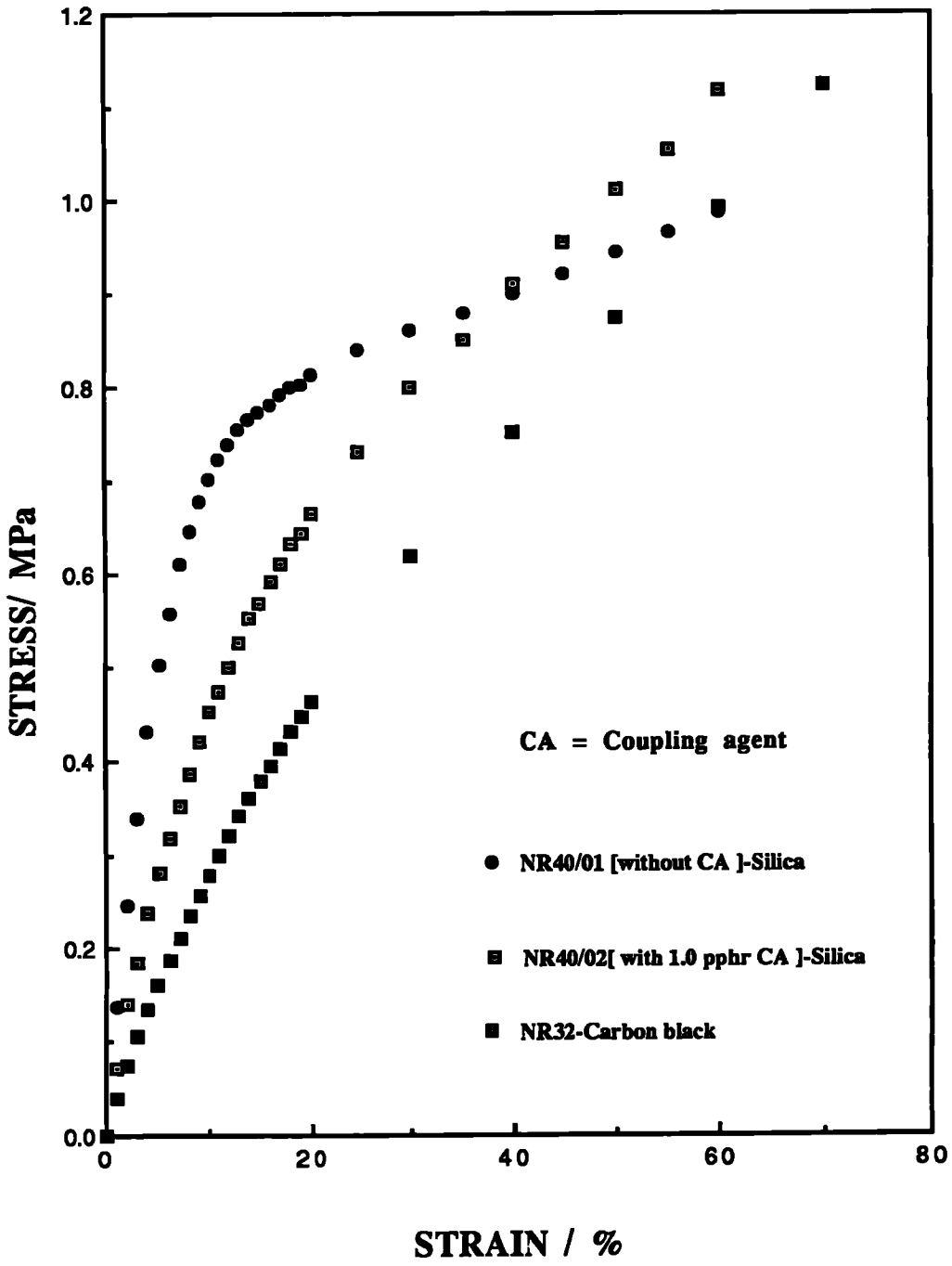

Figure 5.1 : Tensile stress-strain data points for silica filled NR vulcanizates to show the effect of a coupling agent at small strains and compared with a carbon black filled NR vulcanizate (NR32)

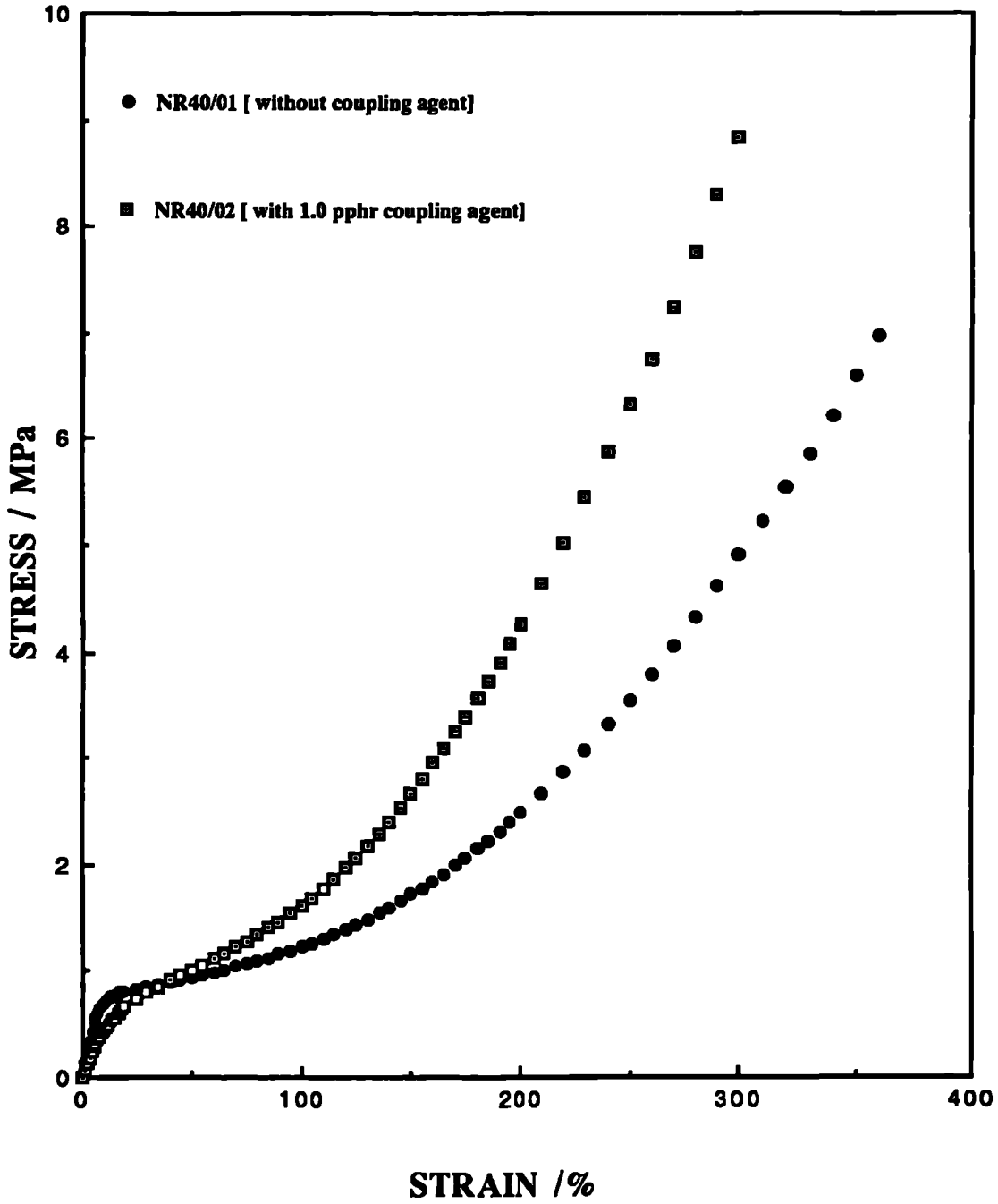

Figure 5.2 : Tensile stress-strain data points for silica filled NR vulcanizates to show the effect of a coupling agent at high strains .

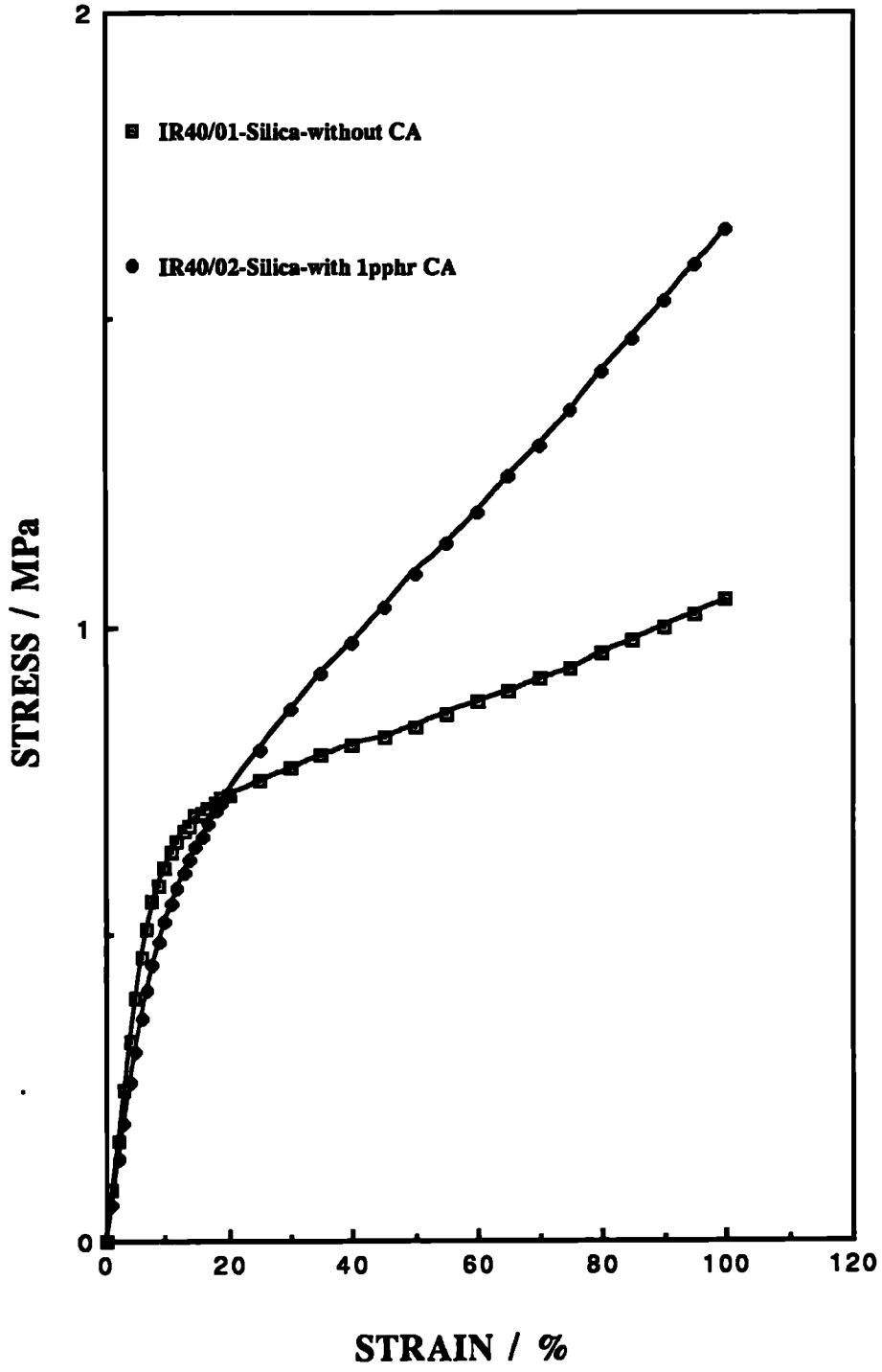

Figure 5.3 : Tensile stress-strain data points for silica filled IR vulcanizates with the curves predicted from equation (4.5) using the values of n, A, K and C.

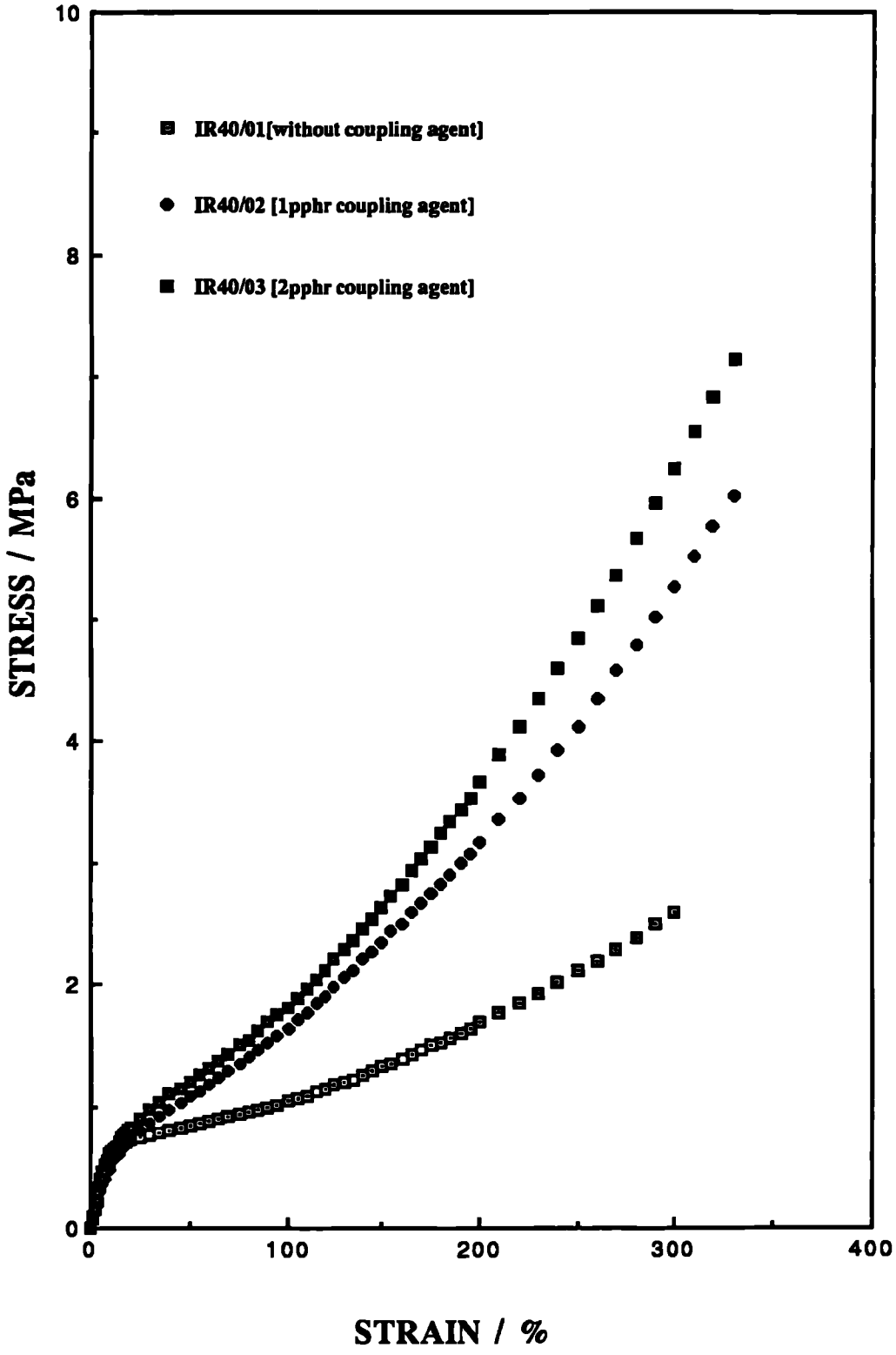

Figure 5.4: Tensile stress-strain data points for silica filled IR vulcanizates to show the effect of a coupling agent at high strains.

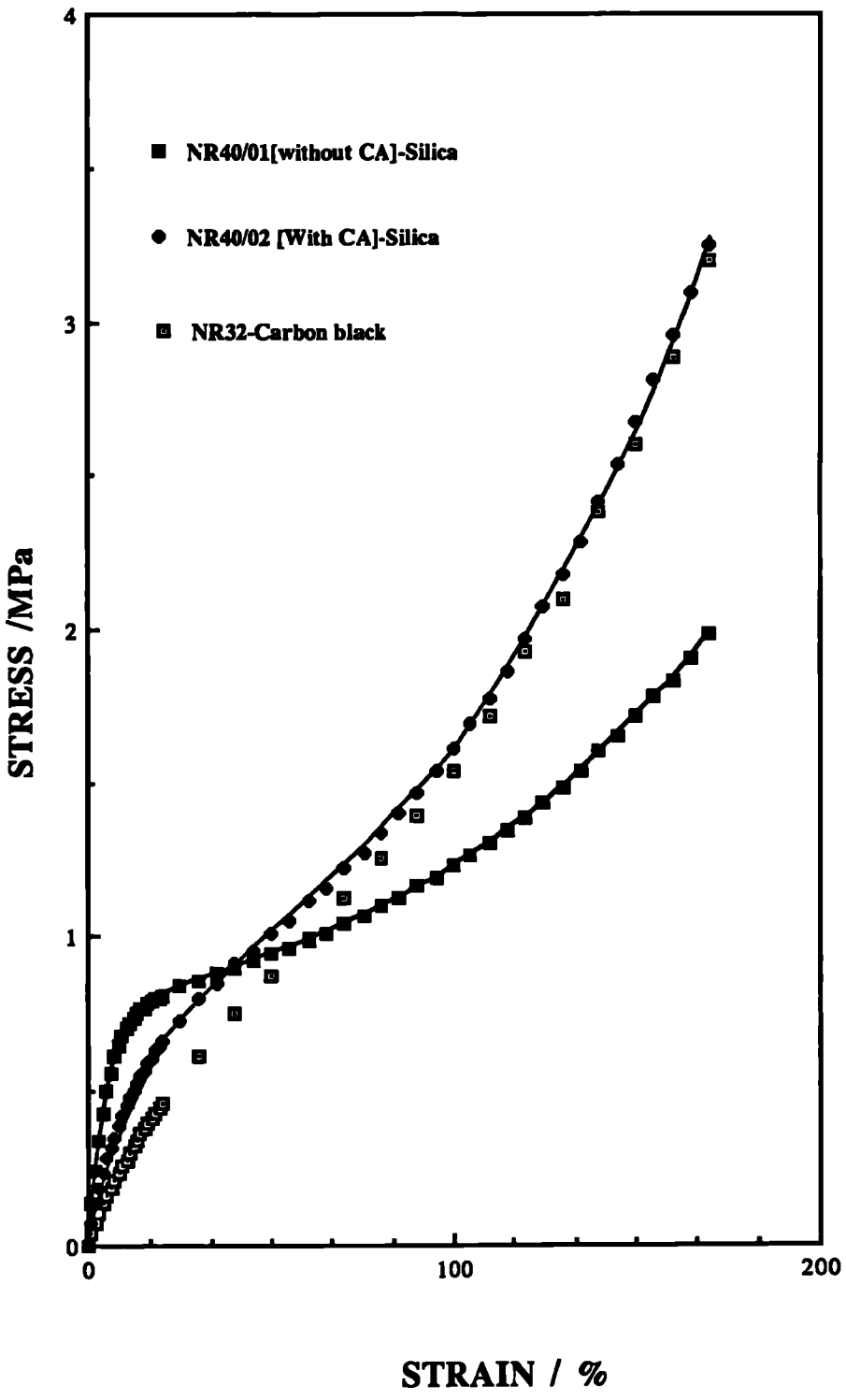

Figure 5.5: Tensile stress-strain data points for silica filled vulcanizates with the curves predicted from equation (4.5) and compared to a carbon black filled vulcanizate (NR32)

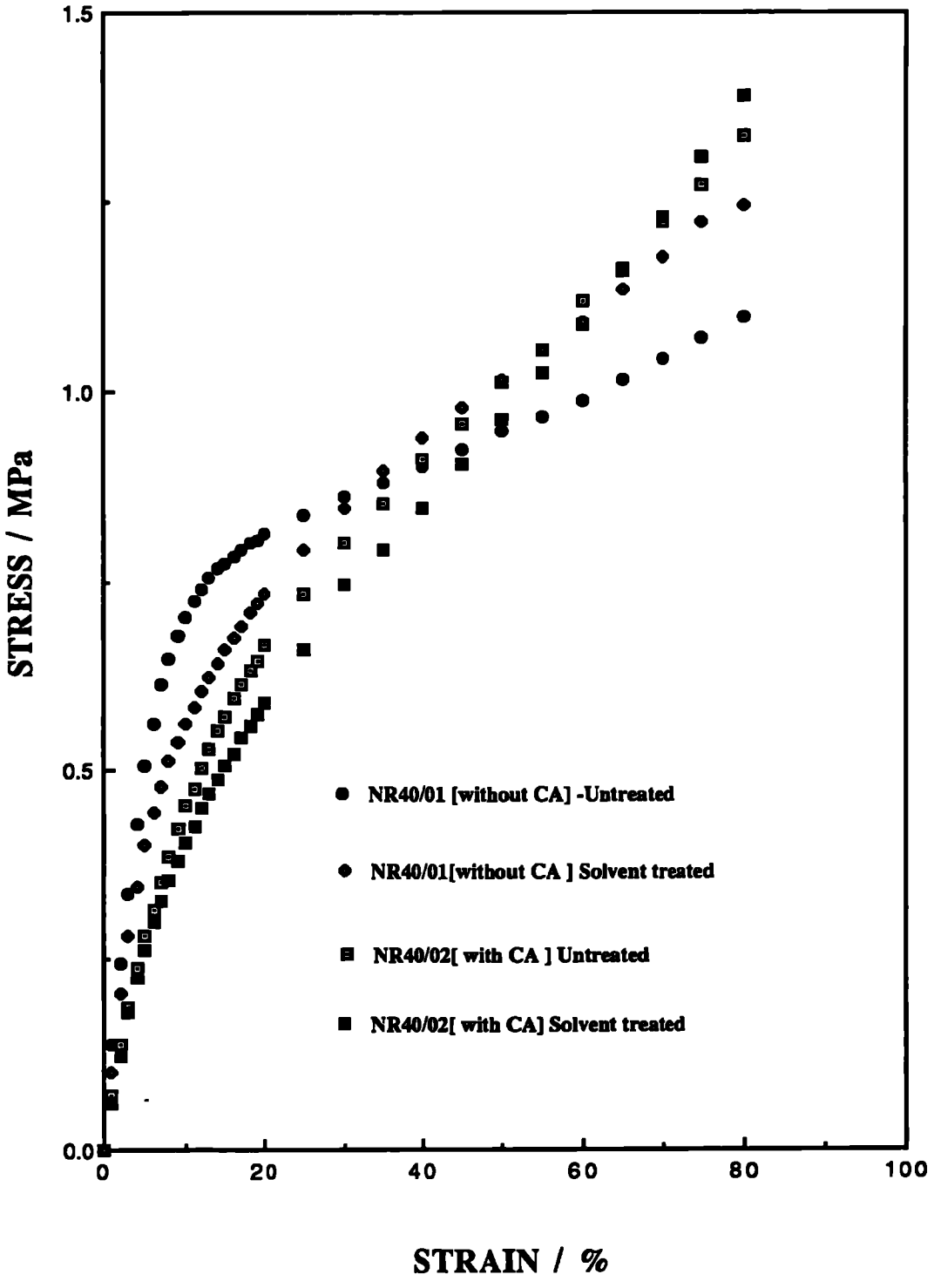

Figure 5.6 : Tensile stress-strain data points for solvent treated and dried silica filled NR vulcanizates without and with coupling agent. [CA = Coupling agent]

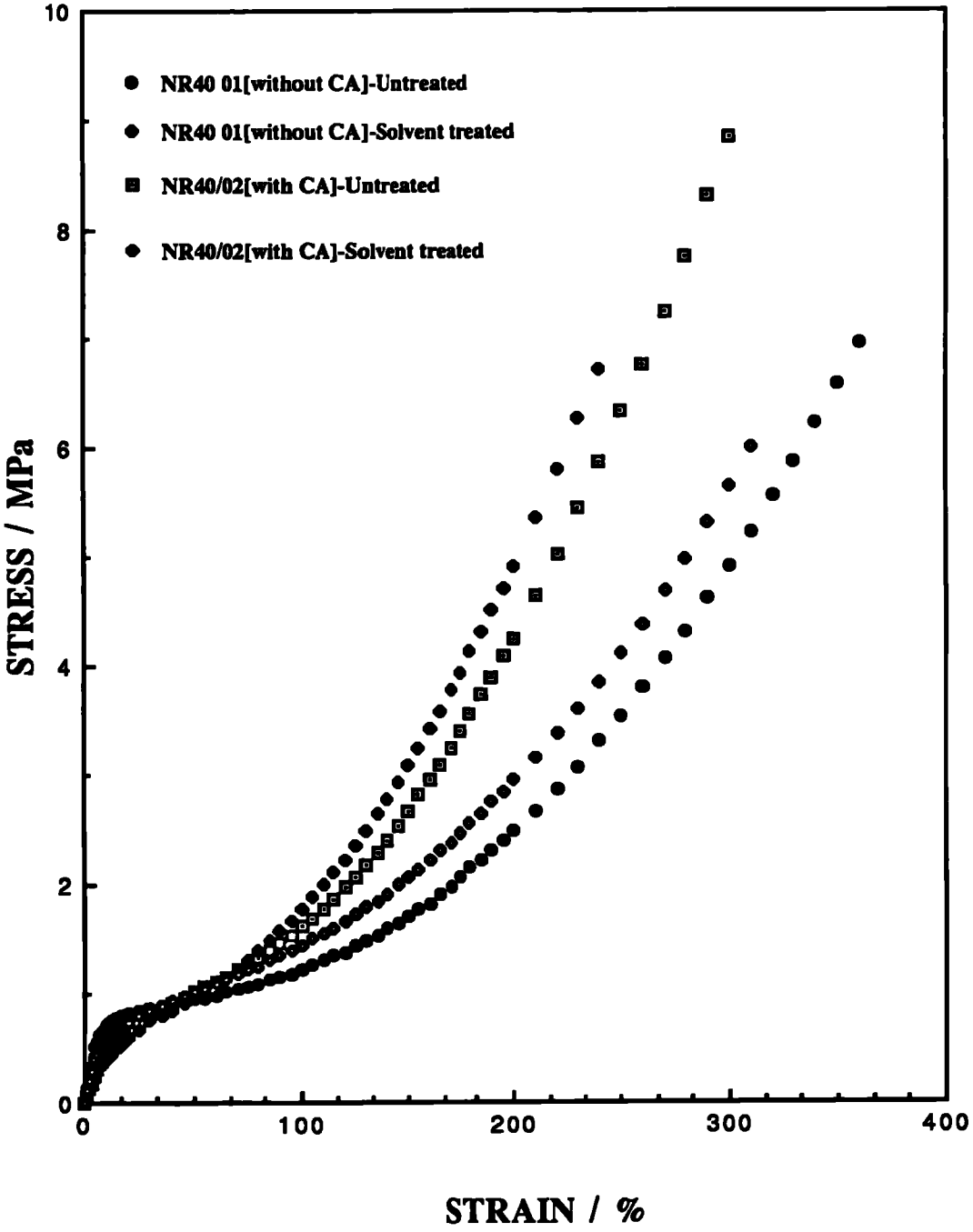

Figure 5.7 :Tensile stress-strain data points for solvent treated and dried silica filled NR vulcanizates to show the effect at high strains.

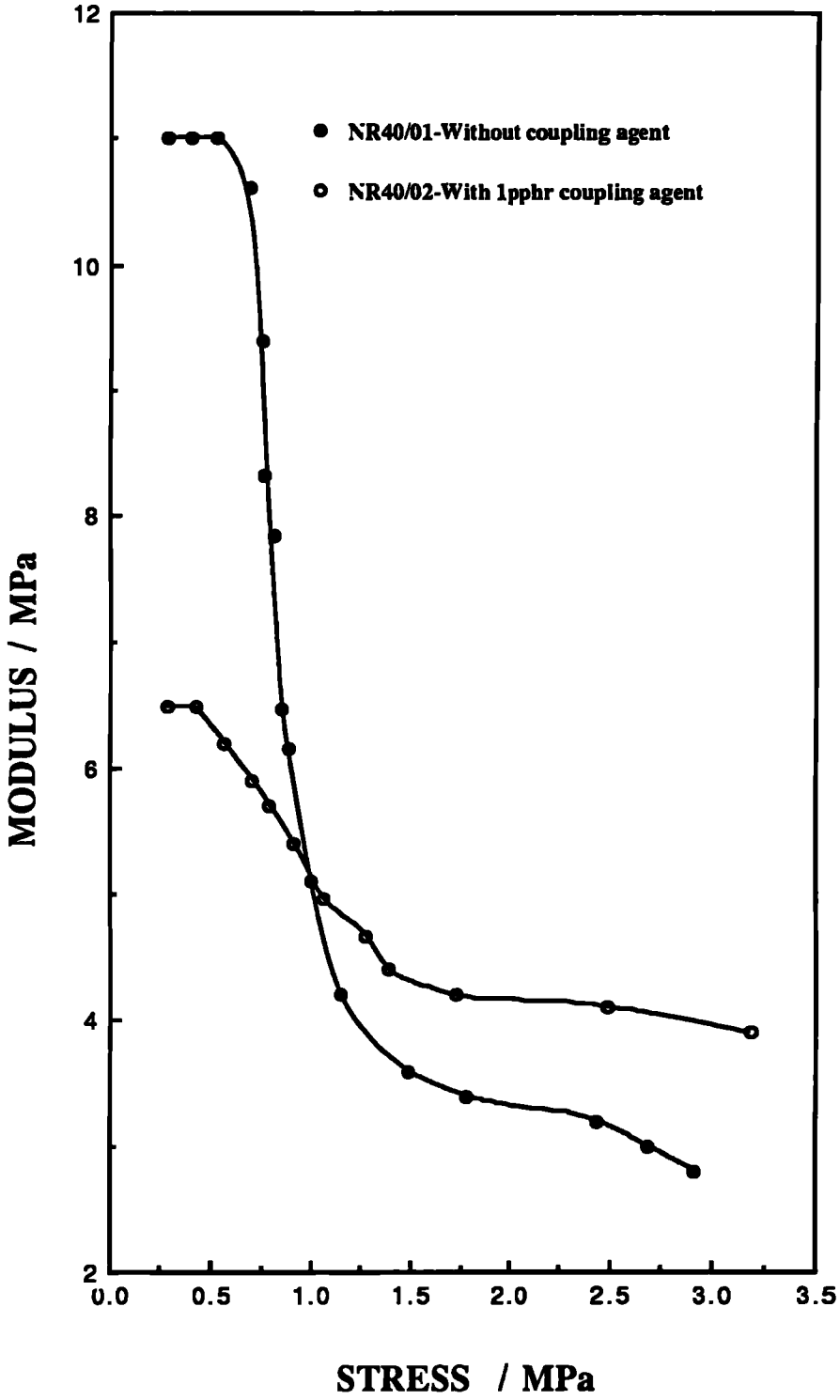

Figure 5.8 : Plot of modulus, obtained from the initial slope of stress-strain curves, against the maximum stresses of silica filled NR vulcanizates.

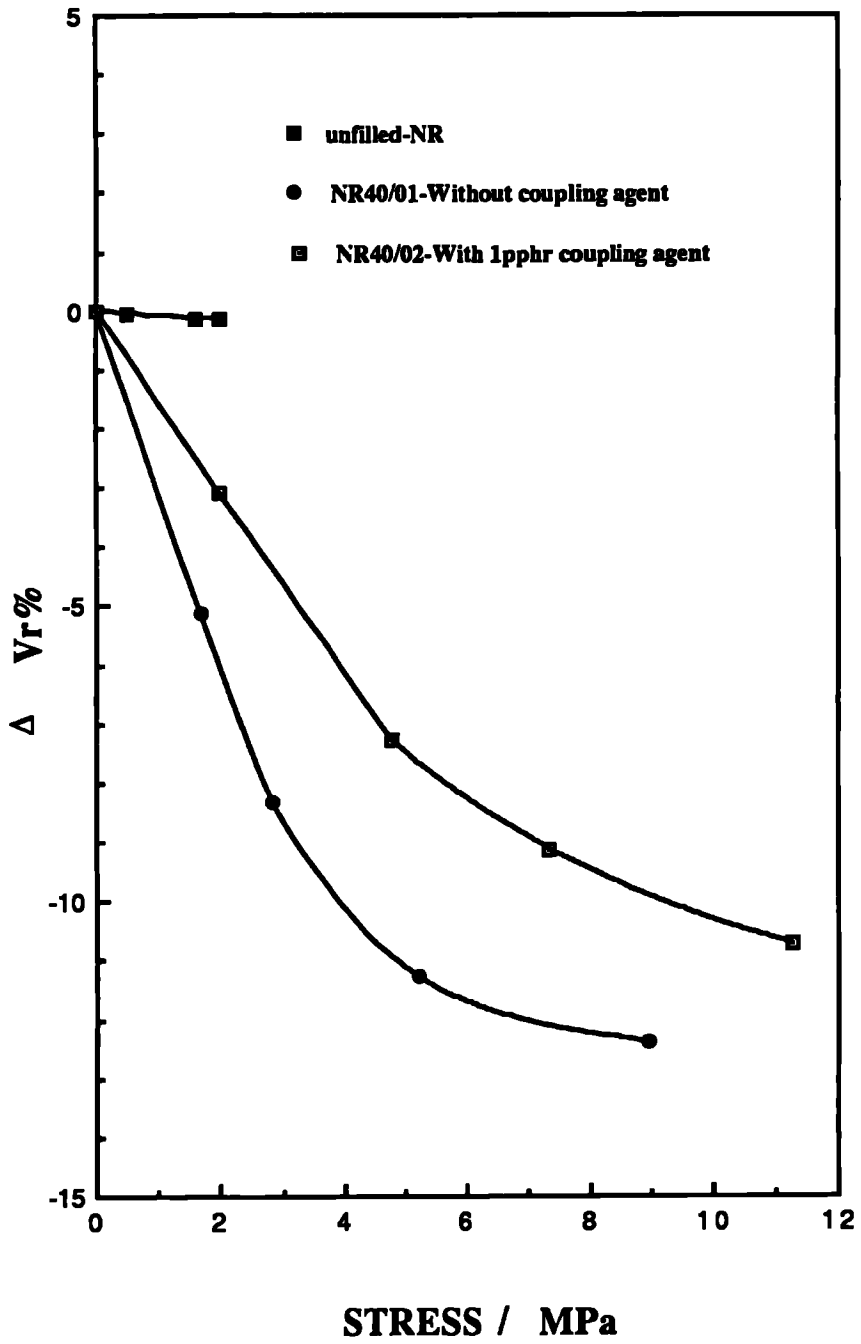

Figure 5.9 : Change in Vr with stressing of silica filled NR vulcanizates.

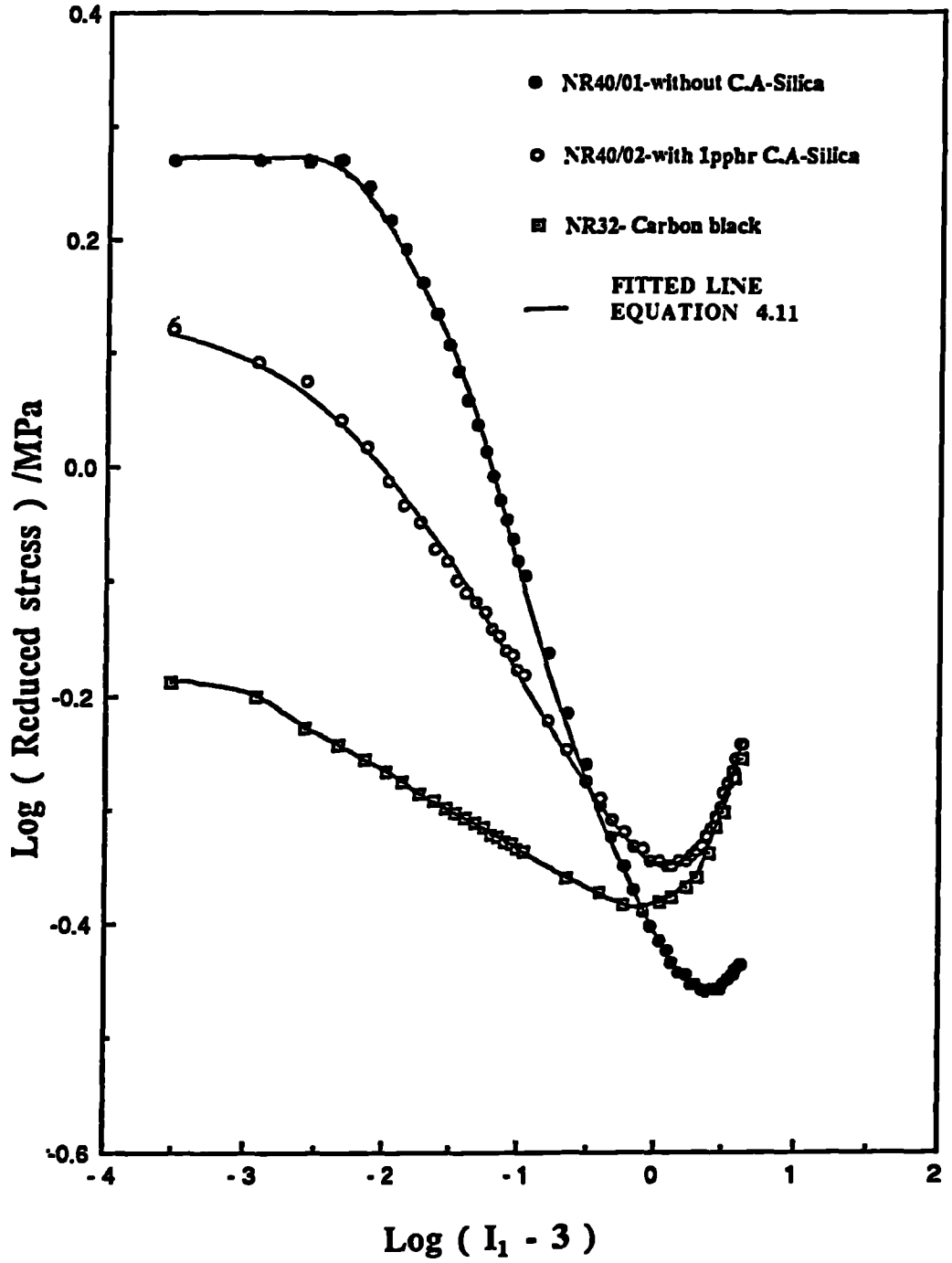

Figure 5.10 : Reduced stress as a function of (I_1 - 3) for silica and carbon black filled NR vulcanizates.

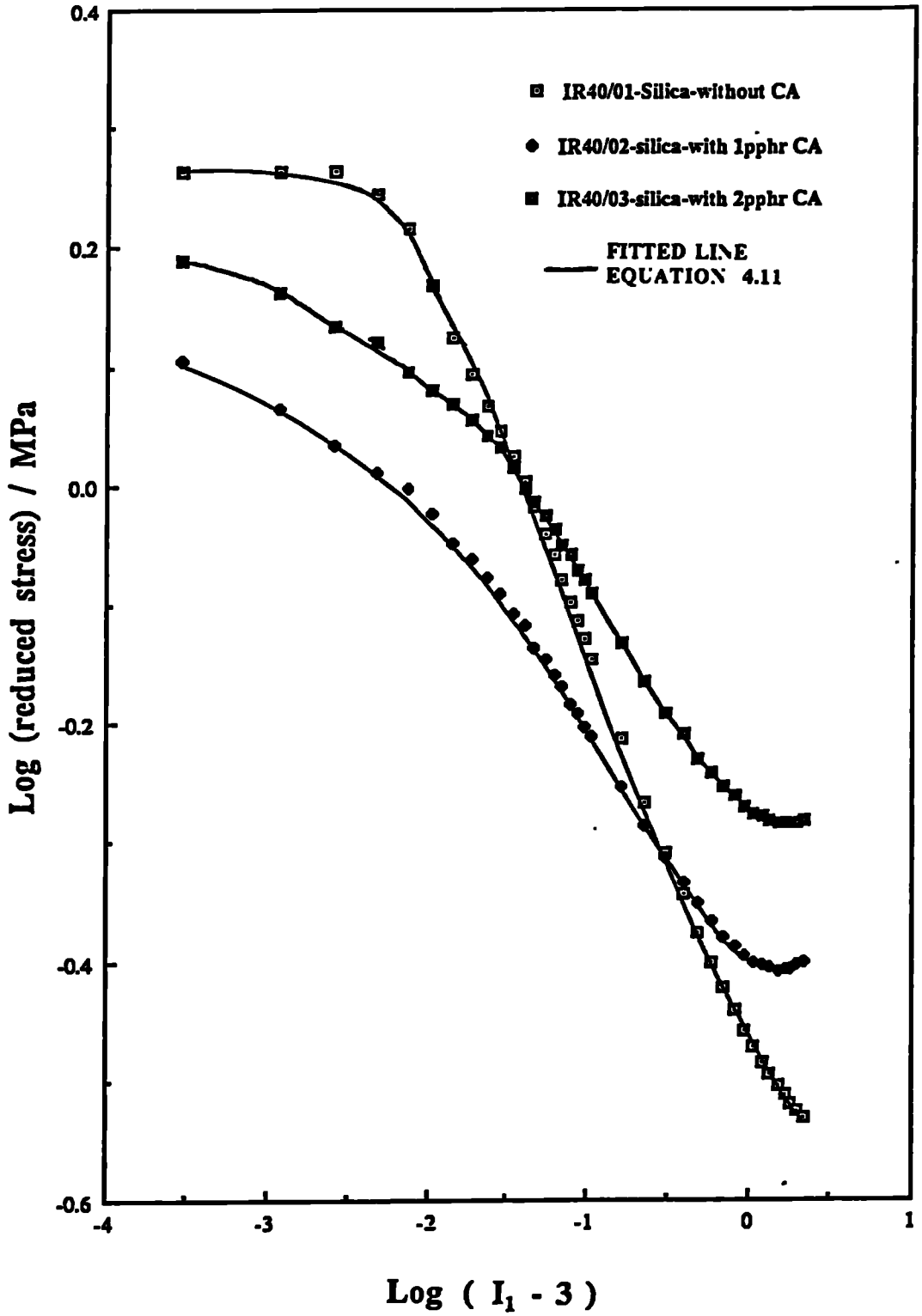

Figure 5.11 : Reduced stress as a function of (I_1 - 3) for silica filled IR vulcanizates.

CHAPTER SIX

6.0 STRESS RELAXATION

6.1 INTRODUCTION

It was observed in chapter four that the modulus of the rubber vulcanizates at a given strain measured dynamically (10th cycle) was less than the static (1st cycle) modulus. This was attributed to the stress-softening effect which occurs to differing extents in both unfilled and filled rubbers. This is an important phenomenon as in many engineering applications rubber components are subject to repeated cycling and the extent of the resulting creep and stress relaxation which results may be significant in determining the effective life of the component.

Derham and Thomas[42] studied the resulting creep strain when either a carbon black filled rubber or an unfilled rubber were loaded and unloaded continuously. They found, contrary to the expectations for an approximately linear visco-elastic material, that the creep rate was greater under cyclic loading (load cycled between zero and F) than under static loading (constant, continuous load, F). The effect was found to be generally more pronounced for the carbon black filled rubber although at high strains (250%) the unfilled rubber exhibited the effect strongly. The enhanced cyclic creep in filled rubbers was thought to result from the cyclic breakdown of the carbon black/rubber interfacial structure. In the highly strained unfilled crystallizing natural rubber, the cyclic creep strain was thought to result from the continuous melting of crystals on unloading yielding additional strain on reloading in the crystal free rubber, prior to subsequent strain crystallization.

In the present case it was decided to investigate the phenomenon of stress relaxation for the carbon black filled Peradin natural rubbers and to carry out similar experiments on both an unfilled NR[25] (EDS19) and a non strain crystallizing SBR (SBR50) containing 50 pphr carbon black, as a basis of comparison. It was decided to measure the dynamic and static stress relaxation (i.e., cycling between 0-50%, 0- 200% etc or maintaining a given λ and measuring the decay of the stress per cycle or per time) rather than creep. The two methods of study should depend on the same basic molecular processes but were expected to yield different results which might throw light on the controlling process.

6.2 EXPERIMENTAL PROCEDURE

Strips of rubber 9.8 mm in width, 2 mm in thickness, were tested either statically and dynamically on an Instron tensile testing machine at 23°C.

For the dynamic tests, the strips were cycled from zero strain to selected constant strains for up 1000 cycles at a given crosshead displacement rate. For each strain level the speed of the crosshead and the gauge length were so chosen that the loading and unloading times were 15 seconds each. The loading-unloading data was continuously recorded on a chart recorder. The maximum stress at each cycle was calculated and plotted against the (number of cycles-1) as a double log plot. A typical plot is as shown in figure 6.1 and all are in general straight lines. From these the stress relaxation rates could be determined and represented as the % decrease per decade of cycles.

The static tests were carried out by rapidly stretching the samples to a given strain (in less than 2 seconds depending on the strain) and subsequently following the force decay as a function of time for up to 120 minutes. The forces were recorded utilizing a video camera system. The resulting data was represented by a plot of log stress versus log time as shown in figure 6.2. The resulting straight lines were used to determine the static stress relaxation rates expressed as % stress decrease per decade of time.

6.3 RESULTS

6.3.1 Effect of strain

Figure 6.3 shows a plot of the cyclic and static stress relaxation rate as a function of cyclic strain for NR49.

The rate increases almost linearly with strain for both cases. However the rates continuously diverge as the strain increases with the cyclic rate always higher than the static.

Also shown on figure 6.3 are the results for an unfilled natural rubber. It can be seen that in this case the two rates are similar up to strains of 200%, after this strain the cyclic rate becomes progressively higher. At low strains the unfilled rubber behaves in a simple visco-elastic manner approximately obeying the Boltzmann superposition principle. Furthermore at very low strains it appears that the static and dynamic rates become similar in magnitude for both unfilled and filled rubbers suggesting simple visco-elastic behaviour in all cases at low strains.

It has been suggested that comparison of the stress-strain behaviour of filled and unfilled rubbers should be carried out on the basis of equal stresses rather than equal strains. This is argued because the filler, being inextensible, causes the rubber matrix to be subjected to a strain higher than that on the material overall (the "strain amplification" effect). Thus the stresses are a better measure of the relative deformation of the rubber itself. Figure 6.4 shows the results presented earlier in figure 6.3 reworked on the basis of stress and it can be seen that the effect of filler content is now much reduced.

6.3.2 Comparison between stress relaxation rates in carbon black filled NR and SBR rubbers

The cyclic and static stress relaxation rates for NR49 and SBR50 are shown in figures 6.5 and 6.6 as a function of strain and stress respectively. It can be seen that the cyclic stress relaxation rate is always greater for the NR rubber and that the difference increases with increasing strain or stress. Furthermore the difference between cyclic and static stress relaxation rates is much greater for NR49 than for SBR50.

These differences may be in part due to an enhanced role for strain crystallization with increasing strain in the case of the NR. The picture is confused however by the fact that the static stress relaxation rate, over the strain range studied, for the SBR is greater than that for NR due to the former being more hysteretic due to its higher glass transition temperature.

6.3.3 Effect of carbon black content on static and cyclic stress relaxation rates in NR

Static

The static stress relaxation rates for the carbon black filled Peradin natural rubbers are shown as a function of strain in figure 6.7 and stress in figure 6.8. In general the rates increases with carbon black content at any strain or stress. The magnitude and form of the curves are consistent with those previously reported for carbon black filled NR by Gregory et al[43]. In the case of the unfilled NR it is only at the higher strains at which strain crystallization occurs that the rate becomes significant.

Cyclic

The cyclic stress relaxation rates for the carbon black filled Peradin natural rubbers are shown in figure 6.9 as a function of strain. In general the rates increase rapidly with increasing strain at a much faster rate than in the static

case (figure 6.8). For a given strain the rate increases with increasing carbon black content. In figure 6.10 the cyclic data is replotted as a function of stress. It can be seen that the differences in rates with carbon black content are now much less suggesting that the molecular network is being subjected to a similar stress cycle in all the materials.

6.4 DISCUSSION

This study has demonstrated the significant enhancement of stress relaxation resulting from cyclic loading compared to that resulting from static loading. The phenomenon is clearly related to the widely observed stress softening effect in rubbers, although this is often mistakenly thought to be virtually complete in a very small number of cycles. This study shows that while the enhanced stress relaxation is logarithmic with time/number of cycles, it continues throughout a component's life.

This enhanced stress relaxation as a result of cyclic loading is at first sight somewhat surprising. For a simple visco-elastic material it would be expected that the cyclic rate, represented as percent per decade, would be rather less than the static as the maximum load in the former case is only applied for a portion of the time. This is in fact what is observed in the case of unfilled natural rubber at low strains (50%,100%, figure 6.9). If the cyclic rate is in fact faster it must result in general, from the process of unloading followed by the extra strain produced during the reloading process.

In the case of unfilled natural rubber both the static and cyclic stress relaxation rates, increase significantly at higher strains, but both appear to be strain independent at the highest strains (figure 6.9). However the cyclic rate is now significantly faster than the static (figure 6.9). It is likely that the process is associated with that of strain crystallization which increases in extent with increasing strain. In a static test the formation of crystallites leads to local stress concentrations (due to the modulus difference) and enhanced strain, as well as some local bond fracture[42]. In this case, when the strain is removed the crystals will melt. Re-application of the strain will require a smaller force to produce a given strain in the regions of bond breakage with new crystals forming at random in all regions. The process would be repeated at each cycle leading to the measured stress relaxation rate. The much lower cyclic rates found with the non-strain crystallizing

SBR gives some support to this view, although the effect on SBR seems rather large for a non-strain crystallizing rubber.

The addition of carbon black to natural rubbers produces a large continuous increase in the cyclic stress relaxation rate when measured at a given strain as the carbon black content increases (figure 6.9). However very similar rates are observed at all carbon black contents at a given stress (figure 6.10). This suggests that while the carbon black significantly stiffens the rubber the molecular stress relaxation processes does not depend significantly on the carbon black. The process is hence still essentially one of molecular breakage at crystal boundaries although a possible minor role of some rubber/carbon black debonding can not be ignored. In the case of carbon black filled SBR (figures 6.5 & 6.6) the smaller (compared to NR) but significantly faster cyclic stress relaxation rates at high strains (compared to static) may be associated with a weak orientation/strain crystallization effect but now, relatively speaking, the role of rubber/carbon black debonding may be significant. It is interesting to note that at low strains/stresses the static rate is actually greater than the cyclic in the filled SBR as would be expected from simple visco-elastic behaviour. This supports the suggestion that some effect akin to crystallization occurs to a minor extent at high strains in SBR.

It is interesting to compare the cyclic creep results determined by Derham and Thomas[42] with the cyclic stress relaxation results from this study. This is shown in figures 6.11 & 6.12 in a limited manner for an unfilled NR compound and NR49 with 49 pphr carbon black (stress relaxation) and NR with 40 pphr carbon black (creep) as functions of strain or stress. The differences in carbon black content should not significantly affect the comparison as the stress relaxation rates as a function of stress are not very sensitive to carbon black content (figure 6.10). It can be seen that for both the filled and unfilled materials the two types of data exhibit a very similar dependence on the applied stress or strain. At low stress, prior to strain crystallization, the rates are low, increasing rapidly with stress as the strain crystallization extent increases. At the highest stresses for the unfilled NR both the cyclic creep rate and the cyclic stress relaxation rate appear to be stress independent. However over this stress range both the cyclic creep rates and cyclic stress relaxation rates continue to increase with stress for NR40 and NR49 respectively. This suggests that carbon black modifies the behaviour significantly in this stress range.

The magnitudes of cyclic creep rates and cyclic stress relaxation rates as a function of strain are surprisingly similar. In general the relation between static creep and static stress relaxation will depend on the form of the stress-strain relation[44] and equality in rate would only be expected for a linear relationship. The first cycle stress-strain curves in the present case are certainly non-linear with considerable hysteresis. It may be however that the effective cyclic stress-strain curves, over any particular range of stress, are more linear with less hysteres's resulting in the surprising agreement between the magnitudes of the creep and stress relaxation results.

This chapter has clearly demonstrated the importance and magnitudes of cyclic stress relaxation in the filled Peradin rubbers and in unfilled rubbers. Some insight has been given as to the mechanisms producing the additional cyclic strain in crystallizing rubbers but the picture for non-strain crystallizing rubbers is far from clear.

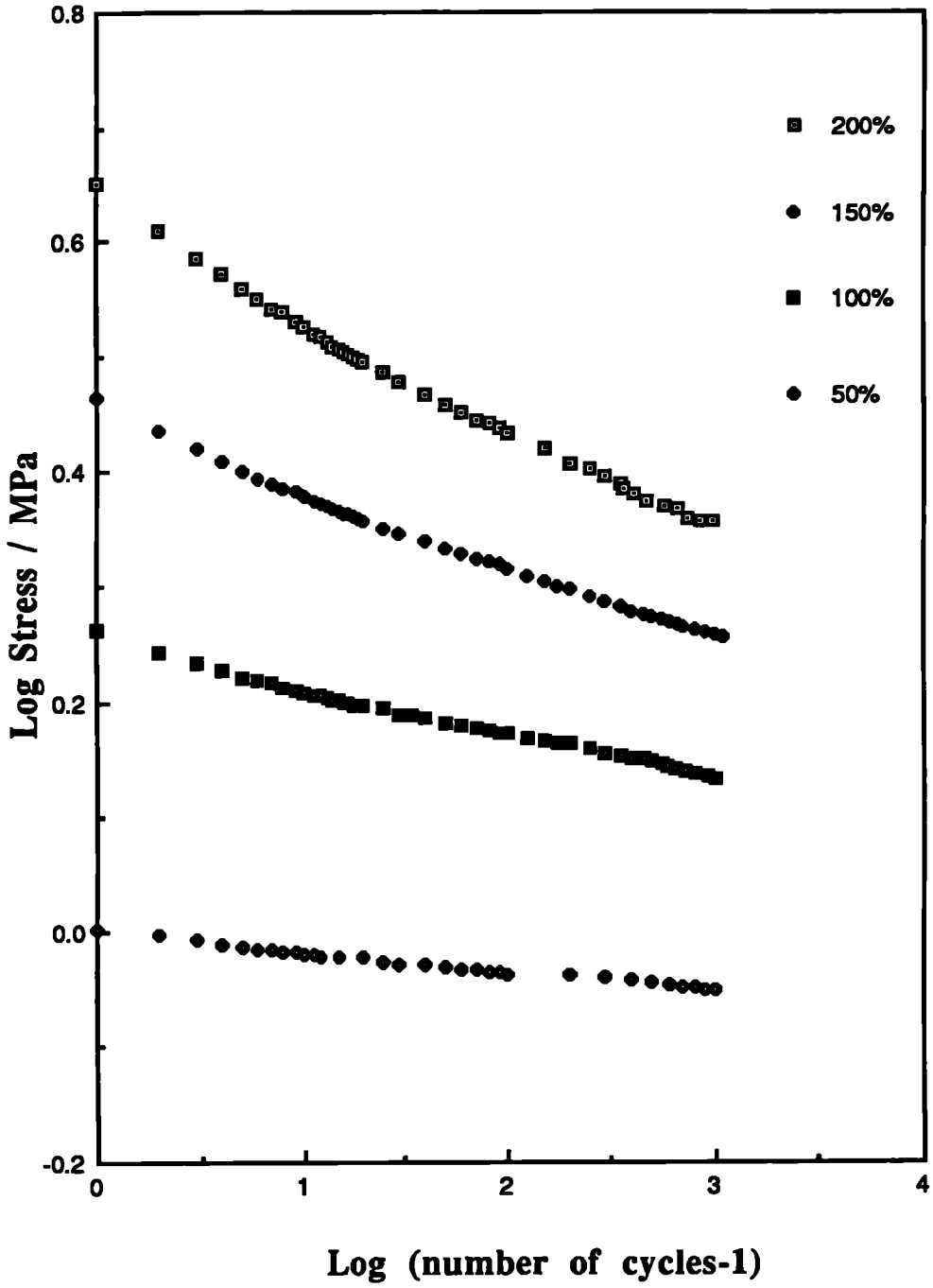

Figure 6.1: Decrease in stress as functions of number of cycles at different cyclic strains for NR49

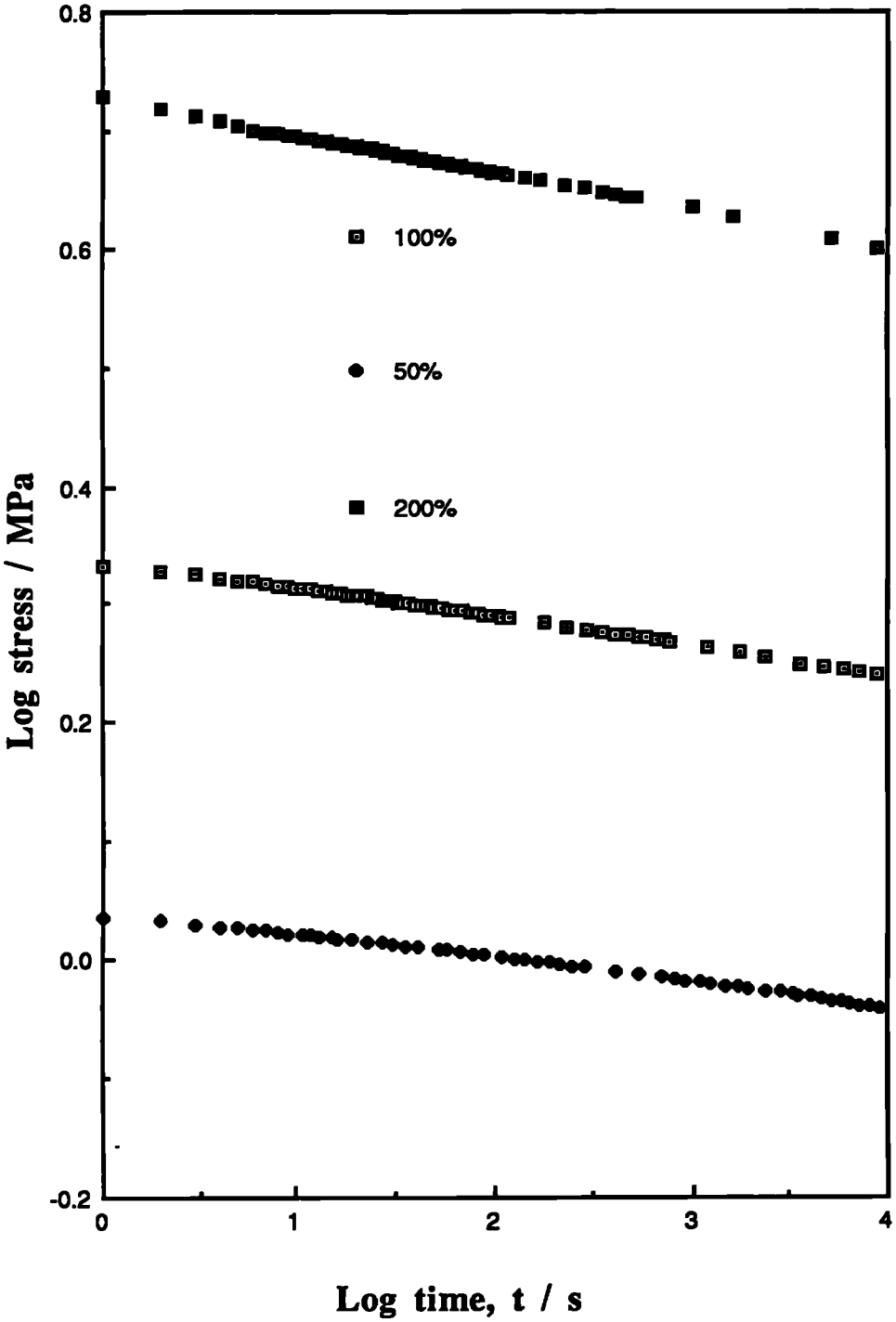

Figure 6.2 :Decrease in stress as functions of time at the different initial static strains for NR49

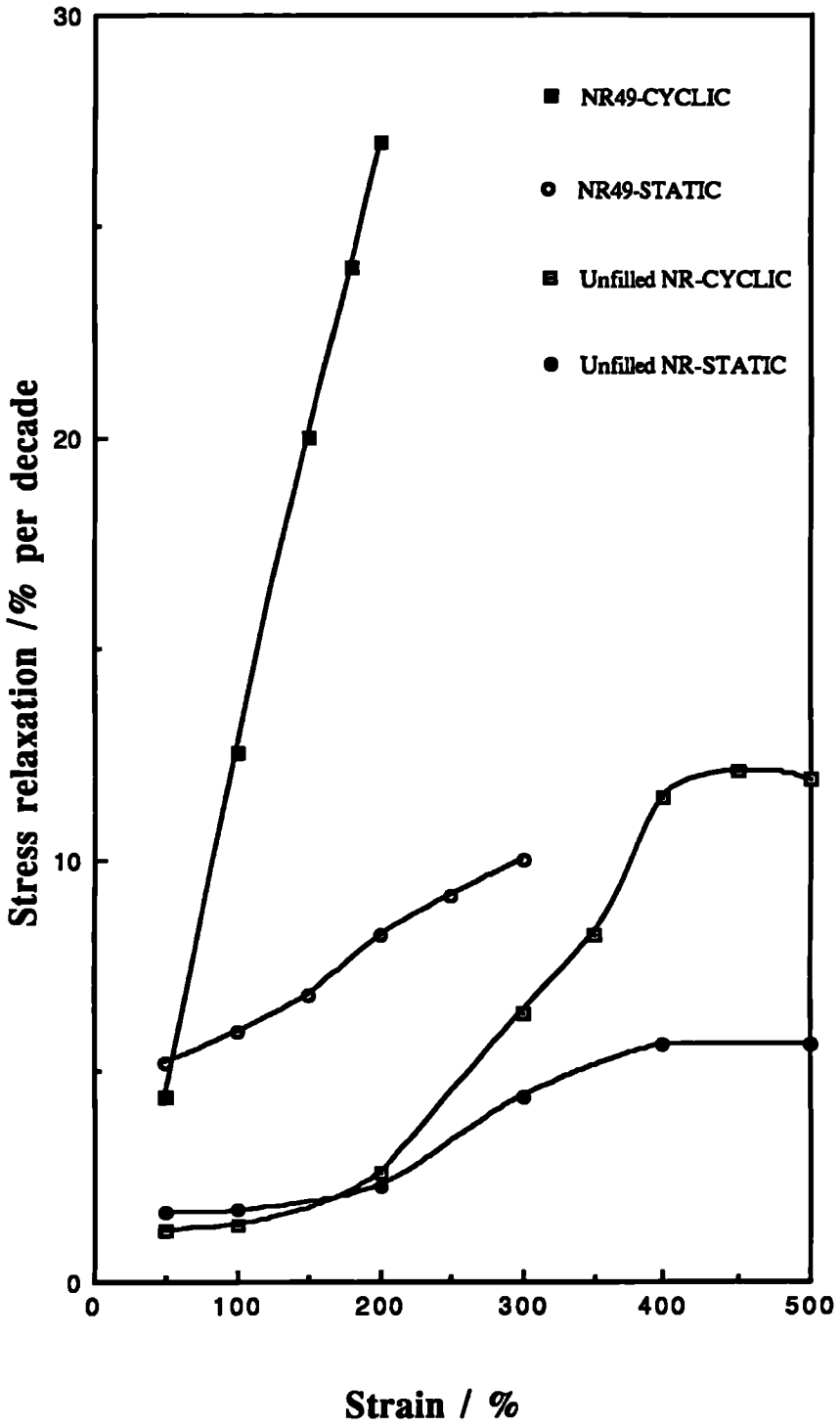

Figure 6.3 : Cyclic and static stress relaxation rates for an unfilled NR and one 49 pphr carbon black filled rubber as functions of the initial strain

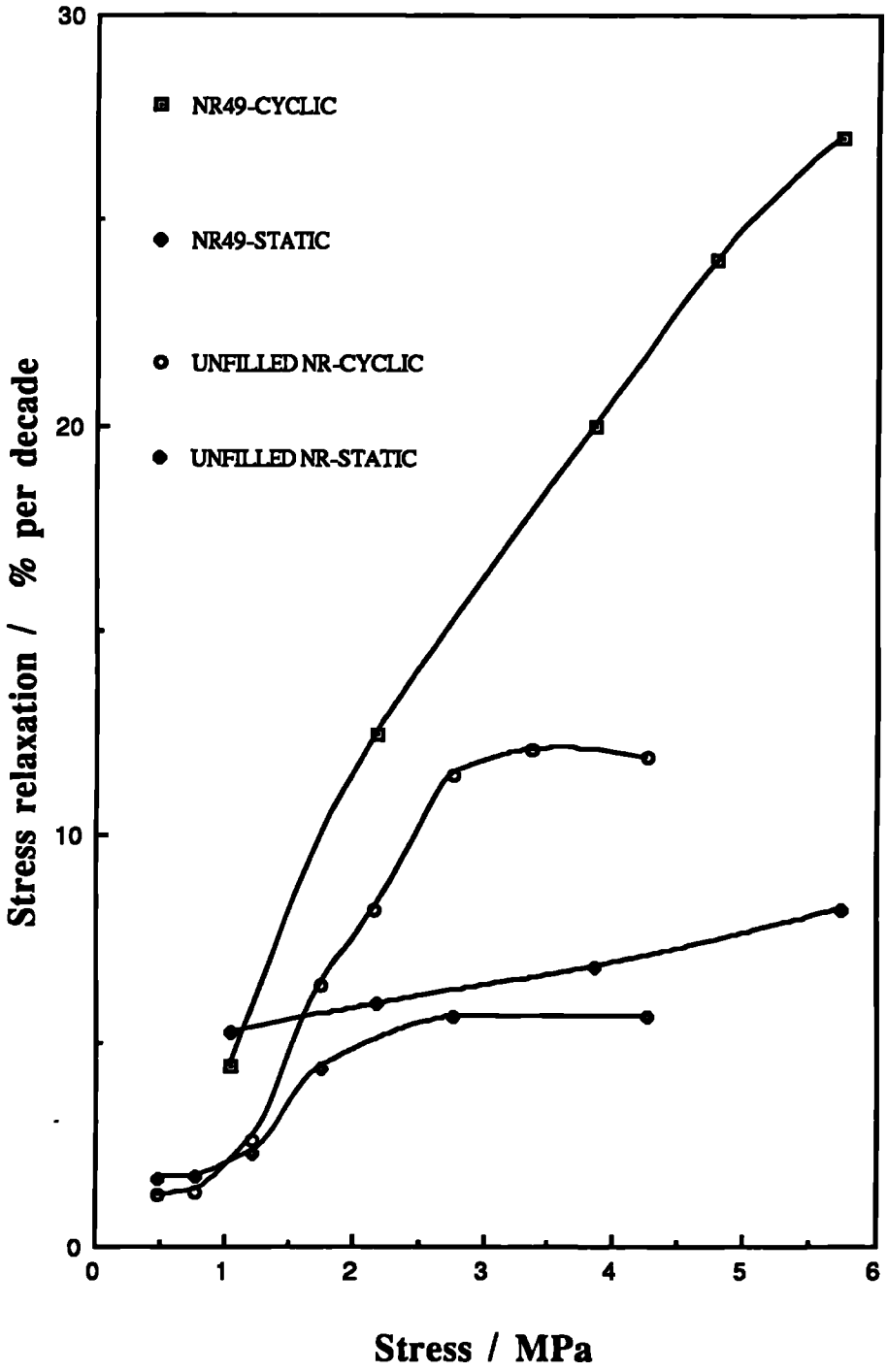

Figure 6.4 : Cyclic and static stress relaxation rates as functions of the applied stress

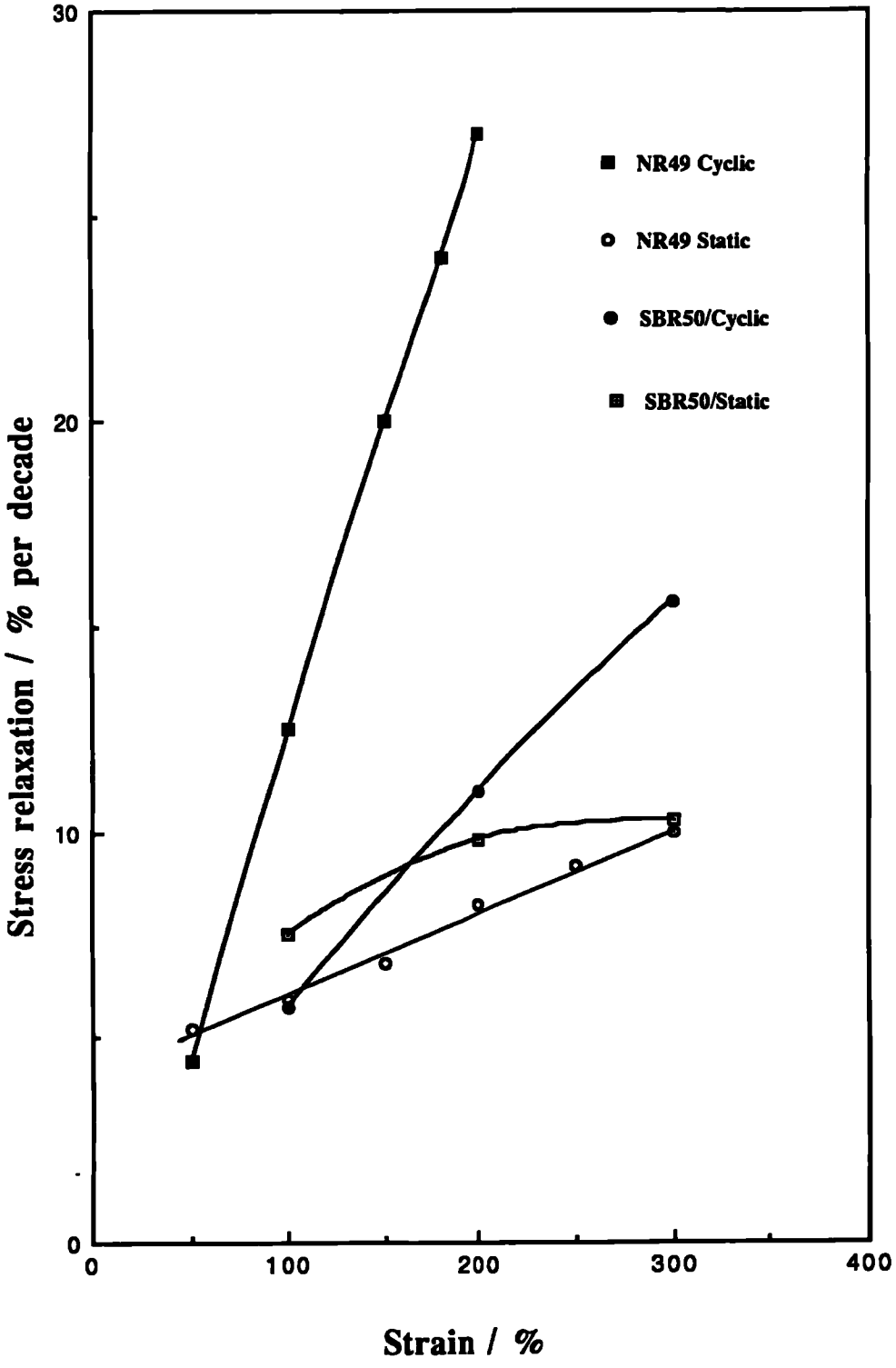

Figure 6.5 :Cyclic and static stress-relaxation rates for the carbon black-filled NR (NR49) and SBR (SBR50) as functions of the initial strain

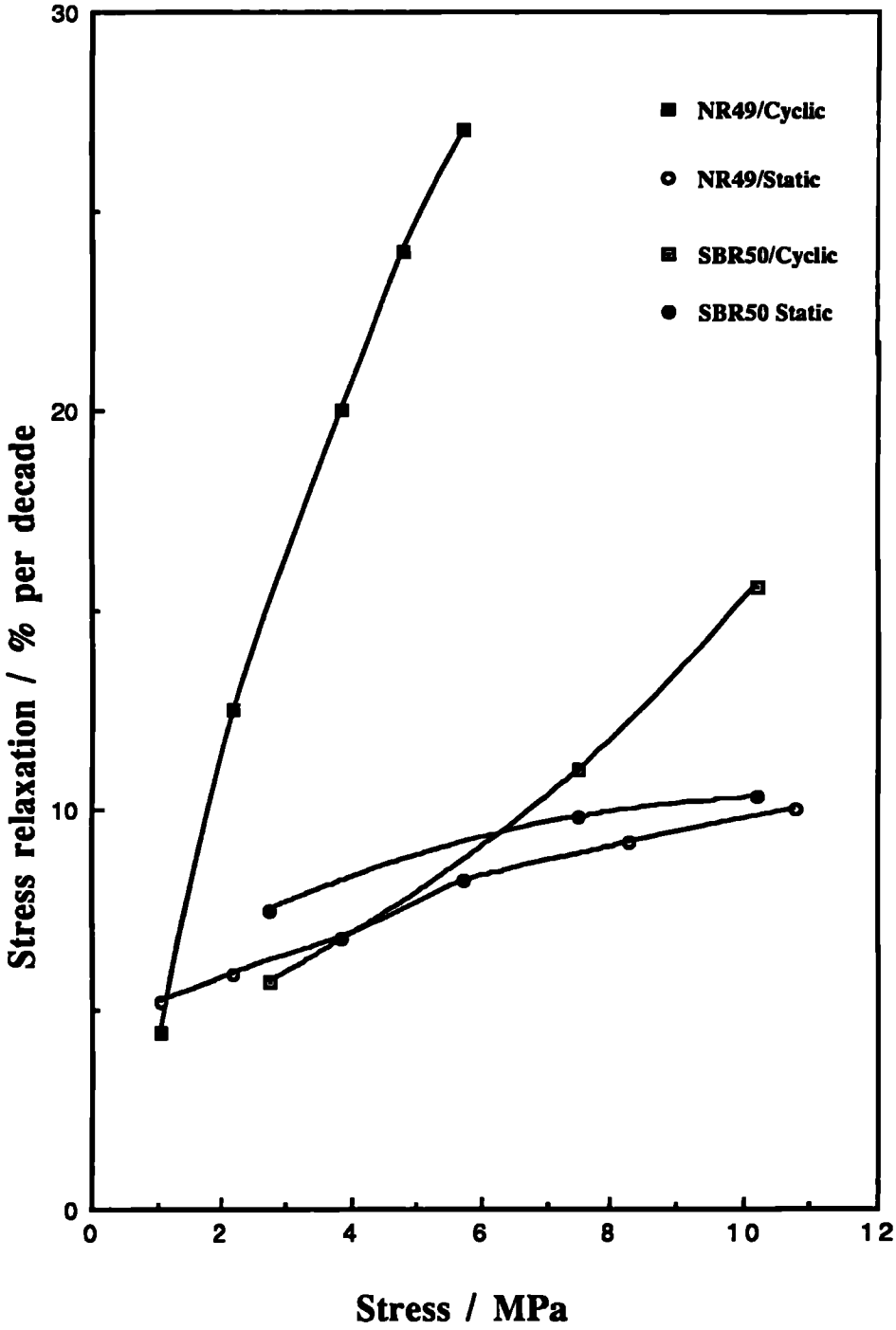

Figure 6.6 :Cyclic and static stress relaxation rates for the carbon black filled NR (NR49) and SBR(SBR50) as functions of the applied stress

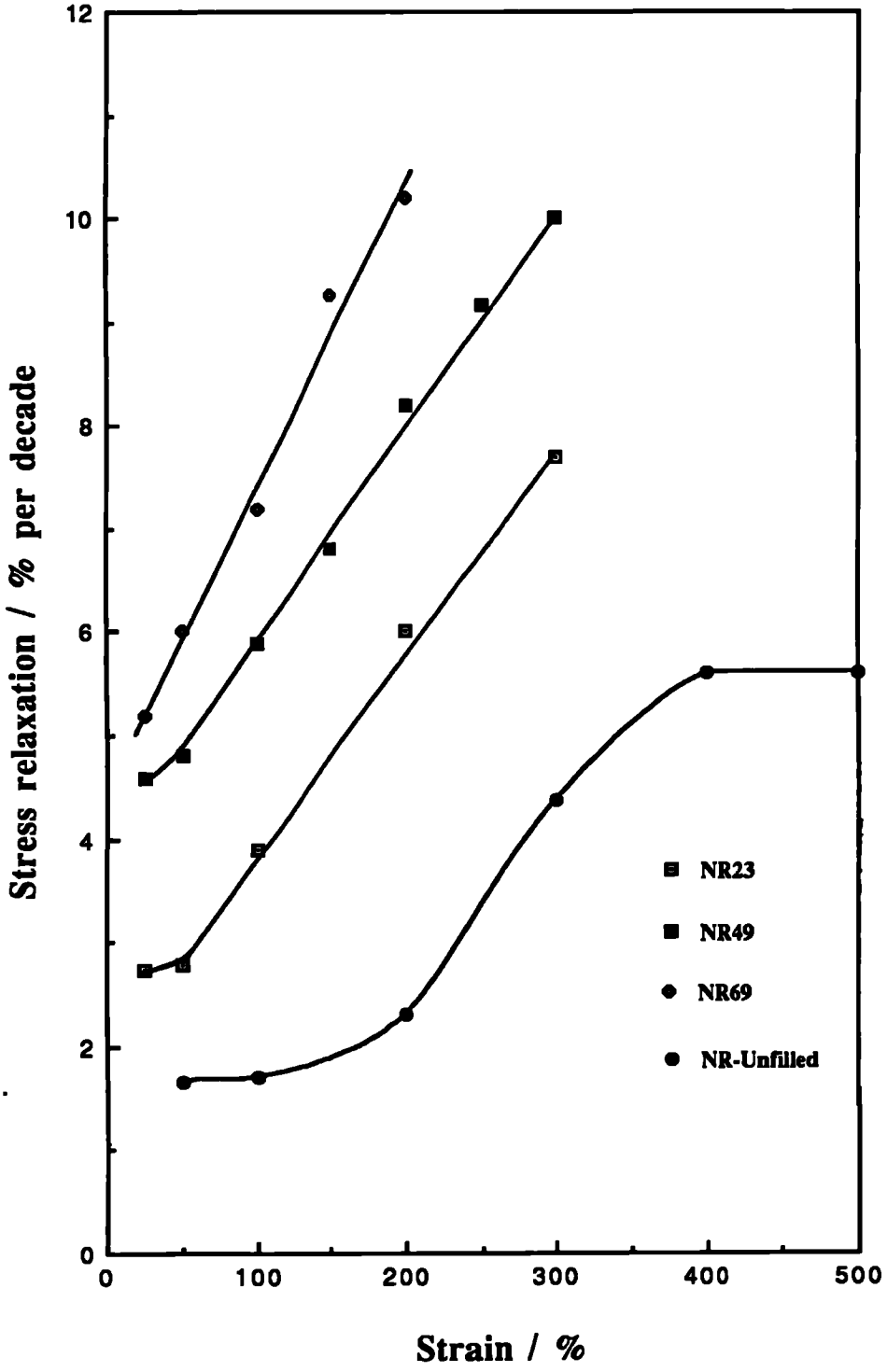

Figure 6.7 :Dependence of static stress relaxation rates on carbon black content as functions of the initial strain

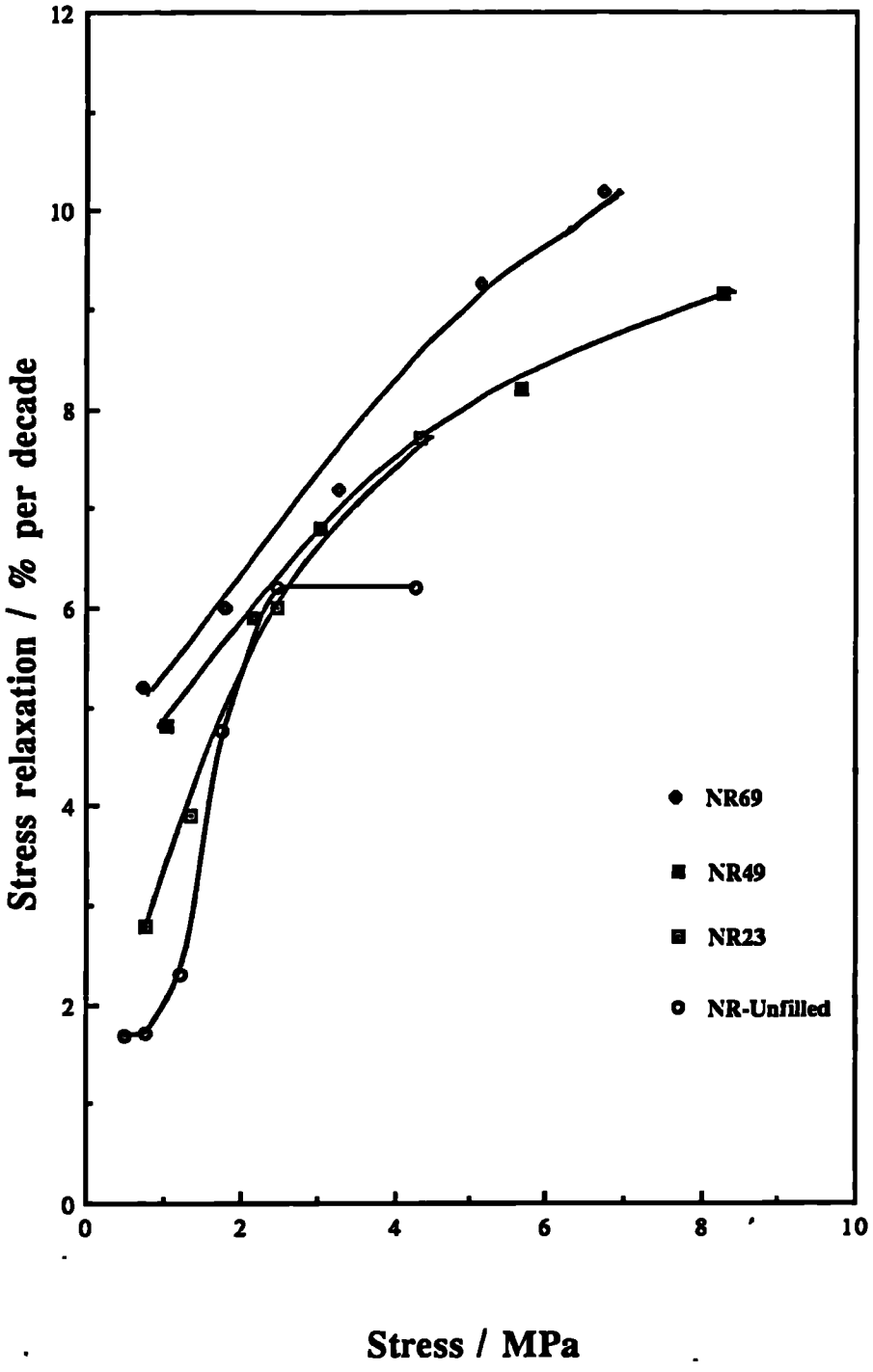

Figure 6.8: Dependence of static stress relaxation rates on carbon black content as function of the applied stress.

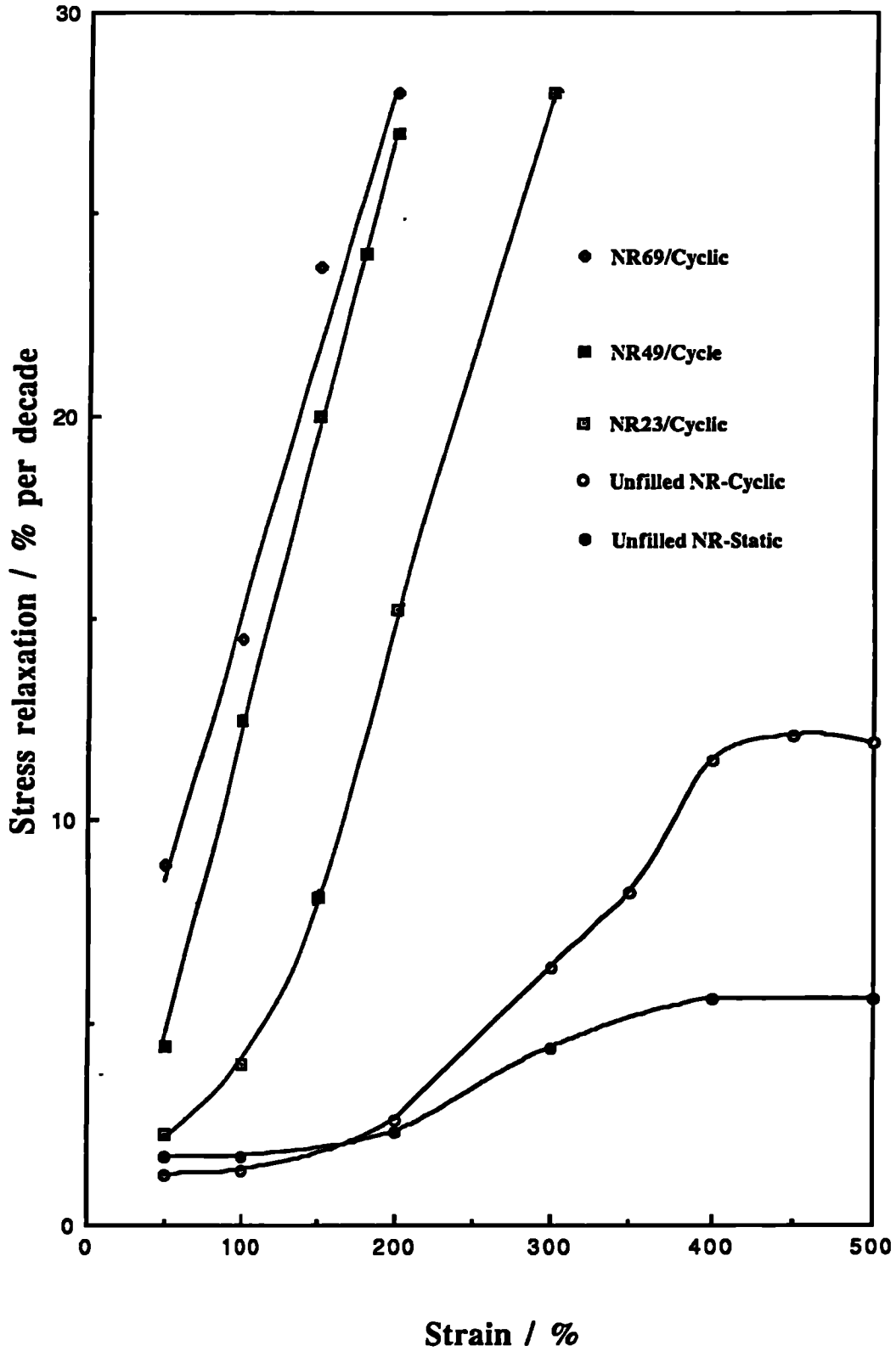

Figure 6.9 :Dependence of cyclic stress relaxation rates on carbon black content as functions of the initial strain

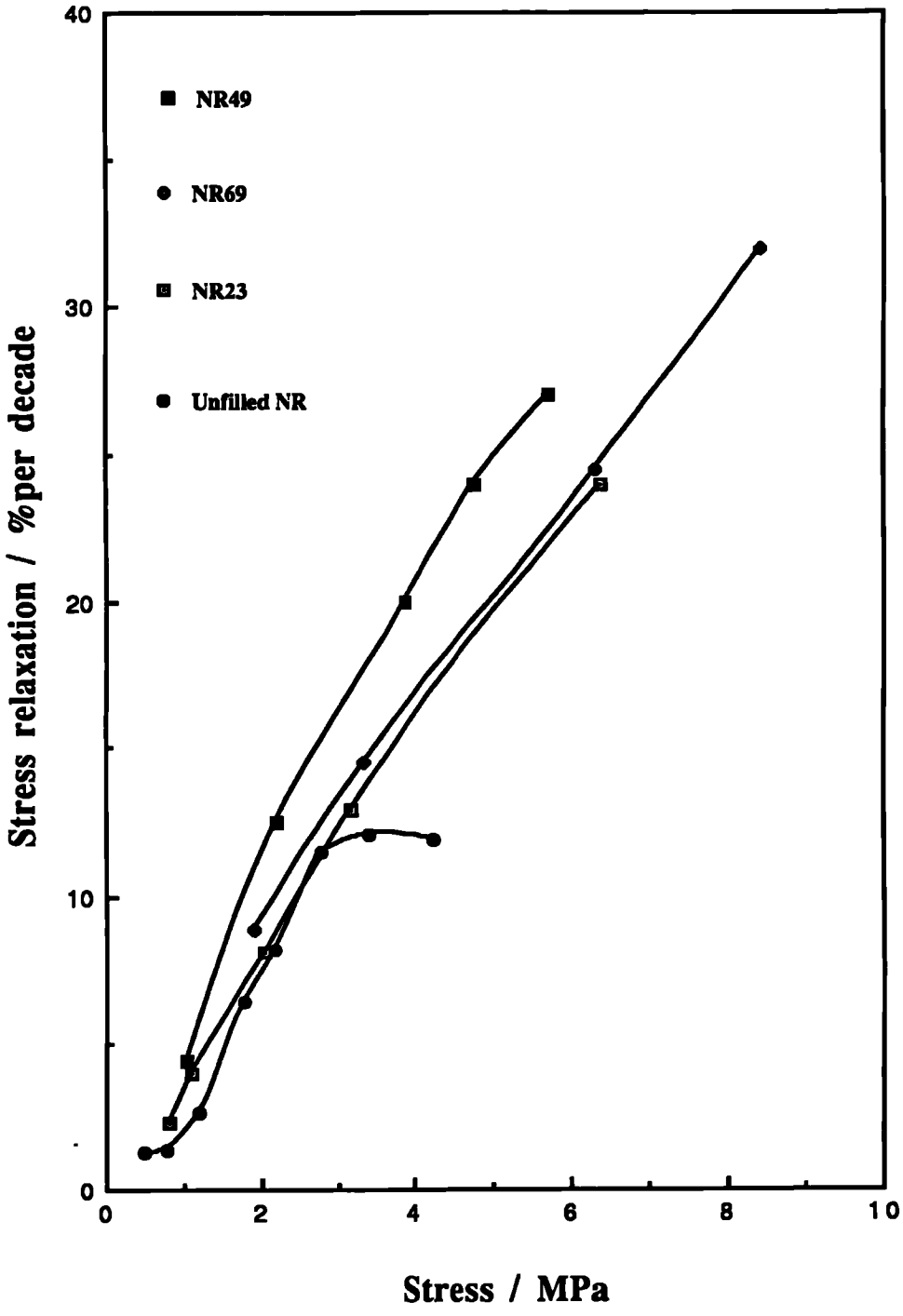

Figure 6.10 :Dependence of cyclic stress relaxation rates on carbon black content as functions of the applied stress

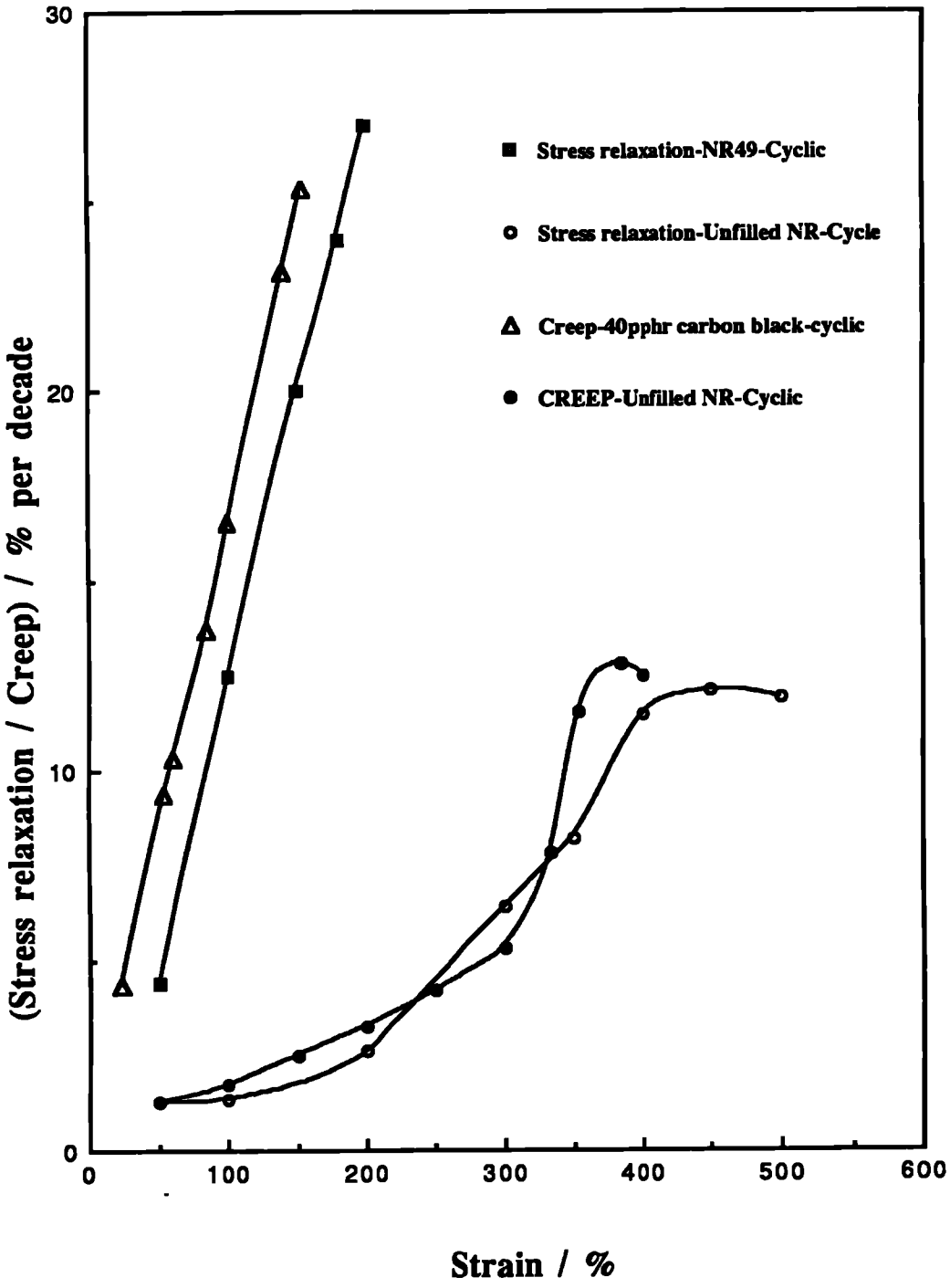

Figure 6.11: Cyclic stress relaxation rates for an unfilled NR and one 49 pphr carbon black filled rubber as functions of the initial strain and compared to creep data of 40pphr carbon black filled NR and an unfilled NR (data from ref 42).

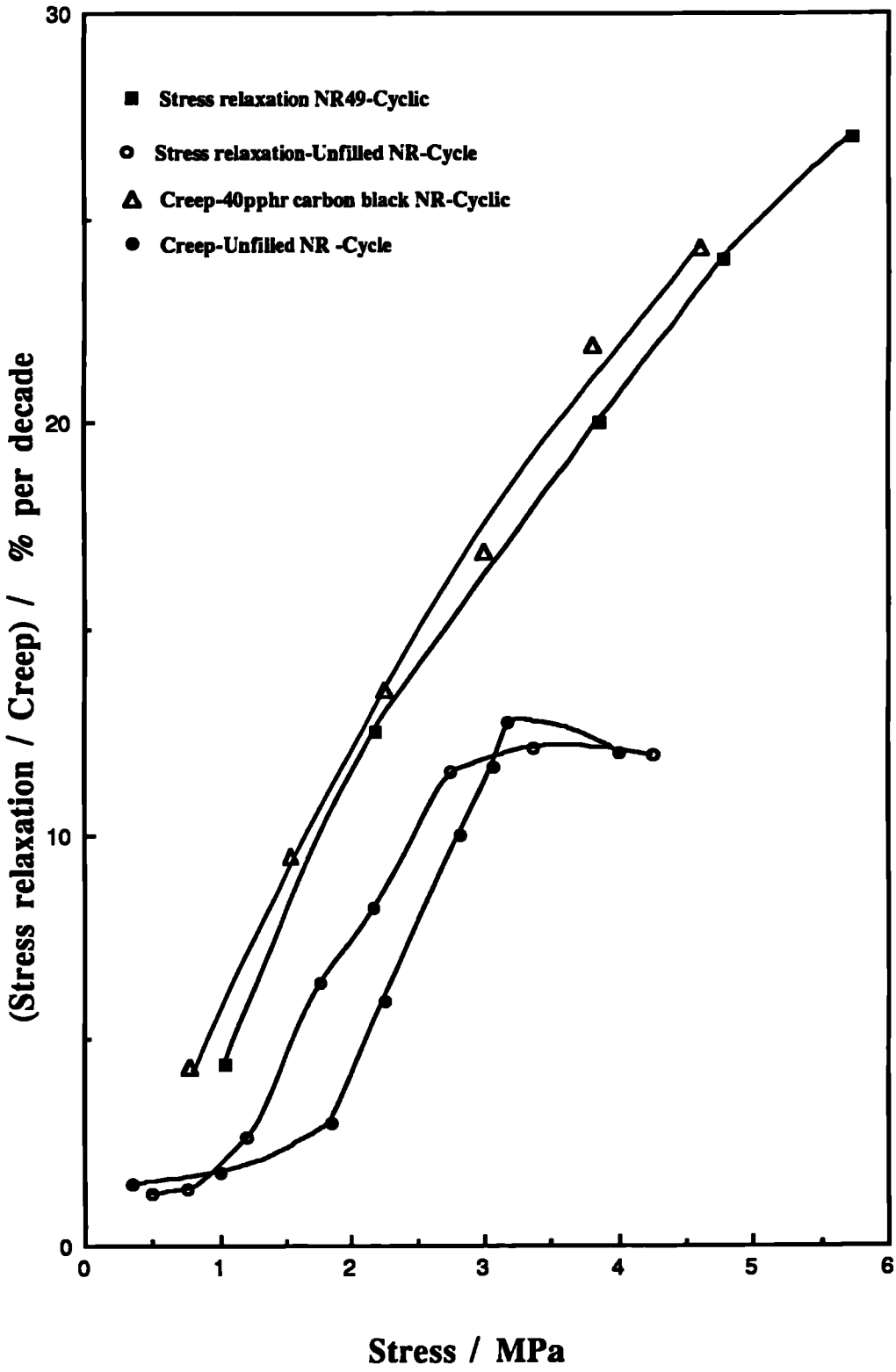

Figure 6.12 : Cyclic and static stress relaxation rates as functions of the applied stress and compared to cyclic creep data (ref 42).

CHAPTER SEVEN

7.0 INTRODUCTION-TEARING

The previous chapters carefully characterized the stress-strain behaviour of both the carbon black and silica filled rubbers used throughout this study as a function of filler content, crosslink density etc. A new strain energy function was proposed which enables the strain/stored energy to be determined relatively easily. Studies of the tear behaviour and fatigue crack growth of rubbers are generally based on a fracture mechanics approach utilizing the concept of the release of elastic stored energy as a tear/crack grows. This chapter deals with the tear behaviour of the study rubbers with cyclic crack growth/fatigue being dealt with in a latter chapter. The chapter reviews previous work particularly with respect to the effect of filler content on mechanisms and regimes of tearing. In the light of this, the aims and scope of the present work are set and are followed by experimental procedures and results sections. The tear data is then discussed particularly with respect to the effect of materials variables on the observed regimes of tearing.

7.1 GENERAL TEARING BEHAVIOUR

The most convenient way to introduce the tearing behaviour is in terms of a trouser tear test, although as will be seen this is not the only test geometry employed by investigators and furthermore the tearing energy measured by the test has a general applicability. The test consists of extending a pre-cut rubber test piece (figure 7.1a) at a constant rate in the geometry shown in figure 7.1(b) and measuring the resultant force (figure 7.1c). There are two extremes of tearing behaviour observed in rubber vulcanizates termed steady and unstable tearing. In the first the tear propagates at a generally constant rate and at a constant force (figure 7.1c.2). In the second (figure 7.1c.1) the tearing force cycles between maximum and minimum values and although an average tearing rate can be calculated it becomes less meaningful as the tear initiation force and the tear arrest force became more widely different. These extremes of tearing behaviour are characterized by relatively smooth torn surfaces (steady tearing) and gross surface roughness (knotty tearing) in the case of unsteady tearing. The actual tearing behaviour observed is not only dependent on materials variables (i.e., strain-

crystallizing/non-strain crystallizing rubbers, filler type/content, crosslink density etc.) but also on the testing regime (i.e., temperature, imposed extension rate).

7.2 GENERAL TEARING ENERGY THEORY-STEADY TEARING

Conventional tear tests results are usually expressed in terms of the tear resistance i.e., the force require to tear a specimen of given thickness. Such tear tests are strongly dependent on the types of specimens used [ASTM D264] and the way the force is applied. Thus measured tear resistance is not a characteristic property of the material.

The need to derive a material specific parameter was treated by Rivlin and Thomas[29] who considered the tear process from an energy stand-point rather than one based on force. In so doing, they applied Griffith's fracture criterion[45], but with a modification to allow for the irreversible energy dissipation which occurs in the highly strained regions around the neighbourhood of the tear tip. The energy required to create new surfaces by the tearing process is defined as the tearing energy. Like Griffith[45], they also postulated that a cut in a strained body would grow only if the elastically-stored strain energy released when the cut grew equalled or exceeded the critical tearing energy or mathematically

$$-1/h \left(\partial W / \partial c \right)_{\ell} \geq T_c \qquad (7.1)$$

Where W is the total elastic strain energy stored in the test-piece, h is the thickness measured in the unstained state, c is the length of a cut, and T_c is the critical tearing energy of the material. The partial derivative indicates that the external forces do not move and hence do no work. The tearing energy represents all the work done during growth of a cut (tear), and has been shown to be largely independent of the overall shape of the test-piece and the way the forces are applied, and as such can be employed as a characteristic property of the material[29]. The validity of this approach has been established by many workers[46,47] and is illustrated in figure 7.2 for an unfilled SBR rubber tested under steady tearing conditions using a variety of test-piece geometries. The geometry of the test pieces are illustrated in Appendix 7.1 together with the relevant equations to determine the tearing energy.

Thomas[48] extended this tearing energy theory by considering the strain-concentration at an incision. Modelling the incision as a parallel-sided slit terminated by a semicircle, he showed that the tearing energy, T is approximately equal to d.W, where d is the diameter of the tip and W is the elastically stored energy per unit volume in the rubber i.e.;

$$T = d.W \qquad (7.2)$$

If the test-piece is pulled to rupture, W represents the work to break per unit volume of rubber W_B and the above relationship becomes;

$$T = d_B.W_B$$

$$\text{or} \quad W_B = T/d_B \qquad (7.3)$$

Thomas examined the validity of equation (7.2) by making incisions of varying tip diameter in the range of 1 mm to 3 mm and measuring the corresponding tearing energies. He showed T/d to be fairly constant and approximately equal to the work to break (W_B) as obtained from uniaxial tensile tests.

Greensmith[49] made further progress by comparing the tearing energy for a tear propagated at various rates and W_B measured in tension on test-pieces extended at various rates (imposed rates varying from 0.1 to 2000% /sec). He expressed the results by plotting T/d and W_B against the reciprocal of the time to break, t, as shown in figure 7.3 for an unfilled and a filled SBR vulcanizate respectively. In both cases, T/d and W_B are comparable in magnitude and showed a similar dependence on time, except that T/d was consistently somewhat higher than W_B. The flaw theory of tensile strength was invoked to account for this[48]. It is known that the tensile strength decreases as the volume of the test piece increases[50]. This is attributed to the fact that, as a matter of probability, there will be more flaws and larger flaws in a large test piece than in a small one. In tearing, the volume at the tip of the tear which is highly stressed is much smaller than in a tensile test specimen, hence in tearing there may be an apparent somewhat greater strength and energy absorption per unit volume than anticipated from a tensile test even at the same rate of elongation.

In the case of steady tearing initiated from a sharp tear tip, the observed roughness of the torn surface is only a few tenths of a millimetre. The observed tearing energy is much higher than that obtained from the

energy to break multiplied by this apparent observed torn surface tip diameter, particularly at high tear rates and in the case of filled SBR rubbers when they tear in a steady manner. The tear hence behaves as if it had a much larger tip diameter than that estimated from the observed surface roughness. Although in steady tearing the tear tip is very sharp, the diameter of the highly strained region at the tear tip (d_H) is larger than the diameter of the tip itself because in order to break a bond laying across the tear path it is necessary to deform a large volume of material around the tear tip[51]. As the tear advances, this highly strained region is relaxed and the dissipation of energy occurs. Thus most of the work done in the case of steady tearing is associated with the hysteresis loss (W_H) in this highly strained region rather than the work to break molecules at the tip of tear. In fact it is this effect which directly gives rise to the observed temperature and strain rate dependences of the tearing energy during steady tearing. It would be expected that the magnitudes of both W_H and W_B change in a similar manner with temperature and strain rate, as W_B, as measured from a tensile test, must be dependent on visco-elastic effects, except at the lowest strain rates and highest temperatures. It is hence not usually possible during steady tearing to distinguish between, $T= W_B.d_B$ and $T = W_H.d_H$, as is not possible to estimate d_B and d_H to the required accuracy.

7.2.1 Threshold tearing energy (T_o)

It has already been mentioned that irreversible energy dissipation occurs in the highly strained region around the tear tip during tearing of a rubber vulcanizate. However, under certain conditions, when this dissipation at the tip of the tear is minimised; the rubber vulcanizate has a minimum tearing energy[52,53]. This minimum tearing energy has been termed the threshold tearing energy. The threshold limit of the tearing energy was first noted by Lake & Thomas[54] in a cyclic crack growth test. They defined T_o as the minimum tearing energy at which cyclic crack growth will occur. The crack growth behaviour under cyclic conditions will be addressed here in a subsequent chapter. The threshold tearing energy of rubbers has been determined experimentally by many workers[52,53,55,56]. They conducted experiments at low rates, high temperatures and/or under swollen conditions, to minimize energy dissipation at the tip of tear, using trouser test-pieces. The magnitude of T_o is found to lie in the range of 0.040-0.080 KJm^{-2} for a wide range of strain and non-strain crystallizing rubbers which differ greatly in tensile strengths and tear strength (force required to tear a

specimen of given thickness). It was shown by Lake and Thomas[54] that, if the long-chain molecular network structure of a rubber was taken into account, then the T_o value could be closely identified with that necessary to break the molecular chains that lie in the path of the growing tear (figure 7.4). In the theory for T_o, Lake and Thomas assumed that d has the minimum possible value (d_o) for an elastomer while W has the maximum possible value (W_o) determined by the bond strength. Thus, on a molecular scale equation 7.2 becomes;

$$T_o = W_o . d_o \qquad (7.4)$$

It should be noted that under the conditions referred to in effect $W_B = W_H = W_o$ and $d_B = d_H = d_o$

In rubber, in order to break a bond crossing the fracture plane it is necessary to stress many other bonds in the same network chain and lying between the crosslinks at the ends of the chain, essentially to their breaking points. Values of T_o calculated from this model were about 0.02 KJm^{-2} which is fairly good considering the assumptions associated with the calculation. This suggests that T_o may be related fairly directly to the strengths of the chemical bonds of the molecules which comprise the material.

The effect of carbon black on T_o has been studied by Bhomick, Gent and Pulford[57]. They carried out the tear test on a pre-scored trouser test-piece swollen with paraffin oil, at high temperatures, 80-150°C, at slow rates, 1-10μms^{-1}. The magnitude of T_o was found to be around 0.2 KJm^{-2}. This indicates that the threshold tearing energy in the case of carbon black-filled rubbers is about four times higher than that for unfilled rubbers. These authors attributed the increase in T_o to the detachment of adhering polymer molecules from particles of carbon black at forces somewhat below those which cause main chain fracture. This process losses energy and increases T_o.

7.2.2 Effect of rate and temperature on tearing energy-visco-elastic effect

The magnitude of the tearing energy depends both on the rate and temperature of tear measurement. This is neatly summarised in the three-dimensional plots of tearing energy versus tear rate and temperature[58] as shown in figures 7.5a for an unfilled SBR (a non-strain crystallizing

rubber). The tearing energy increases with increasing tear rate or decreasing temperature. This increase in the tearing energy is similar to the increase of energy dissipation in a viscous material with rate of deformation and temperature. Indeed, Mullins[59] showed that the tearing energy data for a range of non-strain crystallizing rubbers is proportional to the shear loss modulus which is a direct measure of energy dissipation. Thus, internal energy dissipation (hysteresis) determines the tearing energy which is controlled mainly by the internal viscosity of the material. He also showed as shown in figure 7.6a that the tearing energy data for the unfilled SBR of figure 7.5a at different rates and temperatures could be superposed to yield a single curve using a form of the WLF[60] equation i.e.,

$$\text{Log } a_T = \frac{C_1 (\theta - \theta_S)}{C_2 + \theta - \theta_S} \qquad (7.5)$$

where a_T is the shift factor, θ_S is the reference temperature to which the other isotherms are shifted and C_1 and C_2 are experimental constants. Furthermore, values of tearing energy for five other unfilled non-strain crystallizing rubbers, two butadiene-styrene compolymers having values of θ_g of -72°C and -78°C and three butadiene-acrylonitrile compolymers having values of θ_g of -30°C, -38°C and -56°C, are all seen to fall on a single curve as shown in figure 7.6(b)[59]. The success of this transformation of the data indicates that the visco-elastic behaviour of a rubber can be considered to be a dominating factor in the steady, smooth tearing of non-strain crystallizing unfilled vulcanizates.

7.3 TEARING ENERGY THEORY- KNOTTY TEARING

In the case of knotty tearing, a tear starts to propagate across the direction of extension but halts monetarily and tends to go at right angles, that is, along the line of stretching in either or both directions for a short distance before resuming the main line of progress. The resultant tear surface is rough on a large scale (figure 7.7a) and the force versus distance curves exhibits very large force drops (figure 7.7a). The higher tearing energy usually associated with knotty tearing as compared to steady smooth tearing has been interpreted as arising from blunter tearing tips, the diameters of which are comparable to the scale of the knottyness. The reason for knotty tearing is still not fully understood. The original suggestions were that it might be associated with the development of an anisotropic zone

perpendicular to the direction of the tear, this zone forming barriers in the path of the tear, and resulting in tear deviation or knotty tearing. Greensmith[61] referred to these barriers as the strengthening structures. More recent work[62] has shown that it is the orientation of molecules in the direction of stretching which provides an easy tear path and leads to tear tip deviation or knotty tearing. Tearing is not continuous and the tear does not propagate in a time dependent manner. Equation (7.3) now becomes;

$$T = W_B . d_K \qquad (7.6)$$

d_K can now be measured from the observation of the knot sizes and W_B is now a work to break; i.e., the actually work done in breaking molecules with visco-elastic effects being much less significant compared to steady tearing. The magnitude of T is largely determined by d_K. d_K is determined by the extent of the orientation of the rubber/carbon black structure in carbon black filled rubbers in the direction of stretching. The greater the orientation, the greater will be d_k causing more side wise tear growth and a higher tearing energy. Gent and Henry[63] showed that when a tear deviation is prevented, strengthening due to the addition of carbon black is relatively small. They carried out experiments using a constrained trouser tear test-piece which they prepared by bonding thin steel strips on opposite sides of the two legs at various spacings (0.1 to 3 mm) as shown in figure 7.8(a). They observed knotty tearing over a wide range of tear rates and temperature for different rubber vulcanizates as shown in figure 7.8 (b), when the spacing of the bonded plates was wide. However, when the spacing of the bonded plates was close to zero, steady tearing was observed. They noted that the tearing energy of the reinforced vulcanizates was then only approximately twice that of the unfilled rubbers. Thus the enhancement of tearing energy in filled rubbers is mainly associated with the broadening of the tear tip as a consequence of tear deviation. This indicates that the nature of the tear tip is of paramount importance and a detailed understanding of the way it is affected by visco-elastic properties, strain-induced crystallization, rate, temperature and filler type/content is necessary to explain tear behaviour.

7.3.1 Effect of rate and temperature on tearing energy-knotty tearing

The temperature and rate dependency of the tearing energy for a SBR filled with 30% by weight of FT carbon black is as shown in figure 7.5(b). The flat plateau indicates a large increase in tearing energy in the region where knotty tearing occurs compared to the unfilled SBR shown in figure 7.5(a). Outside this region, the carbon black-filled SBR shows only a relatively small increase in tearing energy when knotty tearing does not occur. This indicates that the development of knotty tearing is both rate and temperature dependent. This also indicates a complex tearing phenomena with reinforced rubbers which involved two opposing processes. In the first place, there is a basic process, observed with non-crystallizing unfilled vulcanizates, in which a continuous increase in T occurs with an increase in the rate of propagation, essentially a visco-elastic effect. A second process may also take place, the development of an oriented structure at the tip which requires a finite time to form. The second process accounts for a tendency for T to decrease as the speed of tearing increases. The observed dependence of T on rate and temperature represents the balance which is stuck between these opposing processes.

7.4 UNFILLED STRAIN-CRYSTALLIZING RUBBERS

Strain crystallizing rubbers, tear over a wide range of temperature and rate in a stick-slip manner (figure 7.7b) which is a less gross form of knotty tearing. The resulting temperature and rate dependency of tearing energy in the case of NR is as shown in figure 7.5(c). As shown in figure 7.5(c), the tearing energy of strain-crystallizing rubbers is greatly increased, over the range of tear rate and temperature at which crystallization occurs on stretching at the tear tip, compared to the tearing energies of a non-strain crystallizing SBR rubber (figure 7.5 a). The occurrence of stick-slip tearing is attributed to the formation of strain induced crystallization at the tear tip resulting in pronounced energy dissipation on stretching and retraction associated with the formation and melting of crystallites under non-equilibrium conditions[64]. The tearing energy is hence relatively less sensitive to temperature and rate in this region being only dependent on the temperature and rate which allow strain crystallization to occur[65]. At temperatures or rates at which crystallization cannot occur NR behaves as a

non-crystallizing rubber, tearing in a steady manner with the tearing energy being determined by visco-elastic effects[61,66].

7.5 DEPENDENCE OF TEARING ENERGY ON THE TYPE AND CONCENTRATION OF CROSSLINKS

Brown, Porter & Thomas[67] studied the effect of type and concentration of crosslinks on the tearing energy of an unfilled non-strain crystallizing isomerized NR which torn in a steady manner. Their findings are as shown in figure 7.9 where the tearing energy is plotted against the shear modulus, which is directly proportional to the crosslink concentration. It can be seen that the tearing energy decreases as the shear modulus increases for each of the three vulcanising systems investigated. At any particular crosslink concentration, the conventional sulphur vulcanising system produces vulcanizates having higher tearing energies than the EV vulcanizing system or the peroxide cured vulcanizates. Recent work by Samsuri and Thomas[62] showed a similar behaviour in the case of carbon black filled NR vulcanizates. They also observed that the conventional vulcanizing system produced knotty tearing over a wider range of crosslink concentrations than that for the EV and the peroxide systems. They concluded that the superiority of the polysulphide vulcanizates might be due to the labile nature of polysulphide crosslinks, which were able to break and reform in the strained state, thus relieving the stress concentration at the tear tip.

7.6 TEAR BEHAVIOUR OF CARBON BLACK FILLED RUBBERS

The extent of reinforcement by fine particle fillers is quite remarkable. The tearing energy of an SBR vulcanizate is increased as much as tenfold when 30 pphr of carbon black is included in the mix formulation a shown in figure 7.5b. However, this strengthening action is restricted to a specific range of tear rate and temperature of the test. Outside this range of effectiveness, the filler does not enhance the observed strength to a comparable degree.

The addition of carbon black to strain crystallizing rubbers generally promotes tear path deviation, leading to knotty tearing and to large increases in tearing energy. This effect is due to the orientation effect at the tip of tear mentioned earlier. The strength anisotropy arising from orientation effects was first observed by Busse[68], who demonstrated that it was easier to

move a pin in a highly-stretched carbon black-filled NR vulcanizate along the stretching direction than to move it in the transverse direction. Lake and Yeoh[69] carried out an investigation of the resistance of carbon black filled vulcanized rubbers to cutting by sharp objects, they found that the tearing energy measured when a tear propagated as a sharp tear tip formed by a sharp blade was about 0.3 kJm^{-2} compare to 50 kJm^{-2} measured using a trouser tear test-piece when knotty tearing occurred. Recently, Samsuri and Thomas[62] investigated the effect of strength anisotropy on the tearing energy of carbon black filled NR vulcanizates using split tear test pieces (figure c in appendix 7.1) which were first pre-strained by applying a pre-straining force, F_B and then a tearing force, F_A. They found that the tearing energy of pre-strained vulcanizates for a tear propagating in the direction of molecular orientation (i.e., parallel to F_B) was very low, being a factor of about 10 or more lower than the tearing energy obtained from measurements using a trouser tear test-piece. They concluded that knotty tearing occurs in trouser tests due to weakening in the stretch direction rather than due to strengthening in the normal direction of tear propagation.

The range of tear rates over which knotty tearing can occur depends upon the type of rubber and the size of filler particles. NR which crystallizes on stretching gives a wider range of tear rate and temperature over which knotty tearing occurs than does SBR which does not strain-crystallize as shown in figures 7.10(a) & 7.10(b) respectively. Thus strain crystallization enhances further the anisotropic orientation of structure so that the net effect is greater than that due to carbon black alone. The results also indicate that fine carbon black particles are more effective in introducing knotty tearing over a wide range of tear rate and temperature than large carbon black particles.

7.7 TEAR BEHAVIOUR OF SILICA FILLED RUBBERS

Silica is the most widely used filler in the rubber industry after carbon black. Silica together with an appropriate coupling agent is now used, in part or as a whole in such applications as tyres, conveyer belts, automotive engine mounts etc. The technological driving force for its use seems, apart from its light colour, to be associated with improved wear/abrasion resistant and low heat build up or thermal properties. Most physical property studies involving silica filled rubbers have hence concentrated on technological studies of things such as abrasion resistance, heat built up[39] with a minimum

of data produced concerning stress-strain behaviour[70] and tear behaviour. The majority of scientific studies in fact have concentrated on the chemistry of the rubber/silica coupling process and the nature of filler particle surfaces[39]. The very limited tear studies suggest that appropriately coupled materials have comparable tear strengths to carbon black filled rubbers[71], although in one case it has been reported that part replacement of carbon black in natural rubber by silica actually improved tear behaviour[72]. In the same study[72], it was found that the addition of 0.3 pphr of a mercapto-silane coupling agent reduced tear strength although it improved abrasion resistance and other mechanical properties.

7.8 AIMS AND SCOPE OF THE PRESENT INVESTIGATION

While extensive studies on the role of carbon black in determining tear behaviour in filled rubbers have been carried out; a detailed understanding of what determines the regimes of tearing observed is not available. In the case of silica filled rubbers no real scientific studies have been carried out, particularly as to the role of coupling agents.

The present investigation hence aims to;

(1) To characterize the tear behaviour of the Peradin carbon black compounds, which are used throughout this study and in which the stress-strain behaviour was carefully charaterized in chapter four. The aim was to study the effect of carbon black content, crosslink density and strain induced crystallization on the regimes of tear behaviour.

(2) To study the tear behaviour of uncoupled and coupled silica filled compounds whose interesting stress-strain behaviour was demonstrated in chapter five. In such systems the mechanisms of tearing are unknown and an important part of the study will be a direct comparison with the tearing behaviour in the carbon black filled rubbers.

7.9 EXPERIMENTAL

In this investigation, vulcanizates based on natural rubber (NR), synthetic cis-polyisoprene (IR, Cariflex 305, 92% cis unit) and styrene butadiene rubber (SBR) filled with carbon black and silica were used. All the formulations are given in tables 3.1 to 3.4 in chapter three. The NR vulcanizates filled with different amounts of carbon black were (Peradin compounds) used to study the effect of filler loading on tearing energy and tearing regime; in particular to investigate the effect of temperature and rate on tearing. The effect of crosslink density was studied using the formulations shown in table 3.2 for NR vulcanizates filled with 49 pphr carbon black but having different ratios of sulphur/accelerator to achieve different crosslink densities. A carbon black filled SBR was used to study the effect of rate and temperature in a filled non-strain crystallizing rubber. The effect of silica filler without and with coupling agent was also studied in the above mentioned base rubbers.

7.9.1 Tear measurement

Tear measurements were carried out using simple extension (trouser type) test-pieces as shown diagramatically in figure 7.1(a) &(b). These test-pieces were prepared by cutting a rectangular parallel sided test-piece from a large moulded sheet. The nominal dimensions of the test piece are given in figure 7.1(a). A longitudinal cut was then made in the middle of the specimen (c).

The tear test was carried out by separating the legs of the test-piece at a uniform rate by a moving crosshead operated at a constant rate by two vertical drive screws in an Instron testing machine. The crosshead speed ranged from 0.05 mm per minute to 1000 mm per minute. This provided a wide range of tear rates from 0.42 μms^{-1} to 8300 μms^{-1}. Figure 7.1(b) shows the test-piece in the deformed state where F is the force applied and λ is the extension ratio in the legs of the trouser test-piece. Typical force-displacement curves obtained from the chart recorder of the machine are as shown in figure 7.1(c). Tear measurements other than those at room-temperature (23°C) were carried out inside a temperature cabinet controlled to ± 1°C. Before each test, the test-piece was pre-warmed to the required testing temperature in the cabinet for 15 minutes .

7.9.2 Determination of tearing energy

The tearing energy for a trouser test-piece can be calculated from the following relationship[29];

$$T = 2F\lambda h^{-1} - w W \qquad (7.7)$$

where T is the tearing energy i.e., elastic stored strain energy released to create unit area of crack, F is the tearing force, λ the extension ratio in the legs, W is the strain energy density in the legs, h the thickness of the test-piece in the unstrained state and w its total width. The tearing force, F, is approximately constant during steady tearing (figure 7.1c2), but is calculated as the mean value of the maximum forces during knotty tearing (figure 7.1c1), consistent with the approach suggested by Greensmith[61]. The nominal stress in the legs of a test piece was calculated and the corresponding extension ratio λ was obtained from the stress versus extension ratio curve for the particular type of rubber vulcanizate being tested. The magnitude of the strain energy density W was obtained from the area under the stress versus extension ratio curve.

However, when the legs of the test pieces are inextensible $\lambda = 1$, the energy stored elastically in the legs is zero and equation (7.7) is reduced to a simple form;

$$T = 2F h^{-1} \qquad (7.8)$$

Tearing energies can be calculated from the above equation without a knowledge of the magnitude of the strain energy density W. Greensmith[61] used this approach with trouser test pieces 40 mm in width to prevent extension of the legs and found it applicable for weak rubber vulcanizates such as un-filled SBR. In the case of strong rubbers such as filled vulcanizates, Samsuri[73] found that the extension in the legs of the test piece was still considerable and significant even when using a trouser test piece having dimensions similar to those used by Greensmith. He proposed an alternative relationship whose computation did not require a knowledge of the strain energy density but in which extension of the legs was considered i.e.,

$$T = F h^{-1}(\lambda + 1) \qquad (7.9)$$

The applicability of equations (7.7.), (7.8), and (7.9) will be investigated in the present study.

7.9.3 Determination of tearing rate

The rate of tearing is related to the rate of extension, S, by the following relationship;

$$r = S / 2\lambda \qquad (7.10)$$

when extension in the legs is absent, λ, becomes unity and equation (7.10) reduces to;

$$r = S/2 \qquad (7.11)$$

i.e., the rate of tearing, r, is equal to half the extension rate i.e., half the crosshead speed. Equation (7.11) is valid provided that tearing occurs in a steady manner (figure 7.1c.2) and extension of the legs is negligible. In the case of stick-slip tearing (figure 7.1c1) where the rate varies between a low value at tear arrest to a very high value at tear initiation, equation (7.11) is not really valid. However, equation (7.11) was used to calculate the tear rate, r, for all types of tear failure to give some idea of the rate dependency of tearing energy. Thus the rate used in the case of knotty tearing is only as means of comparing the results with those obtained during steady tearing.

7.9.4 Method of characterizing the type of tear failure

Table 7.1(a) shows the tearing energy ratio (the ratio of tearing energy at tear initiation to tearing energy at tear arrest) for an unfilled IR vulcanizate (formulation IR00) that failed by stick-slip tearing (rough torn surface, but no knot observed at the tear tip). The tearing energy ratio (T_R) for stick-slip tearing ranged from 1.31 to 1.98. Also shown is the tearing energy ratio for a NR vulcanizate filled with 32 pphr of HAF carbon black (NR32) that failed in a knotty manner which ranges from 2.0 to 4.8. The results show clearly that knotty tearing gave higher tearing energy ratios than those resulting from stick-slip tearing.

The tearing energy ratio $(T_R)^{73}$ is used here to classify the mode of tear failure along with visual observation of the failure surface as described below;

Steady tearing: tearing was classified as steady when, (1) the tear propagated at a steady rate, with a minimum fluctuation of tearing force and a smooth torn surface resulted. (2) the tearing energy ratio did not exceed 1.05. This type of tearing is observed in the case of an unfilled SBR compound.

Stick-slip tearing: tearing was classified as stick-slip when, (1) the tear did not propagate at a steady rate resulting in a rough torn surface and (2) when the tearing energy ratio was within the range of 1.05 to 2.0.

Knotty tearing: tearing was classified as knotty when, (1) the tear propagated in a stick-slip manner, (2) there was evidence of knots on the torn test-pieces. If the knots were not clearly defined, the tearing energy ratio was used to characterize the tear failure. In cases like this, tearing was classified as knotty if $T_R > 2.0$.

7.10 RESULTS AND DISCUSSION

In this section the results of the tearing experiments will be presented and discussed. In the case of the carbon black filled compounds the aim was primarily to characterize the tearing behaviour of the NR Peradin compounds. Tearing energies for these are hence presented as a function of rate and temperature. As discussed in section 7.3.1 understanding the rate and temperature dependence of tearing is not simple in filled compounds particularly in strain crystallizing NR. In an attempt to understand this behaviour a parallel set of experiments is reported for carbon black filled non-strain crystallizing SBR.

The tearing experiments on the silica filled rubbers are reported and discussed largely in terms of the silica dispersion and silica/rubber adhesion. In this repect results are reported on NR, IR and SBR vulcanizates.

7.10.1 Calculation of the tearing energy

Tearing energies calculated for NR49 using equations (7.7), (7.8) and (7.9) are shown in table 7.2. The agreement between those calculated using equations (7.7) and (7.9) is very good. However the tearing energies calculated using equation (7.8) are on average 25% lower. It is hence clear that the assumption that the legs of the trouser test piece are inextensible is invalid in the present case. The agreement resulting from use of equations (7.7) and (7.9) obviates the necessity of calculating the strain energy density (W) in the legs in each test and hence allows equation (7.9) to be used to calculate the tearing energy throughout this study with no loss of accuracy.

7.10.2 Tearing behaviour of carbon black filled NR Peradin compounds

The tearing energy as a function of tearing rate as measured at 23^0C is shown in figure 7.11. All the filled rubbers tear in a knotty manner in the tear rate range from 4.2 μms^{-1} to 8300 μms^{-1}, as has been reported previously for carbon black filled NR[61,62].

For comparison purposes the results for the unfilled NR are also shown on the figure. The unfilled NR tears in a stick-slip manner and exhibits considerable tearing energy compared to SBR under similar condition[58]. The stick-slip tearing and the resultant at high tearing energy are associated with the development of strain crystallization in the high strain region at the tip of the tear[65]. The crystallites formed cause tear path deviation or effective blunting of the tear tip. The work done in forming

the crystals increases the tearing energy as the crystals subsequently melt as the molecules fracture and the tear proceeds. The temperature and rate dependence of the process is hence relatively small (within the crystallization regime). However at high rates the time necessary to form the crystallites could become significant resulting in a decrease in tearing energy. Furthermore the necessity of generating a given molecular strain for crystallization could result in a reduction in tearing energy at the higher temperatures due to the increased molecular mobility and rapid stress relaxation.

The addition of carbon black to NR caused a large increase in the tearing energy due to the development of large scale tear deviation i.e., knotty tearing (figure 7.7a). The process involves the development of anisotropic orientation at the tear tip. The anisotropy is such that it becomes easier for a tear to propagate in the direction of stretching i.e., it is the relative strengths at the tear tip in the stretching direction and the normal tear direction which is important. The orientated structures are a complex mixture of carbon black orientation and crystallization which may depend on the mixing process and be dependent on the type and fraction of carbon black[61]. The structures will take a finite time to form, the degree of orientation hence decreasing with increasing rate and decreasing temperature; with corresponding reductions in tearing energy. At the same time however visco-elastic losses during the tearing process will increase with increasing rate and decreasing temperature hence increasing the tearing energy. The balance between these two processes will itself be dependent on the temperature and rate.

In the case of the Peradin compounds at 23°C (figure 7.11) there is a general decrease in the tearing energy with increasing rate suggesting that the time necessary to develop the orientated structures is the predominant factor. The difference in behaviour of the filled compounds is not that large suggesting that provided sufficient carbon black is present to cause knotty tearing then large increases in tearing energy will result. The compound NR69 is seen to have a lower tearing energy than NR49 at this temperature where as an increase in tearing energy with carbon black content would be expected. It was also observed (figure 6.10) that the stress relaxation rate as a function of stress was also in the order NR49>NR69>NR23. It may be that the carbon black becomes relatively less effective at higher loadings in terms of ability to produce oriented structures and in terms of stress redistribution. However bearing in mind both that the tearing process is

complex and that they are commercial compounds; no general conclusion should be drawn.

The temperature dependence of the tearing energy for the Peradin NR carbon black filled compounds at a rate of 830 μms^{-1} is shown in figure 7.12. All the materials tear in a knotty manner and all in general exhibit a tearing energy which decreases with increasing temperature.

This suggests that at this tearing rate, even though knotty tearing occurs, that visco-elastic processes dominate the temperature dependence. For NR49 and NR69 the temperature dependence appears more complex with evidence of the two competing processes (i.e., time to form the oriented structure and visco-elastic relaxation) affecting the temperature dependence. Again the differences between NR49 and NR69 are small suggesting a decreasing relative effectiveness of the carbon black at high loadings.

The tearing energies for NR49 of different crosslink densities are shown as a function of rate in figure 7.13. It can be seen that except for the highest crosslink density material the effect on tearing energy is minimal even though significant differences in the stress-strain behaviour are observed (figure 4.17). All three lower crosslink density materials have high tearing energies and tear in a knotty manner. At the highest crosslink density a large drop in tearing energy is observed. At the lower rates stick-slip tearing occurs but with tearing energies larger than for the unfilled NR (figure 7.13). It is as if the tight network will only allow a very limited orientation of carbon black to occur with little visco-elastic loss. At higher rates steady tearing occurs with a lower tearing energy that for the unfilled NR, suggesting that at these rates for this crosslink density even strain crystallization is difficult.

7.10.3 Tearing behaviour of a carbon black filled SBR compound

The measured tearing energy of a SBR compound filled with 50pphr HAF carbon black is compared with an equivalent unfilled compound in figure 7.14. Both tear in a steady manner at 23°C. The increase in the tearing energy on the addition of carbon black is very large compared to the very weak unfilled SBR. Strain crystallization does not occur and the increase in tearing energy results directly from an increase in mechanical hysteresis due to visco-elastic effects (i.e., more work has to done in the region of the tear tip to generate the forces necessary to break molecules). The tearing energy hence increases with rate as more visco-elastic work is done.

The measured tearing energies at 23-120°C are shown as a function of rate in figure 7.15. The picture is now very complex as the particular tearing mechanism which operates is determined by the temperature and rate. Furthermore when a particular tearing mechanism occurs the magnitude of the tearing energy is dependent on temperature and rate. At 23°C steady tearing occurs at all rates, the large internal viscosity both preventing the formation of orientated carbon black structures and hence steady tearing, and causing the tearing energy to increase with increasing rate. At 120°C knotty tearing occurs at all rates and the tearing energy is low. The low internal viscosity allows the rapid formation of oriented carbon black structures but the energy loss during knotty growth is small leading to low tearing energies. At 90°C knotty tearing occurs at all rates and the tearing energy is high. The internal viscosity is now higher, but still allows time for the formation of oriented carbon black structures and more energy is dissipated during knotty tear growth leading to higher tearing energies. At 70°C the picture is similar but at the highest rates tearing becomes steady as oriented structures have difficulty forming and the tearing energy falls. The 50°C data exhibits the largest transition. At the slowest rate tearing is knotty and the tearing energy is high. As the rate is increased the tearing remains knotty but the tearing energy falls presumably as a result of a decrease in knot diameter as the relative extent of orientation decreases. At higher rates the tearing becomes steady, as little orientation develops, and the tearing energy falls to below the 23°C value as the visco-elastic losses are less at 50°C than at 23°C. Hence it can be seen that at least in a qualitative sense the complex behaviour can be understood in terms of the models of knotty and steady tearing.

7.10.4 Comparison of tearing behaviour of NR and SBR compounds

It was initially decided to study the tearing of SBR, a non strain crystallizing rubber, as a means of understanding the more complex behaviour of the strain crystallizing Peradin NR compounds. In fact it is now clear that the complex rate and temperature behaviour of the two make this difficult. Nevertheless a comparison of the general behaviour of the two is useful.

Figure 7.16 compares the behaviour of unfilled NR and SBR as a function of rate at 23°C. The strain crystallization in NR causes slip-stick tearing to occur resulting in relatively high tearing energies, with little effect of the rate on tearing energy. The SBR tears in a steady manner with

a much lower tearing energy which increases with rate due to energy loss and visco-elastic effects. The addition of carbon black strengthens both materials but at 23°C in quite different manners (figure 7.16). The filled NR tears in a knotty manner with a tearing energy which falls with increasing rate as orientated structures have less time to form. The filled SBR tears in a steady manner with a tearing energy which increases with increasing rate as a result of increased energy dissipation due to increased visco-elastic loss. The comparison is of course not simple as the two tear in different manners and the relative magnitudes of the visco-elastic effects are different as the glass transition temperatures are different. In figure 7.17 the tearing energies of filled NR and SBR are compared at different temperatures at which the polymer visco-elastic effects should be similar (i.e., same temperature relative to θ_g) and at which knotty tearing occurs in both. The tearing energy now decreases with increasing rate for both due to the time necessary to form oriented structures in both. The tearing energy is however always higher for the NR. It may be that strain crystallization continues to play a significant role in terms of both work to form the crystals and in terms of influencing the extent of orientation of the carbon black structure which develops.

7.10.5 Tearing behaviour of silica filled rubbers

The NR, IR and SBR rubbers which acted as the matrix to be filled with silica were all cured with dicumyl peroxide (formulations in tables 3.3&3.4) to produce translucent rubbers which offered the possibility of studying the rubber/filler interface behaviour as de-adhesion could be apparent as stress whitening. This curing system tended to produce a lower crosslink density than for the sulphur cured carbon black filler rubbers and a greater uncertainty in the molecular crosslink density due to an inability to really distinguish between rubber/rubber and silica/rubber links during swelling experiments (see chapter three, section 3.4.4). Furthermore care must be taken in comparing the carbon black and silica filled rubbers at the same pphr filler by weight as the density of silica is 1.95 gm-cm^{-3} and that of carbon black is 1.69 g-cm^{-3}. Hence the 40pphr silica compounds have a volume fraction of 15.4% silica and while the 32 pphr carbon black compound has a volume fraction of 12.3% carbon black based on the formulations used in this study. As the adhesion of silica to rubber is much poorer than carbon black to rubber, experiments were carried out with and without the addition of coupling agents to the compounds. As was discussed

in chapter five section 5.2, it is not easy to distinguish between the action of the coupling agent in producing a better dispersion of the silica and/or better silica/rubber adhesion. Furthermore either effect is likely to be different in the different rubbers.

7.10.6 Tearing behaviour of the silica filled NR compounds

The tearing energy as a function of tearing rate is shown for the silica filled NR compounds in figure 7.18. The unfilled NR, a crystallizing rubber tears in a slip-stick manner with a relatively high tearing energy. The addition of the silica filler results in steady tearing at all rates at 23^0C. As stick slip tearing in NR is associated with the development of strain crystallization at the tear tip this observation seemed surprising. It seemed unlikely that the addition of silica was reducing the ability of the NR to strain crystallize but this possibility was examined. Strips of the 40 pphr silica filled NR were stretched and a WAXRD photograph taken (figure 7.19). Diffraction arcs resulting from strain crystallization were clearly seen showing that strain crystallization could still occur under appropriate conditions. However, not only did stick-slip tearing not occur but neither did knotty tearing which is usually observed when carbon black is added to NR. Clearly the orientated filler structures necessary for knotty tearing were not being developed.

This type of observation is not however exclusive to silica filled rubber. Samsuri[73] studied, as shown in table 7.3, the type of tearing and the magnitude of the tearing energy for NR vulcanizates cured with different amounts of peroxide and filled with 50pphr HAF carbon black. In vulcanizate containing 1 pphr dicumly peroxide the tear propagated in a steady manner with a tearing energy of only 8.0 kJm^{-2} at tear rate of 830 μms^{-1} at 23°C. However in a similar vulcanizate containing 1.7 dicumyl peroxide the tear propagated in a knotty manner at tear rates of 42-830μms^{-1} , with a tearing energy of 50.0 kJm^{-2} at a rate of 830 μms^{-1} at 23°C. It was suggested that in the 1pphr dicumyl peroxide sample the crosslink density was very low allowing molecular chains to flow easily at high extensions. This resulted in steady tearing as, at the rates studied, stresses of the required magnitude to cause orientation at the tear tip leading to crystallization or carbon structure orientation were not developed. However in the higher crosslink density, 1.7pphr dicumyl peroxide specimen, the higher crosslink density limited flow allowing the necessary orientation to develop leading to knotty tearing[73]. It is possible that a similar explanation for the observation of steady tearing in the silica filled 1pphr dicumyl

peroxide specimens could apply. This is supported by the fact that in a 40pphr silica filled vulcanizate cured with 1.7 pphr dicumyl peroxide (the compound was prepared for this study) tearing occurred in a knotty manner at a rate of 830 μms^{-1} at temperature of 23°C, yielding a tearing energy of 49 kJm^{-2} which is comparable to the value of 50 kJm^{-2} for the 50pphr carbon black filled NR cured with 1.7 pphr dicumyl peroxide and tested at a rate of 830 μms^{-1} and temperature of 23°C.

In the current silica filled NR samples cured with 1pphr dicumyl, steady tearing is always observed. In the vulcanizate containing no coupling agent moderate strengths are observed and the tearing energy increases rapidly at high tearing rates. It is likely that de-bonding between rubber and filler occurs which combined with the high viscosity prevents the formation of oriented structures. Some evidence of debonding was observed in that stress whitening occurred in tensile tests at very high strains although this disappeared on unloading. The de-bonding process itself may require considerable energy making a major visco-elastic contribution to the tearing energy particularly at higher rates of tear. The addition of the coupling agent significantly reduces the tearing energy to below that of the unfilled NR (figure 7.18). The coupling agent alters the silica/rubber bonding and the nature of the silica dispersion. No stress whitening was observed in tensile tests. It may be that the good adhesion prevents any de-bonding hence allowing a tear to propagate with little energy loss.

7.10.7 Tearing behaviour of the silica filled SBR compounds

The tearing energy as a function of rate is shown for the silica filled SBR in figure 7.20. Unfilled SBR tears in a steady manner with a tearing energy increasing with rate due to visco-elastic effects. The addition of carbon black to SBR causes large increases in the tearing energy, with the type of tearing being dependent on temperature and rate (see figures 7.14 & 7.15). The addition of silica also causes large increases in the tearing energy at all rates at 23°C. The tearing is knotty on a small scale presumably due to silica orientation. The tearing energy decreases in general with increasing tear rate. The magnitude of the tearing energy, as in silica filled NR, decreased when a coupling agent was added and further decreased when the amount of coupling agent was increased from 1.0 pphr to 1.5 pphr (figure 7.20). This suggests that improved rubber/silica adhesion and a more homogeneous filler dispersion reduces the energy necessary to propagate a tear. This may

be due to both lower visco-elastic energy losses and may be smaller orientated aggregates of silica particles.

7.10.8 Tearing behaviour of the silica filled IR compounds

The tearing energy as a function of tearing rate at 23°C is shown in figure 7.21 for the silica filled IR (synthetic polyisoprene, cariflex 305, 92% cis). The unfilled IR tears in a stick slip manner with a much higher tearing energy than SBR. This suggests that some strain crystallinity develops at the tear tip even though 8% non-cis units are present on the cis polymer chain. The addition of 40pphr silica without coupling agent at 23°C causes a large increase in tearing energy particularly at the higher rates. Tearing occurs in a steady manner as for the silica filled NR. A whitened zone is observed around either side of the tear and at the tear tip when observed in reflected light, which appears as darkened zone in transmitted light (figure 7.22). This becomes more pronounced as the tear rate increases. It is permanent and remains after the test. It is assumed that this whitening is due to vacuoles forming at the silica/IR rubber interface which scatter light. The zone represents the high stress region where debonding occurs and in which rubber molecules have been cycled nearly to break and then relaxed. It is hence the zone in which visco-elastic losses occurred during tear growth and the energy dissipated in this zone in effect represents the tearing energy. During steady tearing, the tearing energy is given by;

$$T = W_H.d_H \qquad (7.12)$$

where W_H is the hysteresis energy loss and d_H is the diameter of the zone at the tear tip in which this loss occurs. It was pointed out in section 7.2 that this relationship is usually difficult to validate due to the inability to measure the magnitude of d_H. In the present case d_H is equal to twice the thickness of the observed whitened zone (figure 7.22). W_H has been estimated from the area between the loaded and unloaded stress-strain curve for the silica filled IR rubber loaded up to 90% of the breaking strain. This yields an under-estimate of W_H of 18.2 MJm^{-3}. The value of T for the tear specimen tested at 420 mms^{-1} at 23°C is 37 kJm^{-2}. The maximum, overestimated value of d_H would hence be 2.03 mm. This would yield an overestimated predicted width of the whitened zone as 1.02 mm. This length is shown marked on figure 7.22. The actual width observed is 0.88. Considering the overestimate in the predicted width, this is a good agreement.

As for NR and SBR the addition of the coupling agent lowers the tearing energy (figure 7.21). However at low tearing rates stick-slip tearing occurs presumably as a result of the development of orientation due to crystallization and the adhering silica structure orientation. However at high tearing rates steady tearing occurs with a much lower tearing energy than in the uncoupled material. The higher tearing energy in the uncoupled material presumably resulting from the large hysteresis losses occuring during rubber/silica debonding.

The temperature dependence of the tearing energy for the silica filled uncoupled IR is shown in figure 7.23 and table 7.4. A large increase in tearing energy is observed at 90°C when knotty tearing commences. It is interesting to note that a whitened region was formed around the tip of the knot (figure 7.24) indicating the extent of the highly strain region. Presumably knotty tearing occurs at this temperature and rate as the stress is large enough and the time is available to develop the orientation at the tear tip which causes deviation of the tear tip sideways. At 120°C knotty tearing still occurs but the tearing energy falls presumably due to the decreased visco-elastic energy dissipation in the region around the tear tip.

7.10.9 Comparison of tearing in silica filled NR, SBR and IR rubbers

The present experiments should be viewed as an initial study of the tear behaviour of silica filled rubbers. They represent a limited number of experiments in terms of both composition, rates and temperatures. They do however give general ideas as to the effect of silica and illustrate the potential of the system for studying steady tearing in particular.

In all cases the addition of silica increased the tearing energy particularly for uncoupled materials. In all cases the addition of coupling agents reduced the tearing energy. Clearly if the filler permanently adheres to the rubber during steady tearing it has a minimal effect in increasing the tearing energy via visco-elasic effects. Direct comparison between the rubbers is difficult with this limited data, but there is a suggestion that at a given rate and temperature the tearing energies are in the order IR>SBR>NR (figure 7.25) , however this order is not maintained at higher tear rates. In general the silica filled rubbers seem to have lower tearing energies than the carbon black filled rubbers. However when both tear in a knotty manner the tearing energies are comparable.

The process of stress whitening around the tear tip during steady tearing provides a unique opportunity to study steady tearing in a quantitative manner. The present results, using this method, provide the first quantitative validation of the relationship;

$$T = W_H \cdot d_H \qquad (7.12)$$

where T = Tearing energy for steady tearing
W_H = Hysteresis energy loss per volume of rubber
d_H = Tear tip diameter in which the energy loss occurs.

TABLE :7 1(a): The ratio of tearing initiation energy to tear arrest energy, T_R, for the unfilled IR, obtained in this study [Formulation IR00] Temperature: 23°C

TEAR RATE , μms^{-1}	4.2	42	170	420	830	4200	8300
T(Initiation) , kJm^{-2}	6.0	8.0	9.0	9.3	8.6	8.5	7.5
T (Arrest) , kJm^{-2}	4.5	4.4	5.5	4.7	5.1	5.9	5.8
T_R	1.36	1.78	1.67	1.98	1.69	1.44	1.31
Type of tear	S.S	S.S	S.S	SS	S.S	S.S	S.S

(b) The ratio of tearing initiation energy to tear arrest energy, T_R, for the 32pphr carbon black filled NR vulcanizate, obtained in this study [Formulation NR32] Temperature: 23°C

TEAR RATE , μms^{-1}	4.2	42	170	420	830	4200	8300
T(Initiation) , kJm^{-2}	43	31	30	31	33	20	19
T (Arrest) , kJm^{-2}	9.0	8.0	7.3	7.9	7.9	10.0	10.8
T_R	4.8	3.9	4.1	3.9	4.2	2.0	2.0
Type of tear	K	K	K	K	K	K	K

S.S:- Stick-slip tearing

K:- Knotty tearing

TABLE 7.2: Comparison of methods of calculating tearing energy. Tearing condition: Tear rate 420 μms^{-1}, temperature: 23°C, Data obtained from HAF carbon black filled NR vulcanizate (NR49)

Sample no	1	2	3	4	5	
Force, F (N)	46.8	43.5	48.5	38.7	54	
Thickness, h (mm)	1.8	2.14	2.25	1.95	2.11	
Total width,w (mm)	25	25	25	25	25	
Stress, σ, MPa	2.00	1.56	1.66	1.53	1.95	
λ	1.88	1.65	1.75	1.63	1.85	
W, (MJ^{-3})	0.884	0.546	0.686	0.522	0.837	Mean
$T=2\ Fh^{-1}$ - wW, kJm^{-2}, eq 7.7	75.7	53.5	58.3	51.7	79.9	63.8
$T = F\ h^{-1}\ (\lambda+1)$, kJm^{-2}, eq 7.9	74.9	53.9	58.3	51.7	79.9	63.0
$T= 2\ F\ h^{-1}$, kJm^{-2} eq 7.8	52	40.7	43.0	39.7	51.2	51.2

TABLE 7.3 : Comparison of tearing energies of NR vulcanizates filled with carbon black or silica and cured with dicumyl peroxide at a tear rate of 830 μms^{-1} at 23°C

PARAMETERS	NR50*/Black 1pphr dicup	NR50**/Black 1.7pphr di *cup*	NR40/01+ (Silica) 1pphr dicup	NR40/01/1.7@ (Silica) 1.7pphr dicup
Crosslink density $[x]_{phys}\ x10^{-5}$ g mol /g RH	4.98	6.49	6.7	9.4
Cure time,	90"at 150°C	120" at 150°C	45"at 160°C	45"at 160°C
M_{100}, MPa	1.27	1.65	1.35	--
T, kJm^{-2}, Type of tear	8.05 S	50 K	11.5 S	49 (knotty) at 830 μms^{-1}

* and ** are the NR vulcanizates cured with dicumyl peroxide having 50 pphr HAF black-data obtained from Samsuri [ref 73], + and @-data obtained in this study

TABLE 7.4 :The effect of temperature on the tearing energy of a 40 pphr silica-filled IR vulcanizate at a tear rate of 420 μms^{-1}, peroxide cured without coupling agent.

Temperature, °C	23	50	70	90	120
IR40/01 T, kJm^{-2}	37	34	30	86	60
Type of tear	S	S.	S	K	K

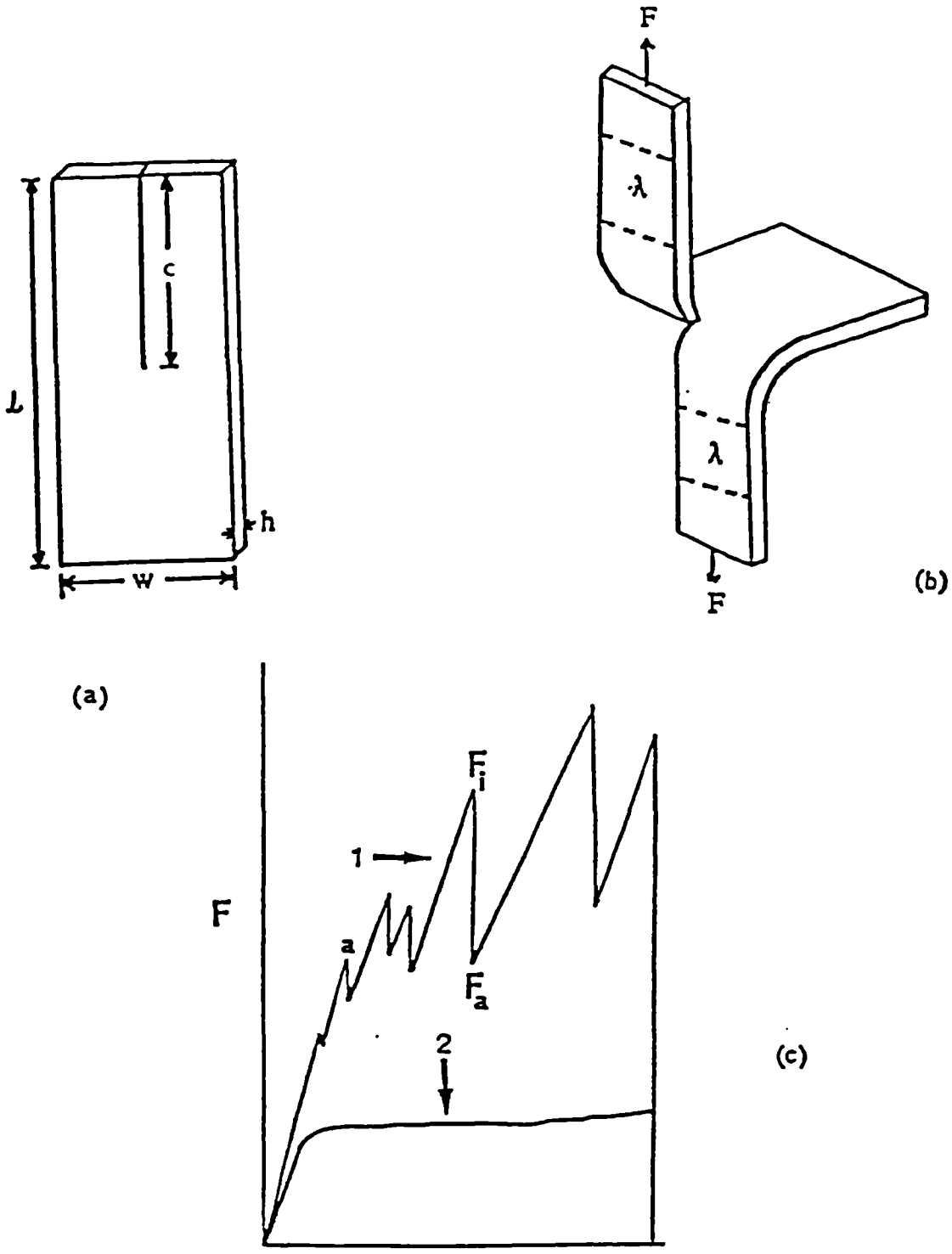

Figure 7.1: Schematic diagrams of trouser test-piece.
(a) Undeformed state; total length, L = 65 mm,
Cut length, C = 37 mm, total width,w = 25 mm
and thickness, h = 1-2 mm. (b) Deformed state
(c) Tearing force-distance chart; (1) knotty tearing
F_i is the force at tear initiation and F_a is the force at
tear arrest (2) steady tearing . Fig 4.2 pg 79

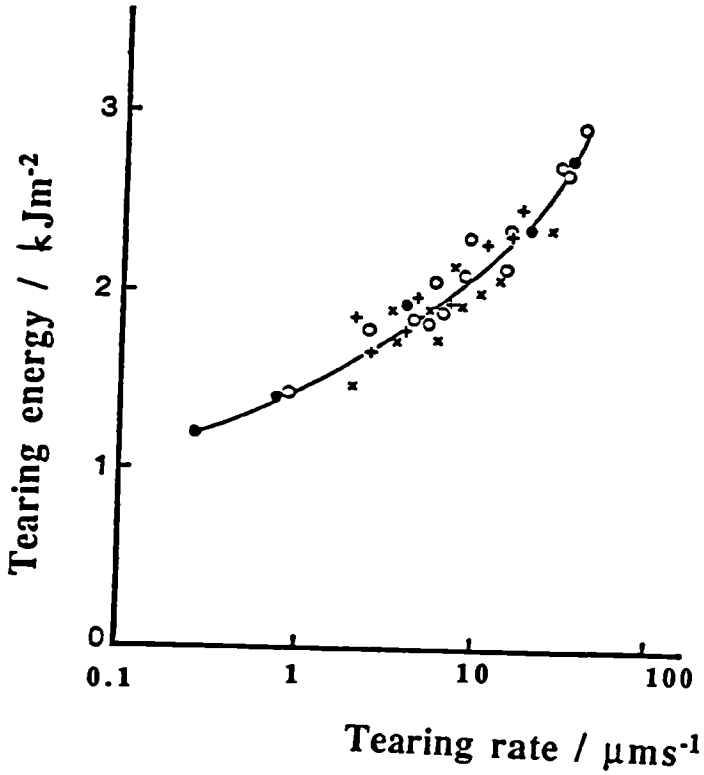

Figure 7.2 Tearing energy T versus rate of tearing r for a SBR vulcanizates using the test pieces shown in Appendix 7.1 (x) trouser, (+) pure shear, (o) split (●) angled

Fig 2, ref 51.

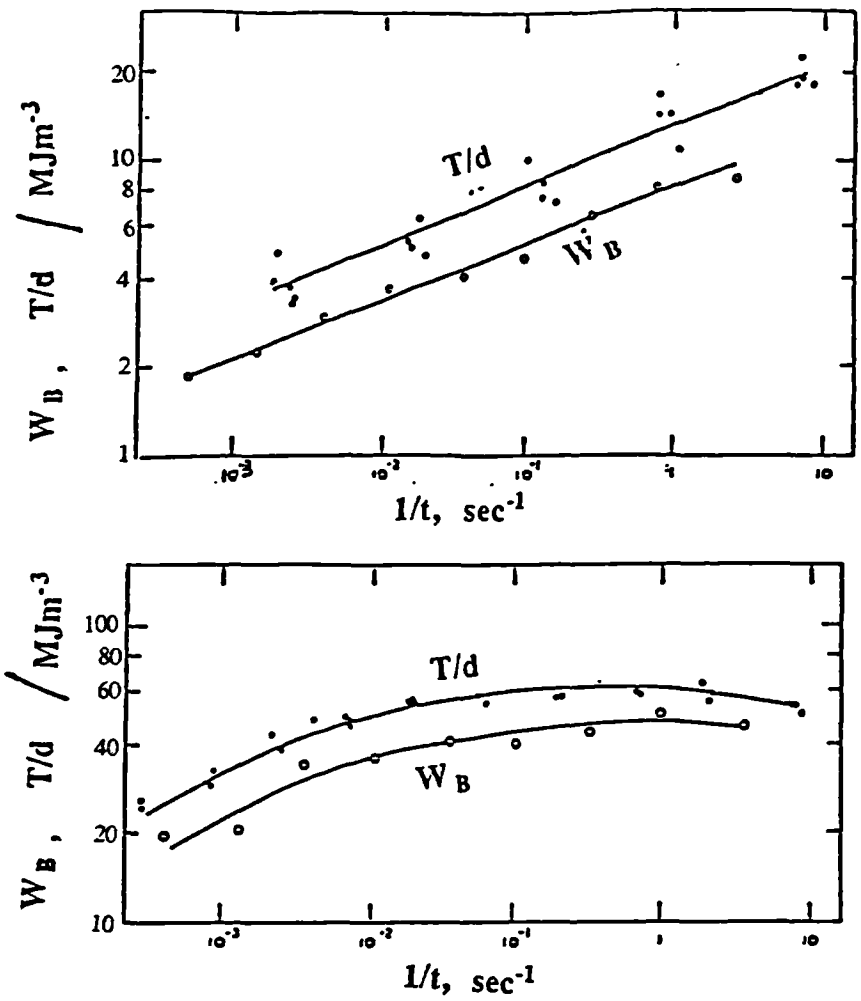

Comparison of W_B vs 1/t and T/d vs 1/t for (a) unfilled SBR vulcanizate, (b) SBR vulcanizate containing SRF carbon black, [figures 3&4, ref 49]

Figure 7.3: Comparison of strain energy density from tensile and tear measurements

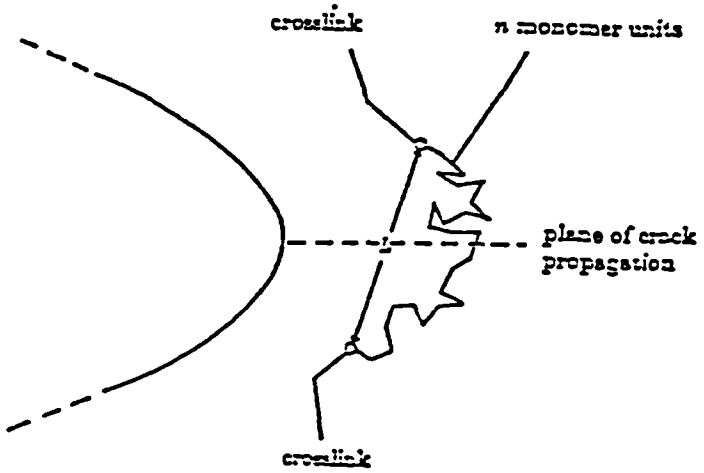

Figure 7.4: Schematic diagram showing a polymer chain laying across the plane of tear propagation
Fig 5, ref 51.

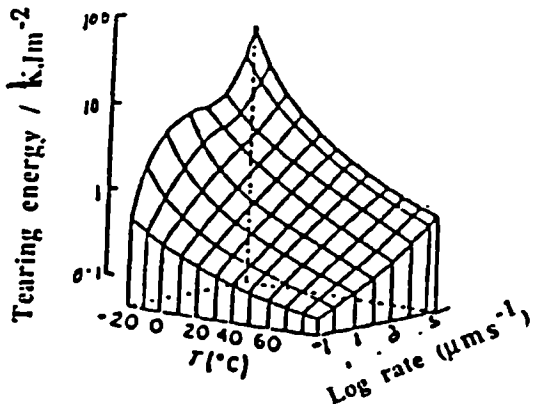

(a) Tearing energy dependence on temperature and rate of tearing for an unfilled SBR

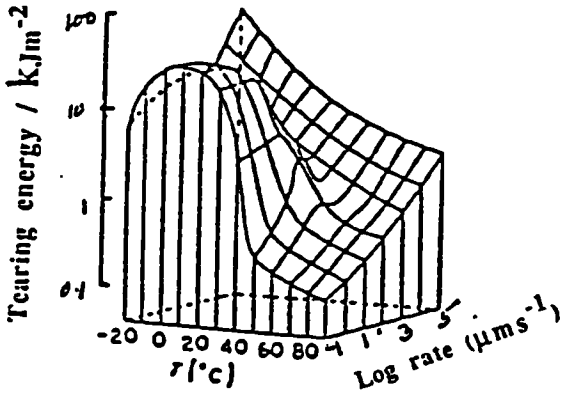

(b) Tearing energy dependence on temperature and rate of tearing for a SBR containing FT carbon black

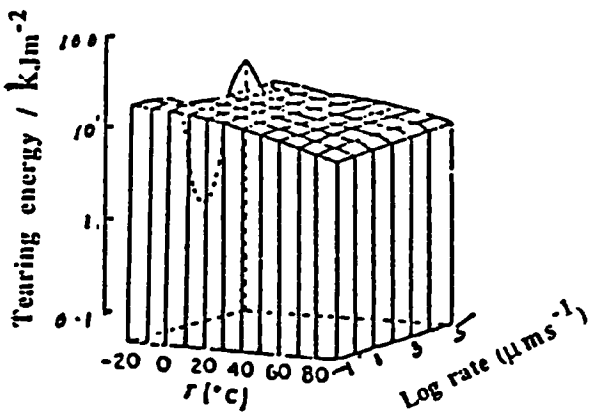

(c) Tearing energy dependence on temperature and rate for an unfilled NR

Figure 7.5: Effects of tear rates and temperatures on tearing energy, ref 58.

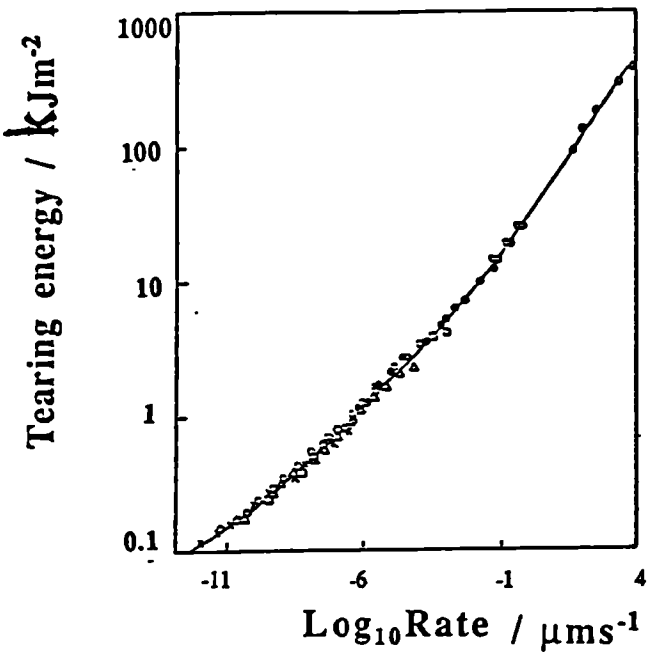

(a) Tearing energy as a function of reduced rate of tearing for a SBR gum vulcanizate, fig 3 ref 59

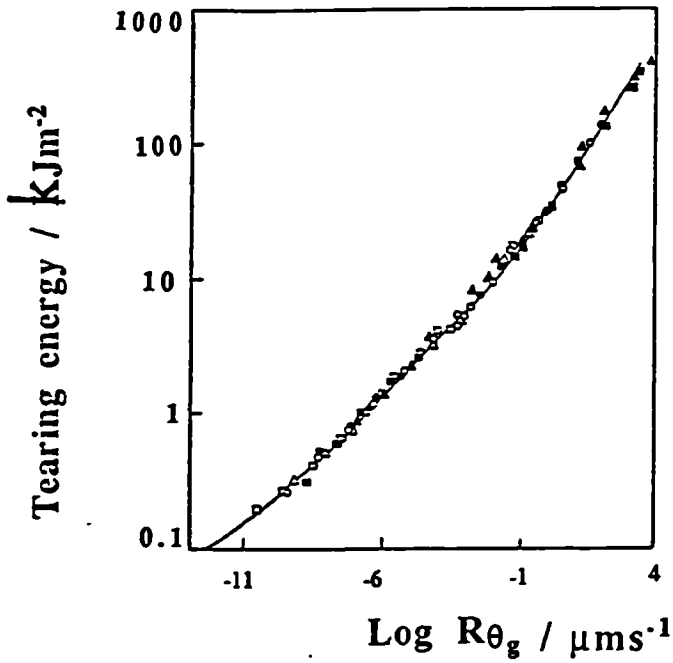

(b) Tearing energy versus tear rate reduced to θ_g for six unfilled amorphous elastomers, fig 5 ref 59

Figure 7.6: Tearing energy master curve

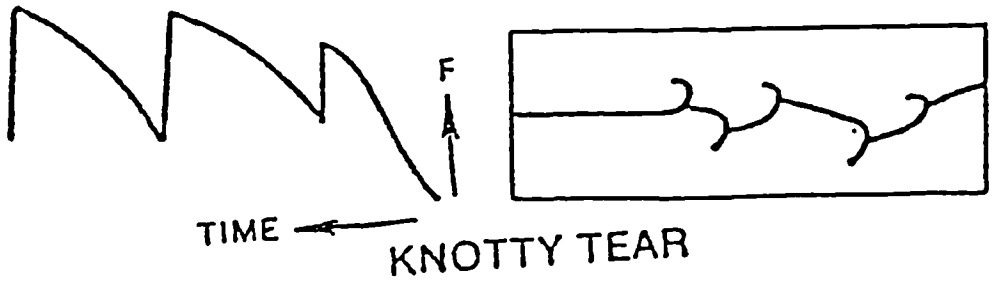

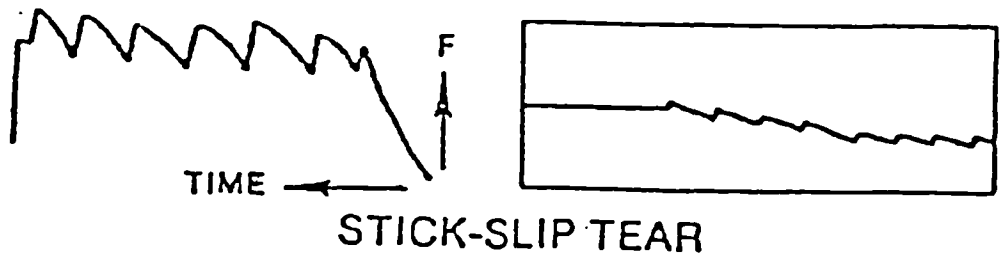

Figure 7.7: Unstable tearing (a) Knotty, (b) stick-slip

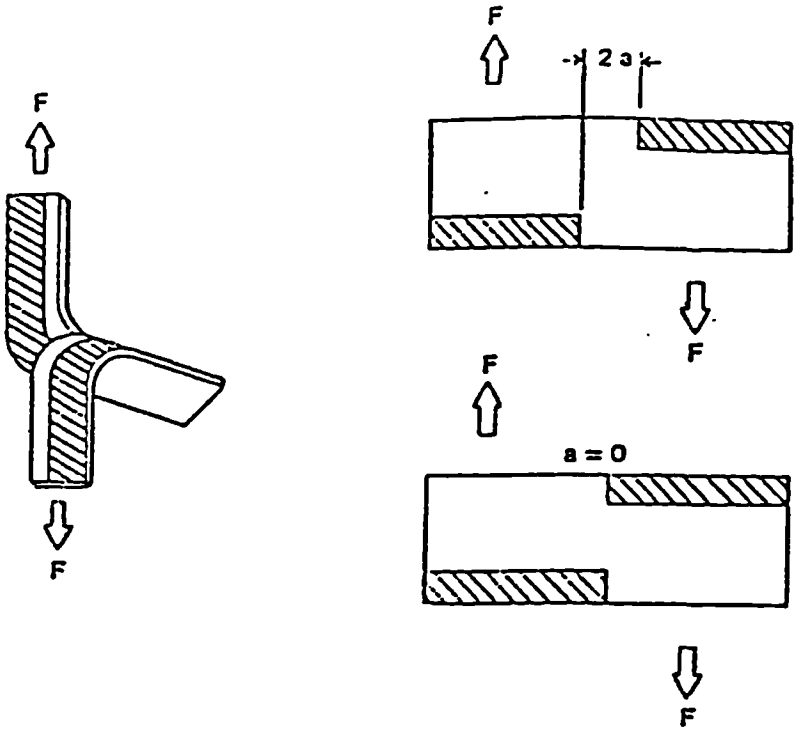

Figure 7.8 (a): Constrained trouser tear test piece with two cross sections indicating different shim spacings.

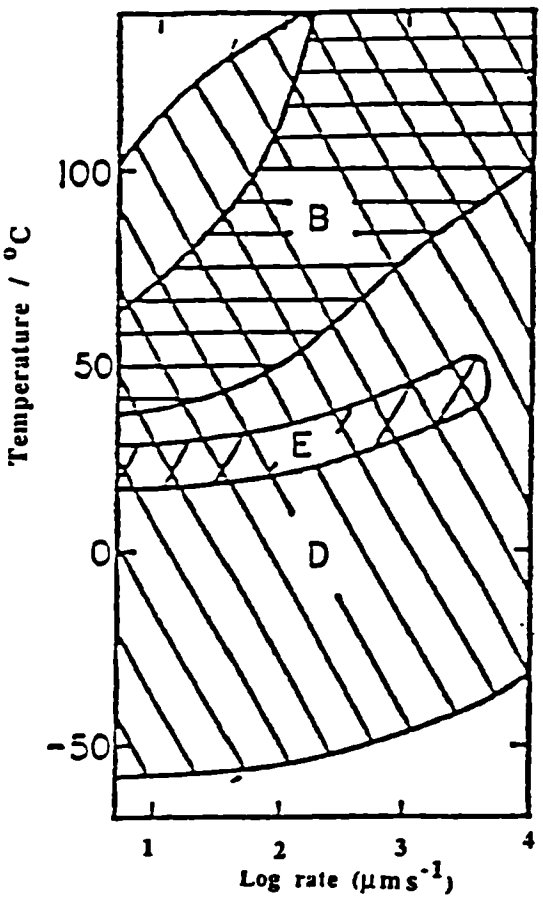

Figure 7.8(b) : Regions of knotty tearing for carbon-black-filled vulcanizates for SBR(B), NR(D), and cis-polybutadiene (E) ref 63.

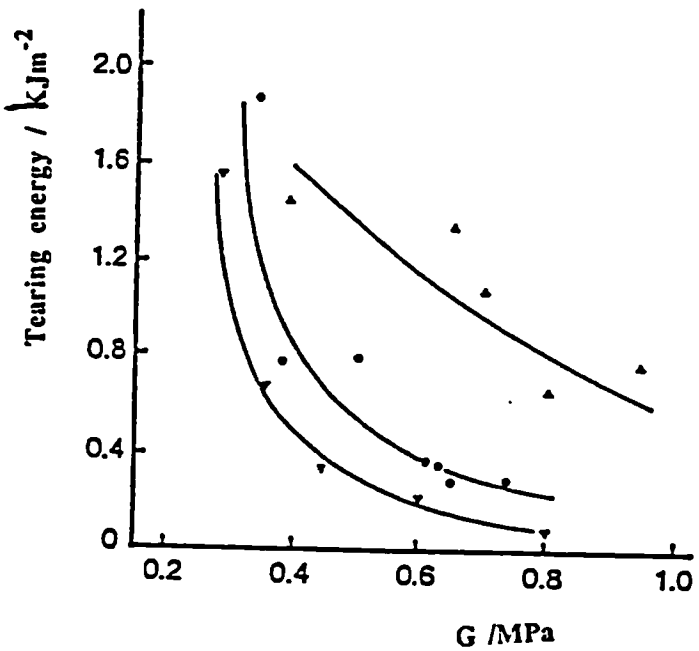

Figure 7.9: Dependence of tearing energy on types of crosslink for isomerized natural rubber
(▼) peroxide (carbon-carbon crosslinks)
(●) EV (mainly monosulphide crosslinks)
(▲) conventional (mainly polysulphide crosslinks)
Fig 6.7467

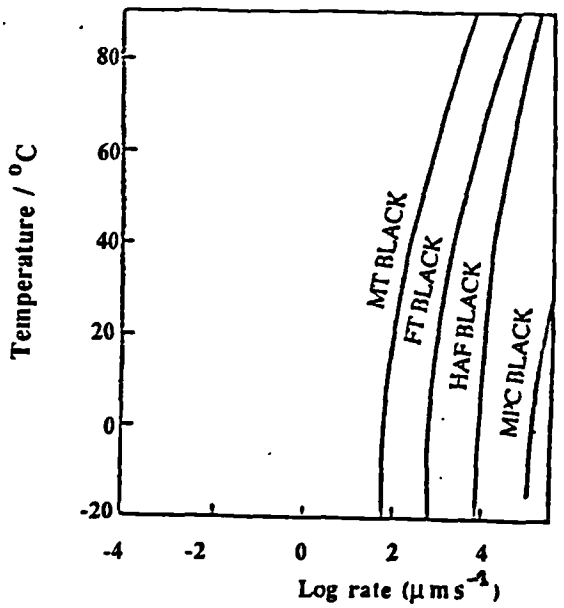

(a) Regions of Knotty tearing for NR containing various carbon blacks. The regions lie to the left of the appropriate curves, [figure 4b, ref 61]

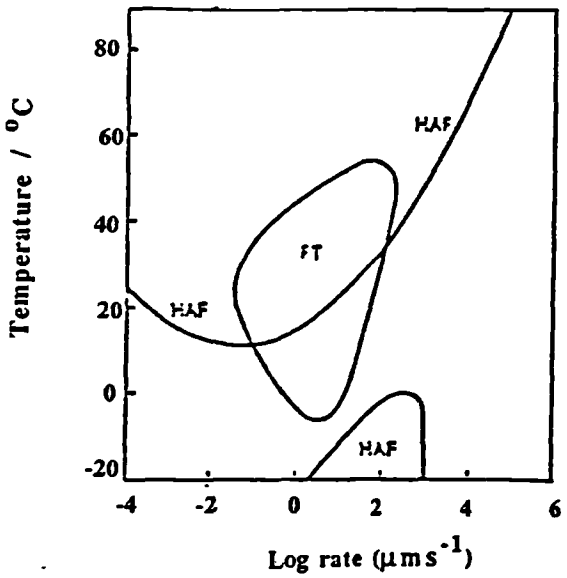

(b) Regions of knotty tearing for SBR containing various carbon blacks, [fig 4a, ref 61]
The knotty tearing occurs within the closed or partially closed curves

Figure 7.10: Regions of knotty tearing as a function of tear rate, temperature and type of carbon black

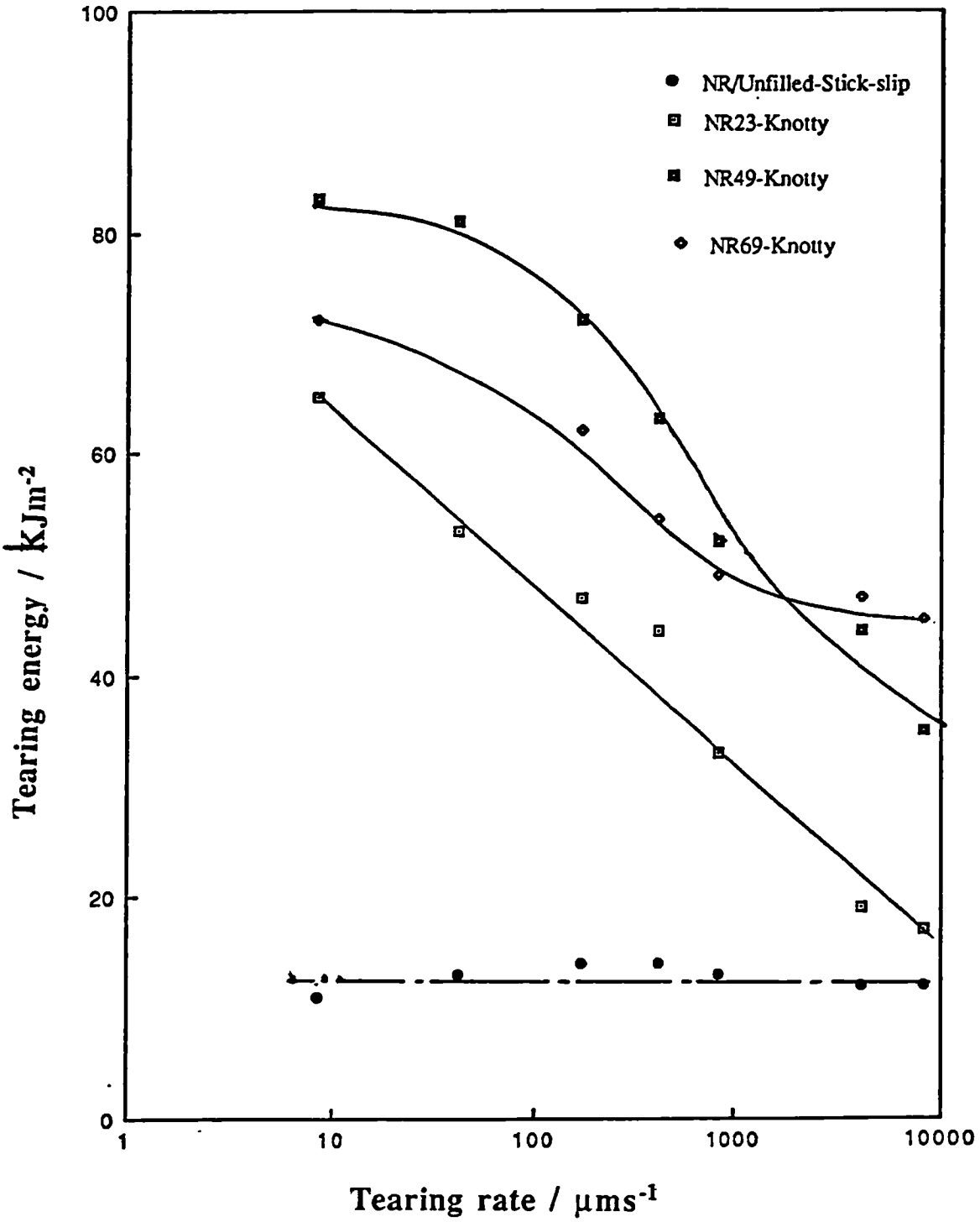

Figure 7.11: Tearing energy as a function of tear rate for carbon black filled NR vulcanizates at 23° C

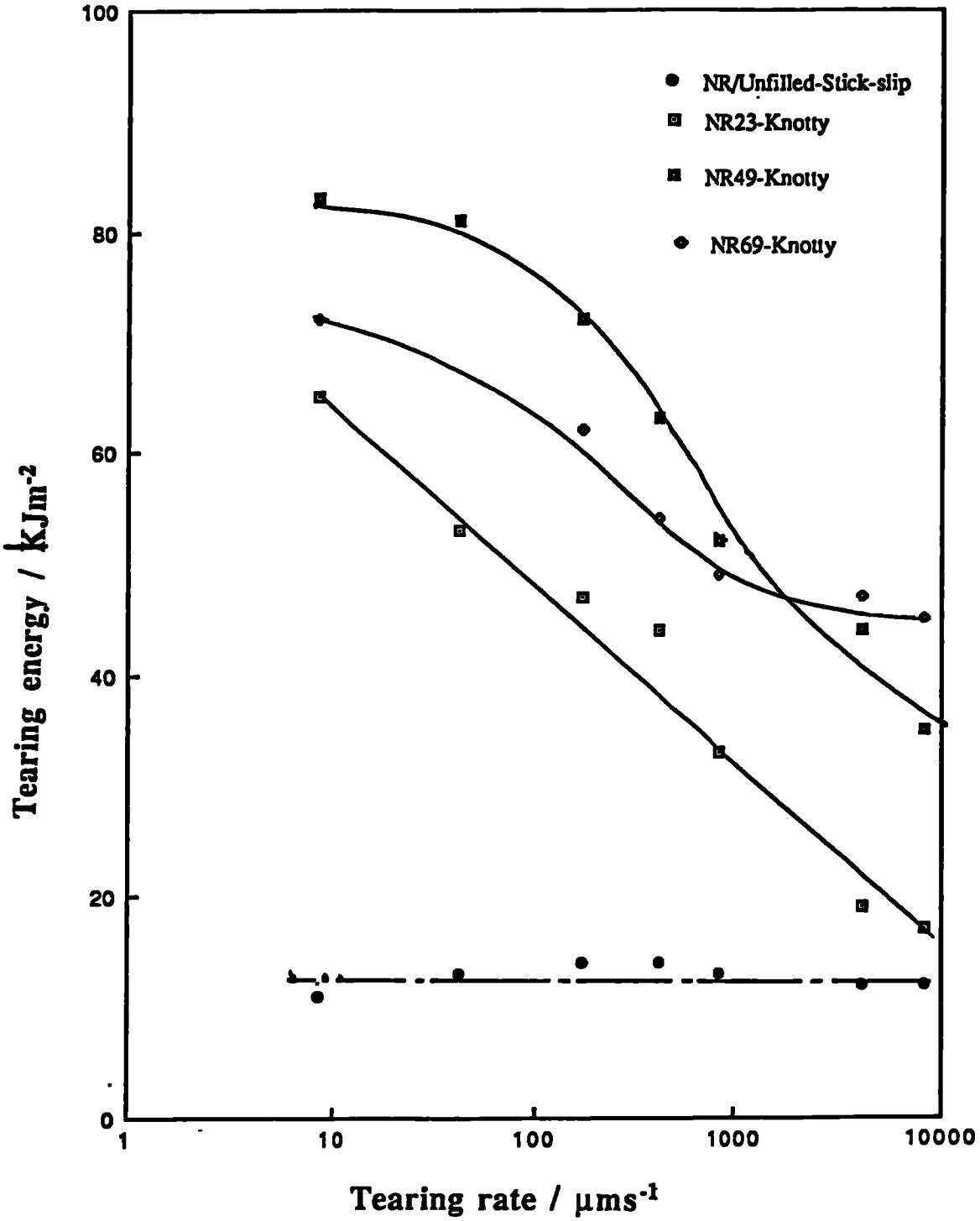

Figure 7.11: Tearing energy as a function of tear rate for carbon black filled NR vulcanizates at 23° C

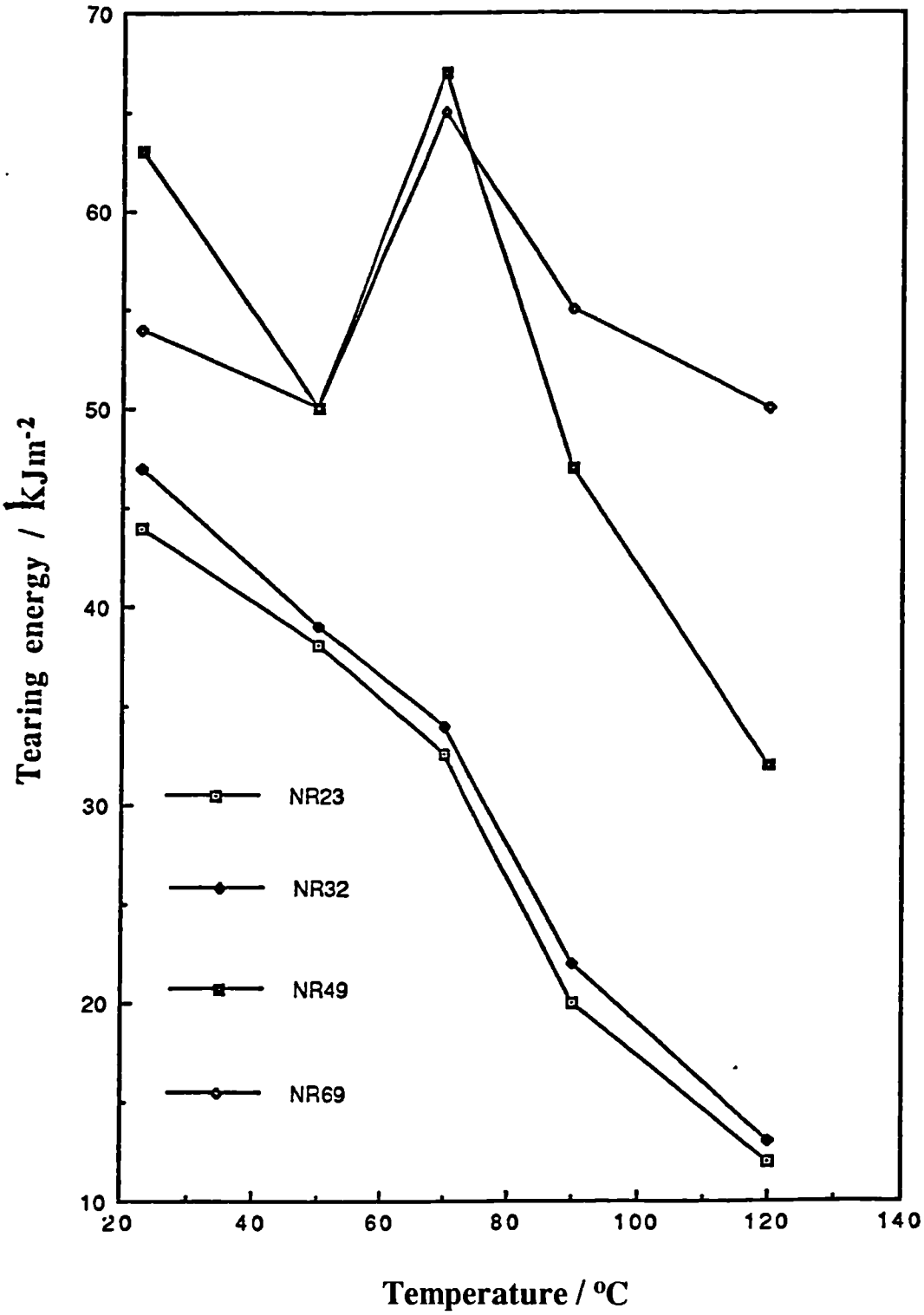

Figure 7.12 : Effect of temperature on the tearing energy of carbon black filled NR vulcanizates at a tear rate of 830μms^{-1}

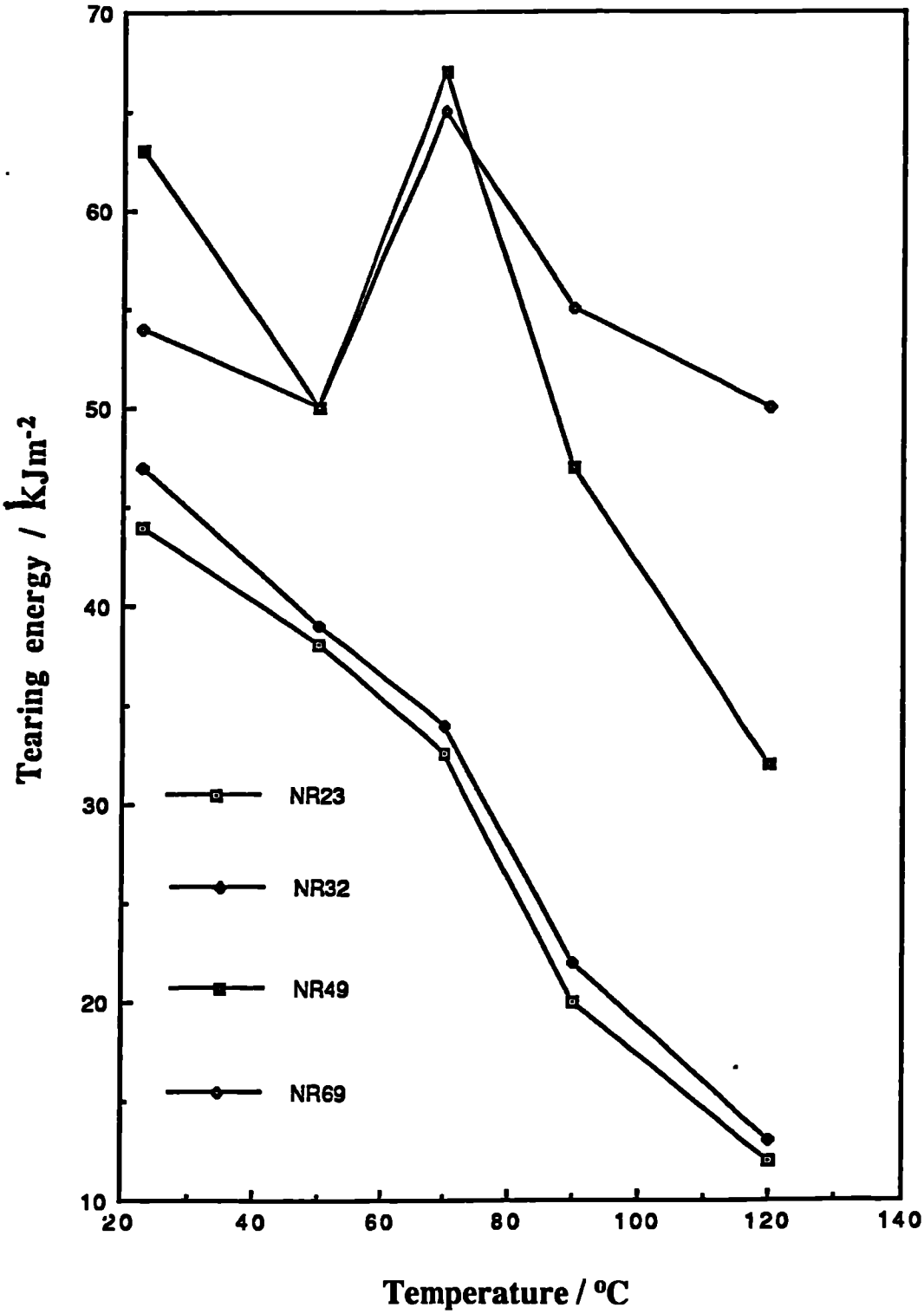

Figure 7.12 : Effect of temperature on the tearing energy of carbon black filled NR vulcanizates at a tear rate of 830μms^{-1}

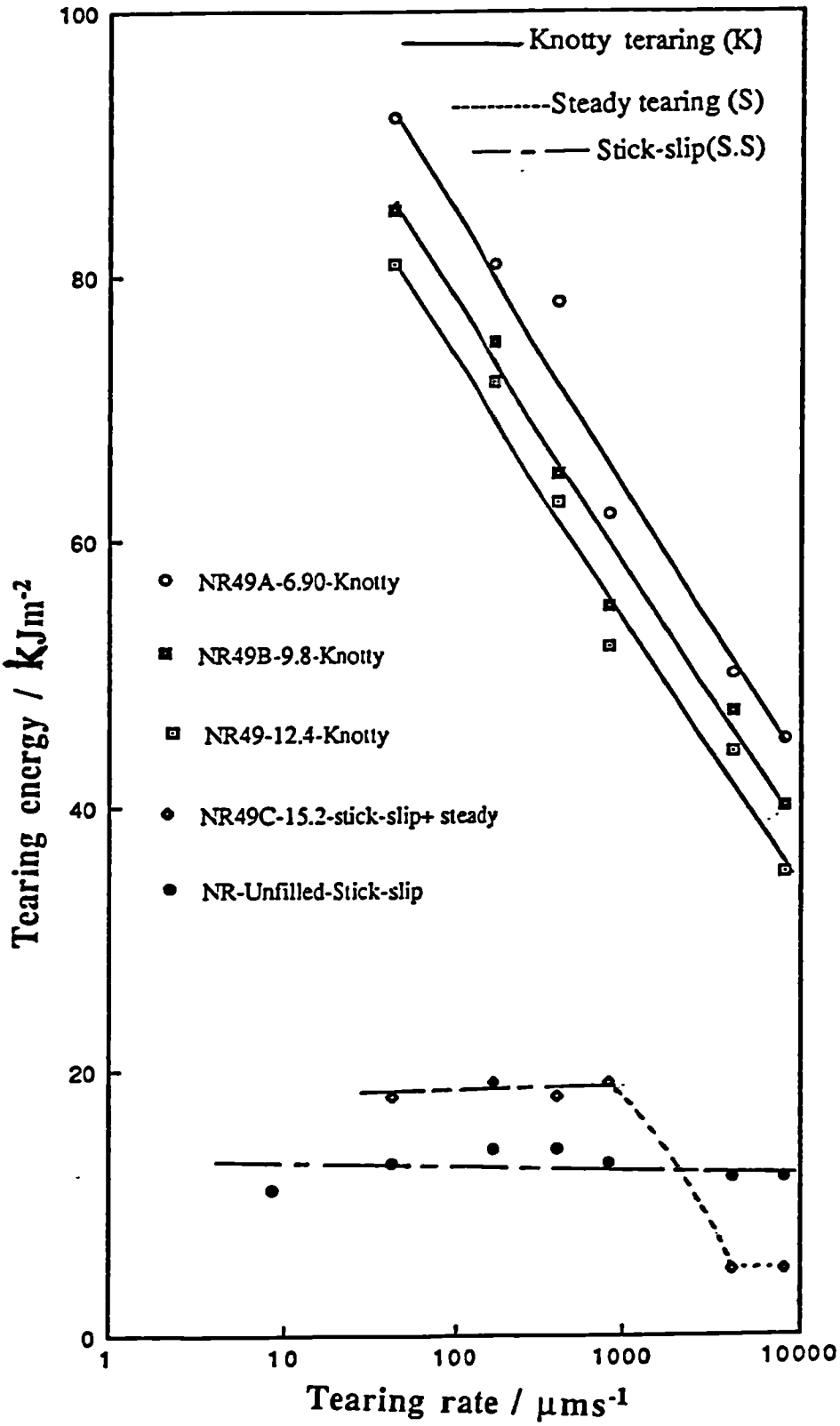

Figure 7.13: Effect of crosslink density on the tearing energy of 49 pphr carbon black-filled NR vulcanizates.

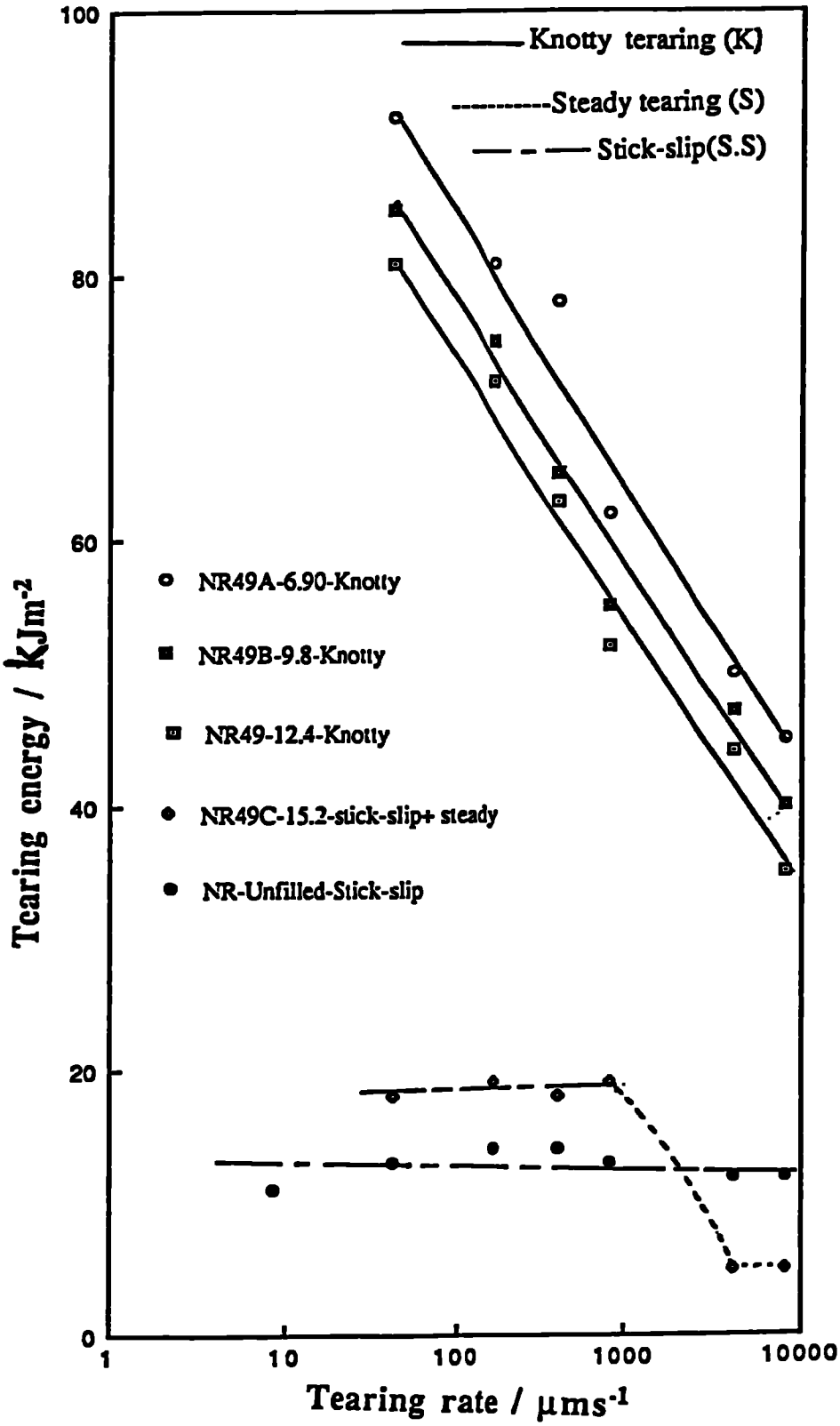

Figure 7.13: Effect of crosslink density on the tearing energy of 49 pphr carbon black-filled NR vulcanizates.

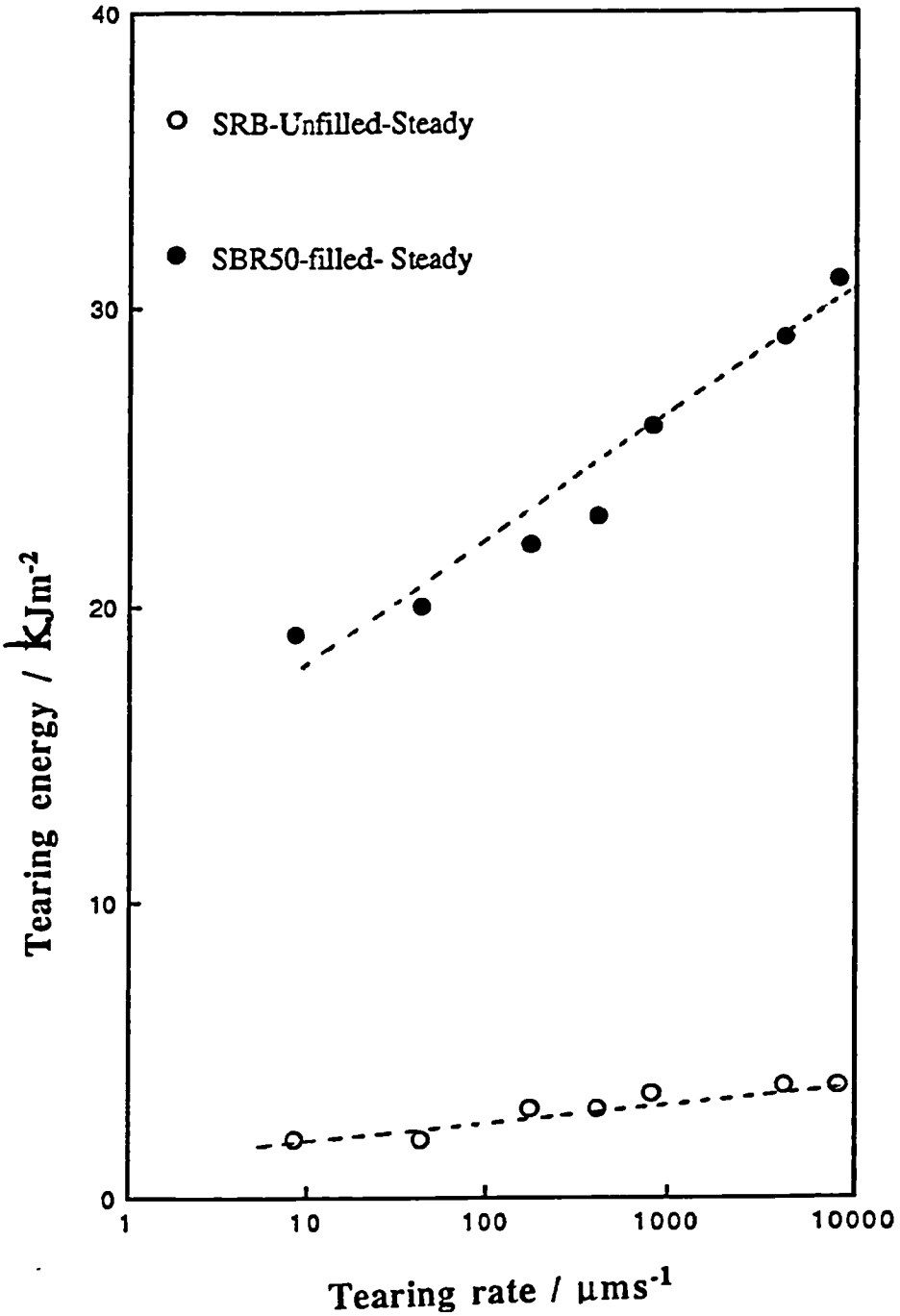

Figure 7.14: Effect of the addition of 50 pphr HAF carbon black on the tearing energy of a SBR vulcanizate at 23°C

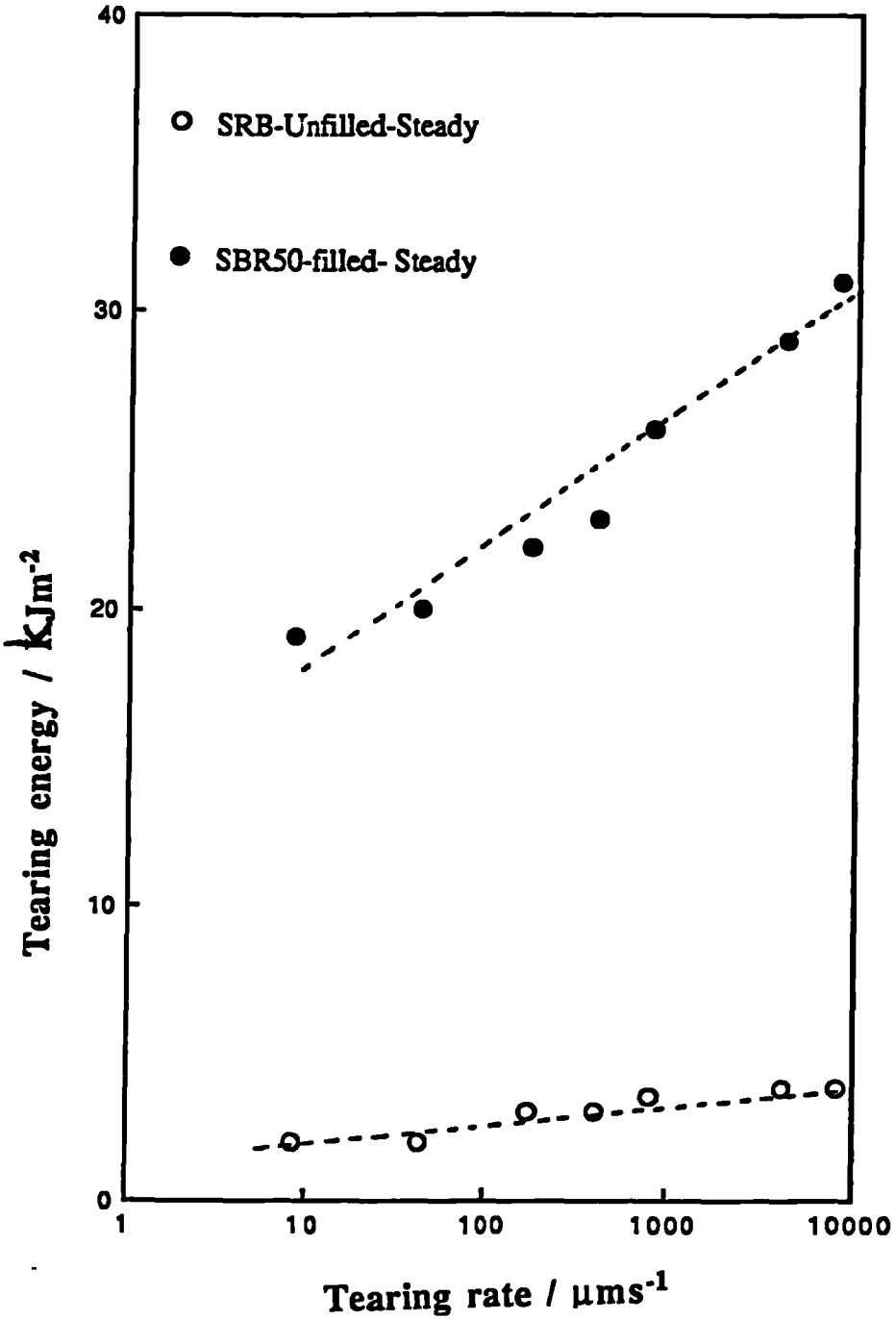

Figure 7.14: Effect of the addition of 50 pphr HAF carbon black on the tearing energy of a SBR vulcanizate at 23°C

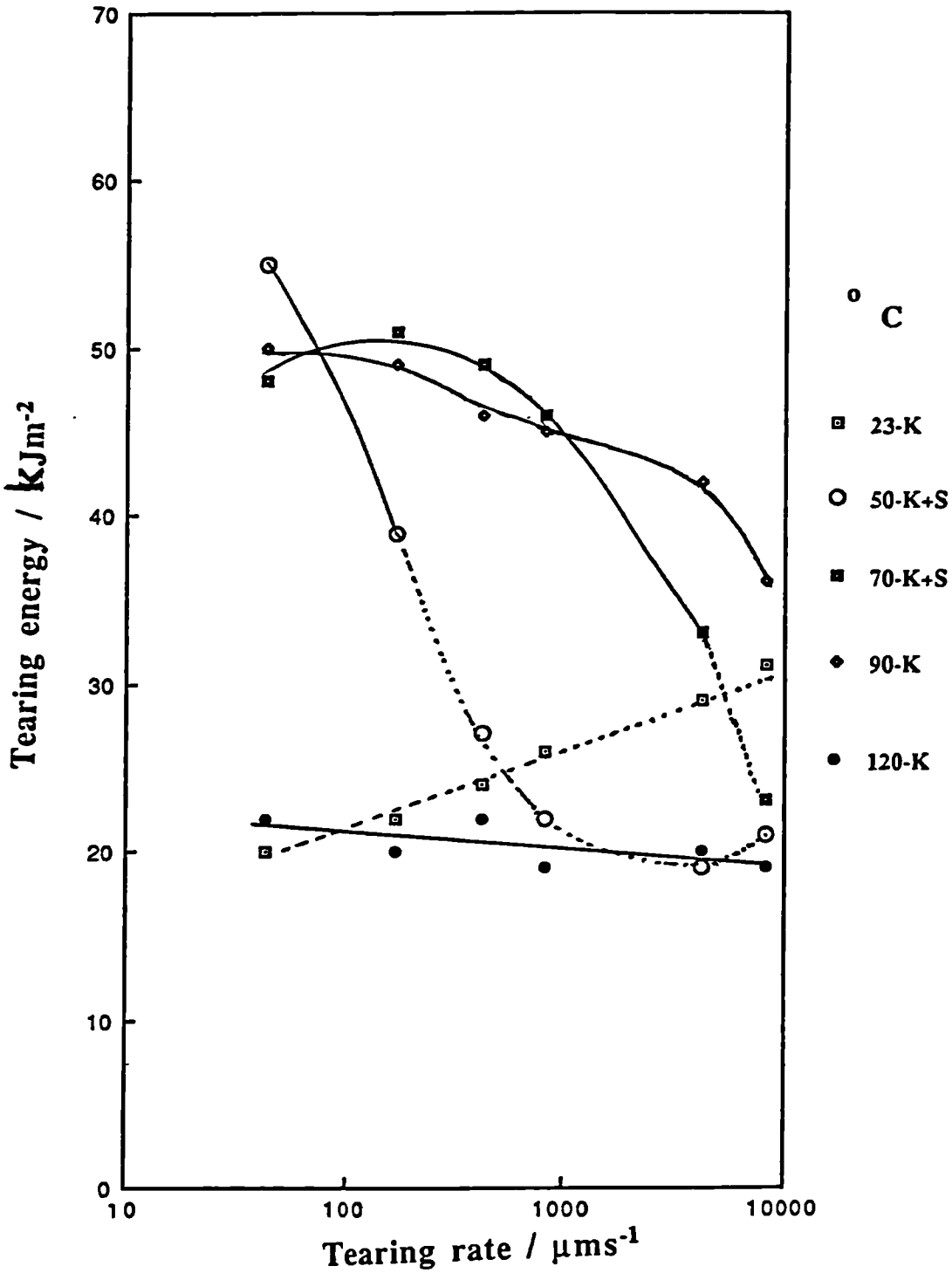

Figure 7.15: Tearing energy versus tear rate at various temperatures of a 50pphr carbon black-filled non-strain crystallizing rubber [SBR]

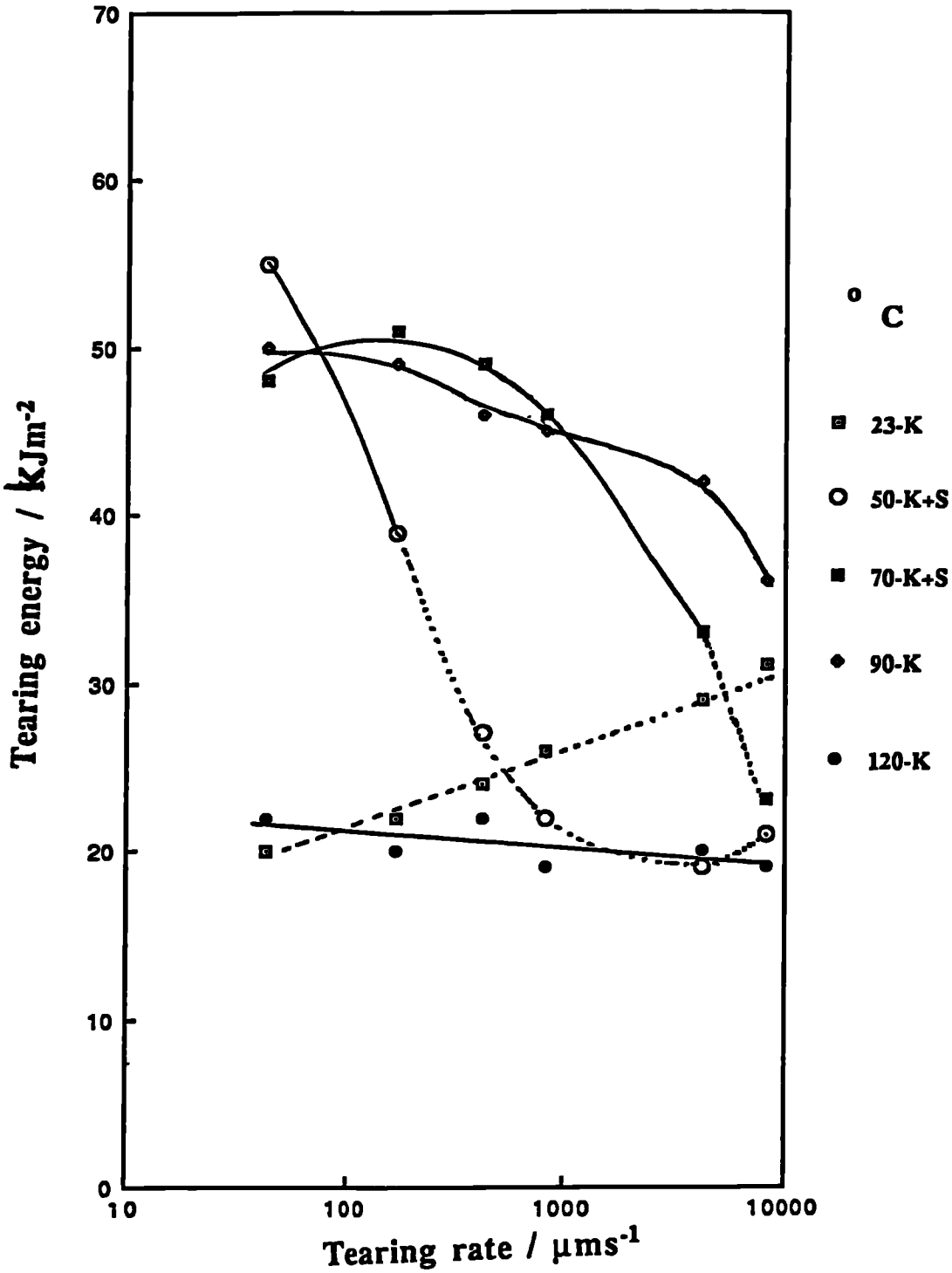

Figure 7.15: Tearing energy versus tear rate at various temperatures of a 50pphr carbon black-filled non-strain crystallizing rubber [SBR]

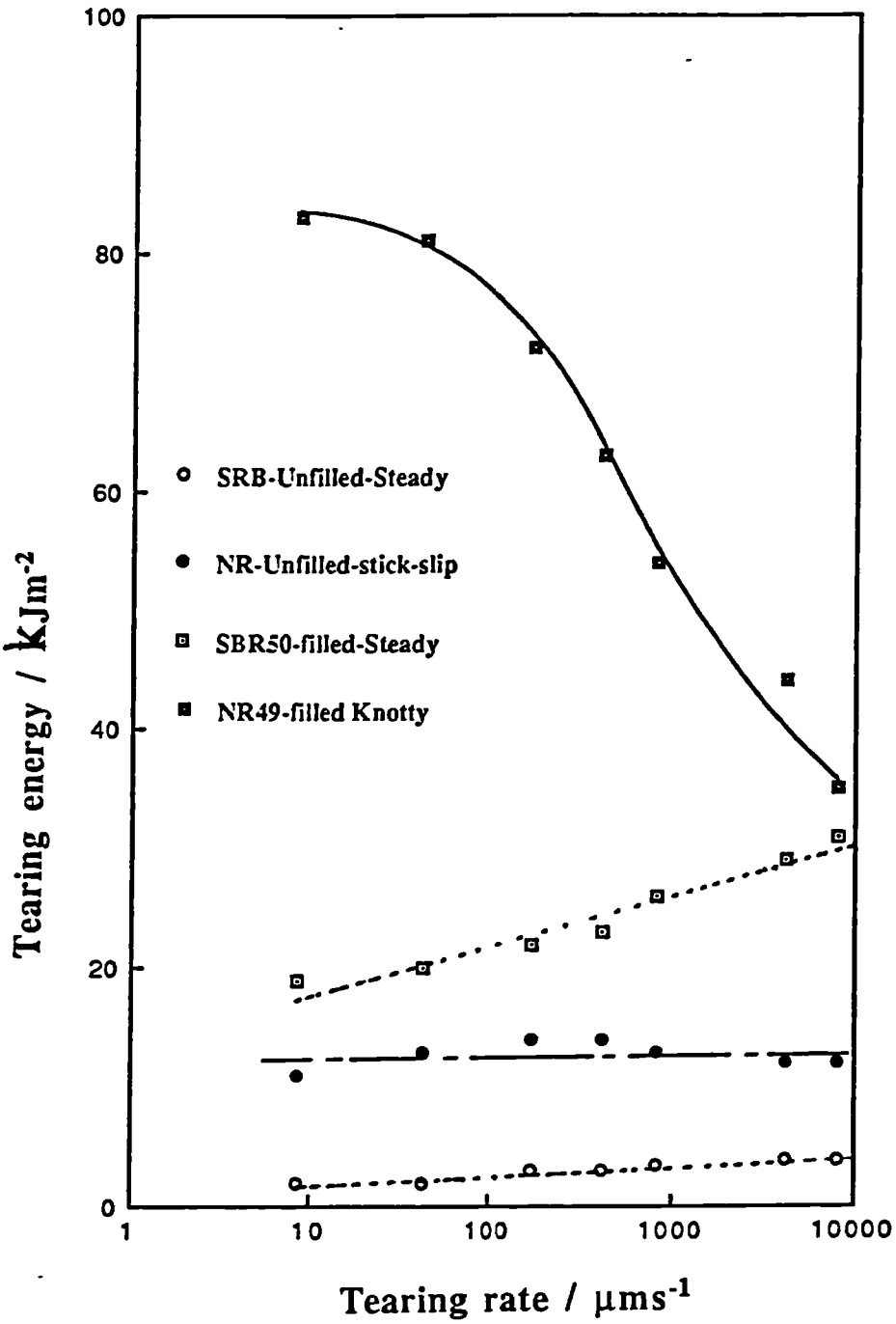

Figure 7.16: Comparison of the tearing energy as a function of tear rate for NR and SBR vulcanizates at 23°C

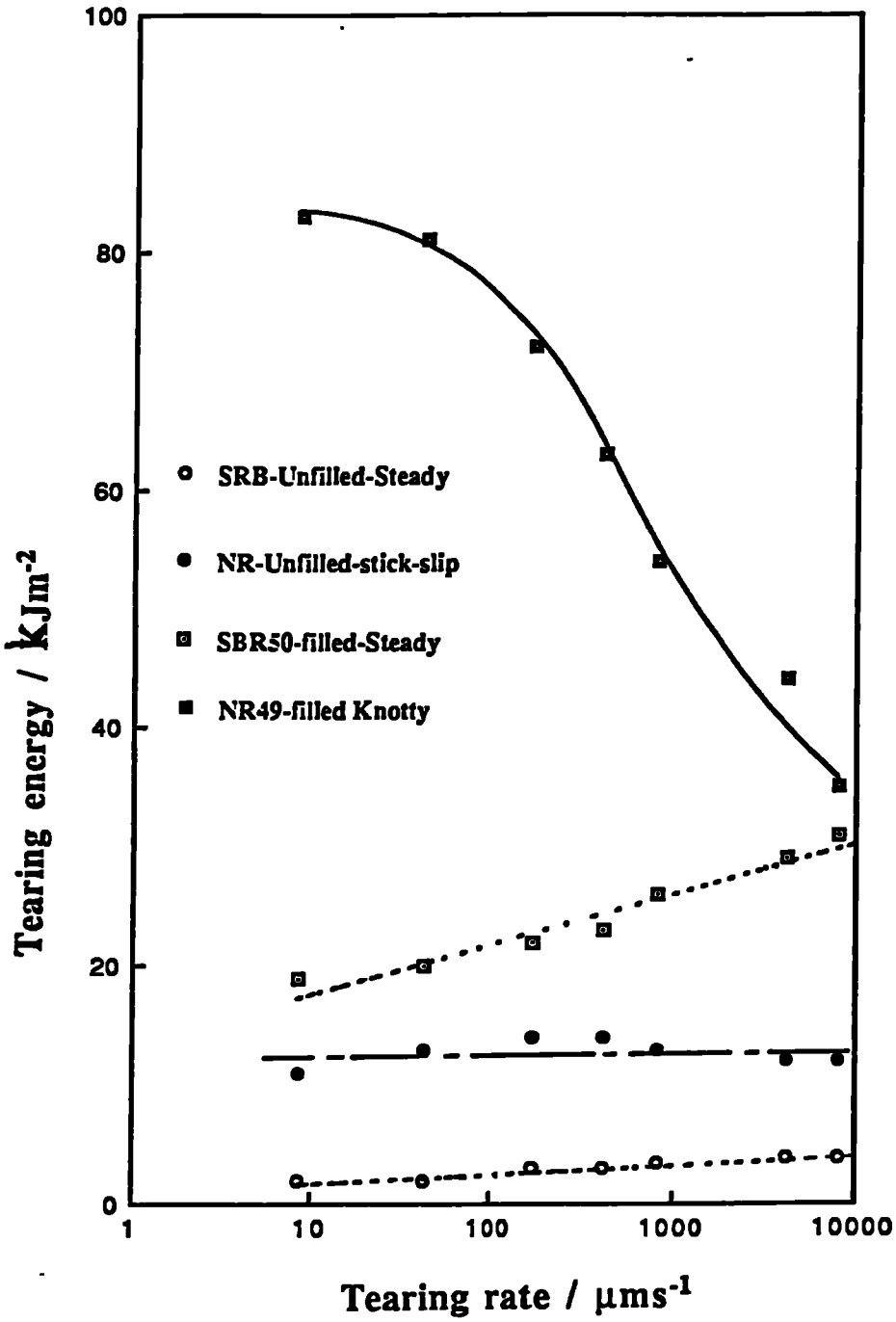

Figure 7.16: Comparison of the tearing energy as a function of tear rate for NR and SBR vulcanizates at 23°C

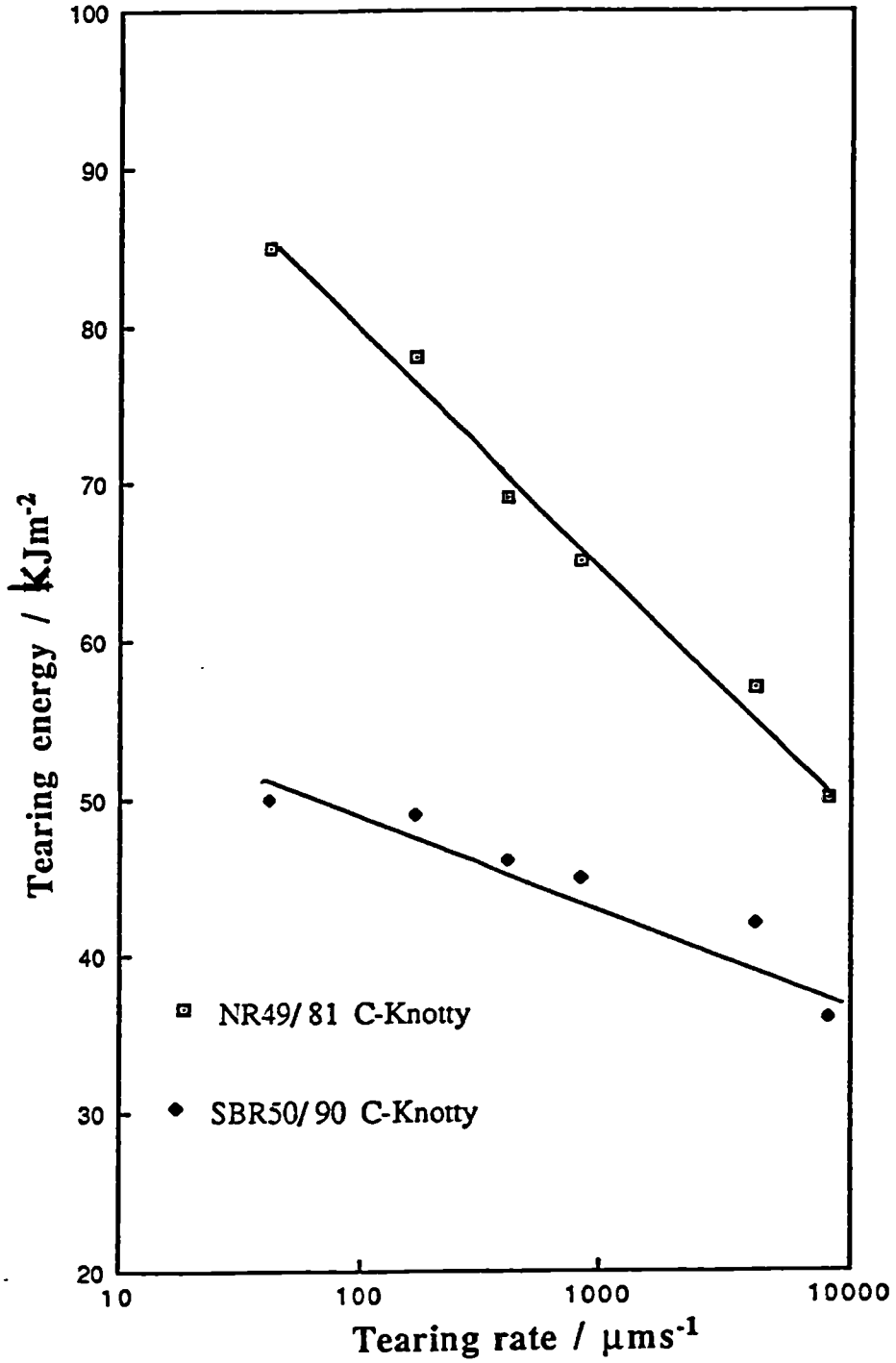

Figure 7.17: Comparison between tearing energy of strain -crystallizing and non-strain-crystallizing carbon black-filled rubbers when both NR and SBR showed knotty tearing

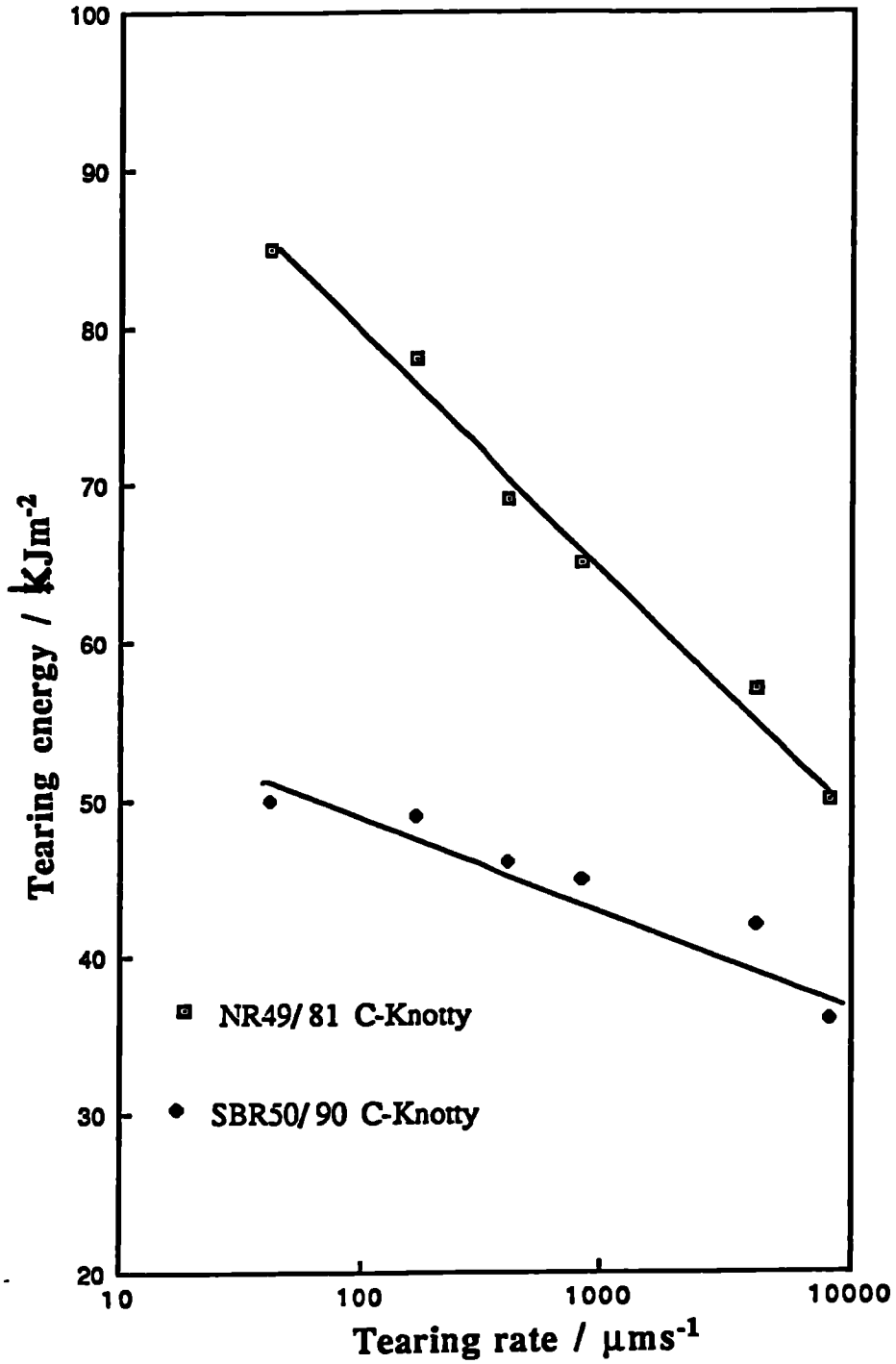

Figure 7.17: Comparison between tearing energy of strain -crystallizing and non-strain-crystallizing carbon black-filled rubbers when both NR and SBR showed knotty tearing

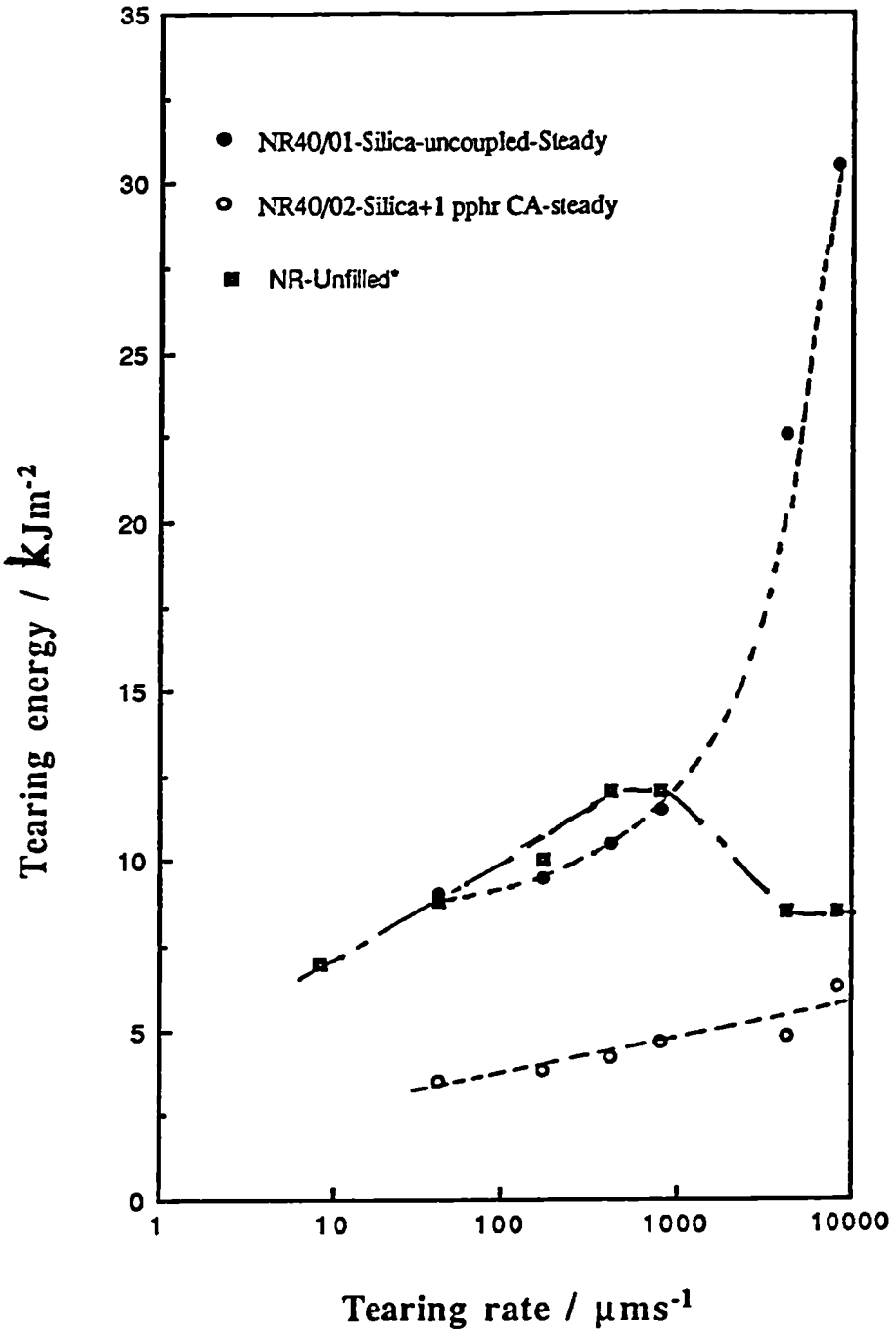

Figure 7.18: Effect of filler and a coupling agent on the tearing energy of the silica-filled NR vulcanizates cured with 1pphr dicumyl peroxide at 23° C, * 1pphr dicumyl cured unfilled NR, data from ref 73 .

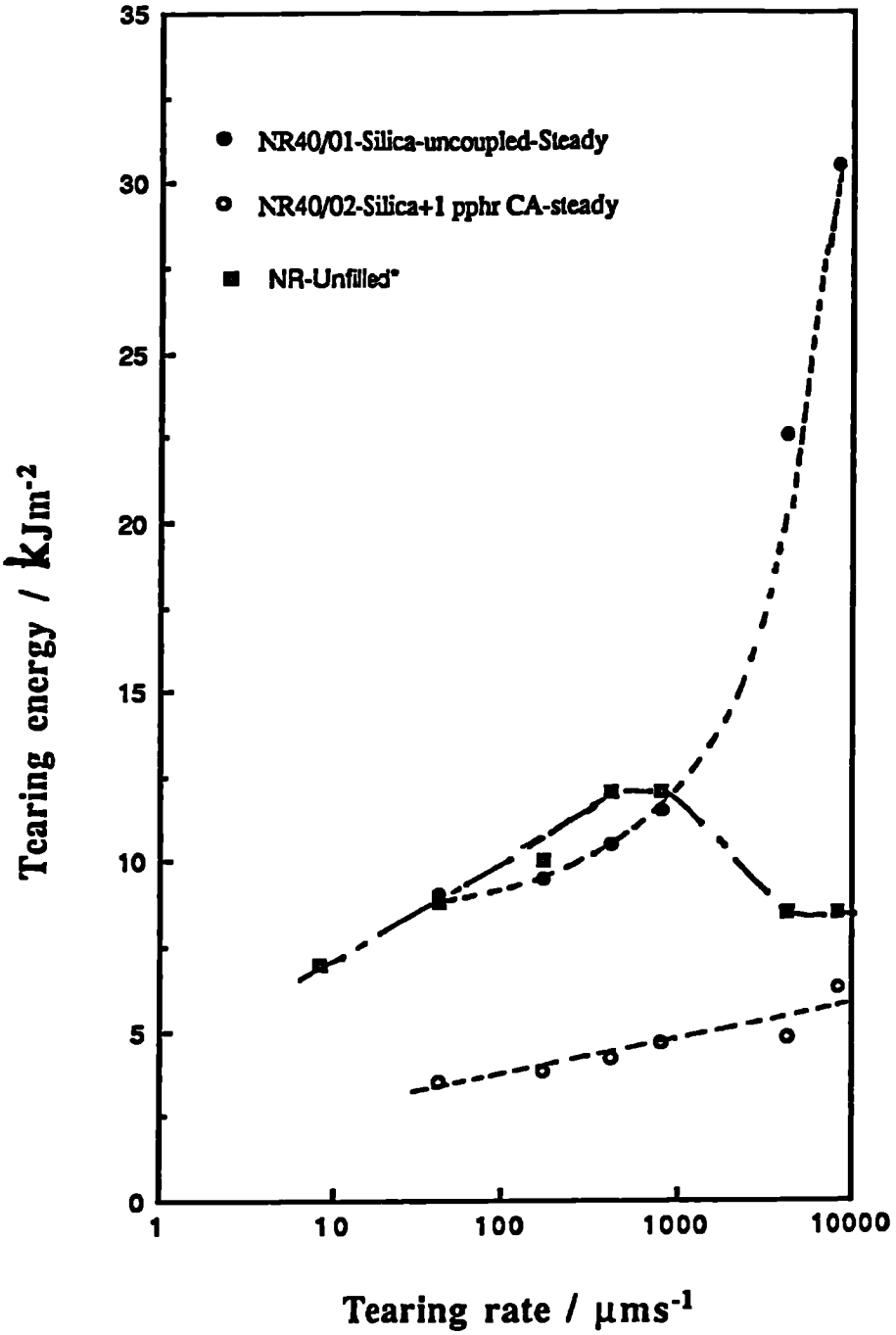

Figure 7.18: Effect of filler and a coupling agent on the tearing energy of the silica-filled NR vulcanizates cured with 1pphr dicumyl peroxide at 23° C, * 1pphr dicumyl cured unfilled NR, data from ref 73 .

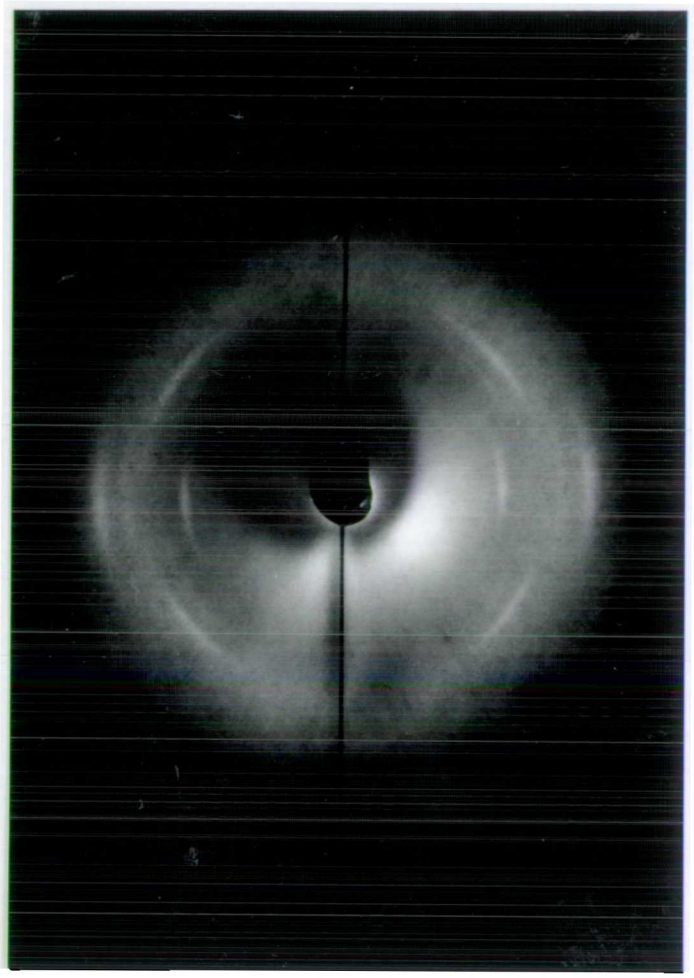

Figure 7.19: Transmission WAXRD photograph of a silica filled NR vulcanizate strained at 300% at 23^0C, Nickel filtered Cu Kα radiation was used with an accelerating voltage of 40 kV and a 30 mA filament current.

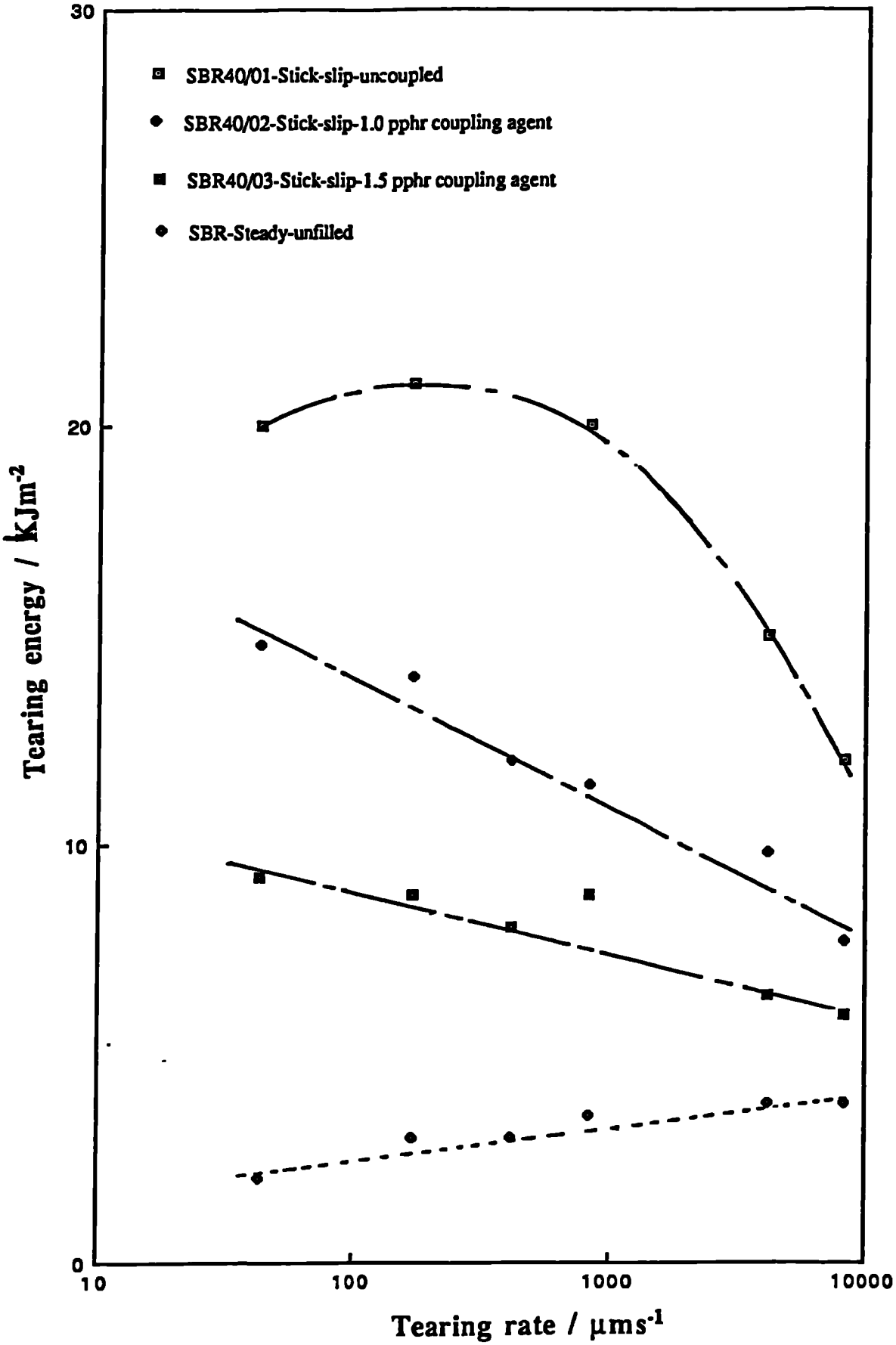

Figure 7.20. The effect of filler and a coupling agent on the tearing energy of silica-filled SBR vulcanizates cured with 1 pphr peroxide.

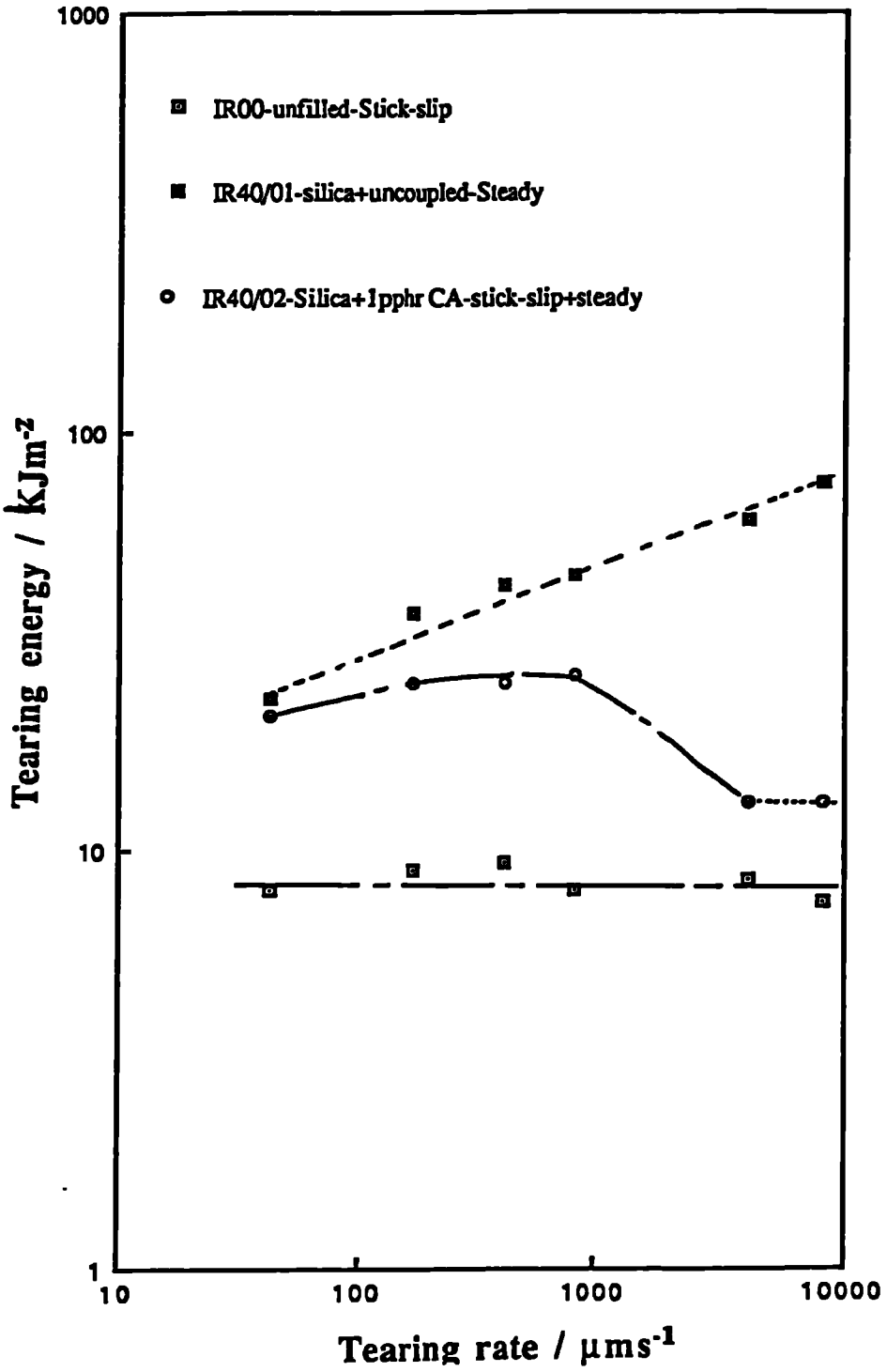

Figure 7.21: The effect of silica filler and a coupling agent on the tearing energy of IR vulcanizates at 23° C.

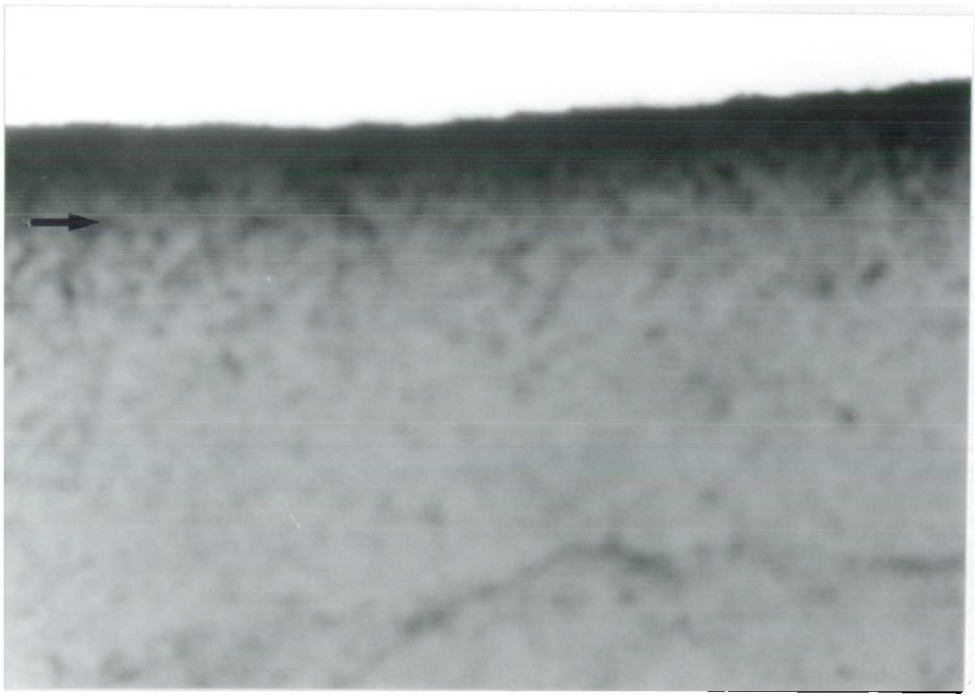

Figure 7.22: Transmission optical micrograph of one side of grown crack in a 40pphr silica filled uncoupled IR vulcanizate at a tear rate of 420 μms^{-1} at 23°C

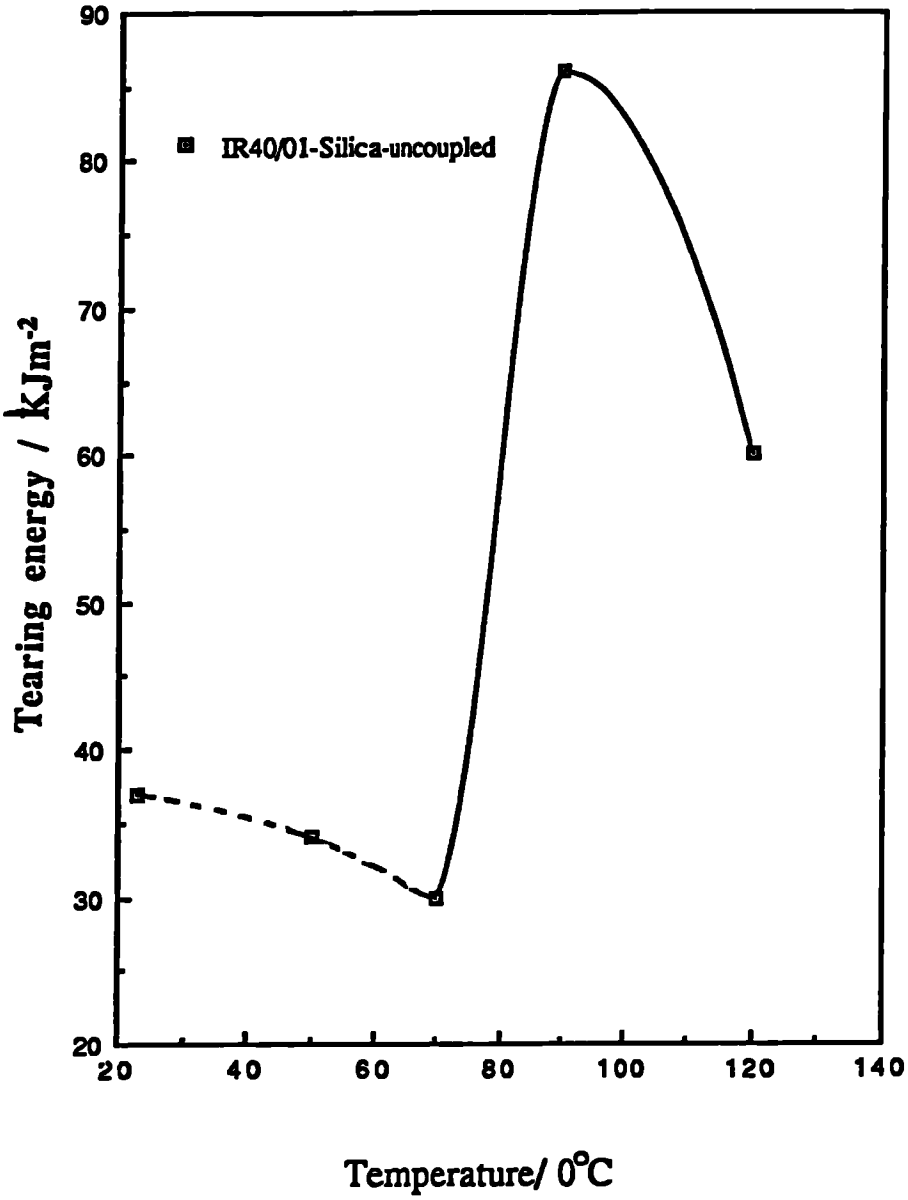

Figure 7.23: The effect of temperature on the tearing energy of silica filled IR vulcanizates at a rate of 420 μms^{-1}

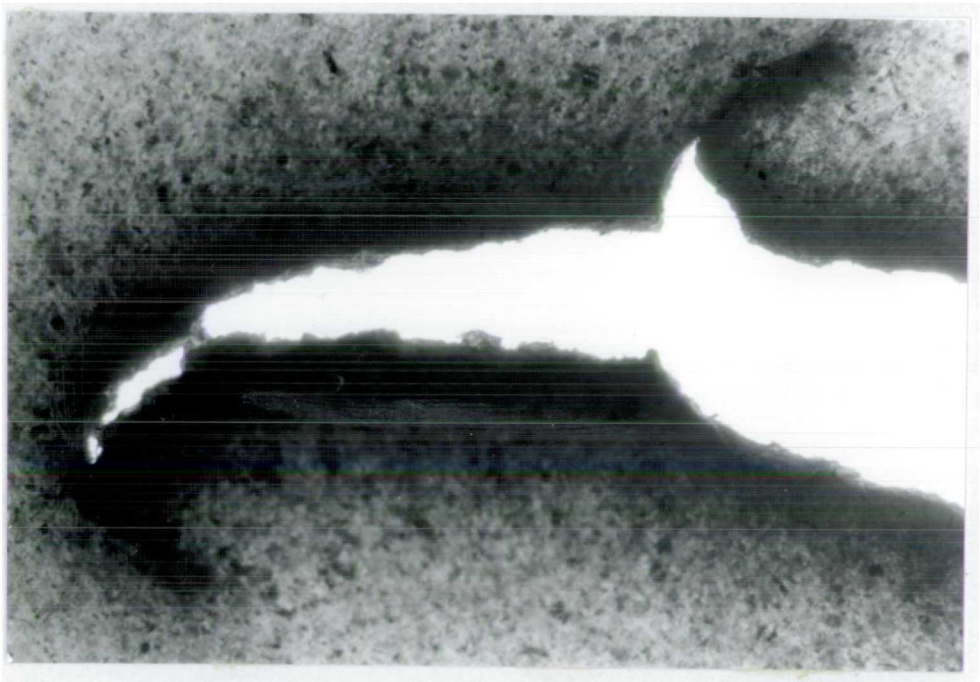

Figure 7.24: Transmission optical micrograph of two sides of grown crack in a silica filled uncoupled IR vulcanizate at a tear rate of 420 μms^{-1} at 90°C (Knotty tearing)

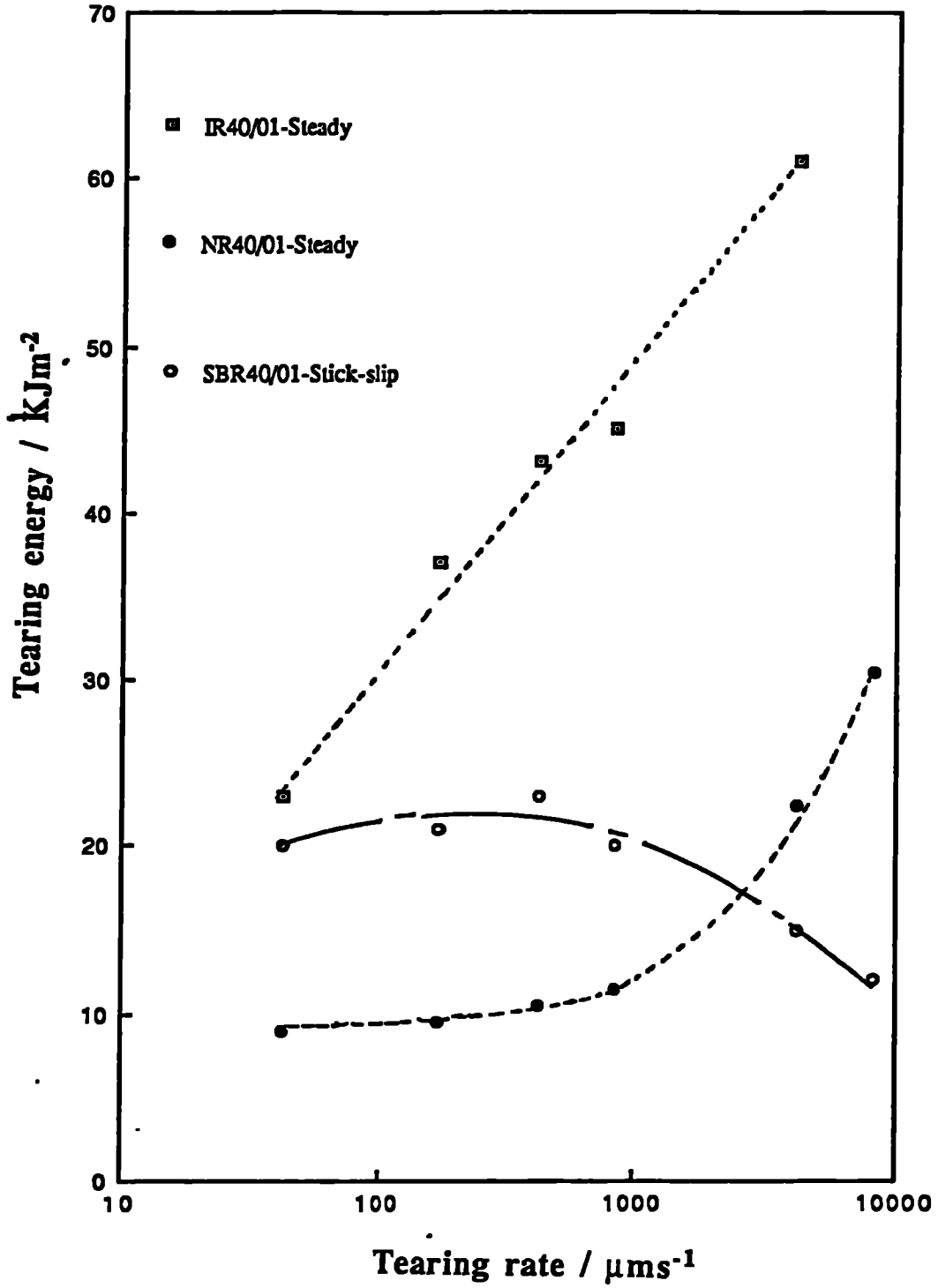

Figure 7.25: The effect of type of rubber on the tearing energy of 40pphr silica filled uncoupled vulcanizates at 23°C

CHAPTER - EIGHT

8.0 INTRODUCTION-CYCLIC CRACK GROWTH

In the previous chapter ideas concerned with tearing in filled rubber vulcanizates were discussed. The concept of tearing energy was introduced and shown to be a materials specific parameter. The tearing referred to concerned rapid crack growth in specimens loaded or strained at a continuous rate usually utilizing the trouser test. However, many rubber components experience repeated cyclic loading in service sometimes causing cyclic crack growth to occur at much slower rates than those normally associated with the tear test. This chapter first briefly reviews how the concept of 'Tearing Energy' can be applied to cyclic crack growth and then discusses existing crack growth data obtained for carbon black filled rubbers.

In the previous chapter results on the tearing behaviour of the Peradin carbon black filled compounds were presented together with limited results on the silica filled compounds. These results were discussed in terms of the effect of materials variables (filler content, crosslink density, coupling agent) and testing variables (rate, temperature) on the resulting measured tearing energy and particularly on the type/regime of tearing. In this chapter the results of cyclic crack growth studies on both the Peradin carbon black compounds and limited data on the silica filled compounds will be presented and discussed. In addition results will be reported from a novel experiment in which specimens were pre-strained in one direction to orientate the rubber/carbon black filler and then subjected to a cyclic loading at right angles to the pre-stained direction. This was carried out in an attempt to both gain some understanding of the role of pre-orientation of the rubber in crack tip growth and to simulate a more complex loading pattern such as may occur in service.

8.1 CRACK GROWTH AND FATIGUE UNDER CYCLIC STRESS

Crack growth during cyclic stressing of pre-cracked (cut) specimens is driven by the release of elastic stored energy in the rubber sample. The process is essentially small scale tearing of the rubber at a crack tip on each application of stress during each cycle. The process can hence be characterized in terms of tearing energy (T) as was discussed for catastrophic tearing in chapter seven. Cyclic crack growth tests can be

carried out using a variety of sample geometries as shown in appendix 7.1 i.e., trouser, pure shear, angle and edge cut tensile strip. Of these the edge cut tensile strip tests result in continuously increasing crack growth per cycle while the pure shear geometry test results in constant crack growth per cycle, for a given applied stress (hence a given tearing energy).

The results from such tests are usually represented as a plot of crack growth per cycle (dc/dn) versus tearing energy. Such plots are shown in figure 8.1 for unfilled SBR and NR vulcanizates over a limited range of tearing energy. The results are plotted as a double logarithmic plot so that the straight lines drawn represent a relationship of the form;

$$dc/dn = B\ T^{\beta} \tag{8.1}$$

Where c is the cut length measured in the unstrained state, n the number of cycles and T is the maximum tearing energy attained during a cycle, B and β are material constants. Results are shown for three test geometries (tensile strip, pure shear and trouser) and it can be seen that dc/dn is independent of test geometry and depends only on the value of the characteristic tearing energy for a given rubber compound. It is found experimentally[74] that this power law relationship adequately represents the behaviour of many rubbers over a useful, but limited range of T. For natural rubber β has a value of about 2 whereas non-strain crystallizing rubbers such as SBR exhibit a β value of about 4.

Figure 8.2(a) shows a plot of the observed cyclic crack growth rates for unfilled NR and SBR vulcanizates over a much wider range of tearing energy (T). It is possible to divide the plot into a number of regions characteristic of a given crack growth behaviour. The full lines represent empirical approximations to the results and are of the forms;

Region A

$$dc/dn = r \qquad T < T_o \tag{8.2}$$

Region B

$$dc/dn = D(T - T_o) + r \qquad T_o < T < T_t \tag{8.3}$$

Region C

$$dc/dn = B\ T^{\beta} \qquad T_t < T < T_c \tag{8.4}$$

Region D

$$dc/dn = \infty \qquad T = T_c \tag{8.5}$$

Region C is that represented by the data in figure 8.1 where B and β are materials constants, At high values of the tearing energy, $T=T_c$, region D, tearing becomes catastrophic akin to the behaviour referred to in chapter seven. Below a critical tearing energy T_t, dc/dn varies linearly with T, (region B) as given by equation (8.3) and as shown by the linear plot in figure 8.2(b). Below a critical value of T, T_o, region A, it is found that crack growth is virtually zero, or occurs at a very small constant rate due to ozone attack.

8.2 FATIGUE LIFE

The crack growth rate at tearing energies $T>T_o$ has been found to be a function of T until catastrophic failure occurs at T_c i.e.,

$$dc/dn = f(T) \tag{8.6}$$

If the fatigue life is defined as the number of cycles required for a crack to grow from a crack length c_1 to a length c_2 then;

$$n = \int_{c_1}^{c_2} dc \,/\, [f(T)] \tag{8.7}$$

This integral can be evaluated provided that the relationship between T and c is known and that values of T can be calculated for the particular sample shape and type of deformation. For example, the tearing energy of a side cut sample deformed in simple extension (see figure 4 in appendix 7.1) is;

$$T = 2\,k\,c\,W \tag{8.8}$$

where k is a slowly varying function of strain[75]. Since T increases with c, rupture of a sample will normally occur when the tearing energy T_c is attained, hence from equation 8.7 & 8.8 , the number of cycles to failure, or fatigue life n, is given by;

$$n = \int_{T_i}^{T_c} dT / [2kWf(T)] \qquad (8.9)$$

Where T_i is the tearing energy at the start of the test, i.e., $T_i = 2kc_iW$

The key is to determine the function f (as shown in equations 8.2-8.4) and to put it in a form which can be integrated directly or numerically. The function must be determined experimentally for each type of material. Then equation 8.7 thus quantitatively relates the fatigue life to the crack growth characteristics of the rubber. The validity of this approach has been examined by carring out experiments on tensile samples containing inserted cuts of various lengths and extended to uncut samples in which it was assumed that natural flaws of a particular size were present initially[74,76,77]. The results were quite satisfactory. However in rubber components, the initial flaw sizes and therefore the initial T values are widely distributed in a given component although it is really the maximum flaw size which is important in determining the failure life. Hence a knowledge of this natural flaw size and shape is necessary in order to predict fatigue life. This is very difficult to measure. Hence a qualitative understanding of the fatigue behaviour of complex rubber components is usually obtained by carring out model experiments on appropriate simply shaped test pieces (see figures a-d in appendix 7.1) and then comparing the results with the measured behaviour of the actual components. This approach is quite useful in a number of applications[78,79,80,81,82]. An alternative approach is to use finite element analysis to assess stress concentrations and distributions of tearing energies in test pieces of complex shape and to attempt to estimate probabilities of crack growth and likely rate. Even here however if fatigue life is to be predicted it would be necessary to predict the initial flaw size and its position in the component.

8.3 MECHANICAL FATIGUE LIMIT

It has been found that at a tearing energy less of than T_o, the threshold value, the crack growth rate is extremely slow (virtually a constant rate in region A in figure 8.2(a), below the T_o value of about $0.01 kJm^{-2}$). This very slow crack growth rate is due to ozone attack. The existence of T_o means that if this value of the tearing energy is not exceeded during cyclic fatigue then the fatigue life of the article will, in the absence of ozone attack, be virtually infinite. Thus rubber can, like other materials such as metals,

exhibit a fatigue limit. The tensile strain e_o corresponding to T_o represents the so called "Mechanical fatigue limit" for a particular rubber. e_o for NR and most of the synthetic rubbers examined to date lies within the range 65-95%. For tensile strains below about 65% strain therefore the fatigue life (usually measured using a dumb-bell specimen repeatedly cycled to a fixed extended length until it breaks in two) is virtually infinite[83]. The magnitude of e_o is extremely important since most rubber components subjected to repeated stressing will be designed to work below it. However in a complex component it is not easy to determine the actual magnitude, point to point, and not easy to determine whether the working conditions are below T_o

8.4 FACTORS WHICH AFFECT CRACK GROWTH AND FATIGUE LIFE

8.4.1 Strain cycle

The strain cycle to which a specimen is subjected during cyclic crack growth may or may not include zero strain. If zero strain is included and the specimen is fully relaxed the crack growth behaviour may be very different from that in the non-relaxing case. This effect is very significant in the case of strain crystallizing rubbers[77].

Figure 8.3 shows some cyclic crack growth results for an unfilled NR. In this instance if the minimum T value is 6% of the maximum tearing energy instead of zero (the tearing energy corresponds to the maximum strain of a cycle and is determined by using the equations shown in appendix 7.1 for different test geometries) the crack growth rate may be reduced by a factor of 10. According to Thomas[84], in a strain crystallizing rubber cyclicly stressed, crystals form as the stress increases at the crack tip and melt at the zero strain part of the cycle. As a consequence of the melting of these crystals, crack growth takes place on subsequent extension before strain-crystallization occurs again. Under non-relaxing conditions, only partial melting of crystals occurs resulting in lower crack growth per cycle at the tip of crack[77]. Crack growth rates are very similar under relaxed and non-relaxed conditions for non-strain crystallizing rubbers, such as SBR, and the crack growth rate increases more rapidly with tearing energy than for strain crystallizing rubbers[85] as seen in figure 8.2(a) which shows the crack growth rates for unfilled NR and SBR under relaxed conditions over a wide range of T values.

8.4.2 Temperature

The effect of temperature on fatigue life is more pronounced for non-strain crystallizing rubbers than for strain-crystallizing rubbers[77] as shown in figure 8.4. According to Lake[86] this difference in behaviour is due to the nature and the extent of mechanical hysteresis in the two rubbers at high strains. NR exhibits a pronounced mechanical hysteresis due to crystallization at high strains at the tip of crack. The origin of this hysteresis is little affected by the temperature[65]. In the case of SBR, the hysteresis is solely governed by the internal viscosity of the material. This internal viscosity decreases considerably with increasing temperature[59,76].

8.4.3 Frequency

The effect of frequency on crack growth per cycle is not simple and depends on the nature of the rubber. In the case of non-strain crystallizing SBR if tearing occurs in a steady time dependent manner then crack growth during each cycle can be considered as the sum of two components[76]. The time dependent component and the increment of crack growth which occurs due to the cycling process itself. At large frequencies, the second of these is dominant and the cyclic crack growth rate at a given tearing energy decreases by a factor of three over a range of 10-1000 cycles per minute. At low frequencies (below 10 cpm), the time dependent component of crack growth dominates and the crack growth per cycle is inversely proportional to the frequency.

Natural rubber, a strain crystallizing rubber, tears in a stick-slip manner. Crack growth does not occur in a time dependent manner and cracks only propagate statically in a catastrophic manner at above a given critical tearing energy. The cyclic component of crack growth hence dominates and the cyclic crack growth rate at a given tearing energy decreases by a factor of three over a range of 10-1000 cycles per minute. At low frequencies, however, below 10 cpm, the rate is virtually independent of frequency. Figure 8.5 shows relative behaviour in air and vacuum depends on T and frequency.

8.4.4 Effect of oxygen

Atmospheric oxygen can influence the cyclic crack growth rate of rubbers. The effect is akin to adding or enhancing a time dependent crack growth process.

At low tearing energies this results in crack growth rates in NR being three times higher in air compared to vacuum (figures 8.5&8.6). However, at higher tearing energies (higher crack growth rates) the effect of oxygen is frequency dependent. At high frequencies dc/dn is the same in air and vacuum (figure 8.5) as the influence of the time dependent crack growth process is minimal. At lower frequencies dc/dn is significantly higher in air as the time dependent crack growth process contributes significantly to the crack growth per cycle (figure 8.5).

Similar effects have been found on fatigue life in NR and for crack growth rates for SBR[87].

It is proposed that a stress-activated oxidative scission process leading to the breakage of the molecular chains in the neighbourhood of the crack tip was responsible for the differences in rate[87]. Suitable anti-oxidants militate against the effect of oxygen and give a crack growth rate typically about mid-way between the two curves for air and vacuum (figure 8.6).

8.4.5 Vulcanization system

Lake and Lindley[77] reported on the effect of the vulcanization system (i.e., polysulphide, monosulphide & peroxide) on the crack growth rate of unfilled NR vulcanizates. They found that the fatigue life of NR containing polysulphidic crosslinks was twice that for systems with mono-sulphide & peroxide crosslinks. They concluded that the superiority of the polysulphidic vulcanizates might be due to the labile nature of polysulphidic crosslinks, which were able to break and reform in the strained state, thus relieving the stress concentration at the tip of the crack. L.C. Yanyo[88] made a similar observation for carbon black-filled NR vulcanizates. He concluded that the longer the crosslinks, the easier it is for individual chains to move (rather than break) when the rubbers are subjected to mechanical stress resulting in larger hysteresis losses and a large tearing energy being needed for a given crack growth rate. The polysulphidic crosslinks may provide this flexibility and hence improve fatigue life.

8.4.6 Effect of filler

Lake and Lindley[77] studied the effect of carbon black on the crack growth rate of several rubbers containing 50pphr MT or HAF carbon black-filler. Figure 8.7 illustrates the results. In all the cases the addition of carbon black causes a decrease in the crack growth rate for a given tearing energy. The threshold tearing energy T_o in the case of HAF carbon black (a

reinforcing filler) is increased by about a factor of two, but MT carbon black (a non-reinforcing filler) has little effect on T_o. The decrease in the cyclic crack growth rate is attributed to the additional source of mechanical hysteresis (i.e., further energy losses at the tip of crack) and also may be due to an effective increase in T_o. Young and Doyle[89] have reported a similar finding for the effect of 50 pphr GPF carbon black in NR and in chloro and bromo-butyl rubbers in cyclic crack growth experiments with pure shear specimens, although their studies did not extend to as low tearing energies as those of Lake and Lindley[77]. A great deal of data exists on the fatigue lives of filled rubbers which are cycled to a given strain or given stress[90-95]. The fatigue lives depend on both the initial flaw sizes and on the crack growth rates at a given tearing energy. Both of these depend on the type of carbon black added[90,93]. Cycling materials containing different carbon blacks to given stresses or strains results in comparisons of fatigue life being made at quite different tearing energies due to the elastic modulus differences. Great care must hence to be taken in interpreting such data. The data does suggest that the type and size of the carbon black particles may be significant in determining the initial flaw size[90] and in determining the crack growth rate[93].

While a great deal of work may have been carried out on the effects of carbon black on fatigue life and more limited studies on the effect of carbon black on cyclic crack growth rate, no systematic study exists on the effect of the magnitude of carbon black content on dc/dn at a given tearing energy nor on the corresponding effect of variable crosslink density. Furthermore no cyclic crack growth data exists in the literature for silica filled vulcanizates.

8.5 AIMS AND SCOPE OF THE PRESENT INVESTIGATION

The present work aims to utilize the carbon black filled NR Peradin compounds to study the effect of carbon black content and crosslink density on cyclic crack growth as a function of tearing energy. A novel part of this work will be to study the effect of pre-straining a carbon black filled rubber in one direction to orientate the rubber/carbon black and then to study cyclic crack growth in this direction. This is analogous to the tearing experiments carried out by Samsuri[73]. It will be used to attempt to gain some understanding of the role of pre-orientation of the rubber in crack tip

growth, compared to crack tip growth in the conventional tests when the orientation is imposed in a direction normal to the crack path.

For the first time crack growth rates in silica filled materials will be measured and in particular the role of a coupling agent will be examined.

8.6 EXPERIMENTAL

In this investigation, vulcanizates based on natural rubber (NR) filled with HAF carbon black or silica filler were used. All the formulations are shown in tables 3.1 to 3.4. The NR vulcanizates filled with different amounts of carbon black (Peradin compounds) were used to study the effect of filler loading on crack growth rates. The effect of crosslink density was studied using the formulations shown in table 3.2 for NR vulcanizates filled with 49 pphr carbon black but having different ratios of sulphur/accelerator to achieve different crosslink densities. An unfilled NR[25] (EDS19) was also used for the purpose of comparison. The effect of pre-straining the rubber in a direction parallel to that of cyclic crack growth was examined using the NR vulcanizate filled with 49 pphr carbon black (NR49). Limited cyclic crack growth studies of silica filled vulcanizates without and with a coupling agent were also carried out using the formulations given in table 3.3.

8.6.1 Crack growth measurement

The test-piece used to investigate the cyclic crack growth behaviour under dynamic conditions was a pure shear test-piece as shown in figure 8.8(a). The tearing energy at a given extension for such a test-piece is independent of crack length and is the product of the strain energy density at that extension, W, and the unstrained height, L_o i.e., (see section 8.6.4 and ref 29)

$$T = W L_o \qquad (8.10)$$

This characteristic of the pure shear test is particularly useful in a crack growth test as it is possible to monitor crack growth over any convenient interval of growth at a given strain level i.e., given tearing energy. Also, reproducibility of the results can be checked on a given sample after other tests at different strains have been performed by reverting to the original strain but using a longer crack. This type of test-piece also allows the surface morphology to be readily correlated with the applied strain and corresponding crack growth rate dc/dn i.e., crack growth per cycle.

The appropriate dynamic strain (i.e., amplitude of the dynamic testing machine) to be imposed on the sample to generate a given tearing energy was determined from the unstrained height (L_o) at zero force and the strain energy density (W). In determining W, the pure shear test-piece was cycled

for about an hour to allow most of the set due to the stress-softening effect to take place. This set was negligible in the case of an unfilled rubber vulcanizate but was more pronounced for filled vulcanizates. The next step was to obtain the stress-strain curve for the pure shear sample at a particular temperature and rate or frequency. The strain energy density, W, at each strain of interest was determined from the area under the stress-strain curve by integration. The strain energy density, W, was then plotted against the strain. A typical plot is as shown in figure 8.9 for the carbon black filled NR vulcanizate (NR69) used in this study. However, the initial unstrained height between the specimen clamps (L_o) changed during the initial cycling process. Thus determination of the unstrained height at zero force was required, after the initial cycling period, to calculate a required dynamic strain for a crack growth test to calculate W from figure 8.9 and in turn to calculate the tearing energy by using equation (8.10). This is particularly important because the crack growth test is usually carried out at relatively small strains (maximum 30%). Thus any errors in the determination of unstrained height may have a significant effect on the determination of tearing energy using equation (8.10). Furthermore, the strain energy density was determined above for a particular temperature and frequency. However, the strain energy density W also depends on the test frequency and other testing conditions such as temperature, enviromental conditions etc., particularly in the case of filled vulcanizates[77]. Thus any such change in the test conditions would require a separate estimation of W. This would complicate the crack growth measurement which itself is a time consuming testing procedure.

Thus a method, which would allow the tearing energy to be measured during a crack growth test without either prior determination of the strain or prior determination of the unstrained height (L_o) after the initial set period, would be very useful for crack growth measurement.

Such a method was introduced in the present work and is illustrated below. A schematic diagram of a pure shear test-piece with a crack length c, width w, unstrained height L_o is as shown in figure 8.8(a). The thickness of the test-piece is h. A straight forward method to estimate the tearing energy was to divide the area under the load-displacement curve for this specimen, (figure 8.10) by the uncut area of the test-piece i.e., **(w-c)h.** This calculation assumes that the cut area of the test-piece is force free. Thus assuming that the cut portion was not contributing anything to the experimentally obtained load-displacement curve. It had been observed by

many workers[29,80] that the force in the cut region near the crack tip region was not zero. A defined portion of the area containing the cut was not force free. This is illustrated in figure 8.8(a) by the shaded length **x**. Thus, the area **x.h** must be deducted from the cut area **c.h** i.e., **(c - x) h** to obtain the force free area which made no contribution to the experimentally obtained load displacement curve. An accurate value of the tearing energy, T, would then be given by;

$$T = \frac{\text{area under the load displacement curve}}{\{ w - (c-x) \} h} \qquad (8.11)$$

In order to use equation (8.11) a value or values of x needed to be obtained.

8.6.2 Determination of the value of x

A series of experiments was carried out on the filled and unfilled rubbers by measuring the change in force measured on a strained pure shear test piece specimen as a longer and longer cut was introduced using a razor blade. The results from such a test for NR69 are shown in figure 8.11. The data points show the measured decrease in force as the cut length is increased. A straight line is shown drawn through these points. Deviation from this line is seen for very short or very long cuts due to the non uniform stress distribution at the pure shear test piece edges. Also plotted on figure 8.11 is the force necessary to extend specimens of widths corresponding to the uncut lengths. The two lines are essentially parallel and the force necessary to extend the cut specimens is clearly greater due to the fact that the force is not zero at the cut near the crack tip. The cut specimens (figure 8.11) hence behave as if the cut length was x = 6.7 mm shorter than the actual cut length and the values of x is independent of cut length. In the test pieces used in the present study this corresponded to an x of 28% of the unstrained height L_o for unstrained heights of 12-34mm. This figure was used throughout this study to calculate x which was then used in equation 8.11 to calculate in situ values of the tearing energy.

The validity of this assumption was checked by comparing the in situ values of T with those determined from prior mensurement of W and L_o using equation 8.10. The results are shown in figure 8.12 and the aggrement is seen to be excellent.

8.6.3 Cyclic crack growth test procedure

Cyclic crack growth tests were carried out using a servo-hydraulic testing machine at room temperature (23°C). A sinusoidal waveform at a frequency of 5Hz was imposed on the specimens. The pure shear test-piece was strained to a maximum strain amplitude of between 5-35% and relaxed to zero strain in each cycle. This is known as a fixed-displacement, fully relaxing test.

A horizontal cut 40 mm in length was introduced on the central axis of one edge of the test piece using a razor blade. This placed the crack/cut tip sufficiently far from the edge to avoid any edge effects[80]. The test piece was cycled to a specific maximum strain amplitude and the crack length was measured using a travelling microscope. The initial rapid crack growth rate due to the extreme crack tip sharpness resulting from the razor blade incision was neglected[76]. Load-displacement curves were simultaneously recorded at regular intervals and always at the time of taking the reading of crack length. Tests were carried out over a range of strain amplitudes and hence a range of tearing energies. The crack length c was plotted against the number, n, of strain cycles in each case. The slopes of these plots are the crack growth per cycle i.e., dc/dn. A typical plot obtained in this study for a carbon black filled NR vulcanizate is as shown in figure 8.13. The cyclic crack growth behaviour for a particular vulcanizate was expressed as the logarithm of the crack growth per cycle (dc/dn) versus logarithm of the tearing energy T (figure 8.14).

8.6.4 Determination of the tearing energy of a pure shear specimen pre-strained (λ_1) in the direction parallel to the crack growth direction and subjected to a maximum cyclic strain amplitude (λ_2) in a direction normal to the crack growth direction.

The derivation of the equation for the tearing energy in a non pre-strained pure shear test specimen was carried out by Thomas[29]. The arguments will be repeated here as they provided the basis for the calculation of the tearing energy in the situation where a specimen is additionally pre-strained by λ_1 (lateral extension) in a direction parallel to that of crack growth.

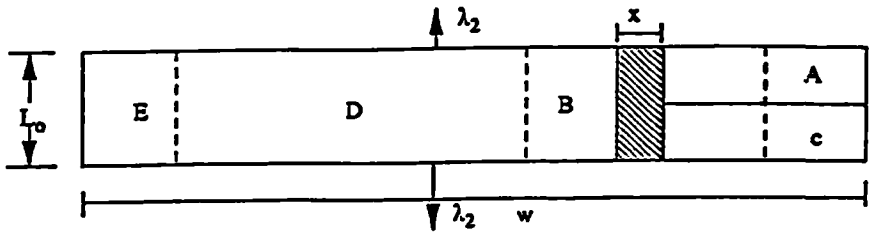

Figure 8.8(a)

Figure 8.8a illustrates a pure shear test-piece containing a cut of length c and having an unstrained height L_o and thickness h. If the specimen grips are held at a constant displacement to produce a strain λ_2, the strain energy density of the deformed pure shear specimen is not the same in all the different regions illustrated. Region A is unstressed and so the assumed strain energy U_A will be zero. In region B, around the cut tip the stress field is complex and the strain energy U_B is difficult to determine. Region D will be in pure shear and so the strain energy in this region will be given by, $U_D = W V_D$ where W is the strain energy per unit volume of the material in pure shear at the relevant strain and V_D is the volume of region D. Region E will not be in pure shear because of its proximity to the ends of the specimen and so U_E will be difficult to calculate.

The lack of knowledge of the magnitudes of U_B and U_E can be overcome by calculating only the change in the stored elastic energy and hence the elastic energy released when crack propagation occurs. If the crack grows by Δc (referred to the unstrained state, $\lambda_2 = 1$) then the net result is an increase in the magnitude of region A at the expense of the magnitude of region D. Thus, an increase in cut length Δc transfers a volume of the rubber (ΔV_D) from a state of pure shear to the undeformed

state (region A). The size of regions B and E are unchanged and so the fact that their strain energies are not known does not matter.

The magnitude of ΔV_D is given by,

$$\text{Now} \quad \Delta V_D = L_o h \Delta c \tag{8.12}$$

Since region A is unstrained, the change in the specimen strain energy ΔU is given by;

$$\Delta U = -W \Delta V_D = - W \Delta c \, h \, L_o \tag{8.13}$$

The tearing energy is hence given by;

$$T = -1/h \, (\Delta U / \Delta c) = W L_o \tag{8.14}$$

where W is the strain energy density of the material in the pure shear region.

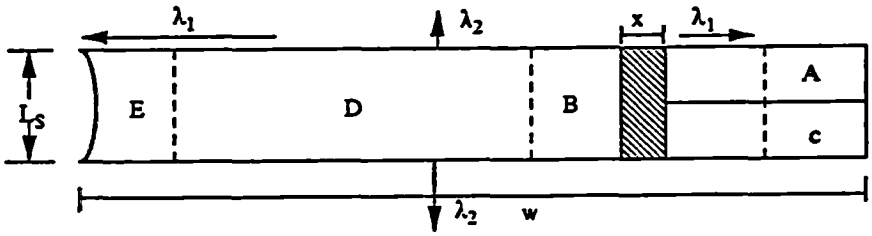

Figure 8.8(b)

Figure 8.8(b) illustrates a pure shear test piece subjected to a lateral pre-extension of λ_1. L_s is the clamped height following this lateral extension. If the specimen grips are held at a constant displacement to produce a strain of λ_2 and the crack grows by Δc referred to unstrained state ($\lambda_1=1$, $\lambda_2=1$) that is $\lambda_1 \Delta c$ in the strained state (when both λ_1 and λ_2 are applied), then the volume of the rubber (ΔV_D) which is transferred from region D to region A is given by;

$$\Delta V_D = (\lambda_1 \Delta c) \text{ x (strained thickness) x (strained height)}$$

$$\Delta V_D = (\lambda_1 \Delta c) \text{ x } (h / (\lambda_1 \lambda_2) \text{ x } (L_S \sqrt{\lambda_1} \quad \lambda_2) = \Delta c \, h \, L_S \sqrt{\lambda_1} \tag{8.15}$$

The change in specimen strain energy ΔU when the crack grows by Δc is given by;

$$\Delta U = -W_S \Delta V_D = - W_S \Delta c \, h \, L_S \sqrt{\lambda_1} \qquad (8.16)$$

where W_S is the difference in elastic energy density between regions A and D. Region D has a zero stress in the λ_2 direction (i.e., when $\lambda_2=1$) but a strain equivalent to λ_1 in the perpendicular direction.
The tearing energy is given by;

$$T = -1/h \, (\Delta U / \Delta c) = W_S \, L_S \sqrt{\lambda_1} \qquad (8.17)$$

$L_S \sqrt{\lambda_1}$ is equal to the unstrained height of the test pieces = L_0 ($\lambda_1=1$, $\lambda_2=1$), hence,

$$T = W_S \, L_0 \qquad (8.18)$$

W_S may be found by integration of the stress/strain curve for the clamped sheet, initially stretched to λ_1 and then stretched to λ_2 in the perpendicular direction. The energy change/unit volume is simply, W_S, as the integration will be carried out from zero force.

8.7 RESULTS AND DISCUSSION

In this section, the results of the cyclic crack growth experiments on carbon black filled and silica filled NR vulcanizates are presented. The effect of filler loading, crosslink density and the effect of pre-straining on the cyclic crack growth rate in the carbon black filled vulcanizates is discussed. The effect of the addition of a coupling agent on the cyclic crack growth rate in the silica filled vulcanizates is discussed.

8.7.1 Crack growth behaviour of carbon black filled vulcanizates

The results of the cyclic crack growth tests are shown in figure 8.14, for the NR vulcanizates filled with various amounts of HAF carbon black, as a double log plot of dc/dn versus tearing energy (T).

The plots are well separated and show a decrease in dc/dn with increasing carbon black content at all tearing energies (T). The plot for each material can be represented by three regions B,C,D as discussed in section 8.1.

In region C the relationship, between cyclic crack growth rate dc/dn, and the tearing energy can be represented by,

$$dc/dn = B (T)^{\beta} \qquad (8.4)$$

This is shown in figure 8.15 where log dc/dn is plotted against log T for the three carbon black filled compounds and an unfilled natural rubber. The numerical values of the constant β calculated from the slope, and the numerical values of the constant B are given in table 8.1. Also shown are values previously determined for carbon black filled rubbers. The present values are seen to be comparable although direct comparison is difficult as details of crosslink density are often not given in the literature. The slopes of the plots for the filled material, β, are all less than the value of 2.0 for the unfilled natural rubber.

In region B (figure 8.14) the relationship between dc/dn and the tearing energy is best represented by a relationship of the form;

$$dc/dn = D (T - T_o) \qquad (8.3)$$

where T_o is threshold tearing energy. This relationship is demonstrated in figure 8.16 for NR23 by plotting dc/dn versus T. The value of T_o is given by the intercept on the T axis at dc/dn = 0. The values of T_o and D

calculated for the present materials are given in table 8.2 together with values determined for other carbon black filled rubbers previously. The T_o values are much larger than those associated with unfilled materals (NR, T_o= 60-80 kJm^{-2}) and are seen to increase with increasing carbon black content. The increase in T_o may be associated with an increased crack tip radius or with the additional work done in rubber/carbon black debonding in the region of the crack tip.

In region D the crack growth rates increase rapidly with tearing energy as the data asymptotes to the catastrophic tearing region. The tearing energies are however very small compared to those for catastrophic tearing of these materials (figure 7.12) where tearing energies of 60-80 kJm^{-2} are observed. These very high tearing energies are associated with knotty tearing which does not occur during cyclic crack growth. However the tearing energies necessary to drive cyclic crack growth in this region are even lower than those necessary to catastrophically tear the materials, under stick-slip tearing conditions in unfilled NR (figure 7.16). Hence even in region D genuine cyclic crack growth is still occurring in which the process of cycling itself allows a crack to grow at relatively low tearing energies.

The mechanism by which cracks grow during cycling is far from clear. As a result no real interpretation of the observed detailed relationship between dc/dn and T exists. In the case of unfilled NR it is suggested that the unloading process allows strain induced crystals at the crack tip to melt which allows increments of crack growth to occur upon reloading prior to subsequent strain induced crystallization. These increments of crack growth occur in a pseudo steady manner and presumably increase in extent with increasing tearing energy, resulting in an increase in dc/dn with increasing tearing energy. This argument is supported by the low temperature dependence of dc/dn[76] as this would depend only on the extent of strain crystallization and melting at the crack tip, which is not very temperature dependent in the crystallization range.

The addition of carbon black causes a systematic reduction in dc/dn at a given T with increasing carbon black content. Part of this reduction may be due to the corresponding increase in the threshold tearing energy (T_o). The major effect however may be associated with blunting or increased curvature at the crack tip due to the carbon black dispersion. This effect is akin to an increasing energy input being necessary to produce a given increment of crack growth with increasing carbon black content. This could be due to the rubber becoming more hysteretic but this does not seem to be

the case in the simple rubber visco-elastic sense as the temperature dependence does not seem to change on the addition of carbon black[77]. Furthermore cyclic crack growth in SBR (a non-strain crystallizing rubber) becomes much less temperature dependent on the addition of carbon black. The hysteretic effect may be associated with the work done in debonding rubber molecules from carbon black during the loading cycle hence reducing the energy available to drive the crack. In the case of filled NR the reduced cyclic crack growth per cycle may in part be due to the strain amplification effect which would result in strain crystallization occurring earlier on the reloading cycle.

The present data illustrates that the crack growth rate (dc/dn) for a given tearing energy decreases systematically with increasing carbon black content. This careful characterization of the Peradin rubbers provides a basis for design and for material selection.

8.8 EFFECT OF CROSSLINK DENSITY ON CYCLIC CRACK GROWTH

The effect of crosslink density on the rate of crack growth was studied for NR49 only. The results are given in figure 8.17 which show that a higher tearing energy is required to produce a given crack growth rate as the crosslink density is decreased

The effect is partly associated with an increase in T_o as the crosslink density decreases. While the same number of rubber molecules need to be broken an increased work needs to be done as the length of molecules between crosslinks increases[54]. In addition the ability of the material to strain crystallize will decrease as the crosslink density increases. This may result in a larger crack growth increment per cycle on reloading prior to the formation of crytals as the crosslink density is increased.

The effect of crosslink density on dc/dn (figure 8.17) is small compared to the effect of carbon black content (figure 8.14). However the effect is not insignificant and in the selection of compounds in design it is a factor to which attention should be given. Furthermore the effect is large enough to require care to be taken in the control of the vulcanization process.

8.9 CYCLIC CRACK GROWTH IN SPECIMEN PRE-STRAINED (λ_1) IN A DIRECTION PARALLEL TO THE CRACK GROWTH DIRECTION AND SUBJECTED TO A MAXIMUM CYCLIC STRAIN AMPLITUDE (λ_2) IN A DIRECTION NORMAL TO THE CRACK GROWTH DIRECTION

Catastrophic tearing studies using trouser test pieces yield knotty tearing and high tearing energies in carbon black filled rubbers in both previous studies[61,62] and for the Peradin rubbers studied here (figure 7.12). These high tearing energies are associated with the development of knots due to crack path deviation in the direction of molecular/carbon black orientation. Samsuri et al[62] demonstrated, using split tear test pieces (figure c in appendix 7.1), that prestraining in the direction parallel to crack growth resulted in a reduction in the tearing energy by a factor of 10. The higher the pre-strain the lower was the tearing energy. Knotty tearing did not occur as the normal growth direction of the crack was now in the direction of molecular/carbon black orientation.

Steady cyclic crack growth in the carbon black filled rubbers in the present study resulted in rough fracture surfaces. These were of a much smaller scale than the roughness resulting from knotty tearing and the associated tearing energies were much smaller. However the roughness may be associated with small scale anisotropy developed in the direction of the application of the strain, normal to the direction of crack growth. If this be the case than pre-straining in the direction of crack growth should very much reduce this anisotropy, may be even producing an anisptropy in the crack growth direction, resulting in lower tearing energies.

To investigate this effect, cyclic crack growth tests were carried out using pure shear test pieces prestrained along the direction of their widths (figure 8.8a) to two different strain levels i.e. 150% and 200%. These specimens were cycled up to maximum strain amplitudes of 30% and the tearing energies were calculated using the relationships derived in section 8.6.4.

The results are shown in figure 8.18 for NR49 as a plot of log T versus log dc/dn. The results for the unstrained NR49 and for an unfilled NR[25] (EDS19) are also shown for comparison purposes. It can be seen that for a given tearing energy the crack growth rate is increased as the pre-strain on the sample is increased. The effect is very large as the cracks in the filled rubber now grow considerably faster than even do cracks in the unfilled unprestrained rubber at a given tearing energy. Furthermore the

crack surfaces in the pre-strained samples are much smoother than those observed in the samples which were not pre-strained. The extent of crack tip deviation had clearly been considerably reduced if not eliminated. In fact the cracks were now almost essentially growing in the direction of pre-orientation of the rubber/carbon black structure resulting in a much lower tearing energy necessary to grow the cracks at a given rate. However the tearing energies necessary for cyclic crack growth remain considerably smaller than those necessary for high speed catastrophic tearing (trouser test piece) even when both are pre-strained by the same amount[73]. It is hence still the loading/unloading process which is responsible for the increments of crack growth at these low tearing energies, albeit growth into a weakened pre-orientated rubber. The crack growth increment on reloading may still be limited by strain crystallization. However the situation is now more complex. In the present case the fully unloaded condition consists of a large pre-strained in the direction of crack growth. This may in fact cause some crystals to form in this direction. On reloading at the crack tip these crystals may 'melt' to be replaced by crystals oriented at right angles as the cyclic strain is increased. The situation at the crack tip during reloading is hence far from simple. In this respect it would be interesting to study cyclic crack growth in pre-strained specimens in which the strain cycle did not include zero strain. The current results are the first of their kind and are significant not only as a means of studying mechanisms of crack growth in filled rubbers but are also significant in terms of crack growth in rubber components which are frequently preloaded in a complex manner.

8.10 SILICA FILLED NR VULCANIZATES WITHOUT AND WITH A COUPLING AGENT

Stress-strain data and tearing behaviour for the silica filled materials were reported in chapters five and seven respectively. Significant differences in behaviour were observed when a coupling agent was added. The first ever cyclic crack growth data for silica filled rubbers is reported in this section. The data is represented as a plot of log T versus log dc/dn in figure 8.19. The effect of the addition of silica to natural rubber on the cyclic crack grow rate is very small. The results are similar whether or not silane coupling agent is present. The effect of addition 40 pphr silica (15.5% by volume) to NR is significantly less than that of 23 pphr (9.9% by volume) HAF carbon black (figure 8.14). As mentioned earlier some caution is

required in making this comparison as the real crosslink density in the silica filled materials is uncertain. In light of the effect of silica on the stress-strain behaviour and on the trouser test tearing data this non effect of silica is some what surprising. Furthermore the significant effect of the addition of a coupling agent on both stress-strain and trouser tear data is clearly not reflected in the cyclic crack growth data.

To some extent this again emphasises the differences in cyclic crack growth and catastrophic tearing. In cyclic crack growth it is the increment of crack growth which occurs during the reloading cycle which is important and which leads to crack growth at such low tearing energies. In the present case silica, coupled or uncoupled, seems to have no effect on this process even though the addition of silica causes significant increases in stiffness. The strain crystallization process which limits the cyclic crack growth increment on cyclic reloading in unfilled NR seems to act in the same way in the silica filled materials. However it is unsafe to make generalisations on the basis of the limited present data and it would require significant further work to understand the apparent differences in the effect of silica on catastrophic tearing and on cyclic crack growth.

TABLE 8.1: Materials constants at the region C (figure 8.14) for carbon black filled NR vulcanizates obtained in this study and compared with published data

Compound	Slope, β	Intercept, B $x10^{-14}$	Compound	Slope, β	Intercept, B $x10^{-14}$
NR23	1.78	5.43	NR based carbon black filled tyre sidewalls compound ref 80	-	
NR49	1.72	3.77		1.91	1.38
NR69	1.88	3.38			

TABLE 8.2: Materials constants at low tearing energies (region B, figure 8.14) for carbon black-filled NR vulcanizates obtained in this study and compared with published data

Compound	T_o, KJm^{-2}	D , $m.cycle^{-1}/Jm^{-2}$	T_o,* KJm^{-2}	D ,** $m.cycle^{-1}/Jm^{-2}$
NR23	0.145	$10.45 X10^{-12}$	0.200	$8.52 X10^{-12}$
NR49	0.180	$8.52 X10^{-12}$		
NR68	0.265	$3.18 X10^{-12}$		

* A NR based carbon black filled tyre compound, Young et al, Rubber chemistry and Technology **55**, 428, (1982)

**A 50pphr HAF carbon black filled compound, ref 82

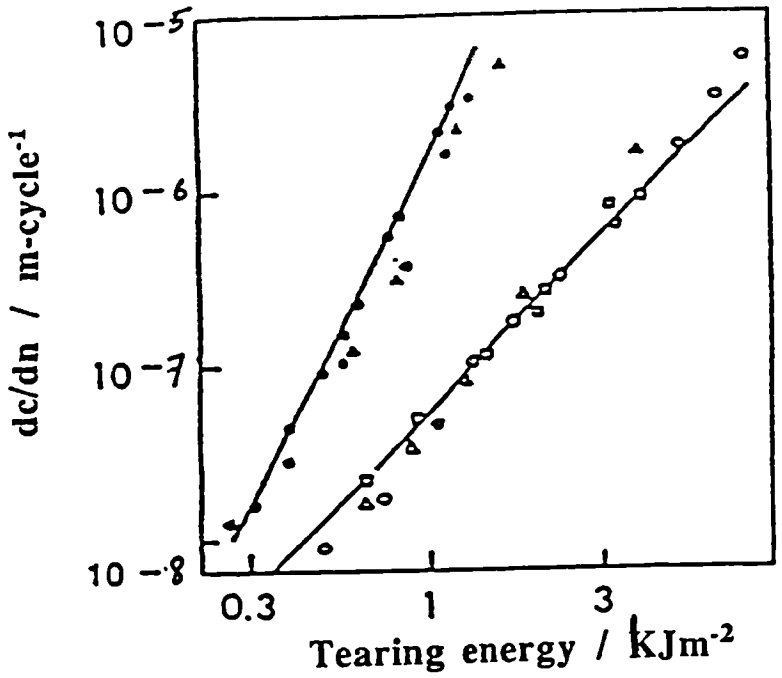

Figure 8.1: Crack growth under repeated loading (a) cyclic crack growth rate as a function of maximum tearing energy of cycles for unfilled vulcanizates of NR (open points) and SBR (filled points): tensile strip test pieces o, •; pure shear, Δ, ▲, trousers. Fig 2, ref 86.

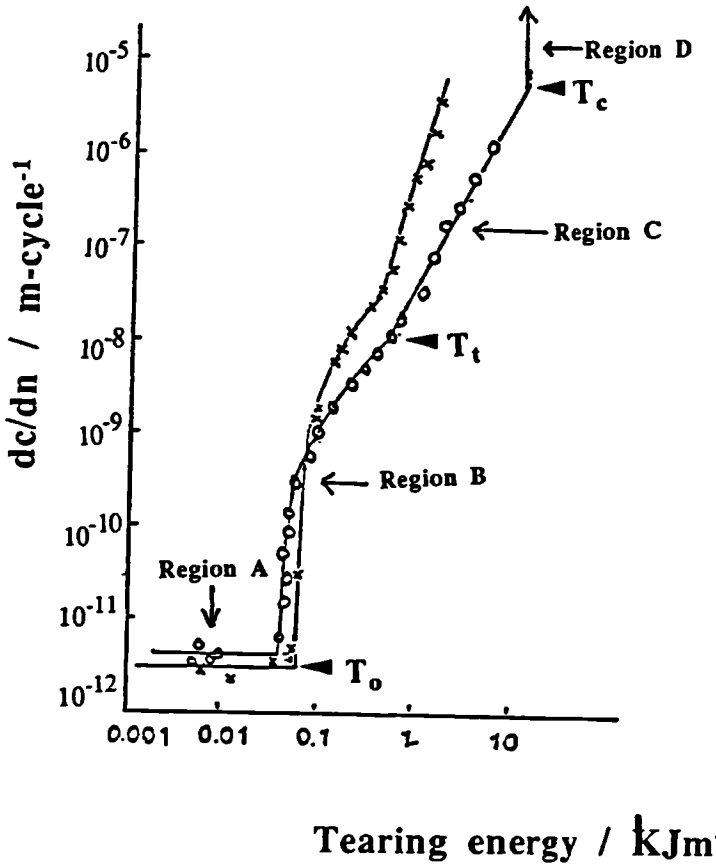

Figure 8.2(a): Crack growth rates (dc/dn) for unfilled NR (o) and SBR(x) vulcanizates as a function of tearing energy (T),
Fig 3, ref 96.

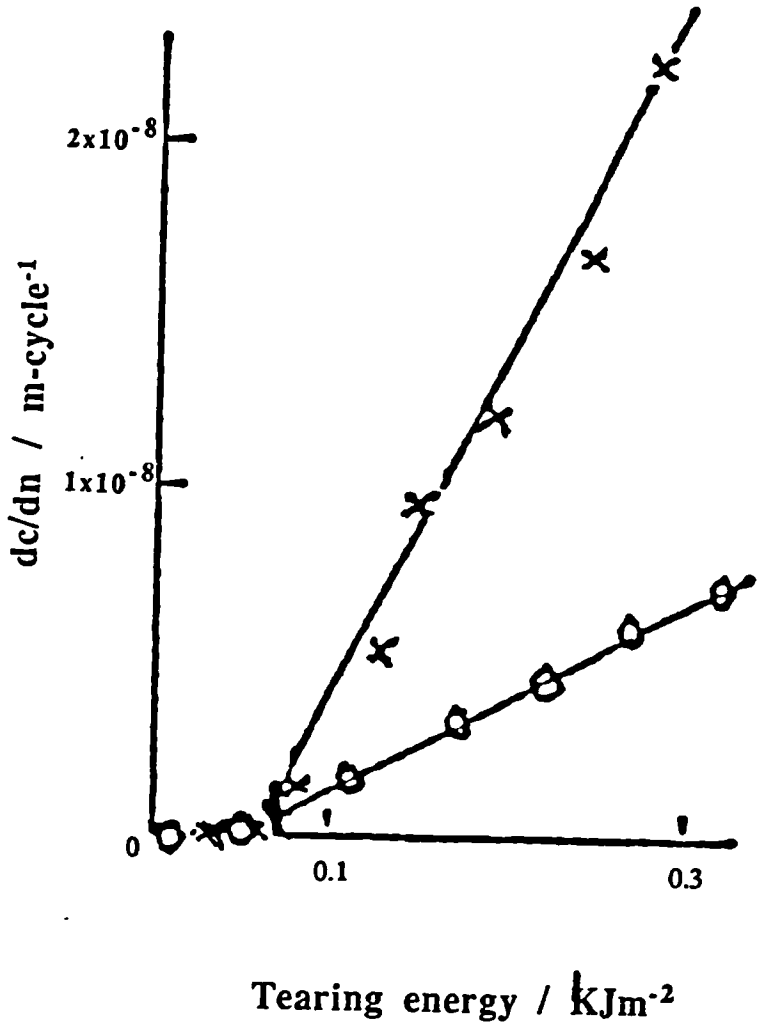

Figure 8.2(b):Crack growth rates (dc/dn) for unfilled NR (o) and SBR (x) vulcanizates as a function of tearing energy (T) in the region near T_o. Fig 4.14 96

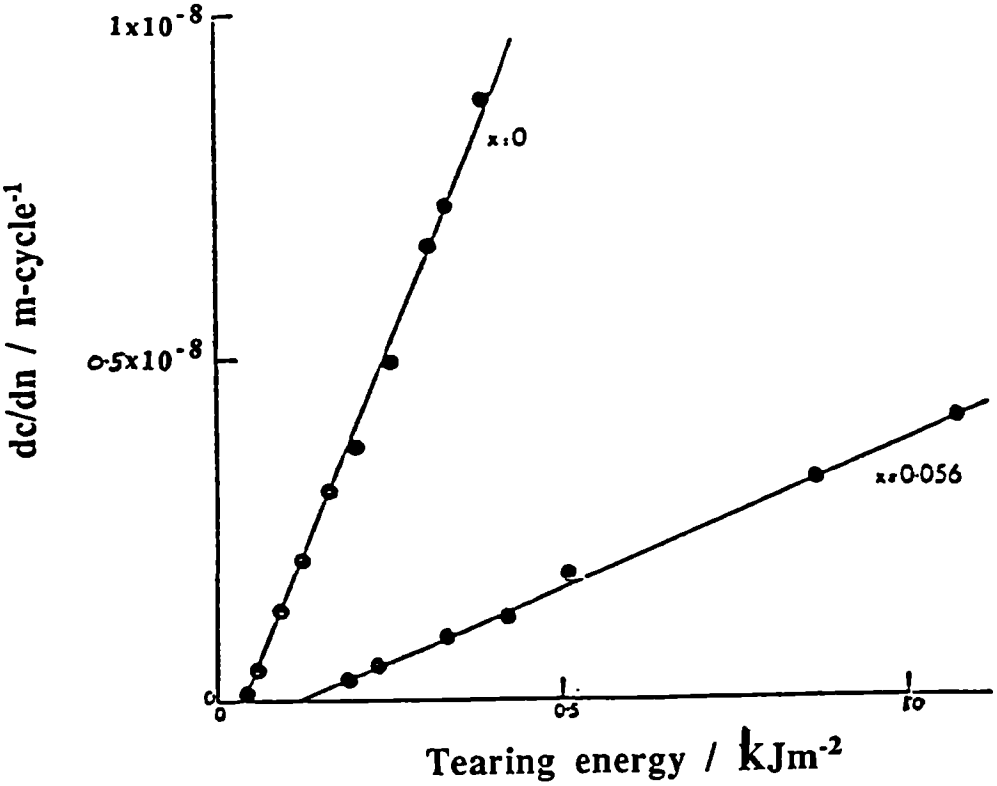

Figure 8.3: Crack growth characteristic of an unfilled NR vulcanizate on linear scales. The left hand points (x= 0) are from experiments in which the test piece is relaxed to zero strain on each cycle. The right hand points, of lower slope, are from a non-relaxing test in which x = T_{min} / T_{max} = 0.056 . Fig 9, ref 73 (Part 2)

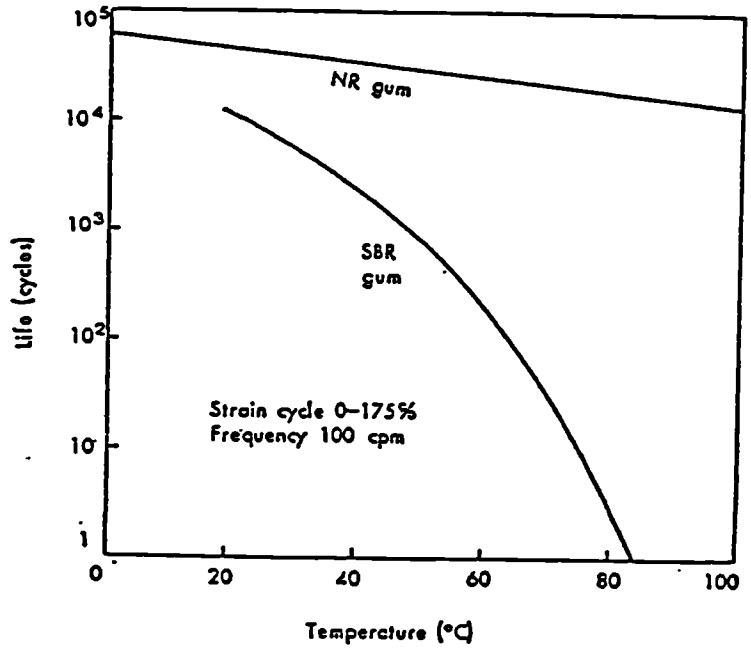

Figure 8.4: Effect of temperature on fatigue life for NR and SBR unfilled vulcanizates cycled to 175% strain at 100 cycles per minute
Fig 33, ref 65

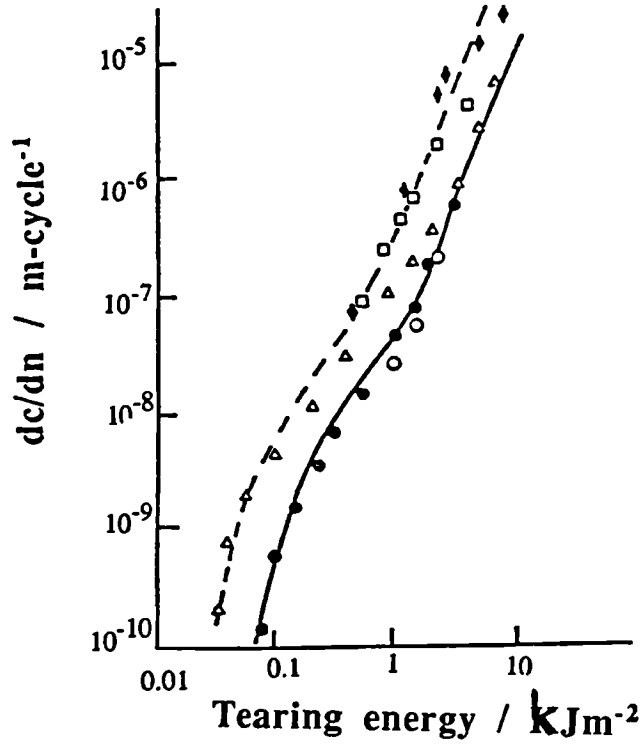

Figure 8.5: Effect of frequency on crack growth rates for an unfilled NR, cycles per minutes in air; (△) 100, (□) 1, (◊) 0.01; vacuum ; (●) 100, (o) 1 . Fig 6(6), ref 86.

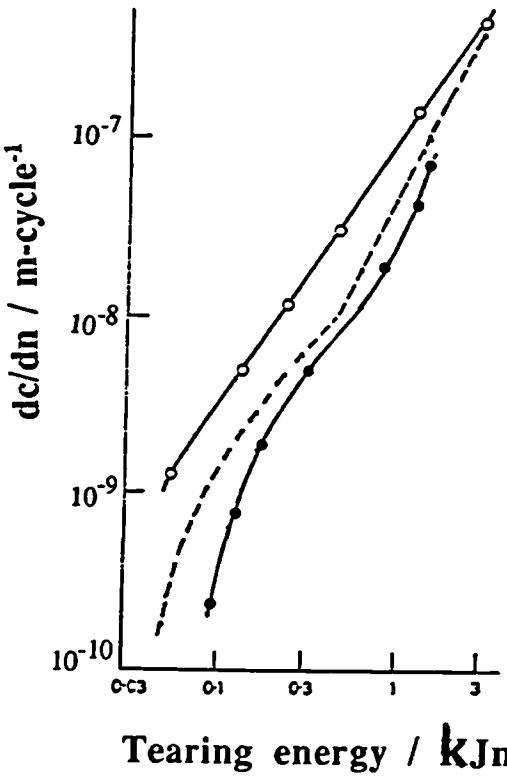

Figure 8.6: Comparison of the crack growth characteristic of unprotected, unfilled NR in air (o) and vacuum (●). The protective action of 1 pphr of an antioxidant in air is indicated by the broken line, frequency 100 cycles per minute. Fig 6, ref 77 (Part II)

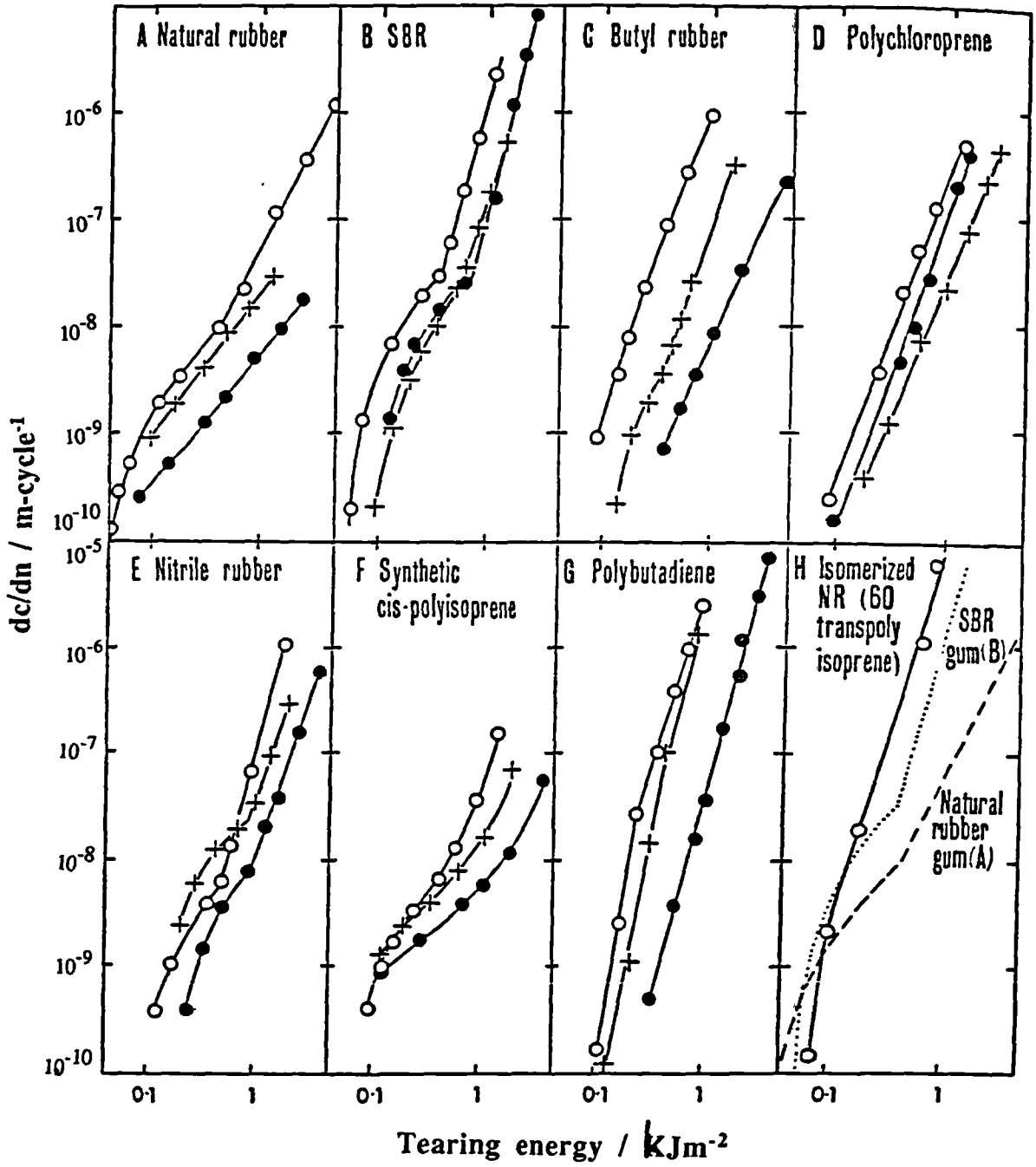

Figure 8.7: Crack growth rate as a function of tearing energy for different vulcanizates unfilled (o), with 50 pphr MT black (+) and with 50 pphr HAF black (•). Fig 2, Ref 99 (Part II)

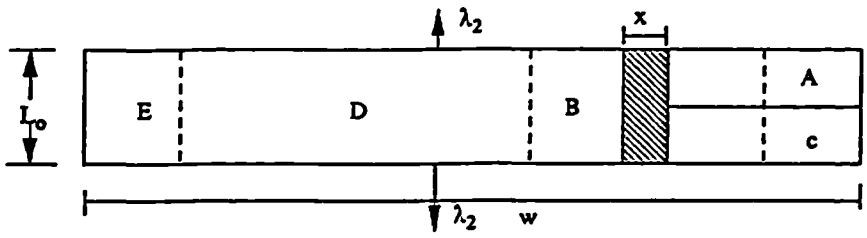

Figure 8.8a: A schematic diagram of a pure shear test piece with a cut length c

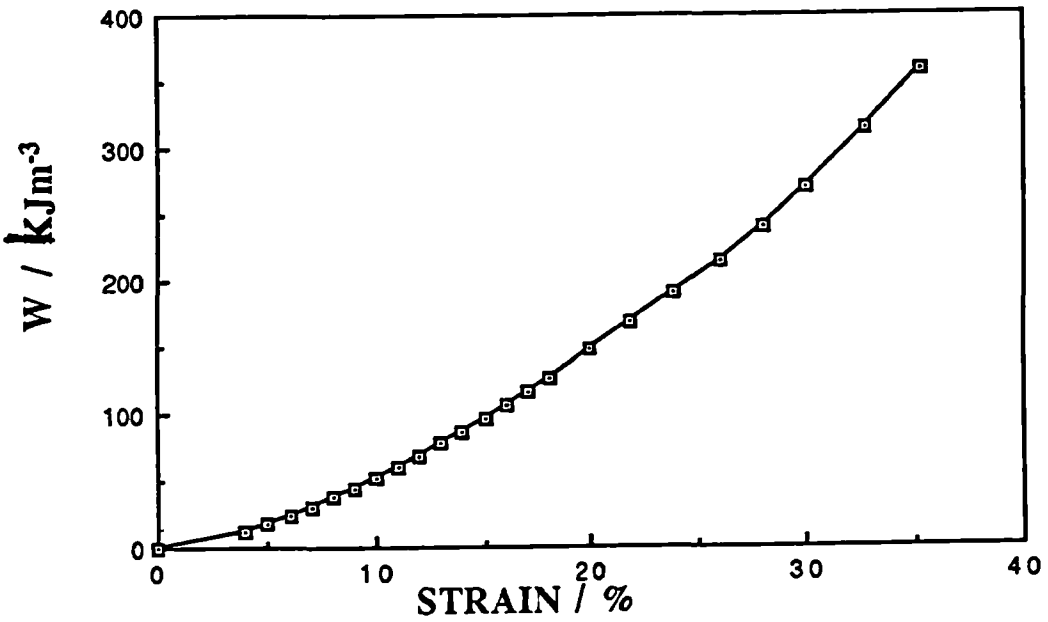

Figure 8.9: A typical plot of strain energy versus % strain for a carbon black filled NR vulcanizate (NR69)

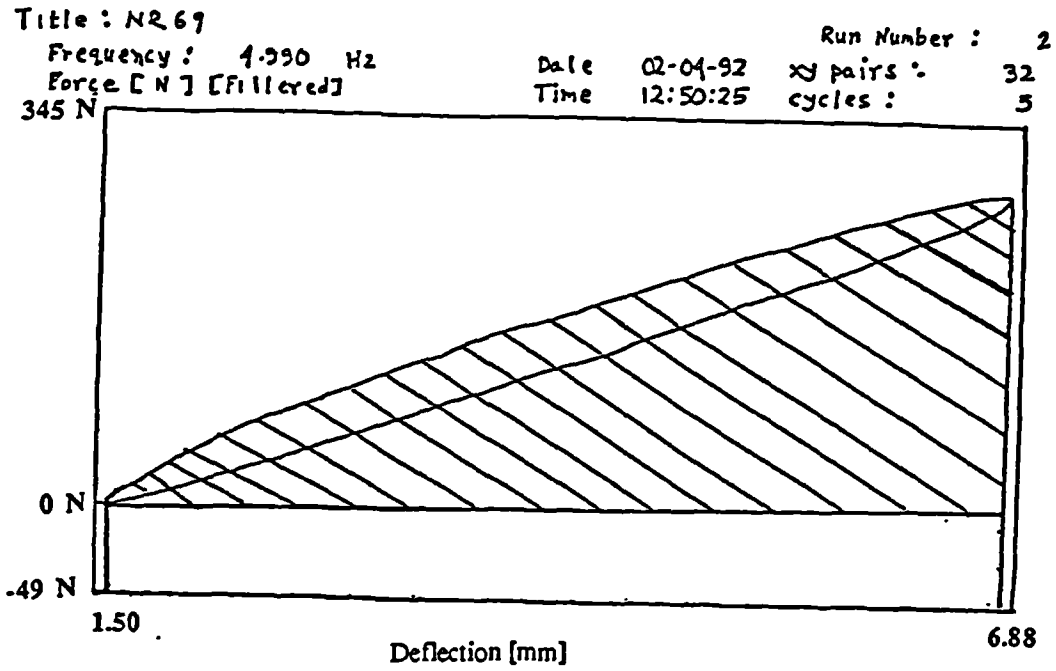

Figure 8.10: A typical load-displacement curve obtained during a cyclic crack growth test.

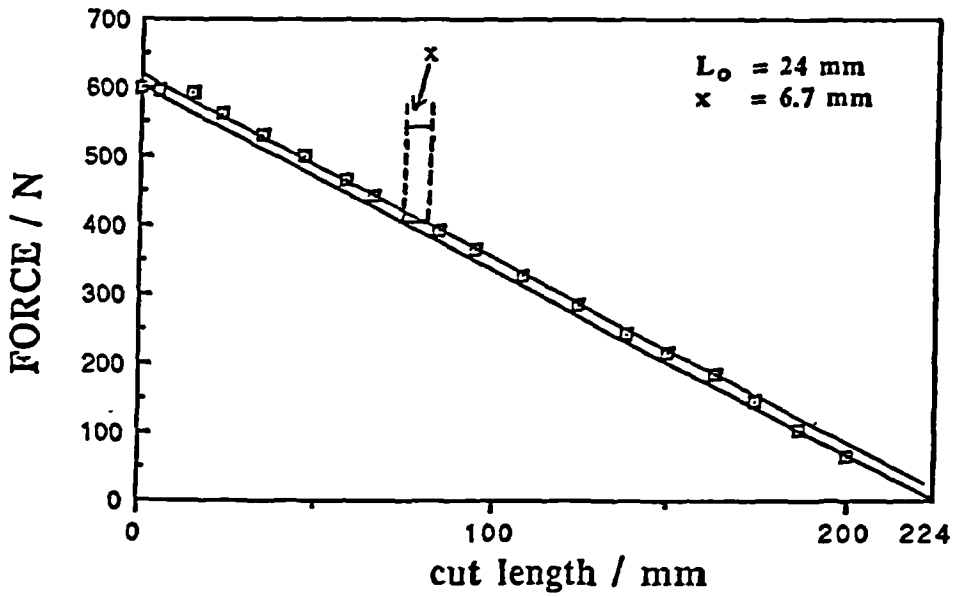

Figure 8.11: Maximum recorded force during cutting a pure shear test specimen under dynamic conditions for a carbon black filled NR vulcanizate (NR69)

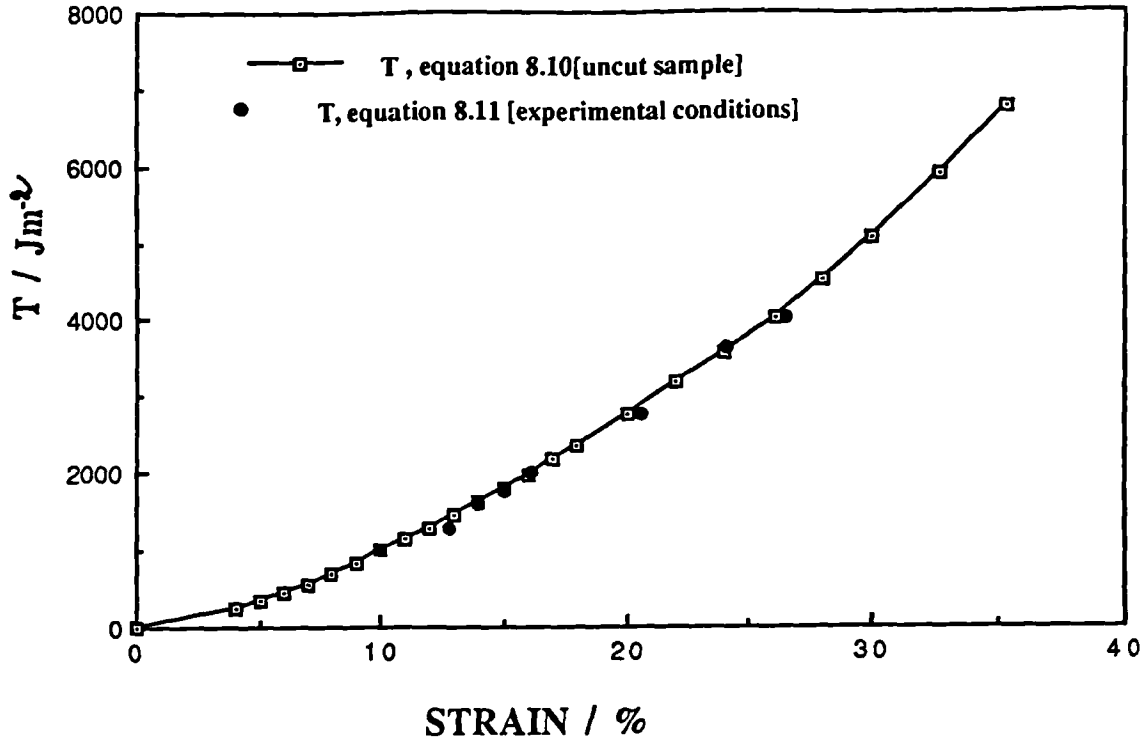

Figure 8.12: Comparison of the tearing energies obtained from equations (8.10) and (8.11)

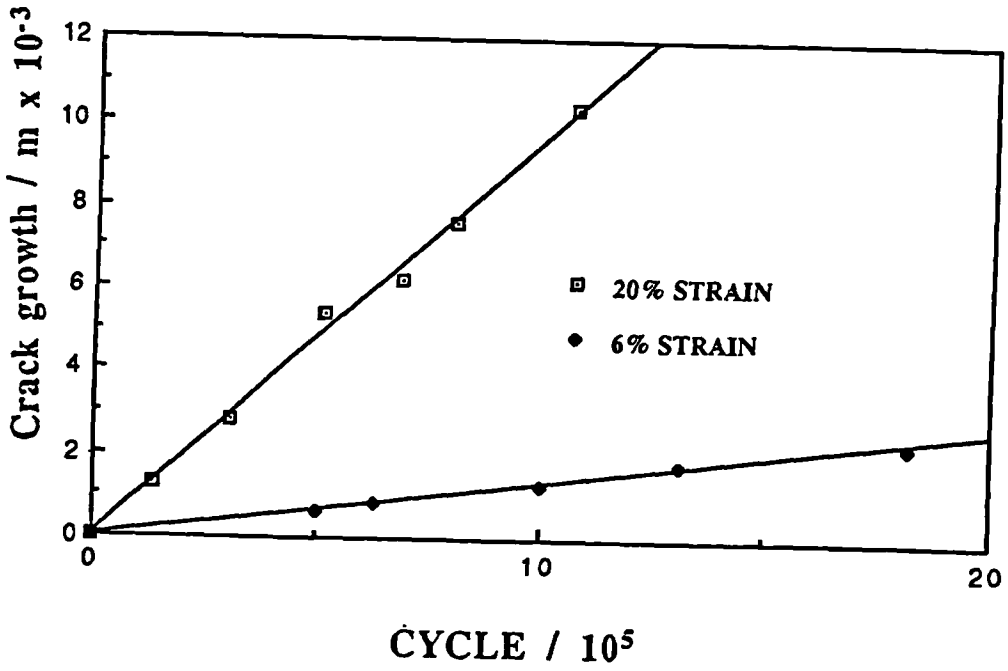

Figure 8.13: Cyclic crack growth, c, versus number of cycles for a carbon black filled NR vulcanizate (NR69)

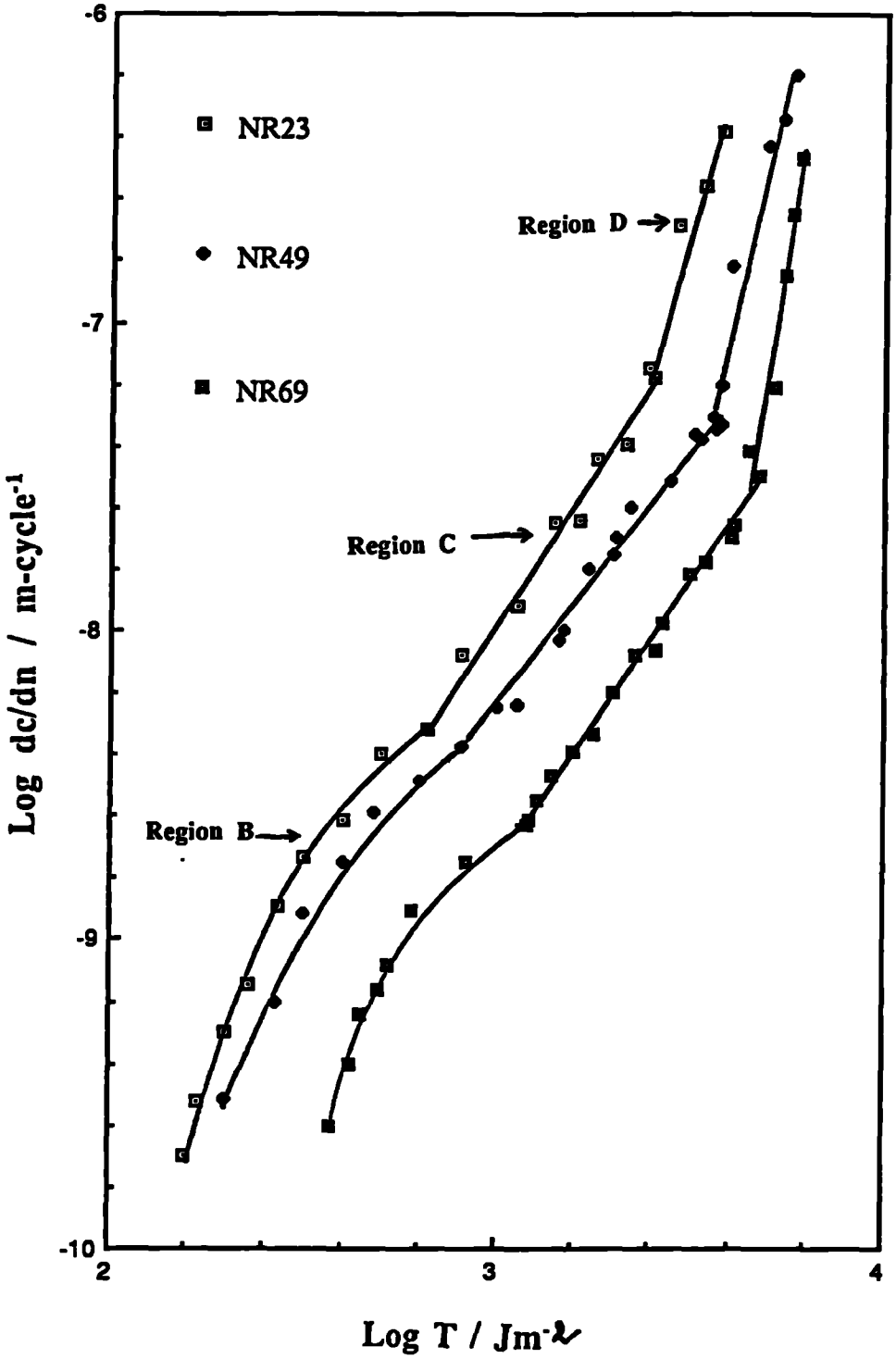

Figure 8.14 : Crack growth per cycle (dc/dn) versus tearing energy (T) for the carbon black-filled NR vulcanizates.

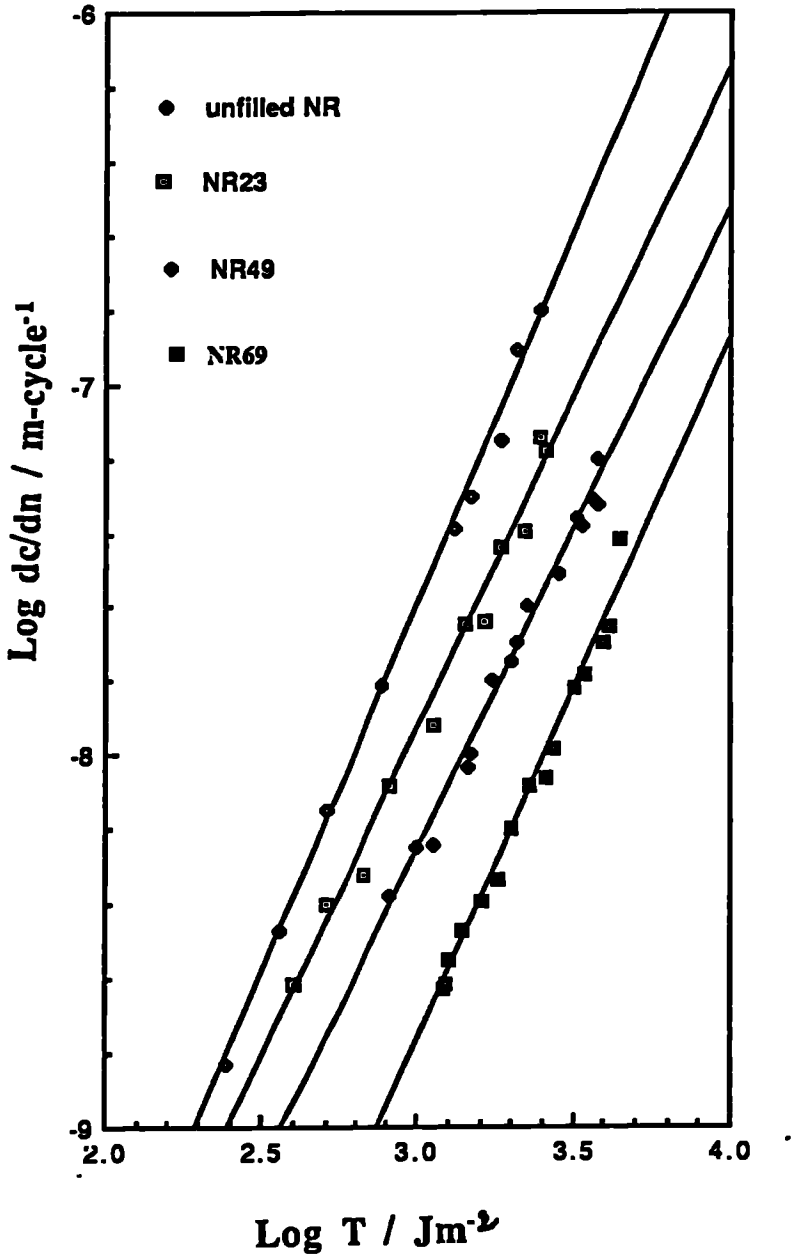

Figure 8.15 :Crack growth per cycle (dc/dn) versus tearing energy (T) for the carbon black-filled NR vulcanizates (Region C).

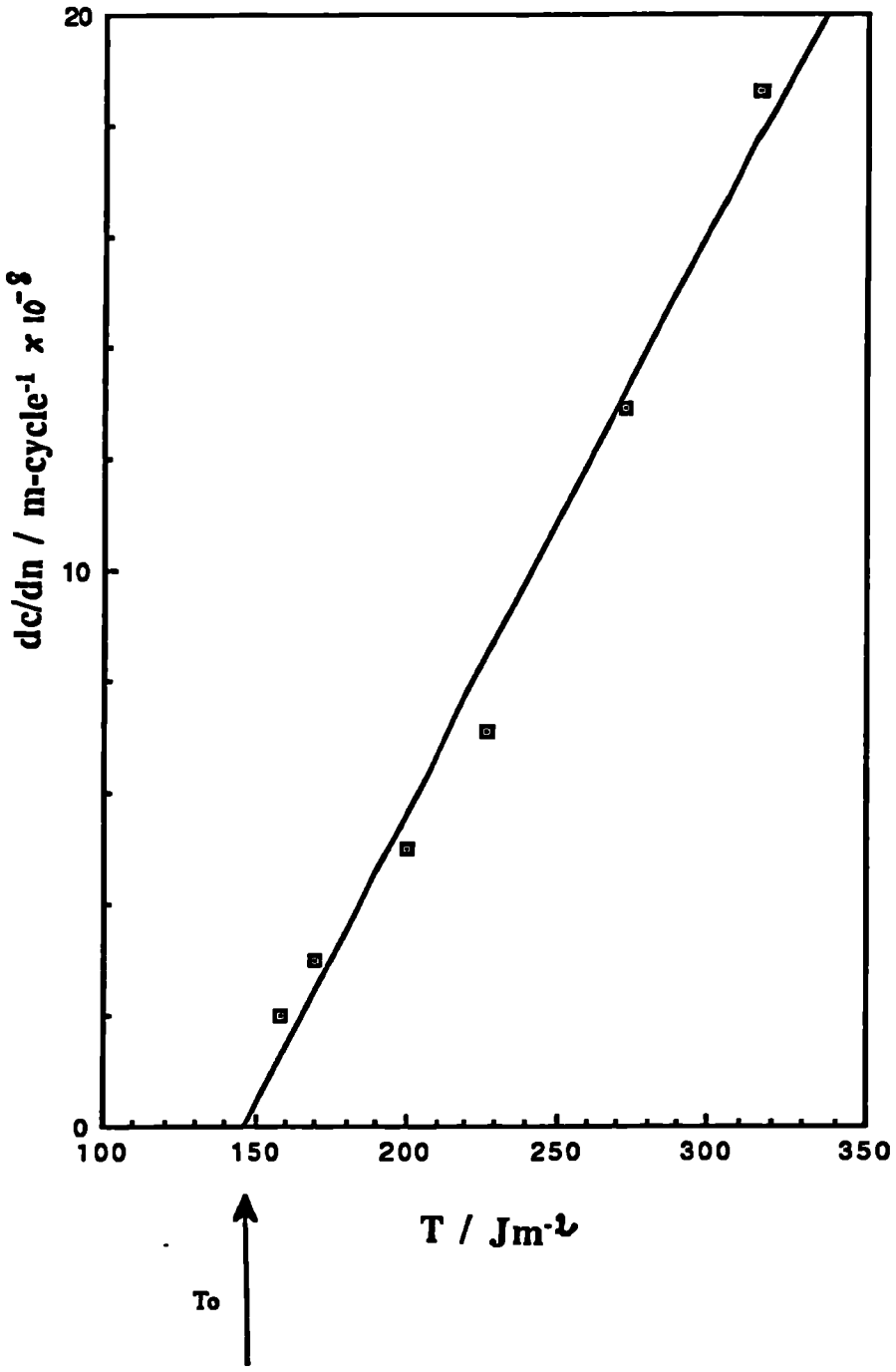

Figure 8.16 :Crack growth per cycle at low tearing energies for a NR vulcanizate filled with 23pphr carbon black (Region B)

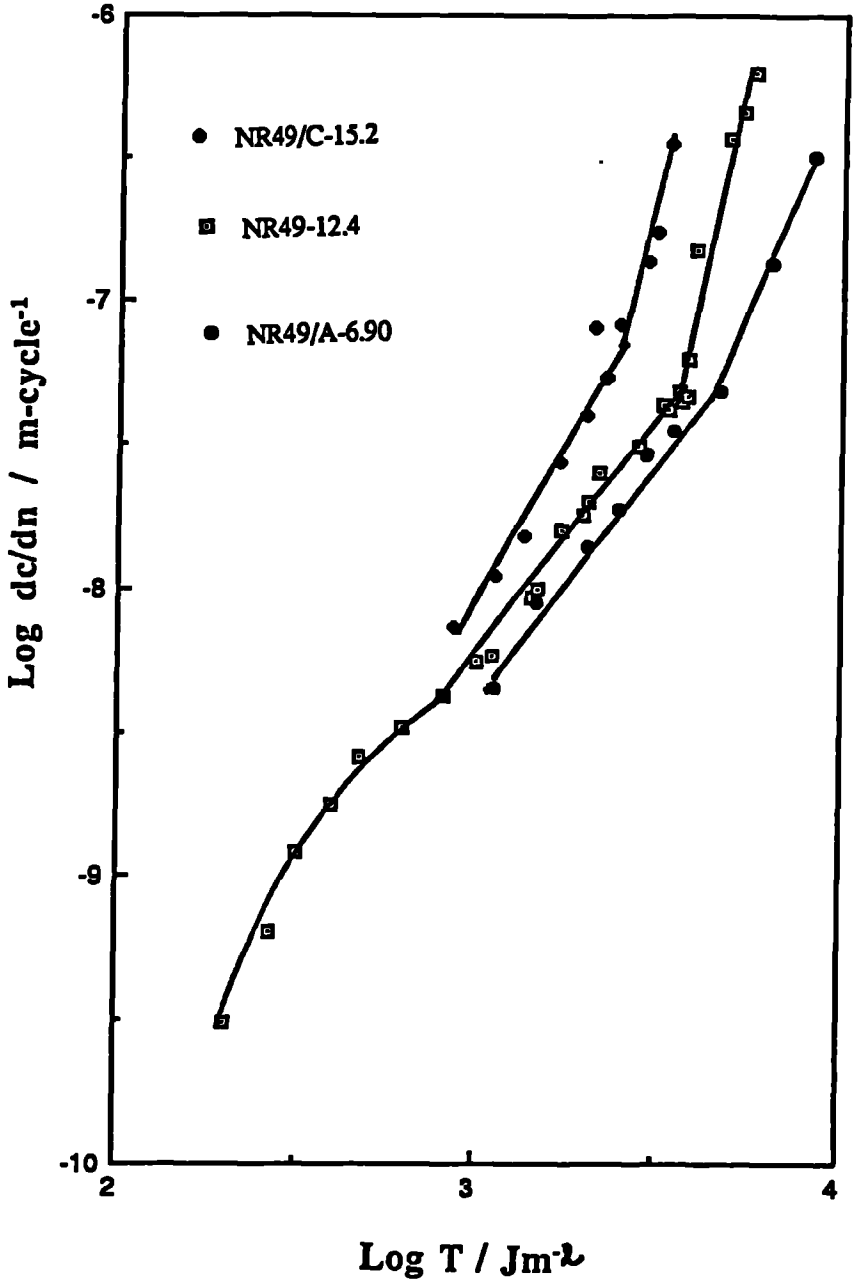

Figure 8.17 : Effect of crosslink density on crack growth per cycle for 49pphr carbon black filled NR vulcanizates

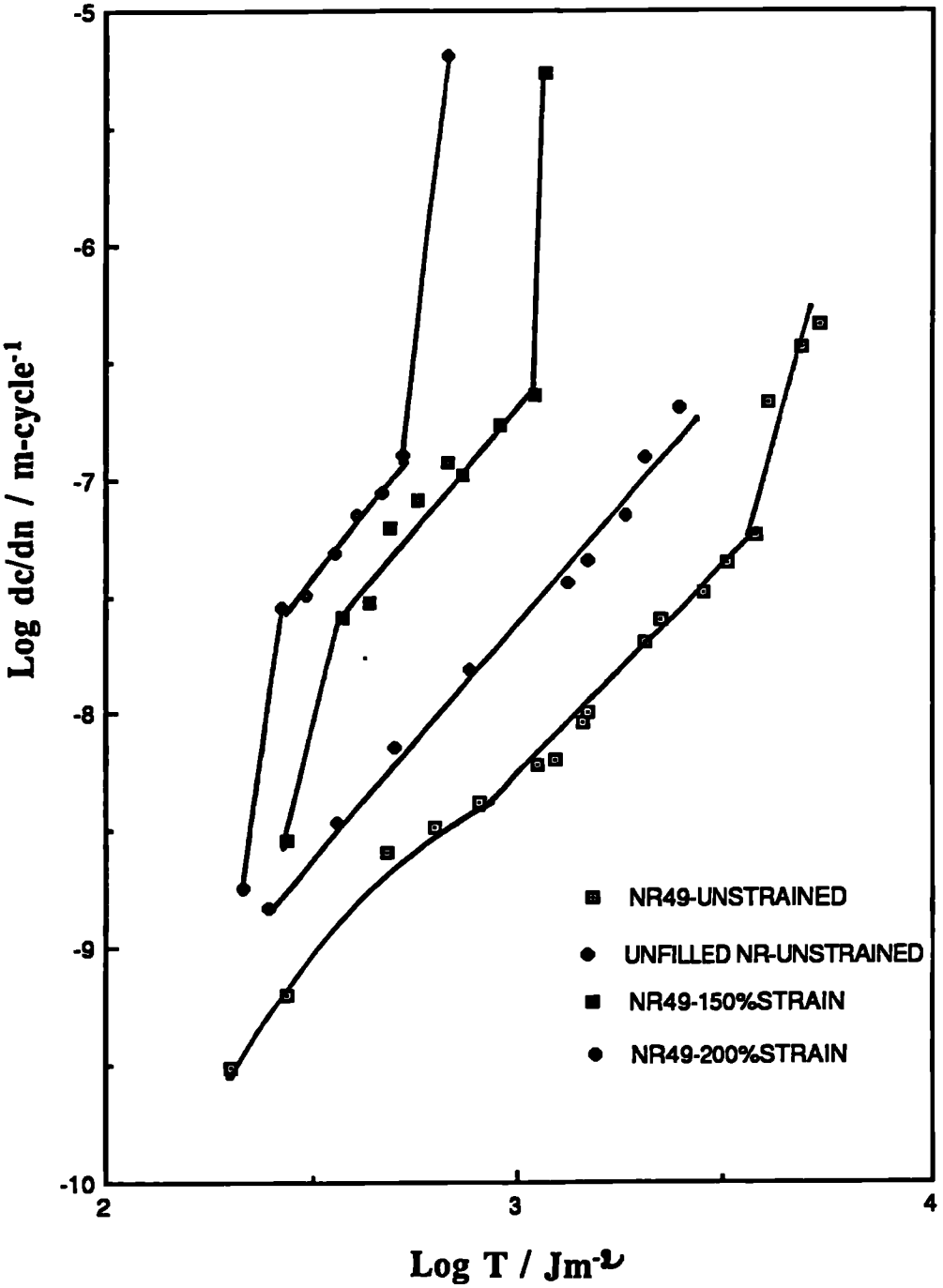

Figure 8.18 : Effect of pre-straining on cyclic crack growth of a carbon black filled vulcanizates [NR49]

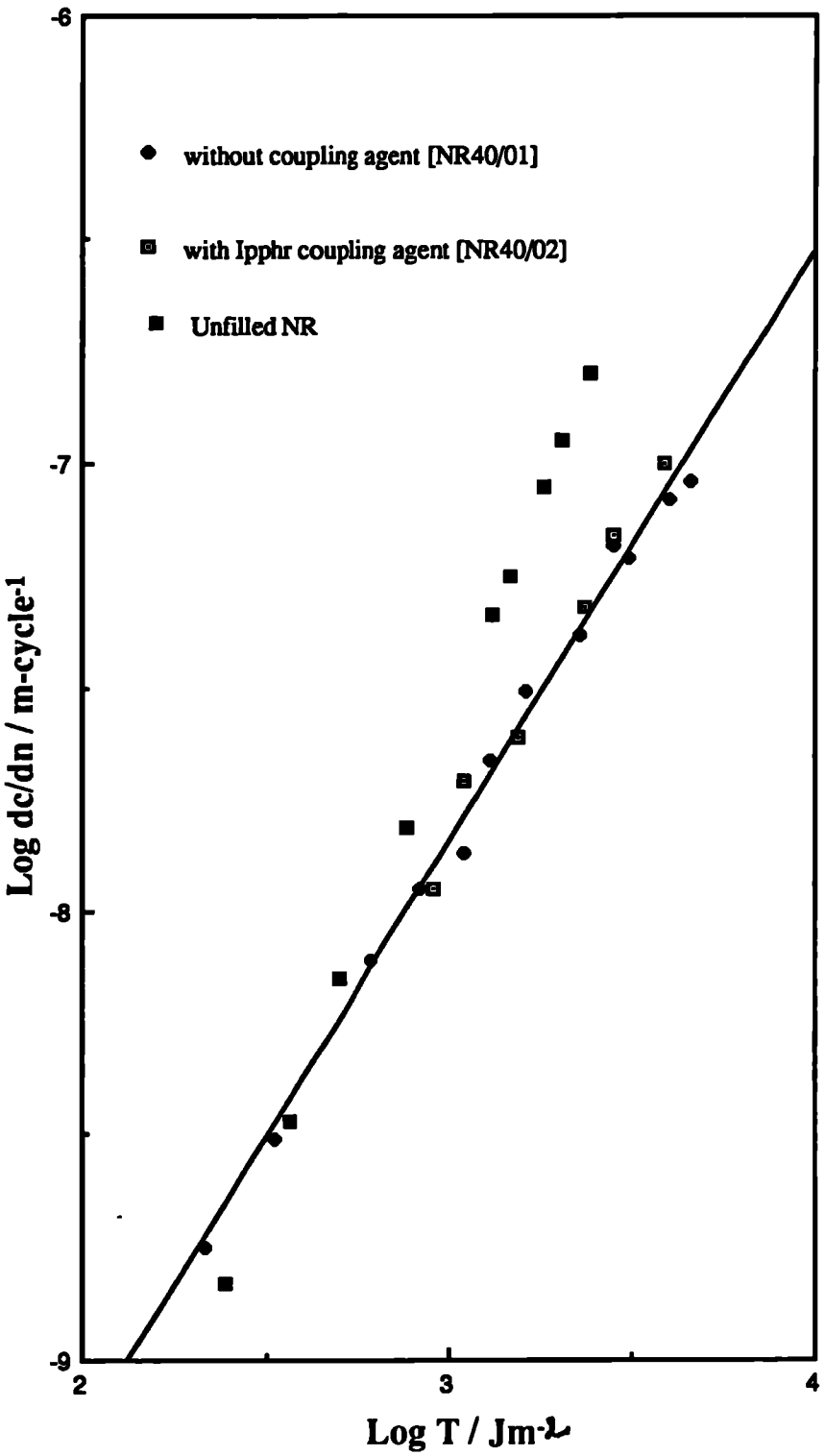

Figure 8.19: Crack growth behaviour of silica filled NR vulcanizates without and with coupling agent

CHAPTER NINE

9.0 SUMMARY AND SUGGESTIONS FOR FUTURE WORK

The thesis consists of a wide ranging study of mechanical behaviour and crack growth in a series of well characterized carbon black and silica filled rubber compounds. As such it represents a significant attempt to relate a variety of mechanical processes in identical materials, which in the literature is complicated by poor materials characterization and materials variability.

It is demonstrated that the stress-strain behaviour of filled rubbers up to strains of 100%, deformed in any manner can be derived from a strain energy function (W) of the form;

$$W = \frac{A}{2\,(\,1 - n/2\,)}\,(\,I_1 - 3 + C^2)^{(\,1 - n/2\,)} + K\,(I_1 - 3)^2$$

where I_1 is the first strain invariant and A, n, K, C are materials constants.

It is demonstrated that the constants can be derived from stress-strain data obtained in any single simple stressing mode. For many engineering purposes it is shown that it is only necessary to define accurately the constants n and A, at least for strains up to 80%.

The numerical values of n are shown to increase with carbon black content and to be independent of crosslink density. It is suggested that n is related to the extent and rate of the breakdown of the carbon black structure. The constant A is in effect the modulus at 100% shear strain and as such increases with crosslink density and carbon black content. The constant K describes the upturn in the stress-strain behaviour at higher strains and is associated with the finite extensibility of the rubber network. As such it increases with carbon black content, due to the strain amplification effect of the filler and with increasing crosslink density. The constant C is the shear strain at which the modulus begins to tend to its finite small strain value and as such decreases with increasing carbon black content. It is only necessary to determine C accurately if very small component strains[36] are of interest e.g., sidewalls of tyres.

The validation of this strain energy function has been carried out here for static (first cycle) deformation of filled rubbers. Using limited literature data it is demonstrated that the function will successfully predict the stress strain behaviour after many cycles if cyclic data is used to determine A, n,

C, K etc. However there is a clear need to validate the function much more systematically and extensively for cyclic data, following stress softening.

The thesis presents an initial study of the effect of the addition of a particulate silica filler on the stress-strain behaviour of rubbers with and without the addition of a coupling agent. The uncoupled materials show a pronounced yield stress at low strains, an effect which is much reduced by the addition of a silane coupling agent. A series of experiments is reported in an attempt to understand this effect. It is clearly associated with both the dispersion of the filler and with silica/rubber coupling. It is difficult to distinguish between these effects as the detailed effect of coupling agent on dispersion is not known. The new strain energy function is fitted to the tensile stress-strain data and yields values of the constants which change in a meaningful manner when the coupling agent is added. This study is interesting but needs to be extended and in particular there is a need to determine quantitatively the effect of the coupling agent on the silica dispersion using translucent rubbers and light scattering.

The thesis reported studies of static and cyclic relaxation rates in carbon black filled rubbers as a function of initial strain. These are the first of their kind and are comparable to previous studies of static and cyclic creep rates. While both the static and cyclic stress relaxation rates increase with carbon black content at a given strain, the effect is much smaller if comparison is made at a given stress. In all cases however the cyclic rates are significantly greater than the static rates. In the case of natural rubber this effect is explained in terms of the melting of crystals on unloading and the increased strain resulting on reloading prior to strain crystallization. The effect of carbon black is largely on the reduced specimen strain necessary to produce a given molecular strain hence enhancing the role of strain crytallization. The situation in filled SBR is far from clear as it is unlikely that the enhanced cyclic relaxation rate is associated with crystallization. In this respect is would be useful to study cyclic stress relaxation in a series of carbon black filled epoxidised natural rubbers in which the extent of strain crystallization could be varied over a wide range.

The thesis reported on the trouser tearing behaviour of both the carbon black and silica filled rubbers. In the case of carbon black the tearing behaviour is complex as both the materials variables and the experimental variables determine the nature of the catastrophic tearing process (Tearing regime). The magnitudes of the tearing energies for a given tear rate and their temperature dependencies can be explained in a

qualitative sense in terms of strain crystallization and carbon black/rubber molecule orientation at the tear tip.

The tearing behaviour of the silica filled materials produced some interesting results. In general the tearing energy is reduced by the addition of a coupling agent, suggesting that silica/rubber debonding is a significant energy absorbing process. In some cases this debonding was evidenced by relatively permanent stress whitening at the tear tip. This whitening was also observed at very large strains in the tensile tests. During steady tearing the width of this zone can be used to calculate the volume of rubber which is cycled nearly to break at the tear tip. If the diameter of this zone is d_H and the hysteresis loss per volume of rubber (determined from the cyclic stress-strain curve) is W_H then it is shown that the tearing energy is given by;

$$T = W_H.d_H$$

This is the first time that this has been demonstrated as it is not usually possible to measure d_H for most systems. The present results in this respect , are limited but it does demonstrate the potential of the system for use as a model material to study the effects of filler content and temperature on tearing energy in a quantitative manner during steady tearing. This is not quite as simple as it may seen but is clearly worthy of future study.

The final part of the thesis dealt with cyclic crack growth in pure shear test pieces for rubbers filled with carbon black and silica. The effect of systematically increasing carbon black content or increasing crosslink density on the observed crack growth rate (dc/dn) at a given tearing energy (T) was investigated for the first time. In all cases cyclic crack growth at a given T occurs at much faster rates than would be predicted from the tearing data. It is hence the additional cyclic crack growth due to the unloading/reloading process which is significant. In a quantitative sense the decrease in dc/dn for a given T with increasing carbon black content can be explained in terms of a combination of strain crystallization occurring earlier in the reloading cycle (due to strain amplification) and hysteresis losses due to the carbon black in NR, but mostly due to second of these in the case of SBR. Increasing the crosslink density causes an increase in dc/dn for a given T. Qualitatively this may be due to a combination of a increase in T_o and an increased rate of crystallization as the crosslink density decreases.

The effect of pre-straining a carbon black filled rubber in the direction of subsequent crack growth and then imposing a cyclic stress at

right angles on dc/dn at a given T is reported. It is shown that dc/dn increases by up to two orders of magnitude as the pre-strain increases to 200%. This is a very important effect particularly with respect to crack growth in components stressed in a complex manner. In this geometry cracks are now growing in the direction of pre-orientation of the rubber/carbon black structure and at 200% pre-strain into a pre-strain crystallized matrix. Cracks clearly require a much lower tearing energy to grow in this direction as has been previously demonstrated for catastrophic tearing using split test pieces[73]. However, the cyclic crack growth dc/dn is much faster than would be predicted from this tearing data. It is hence clearly still the unloading/reloading process which is responsible for this growth. The unloaded crack tip however now has crystals oriented in the direction of crack growth. The fully reloaded crack tip presumably has crystals oriented at right angles to the direction of crack growth. The effect is hence clearly not simple. However a very big effect has been demonstrated for the first time. It is clearly worth if further study utilizing epoxidised natural rubber with different propensities to strain crystallize.

The results for the silica filled materials are surprising as the silica, coupled and uncoupled, seems to have no effect on dc/dn for a given T. This needs to be investigated further as the 'real' crosslink densities of these materials are uncertain and certainly depend on both the silica and the coupling agent.

REFERENCES

1. Treloar, L.R.G., "Physics of Rubber Elasticity" 3rd Ed., Clarendon Press, Oxford (1975)
2. Mooney, M.J., J. Appl. Phys., **11**, 582, (1940)
3. Yeho, O.H., Rubber Chem. Technol., **63**, 792 (1990)
4. Rivlin, R.S., and Saunders, D.W., Phil. Trans. Roy. Soc., London **A243**, 251 (1951)
5. Treloar, L.R.G., J. Polym. Sci.: Polym. symp., **48**, 107 (1974)
6. Rivlin, R.S., in "Rheology vol. 1" Eirich, F.R. Ed., Academic Press, New York 1956, **Ch. 10**, 351
7. Isihara, A., Hashitsume, N., and Tatibana, M., J., Chem. Phys., **19**, 1508 (1951)
8. James, A.G., Green, A., and Simpson, G.M., J. Appl. Polym. Sci., **19**, 2033 (1975)
9. Morman (Jr), K.N., and Pan, T.Y., Rubber Chem. Technol., **61**, 503 (1988)
10. Chow, C. L., and Cundiff, C.H., Tire sci. Technol., **15**, 73 (1987)
11. James, A.G., and Green, A., J. Appl. Polym. Sci., **19**, 2319 (1975)
12. Tschoegl, N.W., Rubber Chem. Technol., **45**, 60 (1972)
13. Verga, O.H., "Stress-strain behaviour of Elastic materials", John wiley and Sons, New York, 1966
14. Ogden, R.W., Rubber Chem. Technol., **59**, 361 (1986)
15. Valanis, K.C., and Landel, R. F., J. Appl. Phys., **38**, 2997 (1967)
16. Hart-Smith, L.J., J. Appl. Math. Phys., **17**, 608 (1966)
17. Alexander, H., Int. J. Engng. Sci., **6**, 549 (1968)
18. Obata, Y., Kawabara, S., and Kawai, H., J. Polym. Sci., Polym. Phys. Ed., **8**, 903 (1970)
19. Jones, D.F., and Treloar, L.R.G., J. Phys. D (Appl. Phys.), **8**, 1285 (1975)
20. Seki, W., Fukahori, Y., Iseda, Y., and Matsunaga, T., Rubber chem. Technol., **60**, 856 (1987)
21. Kawabata, A. and Kawai, H., Adv. Polym. Sci., **24**, 89 (1977)
22. Fukahori, Y., and Seki, W., Polymer, **33**, 502 (1992)
23. Yeho, O.H., Rubber Chem. Technol., **66**, 754 (1993)
24. Gregory, M. J., Plast. Rubber Mater. Applications, **4**, 184 (1979)
25. Natural rubber engineering data sheets, MRPRA, Hertford, UK (1987)

26. Stacer, R.G., Hubner, C., and Husband, D.M., Rubber chem. Technol., **63**, 488 (1990)
27. Porter, M., Rubber Chem. Technol., **40**, 866 (1967)
28. Wagner, M.P., Rubber Chem. Technol., **47**, 697 (1974)
29. Rivlin, R.S., and Thomas, A.G., J. Appl. Polym. Sci., **10**, 291 (1953)
30. Mullins, L.J. Appl. Polym. Sci., **2**, 257 (1959)
31. Mullins, L., and Tobin, N.R., J. Appl. Polym. Sci., **9**, 2993 (1965)
32. Meinecke, E.A., and Maksin, S., Rubber Chem. Technol., **54**, 857 (1981)
33.Payne, A.P., and Whittaker, R.E., Rubber Chem. Technol., **44**, 440 (1971)
34. Kramer, O., and Ferry, J.D., in "Science and Technology of Rubber", Eirich, F.R. Ed., Academic Press, New York 1956, **Ch. 5**, 216
35. Harwood, J.A.C., Mullins, L., and Payne, A.R., J. of the IRI, **Jan-Feb**, 17 (1967)
36. Kraus, G., in "Science and Technology of Rubber", Eirich, F.R. Ed., Academic Press, Newyork 1956, **Ch. 8**, 339
37. Payne, A.P., J. Appl. Polym. Sci., **9**, 2273 (1965)
38. Boonstra, B.B., and Medalia, A.I., Rubber Age, **92**, 892 (1963)
39. Wagner, M.P., Rubber Chem. Technol., **49**, 703 (1976)
40. Wagner, M.P., Wartman, H.J., and Sellers, J.W., Kautsch Gummi Kunstst. **20**, 407 (1967)
41. Voet, A., Morawski, J.C., and Donnel, J.B., Rubber Chem. Technol., **50**, 342 (1977)
42. Derham, C.J., and Thomas, A.G., Rubber Chem. Technol., **50**, 397 (1977)
43. Gregory, M.J., Metherell, C., and Smith, J. F., Plast. Rubber Mater. Applications, 37, (1978)
44. Gent, A.N., J. Appl. Polym. Sci., **6**, 433 (1962)
45. Griffith, A.A., Phil. Trans. Roy. Soc., London, **A221**, 163 (1920)
46. Thomas, A.G., J. Appl. Polym. Sci., **3**, 168 (1960)
47. Lake, G.J., Lindley, P.B., and Thomas, A.G., Proc. 2nd. Int. conf. of Fracture, Brighton, April (1969)
48. Thomas, A.G., J. Polym. Sci., **18** , 177 (1955)
49. Greensmith, W.H., J. Appl. Polym. Sci., **3**, 183 (1960)
50. Higuchi, T., Leeper, H.M., and Davies, D.S., Anal. Chem., **20**, 1029 (1948)
51. Mullins, L.J. Appl. Polym. Sci., Appl. Polym. Symp., **39**, 59 (1984)

52. Mueller, H.K. and Knauss, W. G., Trans. Soc. Rheo., **15**, 217 (1971)
53. Ahagon, A., and Gent, A.N., J. Appl. Polym. Sci., Polym. Phys. Ed., **13**, 1903 (1975)
54. Lake, G.J., and Thomas, A.G., Proc. Roy. Soc., London, **A300**, 108 (1967)
55. Gent, A.N., and Tobias, R.H., J. Appl. Polym. Sci., Polym. Phys. Ed., **20**, 2051 (1982)
56. Yanyo, L.C, and Kelly, F.N., Rubber Chem. Technol., **61**, 100 (1988)
57. Bhomick, A.K., Gent, A.N., and Pulford, C.T.C., Rubber Chem. Technol., **56**, 226 (1983)
58. Greensmith, H.W., Mullins, L., and Thomas, A.G., Trans. Soc.of Rheo. **4**, 1979 (1960)
59. Mullins, L., Trans. IRI, **35**, 213 (1959)
60. Williams, M.L., Landel, R.F., and Ferry, J.D., J. Amec. Chem. Soc., **77**, 3701 (1955)
61. Greensmith, W.H., J. Appl. Polym. Sci., **21**, 175 (1956)
62. Samsuri, A.B., and Thomas, A.G., Int. Rub. Conf., Kuala lumpur (1988)
63. Gent, A.N., and Henry, A.W., Proc. Int. Rub. Conf., 193 (1967)
64. Andrews, E.H., J. Appl. Phy. **32**, 547 (1961)
65. Gent, A.N., in "Science and Technology of Rubber", Eirich, F.R. Ed., Academic Press, Newyork 1956, **Ch. 10**, 419
66. Kadir, A., and Thomas, A.G., Rubber Chem. Technol., **54**, 15 (1981)
67. Brown, P.S., Porter, M., and Thomas, A.G., Int. Rub. Conf., Kuala Lumpur (1985)
68. Busse, W.F., Ind. Eng. Chem., **26**, 194 (1974)
69. Lake, G.J., and Yeoh, O.H., Rubber Chem. Technol., **53**, 210 (1980)
70. Buche, F., J. Appl. Polym. Sci., **5**, 271 (1961)
71. Wagner, M.P., Rubber World, **164**, 46 (1971)
72. Hewitt, N.L., Rubber World, **186**, 24 (1982)
73. Samsuri, A.B., PhD. Thesis, Univ. of London 1989.
74. Gent, A.N., Lindley, P.B., and Thomas, A.G., J. Appl. Polym. Sci., **8**, 455 (1964)
75. Greensmith, W.H., J. Appl. Polym. Sci., **7**, 993 (1963)
76. Lake, G.J., and Lindley, P.B., J. Appl. Polym. Sci., **8**, 707 (1964)
77. Lake, G.J., and Lindley, P.B., Rubber, J.,**146** [10], 24 and **146** [11], 30 (1964)
78. Clapson, B.E., and Lake, G.J., Rubber J., **153** [12], 36 (1970)

79. Grosch, K.A., Kautsch Gummi Kunstst., **26**, 265 (1973)
80. Young, D.G., Rubber Chem. Technol., **58**, 785 (1985)
81. Breidenbach, R.F., and Lake, G.J., Rubber Chem. Technol., **52**, 96 (1979)
82. Huang, Y.S., and Yeoh, O.H., Rubber Chem. Technol., **62**, 709 (1989)
83. Derham, C.J., Lake, G.J., and Thomas, A.G., Rub. Int., Malaya **22 [2]**, 191 (1969)
84. Thomas, A.G., in "Deformation and fracture of high polymers" Kausch, H., Hassel, J.A., and Jaffe, R., Ed., Plenum Press, (1974)
85. Lake, G.J., and Lindey, P.B., Fatigue of Rubber, Proc. conf. Phys. Basic Yield Fracture, Oxford, 176 (1966)
86. Lake, G.J., Rubber Chem. Technol., **45**, 309 (1972)
87. Gent, A.N., J. Appl. Polym. Sci., **6**, 497 (1962)
88. Yanyo, L.C., Int. J. Fracture, **39**, 103 (1989)
89. Young, D.G., and Doyle, M.J., Int. Rub. conf. Japan, **39**,103 (1985)
90. Dizon, E.S., Hicks, A.E., and Chirico, V.E., Rubber Chem. Technol., **47**, 231 (1974)
91. Dizon, E.S., Chirico, V.E., and Hicks, A.E., Int. Rubb. Conf., Brighton, (1977)
92. Killgoar(Jr), P.S., and Lemieux, M.A., and Tabar, R.J., Rubber Chem. Technol., **54**, 347 (1981)
93. Gregory, M.J., NR Technol., **11**, 28 (1980)
94. Baker, C.S.L., NR Technol., **11**, 24 (1977)
95. Beatty, J.R., Rubber Chem. Technol., **37**, 134 (1964)
96. Lake, G.J., and Lindley, P.B., J. Appl. Ploym. Sci. **9**, 1233 (1965)

APPENDIX- 3.1

The measurement of crosslink density can be carried out means of measurement of equilibrium swelling. This is suitable for both unfilled and filled rubber vulcanizates where as measurement utilizing stress strain data from simple extension is only suitable for unfilled rubber vulcanizates.

Various samples, square pieces from flat sheets or thin circular sections from compression buttons or rubber disks (A) from double shear test pieces, were cut for use in swelling measurements. These were carried out by first weighing the rubber samples accurately using an Oetling electronic analytical balance (model R51), and then immersing them in n-decane. The changes in weight of the rubber samples were monitored with respect to time. This was achieved by weighing them every few minutes for four to five hours, then leaving them in the n-decane for a few days in order to reach an equilibrium swelling state.

The n-decane used had a molecular weight of 142.29, while its density was 0.7264 g cm^{-3} at 25°C. The volume of solvent absorbed, V_s, was calculated from the differences in the weights of the swollen and unswollen samples. Hence, the volume fraction of rubber, v_r, in the swollen sample could be calculated using the relationship;

$$v_r = \frac{V_{rn}}{V_{rn} + V_s} \qquad (3A)$$

where V_{rn} is the volume of rubber network. The rubber network (rn) refers to the network formed from the rubber hydrocarbon and the curative by the vulcanization process, including any atoms or groups introduced in crosslinks or as modifications of the main rubber chains. V_{rn} was calculated from the initial weights of the samples and the mix compositions, using the relationship;

$$V_{rn} = \frac{(M_0)\ (M_{rn})}{(M_m)\ (\rho_{RH})} \qquad (3B)$$

where M_{rn} is the weight of rubber network, i.e, the weight of rubber hydrocarbon (RH) and sulphur combined. M_m is the total weight of a mix

formulation, M_0 is the initial weight of the sample and ρ_{RH} is the density of rubber hydrocarbon.

The value of v_r was then substituted into the Flory-Rehner equation for the determination of $[X]_{phys}$ i.e., the physical manifested crosslink density or apparent crosslink density.

$$\ln(1- v_r) + v_r + \chi v_r^2 + 2 \rho v_o [X]_{phys} (v_r)^{1/3} = 0 \qquad (3C)$$

Where v_o is the molar volume of the solvent, of value of 195.88 cm^3 for n-decane, χ is the rubber-solvent interaction parameter, of value of 0.42 for NR and IR in n-decane, ρ is the density of rubber hydrocarbon, of value of 0.92 gm per cm^3 for NR and IR. For a network containing tetrafuntional crosslinks only, the number of network chains is twice the number of crosslinks. Hence the number of crosslinks per unit weight of rubber is $N/2M_c$, where N is Avogadro's number, and M_c is the average molecular weight between crosslinks. The crosslink density expressed in "gram molecules" per gram of rubber is thus

$$[X]_{phys} = \frac{1}{2M_c} \qquad (3D)$$

APPENDIX-4.1

STRESS-STRAIN FITTING ROUTINE

Consisting of;

(1) Flow chart

(2) Programme

(3) Example of input and output data for NR69

(1) Flow Chart

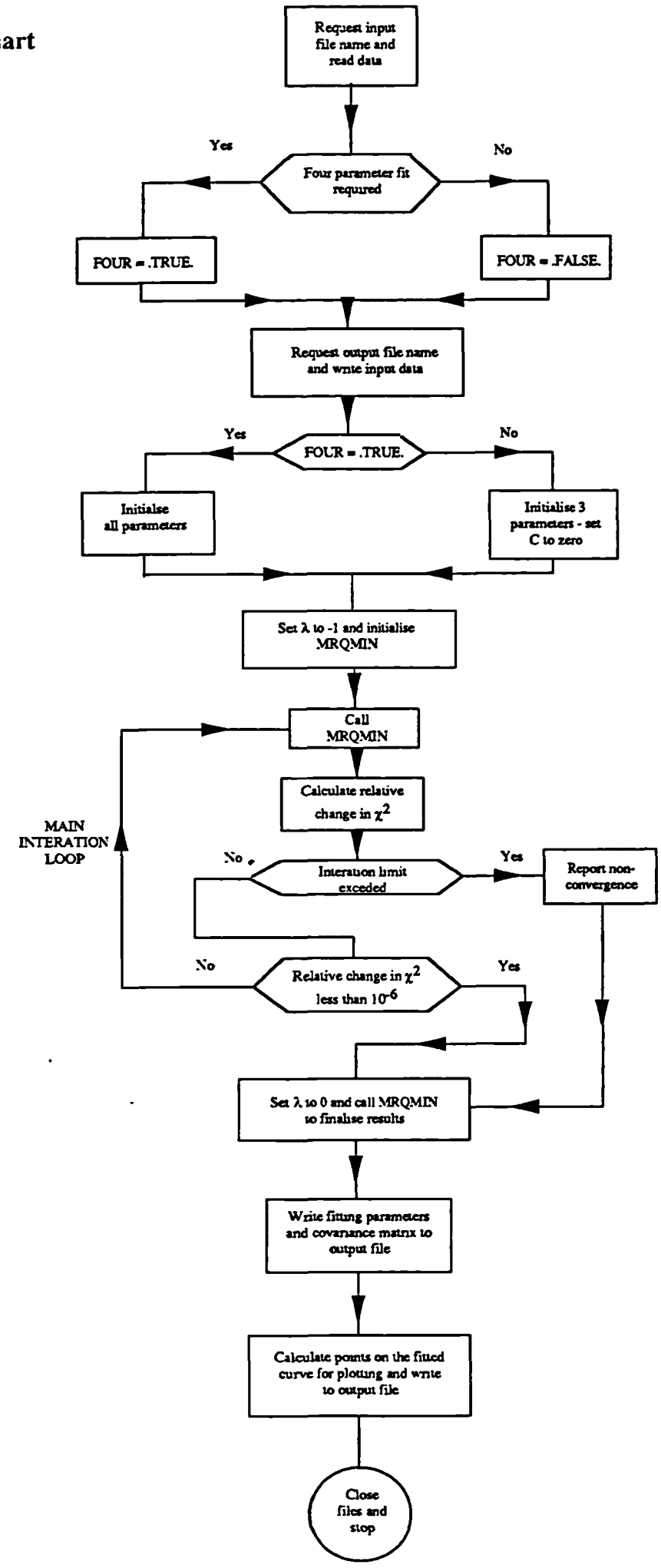
Request input file name and read data
Four parameter fit required
Yes
No
FOUR = .TRUE.
FOUR = .FALSE.
Request output file name and write input data
FOUR = .TRUE.
Yes
No
Initialse all parameters
Initialise 3 parameters - set C to zero
Set λ to -1 and initialise MRQMIN
Call MRQMIN
Calculate relative change in χ^2
MAIN INTERATION LOOP
Interation limit exceded
No
Yes
Report non-convergence
Relative change in χ^2 less than 10^{-6}
No
Yes
Set λ to 0 and call MRQMIN to finalise results
Write fitting parameters and covariance matrix to output file
Calculate points on the fitted curve for plotting and write to output file
Close files and stop

(2) Programme

```
C     This programme uses routines from Numerical Recipes (W. Press,
C     B.P. Flannery, S. A. Teakolsky and W. T. Vettering) 14.4 pp521
C      - 528 to fit an expression to normalised stress/strain invariant
C     data for elastomers.  Details of the method are given in the
C     reference.  The expression has four parameters:- A (= A(1)),
C     n (= A(2)), K (= A(3) and C (= A(4)) and gives the relation
C     between the reduced stress, Y, and the first strain invariant
C     (minus 3), X.   The expression is
C
C     Y = (A/2)*(X+C**2)**(-n/2)+2.*K*X
C
C     However the program allows a choice of a three parameter function
C     (obtained by setting C to zero) or a four parameter function as
C     above.  For details of this see the reference pages 513 & 526.
C
C     Page numbers refer to the first edition of Numerical Recipes.
C
C     Reserve space:
C
      DIMENSION X(200), Y(200),SIG(200)
      DIMENSION A(4),LISTA(4), COVAR(4,4), ALPHA(4,4),NPTS(8)
      EXTERNAL FUNCS
C
C     X,Y hold the sub-sets of NPTS data points for the
C     different deformation modes. SIG holds the standard deviations
C     of the individual data values (i.e. the weight functions - not
C     used in this application), A the parameters to be determined,
C     LISTA the indices of the parameters which are to be fitted,
C     COVAR the elements of the covariance matrix and ALPHA the
C     curvature matrix.
C
C     Set the number of parameters required for the fitting
C     equation and the string marking end of input file.
C
      PARAMETER (MA=4)
C
C     Reserve space for the filenames from which input values of
C     data to be are read and in which the results are to be stored.
C     Also reserve space for an identity code for the data set and
C     codes to identify the deformation mode for each data sub-set.
C
      CHARACTER FILEIN *40, FILEOUT *40, CODE *70
      CHARACTER MODE(8)*40, EXIT *40
      LOGICAL FOUR
      EXIT='****                                              '
C
C     Print heading.
C     Ask whether a four or three parameter fit is required.
C
      WRITE(*,198)
  198 FORMAT(/////////////// ////////30X,'E L A S T O M E R  II'/
     $       30X,'----------------------'////13X,'Do you want to fit a ',
     $       'three or four parameter function?'///)
      WRITE(*,197)
  197 FORMAT(24X,'Type "3" for three parameters, or'/24X,'Type "4"',
     $        ' for four parameters.'/18X,'Carriage Return or Enter',
     $        ' after number, please.'/)
   62  READ(*,*)IPARAM
       IF(IPARAM.NE.3.AND.IPARAM.NE.4) THEN
        WRITE(*,57)
```

```
 57     FORMAT(15X,'Sorry, either a 3 or a 4 is required.  Try again.')
       GOTO 62
      ELSE
       IF(IPARAM.EQ.4)THEN
          FOUR=.TRUE.
       ELSE
          FOUR=.FALSE.
       ENDIF
      ENDIF
C
C     Open the input file and read in the data
C
      WRITE(*,56)
 56   FORMAT(15X,'Please input the filename (maximum of 40 characters)'/
     $       15X,'in which data is to be found.'//
     $       15X,'Consult the documentation for the required format'/
     $       15X,'of the input file.'//)
      READ (*, 199) FILEIN
 199  FORMAT(A40)
      OPEN(UNIT =4, FILE=FILEIN,STATUS='OLD')
      READ(UNIT=4,FMT=800)CODE
      WRITE(*,*)CODE
 800  FORMAT(A70)
      NMODE=0
      I=1
      IEND=0
      IBEG=1
C
C     Now begin the loop to read in the data sets.
C
 81   CONTINUE
       READ(UNIT=4,FMT=702)MODE(I)
 702     FORMAT(A40)
       IF(MODE(I).NE.EXIT)THEN
C
C        Not finished yet
C
         NMODE=NMODE+1
         READ(UNIT=4,FMT=*)NPTS(I)
         IEND=IEND+NPTS(I)
C
C     Now read in the data points for this deformation mode.
C
         WRITE(*,51)MODE(I)
 51        FORMAT(20X,A40)
         READ(UNIT=4,FMT=*)(X(K),Y(K),K=IBEG,IEND)
         I=I+1
         IBEG=IEND+1
C
C     Now go round the loop again for the next data sub-set.
C
         GOTO 81
      ENDIF
C
C     All data read, close the input file.
C
      CLOSE(UNIT=4)
      WRITE(*,52)
 52   FORMAT(17X,'All data read successfully, input file closed.')
C
C     Check to see if there was any data in the file.
C
      IF(NMODE.EQ.0)THEN
```

```
      WRITE(*,53)
   53   FORMAT(19X,'There was no valid data in the input file. '/
     $         28X,'Program is terminating.')
      CLOSE(UNIT=4)
      STOP
      ENDIF
C
C     Calculate the total number of data points and then
C     set the all standard deviations (weight functions) to 1.
C
      NDATA=0
      DO 67 I=1, NMODE
       NDATA=NDATA+NPTS(I)
   67 CONTINUE
      DO 20 I=1,NDATA
       SIG(I)=1.
  20  CONTINUE
C
C     Open the output file and write the original data in comma-
C     separated value format together with the mode headings.
C
      WRITE(*,150)
  150 FORMAT(20X,'Please enter the name of the output file'/
     $       28X,'(maximum 40 characters).')
      WRITE (*,*)
      READ(*,199)FILEOUT
      OPEN(UNIT=4,FILE=FILEOUT, STATUS = 'NEW')
      WRITE(UNIT=4,FMT=626)CODE
  626 FORMAT(20X,'NON-LINEAR LEAST SQUARES FITTING PROGRAM'//
     $       30X,'E L A S T O M E R II'/30X,'======================'//
     $       'Data set:-',A70//17X,'Original data in comma separated',
     $        ' value format.'////)
      IEND=0
      IBEG=1
      DO 35 I=1,NMODE
      IEND=IEND+NPTS(I)
      WRITE(UNIT=4,FMT=627)MODE(I)
  627   FORMAT(/A40)
      WRITE(UNIT=4,FMT=629)(X(K),Y(K),K=IBEG,IEND)
  629   FORMAT E14.8,',',E14.8)
      IBEG=IEND+1
   35 CONTINUE
C
C     Now the the NMODE data sub-sets are sorted into a single set in
C     ascending order of X.  First check if this is necessary.
C
      IF(NMODE.GT.1) THEN
C
C        Yes, it is.
C
      CALL SORT2(NDATA,X,Y)
      ENDIF
C
C     Now set the initial values of the parameters and
C     the indices of those to be fitted.  The former may have
C     to be improved for special cases.
C
      A(1)=1.
      A(2)=1.
      A(3)=1.
      DO 21 I=1,4
       LISTA(I =I
  21  CONTINUE
```

```
C
C     Adjust LISTA(4) and A(4) depending on whether a 3 or 4
C     parameter fit is required.
C
      IF(.NOT.FOUR)THEN
       LISTA(4)=0
       A(4)=0.
       MFIT=3
      ELSE
       MFIT=MA
       A(4)=0.1
      ENDIF
      NCA=MA
C
C     Now call the fitting routine with ALAMDA=-1 to
C     initialise it.
C
      ALAMDA=-1.
      CALL MRQMIN(X,Y,SIG,NDATA,A,MA,LISTA,MFIT,COVAR,ALPHA,
     $            NCA,CHISQ,FUNCS,ALAMDA)
C
C     Write  some headings in the file and then set up the loop to
C     minimise CHISQ and find the best fit parameters.
C
      WRITE(UNIT=4,FMT=501)IPARAM
 501  FORMAT(//30X,'INTERMEDIATE RESULTS'/30X,'--------------------'//
     $       20X,'A ',I1,' parameter function is being fitted.'///
     $       'Iter',3X,'Relative',10X,'A',14X,'n',14X,
     $       'K',14X,'C'/8X,'change'/)
      WRITE(*,501)IPARAM
      NITER=0
 27   CONTINUE
       NITER=NITER+1
       C1=CHISQ
       CALL MRQMIN(X,Y,SIG,NDATA,A,MA,LISTA,MFIT,
     $                 COVAR,ALPHA,NCA,CHISQ,FUNCS,ALAMDA)
       C2=CHISQ
       ACC=ABS((C2-C1)/C2)
       WRITE(UNIT=4,FMT=502)NITER,ACC,A(1),A(2),A(3),A(4)
 502     FORMAT(I2,2X,E14.8,1X,E14.8,1X,E14.8,1X,E14.8,1X,E14.8)
       WRITE(*,502)NITER,ACC,A(1),A(2),A(3),A(4)
       IF(ACC.GT.1.E-6)THEN
          IF(NITER.LT.50)GOTO 27
       ENDIF
C
C     Check whether the set limit on number of iterations
C     has been exceeded.  If so print a warning.
C
      IF(NITER.EQ.100)THEN
       WRITE(*,151)
 151     FORMAT(/27X,'The algorithm has failed to converge in 50',
     $           'iterations.')
      ELSE
       WRITE(*,152)FILEOUT
  152    FORMAT(/27X,'Successful convergence'/20X,' - final results',
     $          ' in file ',A40)
      ENDIF
C
C     Now complete the process by calling MRQMIN
C     with ALAMDA=0.
C
      ALAMDA=0.
      CALL MRQMIN(X,Y,SIG,NDATA,A,MA,LISTA,MFIT,COVAR,
```

```
     $            ALPHA,NCA,CHISQ,FUNCS,ALAMDA)
C
C     Now write the final results to the output file
C

      IF(NITER.LT.100)THEN
        WRITE(4,990)
 990      FORMAT(/32X,'PROCESS CONVERGED')
      ELSE
        WRITE(4,991)
 991      FORMAT(/6X,'WARNING - PROCESS DID NOT ',
     $              'CONVERGE, ITERATION LIMIT EXCEEDED')
      ENDIF
      WRITE(4,992)
 992  FORMAT(////31X,'Fitting Parameters'/
     $           31X,'-----------------')
      WRITE(4,993)A(1),A(2),A(3),A(4)
 993  FORMAT(/30X,'A = ',E15.8/30X,'n = ',E15.8/30X,'K = ',E15.8
     $       /30X,'C = ',E15.8)
      WRITE(4,994)CHISQ
 994  FORMAT(/7X,'Squares of the residuals = ',E15.8//)
      WRITE(4,996)
 996  FORMAT(30X,'The covariance matrix'/30X,'--------------------'/)
      WRITE(4,995)((I,J,COVAR(I,J),J=1,4),I=1,4)
 995  FORMAT('C(',I1,I1,')=',E13.6,1X,'C(',I1,I1,')=',E13.6,1X,
     $       'C(',I1,I1,')=',E13.6,1X,'C(',I1,I1,')=',E13.6)
C
C     Now calculate values of reduced stress from values of the strain
C     invariant using the fitted parameters in the given equation.
C     First we calculate the range of values of the strain invariant
C     given on a logarithmic scale and the increment required to give
C     50 points on the fitted curve equally spaced on a log scale.
C
      XLINC=(LOG(X(NDATA)/X(1)))/49.
C
C     Now write heading.
C
      WRITE(4,997)CODE
 997  FORMAT(///16X,'Fitted values of strain invariant/reduced stress'
     $       /16X,'================================================='///
     $       'Data set: ',A70///
     $       5X,'Strain',6X,'reduced'/4X,'invariant',4X,'stress'/)
C
C     Now calculate the points on the fitted curve and write to the
C     results file. Note that the results are written in comma-
C     separated value format and after editing the file to remove the
C     redundant lines it can be imported into Cricket Graph for
C     plotting.
C
      XLFIT=LOG(X(1))
      DO 23 I=1,50
       XFIT=EXP(XLFIT)
       PHIFIT=RSIGMA(XFIT,A(1),A(2),A(3),A(4))
       WRITE(4,998)XFIT,PHIFIT
 998     FORMAT(E14.8,',',E14.8)
       XLFIT=XLFIT+XLINC
  23  CONTINUE
      STOP
      END
C
C
C     ********************************************************************
C
```

```
C
      SUBROUTINE FUNCS(AI,A,PHI1,DYDA,NA)
C
C     Calculates the value of the function PHI for a
C     given X with the parameters, A, n and K in
C     array A and calculates the values of the NA
C     partial derivatives with respect to the parameters
C     at X, returning them in the array DYNA.
C
      DIMENSION A(NA), DYDA(NA)
C
C     First check the validity of the values of AI.
C
      IF(AI.LT.0.)THEN
        WRITE(*,997)
 997      FORMAT(1X,'Invalid data in FUNCS:- AI less than 0')
        WRITE(*,998)
 998      FORMAT(1X,'Execution terminated.')
        STOP
      ENDIF
C
C     Now calculate the function value, PHI.
C
      AINO2=(AI+A(4)*A(4))**(-A(2)/2.)
      PHI1=A(1)/2.*AINO2+2.*A(3)*AI
C
C     Now calculate the three partial derivatives
C     w.r.t. A(1), A(2) and A(3).
C
      DYDA(1)=AINO2/2.
      DYDA(2)=-A(1)*AINO2*LOG(AI+A(4)*A(4))/4.
      DYDA(3)=2.*AI
      DYDA(4)=-A(1)*A(2)*A(4)*AINO2/(AI+A(4)*A(4))/2.
      RETURN
      END
C
C
C     ****************************************************************
C
C
      FUNCTION RSIGMA(AI,A,EXPT,AK,C)
C
C     Calculates the values of the fitting function and does it more
C     efficiently than FUNCS (i.e. without the derivatives).
C
C     First check the validity of the values of AI
C
      IF(AI.LT.0.)THEN
        WRITE(*,800)
 800      FORMAT(1X,'Invalid data in SIGMA:- AI less than 0.')
        WRITE (*,801)
 801      FORMAT(1X,' Execution terminated.')
      STOP
      ENDIF
C
C     Now calculate the function value of the reduced stress.
C
      RSIGMA=A*(AI+C*C)**(-EXPT/2.)/2.+2.*AK*AI
      RETURN
      END
C
C
C     ****************************************************************
```

```
C
C
      SUBROUTINE MRQMIN(X,Y,SIG,NDATA,A,MA,LISTA,MFIT,
     *     COVAR,ALPHA,NCA,CHISQ,FUNCS,ALAMDA)
C
C     Levenberg-Marquardt method for minimising the sum of the squares
C     of the residuals of a fit between a set of NDATA points X(I),
C     Y(I) with individual standard deviations SIG(I) and a non-linear
C     function dependent on MA coefficients, A.  See Numerical Recipes
C     (first edition) by Press, Flannery, Teukolsky and Vettering
C     (Cambridge) section 14.4 pp 521 - 528 for details.
C
      PARAMETER (MMAX=20)
      DIMENSION X(NDATA),Y(NDATA),SIG(NDATA),A(MA),LISTA(MA),
     *  COVAR(NCA,NCA),ALPHA(NCA,NCA),ATRY(MMAX),BETA(MMAX),DA(MMAX)
      EXTERNAL FUNCS
      IF(ALAMDA.LT.0.)THEN
      KK=MFIT+1
C
C     Does LISTA contain a proper permutation of the coefficients?
C
      DO 12 J=1,MA
        IHIT=0
        DO 11 K=1,MFIT
          IF(LISTA(K).EQ.J)IHIT=IHIT+1
 11       CONTINUE
        IF (IHIT.EQ.0) THEN
          LISTA(KK)=J
          KK=KK+1
        ELSE IF (IHIT.GT.1) THEN
          PAUSE 'Improper permutation in LISTA'
        ENDIF
 12     CONTINUE
      IF (KK.NE.(MA+1)) PAUSE 'Improper permutation in LISTA'
      ALAMDA=0.001
      CALL MRQCOF(X,Y,SIG,NDATA,A,MA,LISTA,MFIT,ALPHA,BETA,NCA,CHISQ,
     *                FUNCS)
      OCHISQ=CHISQ
      DO 13 J=1,MA
        ATRY(J)=A(J)
 13     CONTINUE
      ENDIF
C
C     Alter linearized fitting matrix by augmenting diagonal elements
C     .
      DO 15 J=1,MFIT
      DO 14 K=1,MFIT
        COVAR(J,K)=ALPHA(J,K
 14     CONTINUE
      COVAR(J,J)=ALPHA(J,J)*(1.+ALAMDA)
      DA(J)=BETA(J)
 15   CONTINUE
C
C     Matrix solution
C
      CALL GAUSSJ(COVAR,MFIT NCA,DA,1,1)
C
C     Once converged evaluate covariance matrix with ALAMDA=0.
C
      IF(ALAMDA.EQ.0.)THEN
      CALL COVSRT(COVAR,NCA,MA,LISTA,MFIT)
      RETURN
      ENDIF
```

```
C
C     Did the trial succeed?
C
      DO 16 J=1,MFIT
      ATRY(LISTA(J))=A(LISTA(J))+DA(J)
 16   CONTINUE
      CALL MRQCOF(X,Y,SIG,NDATA,ATRY,MA,LISTA,MFIT,COVAR,DA,NCA,CHISQ,
     *FUNCS)
      IF(CHISQ.LT.OCHISQ)THEN
C
C     Success, accept the new solution.
C
      ALAMDA=0.1*ALAMDA
      OCHISQ=CHISQ
      DO 18 J=1,MFIT
        DO 17 K=1,MFIT
          ALPHA(J,K)=COVAR(J,K)
 17       CONTINUE
        BETA(J)=DA(J)
        A(LISTA(J))=ATRY(LISTA(J))
 18     CONTINUE
      ELSE
C
C     Failure, increase ALAMDA and return.
C
      ALAMDA=10.*ALAMDA
      CHISQ=OCHISQ
      ENDIF
      RETURN
      END
C
C
C     ******************************************************************
C
C
      SUBROUTINE MRQCOF(X,Y,SIG,NDATA,A,MA,LISTA,MFIT,ALPHA,BETA,NALP,
     *CHISQ,FUNCS)
C
C     Used by MRQMIN to evaluate the linearised fitting matrix ALPHA,
C     and vector BETA as in NR 14.8 (Numerical Recipes pp 527)
C
      PARAMETER (MMAX=20)
      DIMENSION X(NDATA),Y(NDATA),SIG(NDATA),ALPHA(NALP,NALP),BETA(MA),
     *    DYDA(MMAX),LISTA(MFIT),A(MA)
      EXTERNAL FUNCS
      DO 12 J=1,MFIT
      DO 11 K=1,J
        ALPHA(J,K)=0.
 11     CONTINUE
      BETA(J)=0.
 12   CONTINUE
      CHISQ=0.
      DO 15 I=1,NDATA
      CALL FUNCS(X(I),A,YMOD,DYDA,MA)
      SIG2I=1./(SIG(I)*SIG(I))
      DY=Y(I)-YMOD
      DO 14 J=1,MFIT
        WT=DYDA(LISTA(J))*SIG2I
        DO 13 K=1,J
          ALPHA(J,K)=ALPHA(J,K)+WT*DYDA(LISTA(K))
 13       CONTINUE
        BETA(J)=BETA(J)+DY*WT
 14     CONTINUE
```

```
      CHISQ=CHISQ+DY*DY*SIG2I
 15   CONTINUE
      DO 17 J=2,MFIT
      DO 16 K=1,J-1
        ALPHA(K,J)=ALPHA(J,K)
 16     CONTINUE
 17   CONTINUE
      RETURN
      END
C
C
C     ******************************************************************
C
C
      SUBROUTINE COVSRT(COVAR,NCVM,MA,LISTA,MFIT)
C
C     Given the covariance matrix COVAR of a fit of MFIT of NA total
C     parameters, and their ordering, LISTA, repack the covariance
C     matrix to the true order of the parameters.  Elements associated
C     with fixed parameters will be zero.  NCVM is the physical
C     dimension of COVAR. (Numerical Recipes pp 515)
C
      DIMENSION COVAR(NCVM,NCVM),LISTA(MFIT)
C
C     Zero all elements below diagonal.
C
      DO 12 J=1,MA-1
      DO 11 I=J+1,MA
        COVAR(I,J)=0.
 11     CONTINUE
 12   CONTINUE
C
C     Repack off-diagonal elements of fit into correct locations below
C     diagonal.
C
      DO 14 I=1,MFIT-1
      DO 13 J=I+1,MFIT
        IF(LISTA(J).GT.LISTA(I)) THEN
          COVAR(LISTA(J),LISTA(I))=COVAR(I,J)
        ELSE
          COVAR(LISTA(I),LISTA(J))=COVAR(I,J)
        ENDIF
 13     CONTINUE
 14   CONTINUE
      SWAP=COVAR(1,1)
      DO 15 J=1,MA
      COVAR(1,J)=COVAR(J,J)
      COVAR(J,J)=0.
 15   CONTINUE
      COVAR(LISTA(1),LISTA(1))=SWAP
C
C     Now sort elements into proper order on diagonal.
C
      DO 16 J=2,MFIT
      COVAR(LISTA(J),LISTA(J))=COVAR(1,J)
 16   CONTINUE
C
C     Finally fill in above diagonal by symmetry.
C
      DO 18 J=2,MA
      DO 17 I=1,J-1
        COVAR(I,J)=COVAR(J,I)
 17     CONTINUE
```

```
 18   CONTINUE
      RETURN
      END
C
C
C     ****************************************************************
C
C
      SUBROUTINE GAUSSJ(A,N,NP,B,M,MP)
C
C     Linear equation solution by Gauss-Jordan elimination,  A is an
C     input matrix of N by N elements, stored in an array of physical
C     dimensions by NP by NP.  B is an input matrixs of N by M elements
C     containing the M right-handed side vectors, stored in an array of
C     phyiscal NP by MP.  On output A is replaced by its matrix invers,
C     and B is replaced by the corresponding solution vectors.
C     (Numerical Recipes pp 28)
C
      PARAMETER (NMAX=50)
      DIMENSION A(NP,NP),B(NP,MP),IPIV(NMAX),INDXR(NMAX),INDXC(NMAX)
C
C     The integer arrays IPIV, INDXR and INDXC are used for bookkeeping
C     on the pivoting.  NMAX should be as large as the largest
C     anticipated value of N.
C
      DO 11 J=1,N
      IPIV(J)=0
 11   CONTINUE
C
C     This is the main loop over the columns to be reduced.
C
      DO 22 I=1,N
      BIG=0.
C
C     This is the outer loop of the search for a pivot element.
C
      DO 13 J=1,N
        IF(IPIV(J).NE.1)THEN
          DO 12 K=1,N
            IF (IPIV(K).EQ.0) THEN
            IF (ABS(A(J,K)).GE.BIG)THEN
               BIG=ABS(A(J,K))
               IROW=J
               ICOL=K
            ENDIF
            ELSE IF (IPIV(K).GT.1) THEN
            PAUSE 'Singular matrix'
            ENDIF
 12         CONTINUE
        ENDIF
 13     CONTINUE
      IPIV(ICOL)=IPIV(ICOL)+1
C
C     We now have the pivot element so we interchange rows, if needed,
C     to put the pivot element on the diagonal.  The columns are not
C     physically interchanged only relabeled:  INDXC(I), the column of
C     the Ith pivot element, is the Ith column that is reduced, while
C     INDXR(I) is the row in which that pivot element was originally
C     located.  If INDXR(I) is not equal to INDXC(I) there is an implied
C     column interchange.  With this form of book-keeping, the solution
C     B's will end up in the correct order, and the inverse matrix will
C     be scrambled by columns.
C
```

```
      IF (IROW.NE.ICOL) THEN
        DO 14 L=1,N
          DUM=A(IROW,L)
          A(IROW,L)=A(ICOL,L)
          A(ICOL,L)=DUM
 14       CONTINUE
        DO 15 L=1,M
          DUM=B(IROW,L)
          B(IROW,L)=B(ICOL,L)
          B(ICOL,L)=DUM
 15       CONTINUE
      ENDIF
C
C     We are now ready to divide the pivot row by the pivot element,
C     located at IROW  and ICOL.
C
      INDXR(I)=IROW
      INDXC(I)=ICOL
      IF (A(ICOL,ICOL).EQ.0.) PAUSE 'Singular matrix.'
        PIVINV=1./A(ICOL,ICOL)
        A(ICOL,ICOL)=1.
        DO 16 L=1,N
          A(ICOL,L)=A(ICOL,L)*PIVINV
 16       CONTINUE
        DO 17 L=1,M
          B(ICOL,L)=B(ICOL,L)*PIVINV
 17       CONTINUE
C
C     Next we reduce the rows ...
C
        DO 21 LL=1,N
          IF(LL.NE.ICOL)THEN
C
C     ... except for the pivot one, of course.
C
            DUM=A(LL,ICOL)
            A(LL,ICOL)=0.
            DO 18 L=1,N
            A(LL,L)=A(LL,L)-A(ICOL,L)*DUM
 18           CONTINUE
            DO 19 L=1,M
            B(LL,L)=B(LL,L)-B(ICOL,L)*DUM
 19           CONTINUE
      ENDIF
 21     CONTINUE
 22   CONTINUE
C
C     This is the end of the main loop over columns of the reduction.
C     It only remains to unscramble the solution in view of the column
C     interchanges.  We do this by interchanging pairs of columns in the
C     reverse order that the permutation was built up.
C
      DO 24 L=N,1,-1
      IF(INDXR(L).NE.INDXC(L))THEN
        DO 23 K=1,N
          DUM=A(K,INDXR(L))
          A(K,INDXR(L))=A(K,INDXC(L))
          A(K,INDXC(L))=DUM
 23       CONTINUE
      ENDIF
 24   CONTINUE
      RETURN
      END
```

```
C
C
C     ******************************************************************
C
C
      SUBROUTINE SORT2(N,RA,RB)
C
C     Sorts an array RA of length n into ascending numerical order
C     using the Heapsort algorithm, while making the corresponding
C     rearrangement of the array RB.  For mor detailed comments see
C     the routine SORT
C
      DIMENSION RA(N),RB(N)
      L=N/2+1
      IR=N
 10   CONTINUE
      IF(L.GT.1)THEN
        L=L-1
        RRA=RA(L)
        RRB=RB(L)
      ELSE
        RRA=RA(IR)
        RRB=RB(IR)
        RA(IR)=RA(1)
        RB(IR)=RB(1)
        IR=IR-1
        IF(IR.EQ.1)THEN
          RA(1)=RRA
          RB(1)=RRB
          RETURN
        ENDIF
      ENDIF
      I=L
      J=L+L
 20     IF(J.LE.IR)THEN
        IF(J.LT.IR)THEN
          IF(RA(J).LT.RA(J+1))J=J+1
        ENDIF
        IF(RRA.LT.RA(J))THEN
        RA(I)=RA(J)
        RB(I)=RB(J)
        I=J
        J=J+J
      ELSE
        J=IR+1
      ENDIF
      GO TO 20
      ENDIF
      RA(I)=RRA
      RB(I)=RRB
      GO TO 10
      END
C
C
C     ******************************************************************
C
C
```

(3)Example of input and output data for NR69

NON-LINEAR LEAST SQUARES FITTING PROGRAM

E L A S T O M E R

Data set:-Preliminary test data: tension, four deformation modes

Original data in comma separated value format.

```
TENSION/NR69
0.29801982E-03,0.22337201E+01
0.11843137E-02,0.18465505E+01
0.26475727E-02,0.16809299E+01
0.46769231E-02,0.15189699E+01
0.72619044E-02,0.14254000E+01
0.10392454E-01,0.13660290E+01
0.14058879E-01,0.13109683E+01
0.18251851E-01,0.12451740E+01
0.22962385E-01,0.12119361E+01
0.28181818E-01,0.11694451E+01
0.33901804E-01,0.11356900E+01
0.40114283E-01,0.11186252E+01
0.46811503E-01,0.10961986E+01
0.53985965E-01,0.10674769E+01
0.61630433E-01,0.10502752E+01
0.69737935E-01,0.10257578E+01
0.78301703E-01,0.10110054E+01
0.87315255E-01,0.99718940E+00
0.96772003E-01,0.98283565E+00
0.10666667E+00,0.96885371E+00
0.16249999E+00,0.91317492E+00
0.22846153E+00,0.87720000E+00
0.30398148E+00,0.85421097E+00
0.38857141E+00,0.83883571E+00
0.48181033E+00,0.82630831E+00
0.58333331E+00,0.82157999E+00
0.69282257E+00,0.82721579E+00
0.81000000E+00,0.83724999E+00
0.93462115E+00,0.84542465E+00
0.10664706E+01,0.85986751E+00
0.12053572E+01,0.88290852E+00
0.13511112E+01,0.90423142E+00
0.16626314E+01,0.94898229E+00
0.20000000E+01,0.10044001E+01

PURE SHEAR
0.39604941E-03,0.21470899E+01
0.15687812E-02,0.17990599E+01
0.34959089E-02,0.16444599E+01
0.61562132E-02,0.15352609E+01
0.95294791E-02,0.14495408E+01
0.13596440E-01,0.14001905E+01
0.18338726E-01,0.13486288E+01
0.23738820E-01,0.13045668E+01
0.29779994E-01,0.12576596E+01
0.36446282E-01,0.12265649E+01
0.43722432E-01,0.11944423E+01
0.51593875E-01,0.11691007E+01
0.60046678E-01,0.11416300E+01
0.69067525E-01,0.11191035E+01
0.78643667E-01,0.10972951E+01
```

0.88762903E-01,0.10774974E+01
0.99413549E-01,0.10578150E+01
0.11058444E+00,0.10437386E+01
0.12226482E+00,0.10291088E+01
0.13444444E+00,0.10151919E+01
0.16026240E+00,0.98897624E+00
0.20250000E+00,0.95485097E+00
0.28171595E+00,0.91406136E+00
0.37119683E+00,0.88959032E+00
0.47020408E+00,0.87539839E+00
0.57812428E+00,0.86782491E+00
0.69444441E+00,0.86734801E+00
0.81873309E+00,0.87335759E+00
0.95062500E+00,0.88557481E+00
0.10898094E+01,0.90168529E+00
0.12360207E+01,0.92096447E+00
0.13890306E+01,0.94491672E+00
0.15486419E+01,0.96751624E+00
0.17146840E+01,0.99510449E+00
0.18870082E+01,0.10226188E+01
0.20654749E+01,0.10523000E+01
0.22499868E+01,0.10839401E+01

SIMPLE SHEAR
0.99999994E-04,0.29308900E+01
0.39999997E-03,0.23550489E+01
0.89999997E-03,0.20906400E+01
0.15999999E-02,0.19108475E+01
0.25000000E-02,0.18165791E+01
0.35999998E-02,0.17060799E+01
0.49000000E-02,0.16378693E+01
0.63999998E-02,0.15525636E+01
0.81000000E-02,0.15003691E+01
0.10000000E-01,0.14496962E+01
0.12100000E-01,0.14070786E+01
0.14399999E-01,0.13641327E+01
0.16899999E-01,0.13228943E+01
0.19600000E-01,0.12966464E+01
0.22500000E-01,0.12696519E+01
0.25599998E-01,0.12460318E+01
0.28900000E-01,0.12176969E+01
0.32400000E-01,0.11960490E+01
0.36100000E-01,0.11733274E+01
0.40000000E-01,0.11592476E+01
0.62500000E-01,0.10700747E+01
0.90000003E-01,0.10089275E+01
0.12250000E+00,0.95942747E+00
0.15999999E+00,0.93039977E+00
0.20250000E+00,0.90346461E+00
0.25000000E+00,0.88149452E+00
0.30250000E+00,0.86492997E+00
0.36000001E+00,0.84934049E+00
0.42250001E+00,0.84571599E+00
0.49000000E+00,0.83826500E+00
0.56250000E+00,0.83921998E+00
0.63999998E+00,0.84463357E+00
0.72250002E+00,0.84372800E+00
0.81000000E+00,0.84978002E+00
0.90249997E+00,0.85391002E+00
0.10000000E+01,0.85900002E+00

COMPRESSION
0.30202019E-03,0.23751959E+01

0.12163265E-02,0.18565443E+01
0.27556702E-02,0.16331051E+01
0.49333333E-02,0.15136586E+01
0.77631574E-02,0.14257623E+01
0.11259575E-01,0.13429901E+01
0.15437634E-01,0.12885583E+01
0.20313043E-01,0.12506651E+01
0.25902199E-01,0.12167041E+01
0.32222223E-01,0.11782506E+01
0.39291009E-01,0.11489394E+01
0.47127273E-01,0.11255475E+01
0.55750572E-01,0.11026540E+01
0.65181398E-01,0.10777686E+01
0.75441175E-01,0.10656519E+01
0.86552381E-01,0.10464511E+01
0.98538553E-01,0.10088214E+01
0.11142439E+00,0.98985266E+00
0.12523579E+00,0.97854989E+00
0.14000000E+00,0.96315002E+00
0.22916667E+00,0.90879666E+00
0.34714284E+00,0.87731140E+00
0.49942305E+00,0.86286312E+00
0.69333332E+00,0.86008334E+00
0.93886363E+00,0.88422268E+00
0.12500000E+01,0.92509967E+00

Fitting Parameters

A = 0.14047218E+01
n = 0.30064653E+00
K = 0.90090941E-01
C = 0.22236500E-02

Squares of the residuals = 0.24296832E+00

Fitted values of strain invariant/reduced stress
==========

Data set: Preliminary test data: tension, four deformation modes

Strain invariant	reduced stress
0.99999988E-04	0.27970165E+01
0.12269303E-03	0.27156445E+01
0.15053580E-03	0.26360207E+01
0.18469697E-03	0.25582343E+01
0.22661033E-03	0.24823462E+01
0.27803510E-03	0.24083933E+01
0.34112972E-03	0.23363924E+01
0.41854241E-03	0.22663453E+01
0.51352244E-03	0.21982416E+01
0.63005632E-03	0.21320624E+01
0.77303522E-03	0.20677812E+01
0.94846040E-03	0.20053645E+01
0.11636950E-02	0.19447784E+01
0.14277727E-02	0.18859840E+01
0.17517778E-02	0.18289414E+01
0.21493095E-02	0.17736096E+01
0.26370531E-02	0.17199483E+01
0.32354807E-02	0.16679170E+01

0.39697098E-02,0.16174766E+01
0.48705577E-02,0.15685883E+01
0.59758353E-02,0.15212163E+01
0.73319345E-02,0.14753267E+01
0.89957737E-02,0.14308878E+01
0.11037188E-01,0.13878718E+01
0.13541860E-01,0.13462547E+01
0.16614921E-01,0.13060168E+01
0.20385359E-01,0.12671437E+01
0.25011423E-01,0.12296279E+01
0.30687281E-01,0.11934687E+01
0.37651169E-01,0.11586752E+01
0.46195375E-01,0.11252672E+01
0.56678527E-01,0.10932774E+01
0.69540619E-01,0.10627550E+01
0.85321533E-01,0.10337679E+01
0.10468360E+00,0.10064081E+01
0.12843953E+00,0.98079550E+00
0.15758638E+00,0.95708525E+00
0.19334754E+00,0.93547487E+00
0.23722401E+00,0.91621351E+00
0.29105737E+00,0.89961427E+00
0.35710719E+00,0.88606756E+00
0.43814575E+00,0.87605899E+00
0.53757441E+00,0.87019068E+00
0.65956652E+00,0.86920750E+00
0.80924230E+00,0.87402921E+00
0.99288415E+00,0.88578999E+00
0.12182000E+01,0.90588700E+00
0.14946469E+01,0.93603998E+00
0.18338279E+01,0.97836387E+00
0.22499796E+01,0.10354588E+01

APPENDIX-7.1

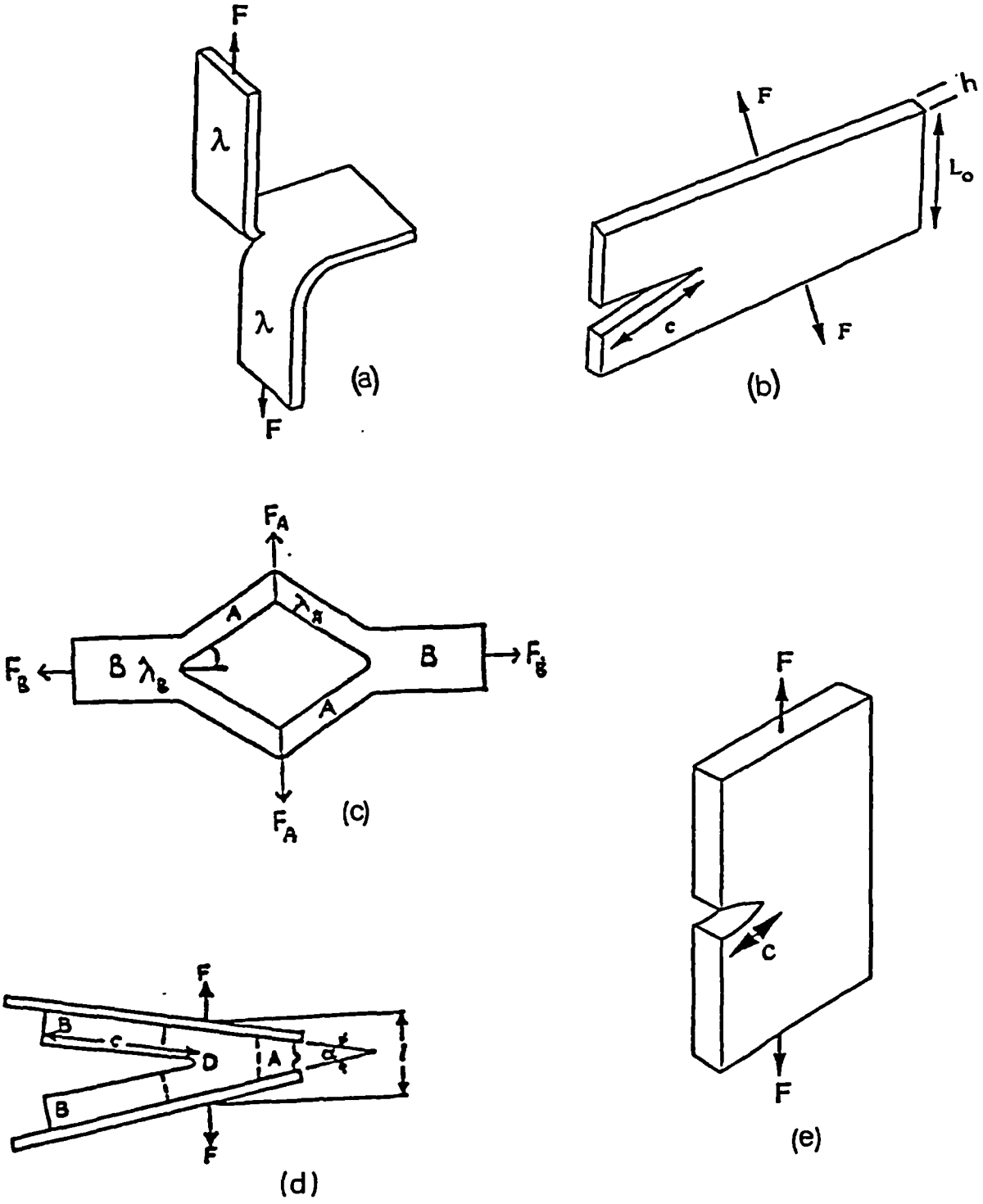

Types of tear test- pieces (a) trouser (b) pure shear (c) split (d) angled (e) edge crack . Fig 1, Pg 51.

Relation between tearing energy and strain energy density for differently-shaped test pieces

(a) Simple extension test piece, commonly known as trouser test piece (figure a)

$$T = 2F\lambda/h - wW$$

Where F is the force applied to each leg, λ is the extension ratio in each leg, h is the thickness in unstrained state, w is the total width of the test piece, and W is the strain energy density in the legs of the test piece that are in simple extension.

(b) Pure shear test-piece (figure b)

$$T = WL_o$$

Where W is the strain energy density in that region of the test piece which is in a state of pure shear, and L_o is the distance between the two parallel clamps at unstrained state,

(c) Split tear teat-piece (figure c)

$$T = \frac{F_A \lambda_A \sin \Phi}{h} + \frac{F_B(\lambda_B \cos \Phi - \lambda_B)}{h} - w\,(W_A - W_B)$$

Where λ_A, λ_B and W_A, W_B are extension ratios and strained energy densities in regions in regions A and B respectively, Tan $\Phi = F_A / F_B$, and w is the width.

(d) Angle test-piece (figure d)

$$T = \frac{2F \sin \alpha}{h}$$

Where F and h are the force and test piece thickness and α is the angle between the clamps.

(e) Edge crack (figure e)

$$T = 2KWc$$

Where W is the strain energy density , K a slowly varying function of strain and c is the cut length.

BIBL LO D N U IV